Surface-Decorated Magnetic Particles in Combination with Isothermal Nucleic Acid Amplification for Rapid Pathogen Detection

Thesis submitted in fulfilment of the requirements for the Degree of

DOCTOR OF PHILOSOPHY

By

SAYANTAN TRIPATHY

Department of Chemistry

BENNETT UNIVERSITY

(Established under UP Act No 24, 2016)

Plot Nos 8-11, Tech Zone II,

Greater Noida-201310, Uttar Pradesh, India

May, 2022

TABLE OF CONTENTS

ACKNOWLEDGEMENT

To begin with, I would like to express my deep and genuine gratitude to my Ph.D. supervisor, Dr. Souradyuti Ghosh at the Department of Chemistry, Bennett University (BU) for his constant support, guidance, suggestions, and encouragement during the days of my Ph.D. I feel grateful to have a supervisor who has kept his door open for any scientific discussions at any time. He has helped in shaping me through all these years not only in the scientific field but also in improving other skills. The good thing about his lab, he also guided me to learn both chemistry and biology in his lab. Along with chemistry, Dr. Ghosh inspired and guided me to stabilize and learn the biological work in his lab at BU. Moreover, his broad research experience in chemistry and biology, and his way of tackling problems have inspired me a lot. Over the last four years, working with him had helped me to grow as an individual in the field of research and no doubt, it will remain the most significant part of my professional life.

I also take this opportunity to thank Prof. Rajinder Singh Chauhan and Dr. Sreekanth Ramachandran as my research advisory committee (RAC) members for their valuable comments and suggestion during every RAC presentation. I am extremely thankful to Prof. Rajinder Singh Chauhan for his fantastic course in genetics. He is an excellent teacher and always teaches from the bottom of his heart. I would like to thank Dr. Saurabh Jyoti Sharma for his valuable suggestion. The good thing about him is that he is so practical in his professional life and always gives me suggestions which are very useful to me. I am personally grateful to the late Dr. Vinayak Gupta for his help to gain knowledge in the genetics course. I am personally thankful to Dr. Mrittika Sengupta, Dr. Deepa Khare, and Dr. Sarika Chaudhuri for their guidance and suggestions during the course work. I would also like to thank Dr. Manu Smriti Singh, Dr. Vaishali Verma, and Dr. Vibhuti Joshi for their advice on different occasions.

I would like to show my sincere gratitude to BU for the funding which enabled me to carry out my research here at BU. I would like to thank all the departmental staff for their continuous help and assistance throughout my Ph.D. I am thankful to Mr. Ved Prakash Gangawar, Mr. Jitendra Khare, and Mr. Pawan Sharma for being a little more generous in providing extra glassware and working places.

Now coming to my groupmates, first of all, I would like to thank Dr. Vandana K Nair my super senior and first postdoctoral researcher in SG's Research group. She has taught me how to become a smart and professional scientist. Next, my junior, Mr. Shrawan Kumar is one of the finest researchers, the person whom I met in my life and a very good friend of mine. He is very talented and innovative in his professional as well as personal life. I would like to thank Mr. Hira Singh Gariya and Ms. Deepika Chaubey, the other juniors who have stayed for a short period in our research group. They both have helped me at BU in different modes.

Personally, thank my family members and relatives. Even though, I take this occasion to pay my deep respect to my family, who stood silently and strong till today. Most importantly I am

proud of the way he kept their patience. I also would like to thank my childhood friends, Nilanjan, Ashish. They were good support in my life till today.

Finally, I like to express my sincere thanks to Bennett University Foundation for providing scholarship and infrastructure; otherwise, this work would not have been possible.

Sayantan Tripathy

ABSTRACT

Nucleic acid extraction from clinical samples followed by nucleic acid amplification tests (NAATs) is the key step of conventional molecular diagnostics. Recently, isothermal nucleic acid amplification tests (iNAATs) draw the attention of scientists. These techniques have a significant advantage over conventional NAATs as the detection of the amplicons by iNAATs can be pushed forward using a thermal cycler-free manner, therefore enabling field detection. It helps obtain rapid, quantitative results either in the laboratory or, more importantly, in a resource-limited area. Despite these advantages, prior nucleic acid extraction from the clinical sample is necessary for both NAATs and iNAATs, which need high-cost instruments, a centralized lab, and highly trained personnel. Microfluidic devices can overcome the issue of prior nucleic acid extraction but the complex fabrication procedure of the analytical device makes it non-compatible in the resource-constrained settings by the end-users. Immunoassays could also be applied to detect the viable pathogen, but the high cost and uncertainty of antibodies are still limitations for those methods. Keeping in mind these research gaps, our primary research is mainly focused on surface-modified magnetic particle-mediated nucleic acid extraction from infectious pathogen followed by downstream isothermal amplification for near-point-of-care diagnostics, especially for the resource-constrained area. Our second area of research explores the alternatives to costly antigen-based detection methods by employing aptamers to detect viable pathogen. Our first objective explores two chitosan-coated magnetic particle preparation methods that can be executed within 6 hours from commonly available chemicals with nothing but a magnetic stirrer and water bath. It is also doable by a minimally trained person followed by downstream loop-mediated isothermal amplification (LAMP). Our second objective explores sequence-specific magneto capture of RNA containing the RdRp gene of SARS-CoV-2 followed by in situ electrochemical reverse transcriptase LAMP. In this assay, we have employed sequence-specific capture of the target on solid-phase support followed by reverse transcriptase LAMP. The amplicons are subsequently detected by square wave voltammetry (SWV). In the third objective, we performed a sandwich aptamer assay. The aptamer was coupled with streptavidin-coated magnetic nanoparticles bound with aptamer for detecting the live pathogen from a biological sample by an enzyme-free hybridization chain reaction (HCR) coupled with colorimetry.

DECLARATION BY THE SCHOLAR

I hereby declare that the work reported in the Ph.D. thesis entitled **"Surface-Decorated Magnetic Particles in Combination with Isothermal Nucleic Acid Amplification for Rapid Pathogen Detection"** submitted at **Bennett University, Greater Noida, India**, is an authentic record of my work carried out under the supervision of **Dr. Souradyuti Ghosh**. I have not submitted this work elsewhere for any other degree or diploma.

I am fully responsible for the contents of my Ph.D. Thesis.

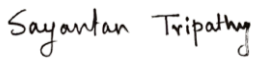

Sayantan Tripathy

Department of Chemistry

Bennett University, Greater Noida, India

26.05.2022

SUPERVISOR'S CERTIFICATE

This is to certify that the work reported in the Ph.D. thesis entitled "**Surface-Decorated Magnetic Particles in Combination with Isothermal Nucleic Acid Amplification for Rapid Pathogen Detection**", submitted by **Sayantan Tripathy** at **Bennett University, Greater Noida, India** is a bonafide record of his original work carried out under my supervision. This work has not been submitted elsewhere for any other degree or diploma.

Dr. Souradyuti Ghosh
Associate Professor

26.05.2022

LIST OF ABBREVIATIONS

AMR	Antimicrobial Resistance
BSL2	Biosafety Level 2
CCCMP	Co-precipitation Cured Magnetic Particles
CHI-g-PEI	Chitosan-graft- poly-ethylenimine
COVID-19	Coronavirus disease
CRISPR	Clustered Regularly Interspaced Short Palindromic Repeats
CsCl	Caesium Chloride
CTAB	Cetyl Trimethyl Ammonium Bromide
Ct-DNA	Calf thymus DNA
Ct	Cycle Threshold
cDNA	Complementary DNA
DLS	Dynamic Light Scattering
DMSO	Dimethyl sulfoxide
DNA	Deoxynucleic Acid
E. coli	*Escherichia coli*
ECCMP	Electrostatically conjugated chitosan-coated magnetic particles
EDL	Electric Double Layer
EDX	Energy-Dispersive X-ray Spectroscopy
eLAMP	electrochemical end-point LAMP
ELISA	Enzyme-linked Immunoassay

eRT-LAMP	electrochemical reverse transcription end-point LAMP
EtBr	Ethidium Bromide
FBS	Fetal Bovine Serum
FE-SEM	Field Emission Scanning Electron Microscope
FT-IR	Fourier Transform infrared Spectroscopy
gDNA	Genomic Deoxynucleic Acid
GlcNAc	N-acetyl glucosamine
GlcN	Glucosamine
GuSCN	Guanidinium thiocyanate
H1-i21	Hairpin1-DNAzyme-i21
H1-i221	Hairpin1-DNAzyme-i22
HCR	Hybridization Chain Reaction
hg DNA	Human Genomic DNA
HIV	Human Immunodeficiency Virus
ICDD	International Center for Diffraction Data
INAATs	Isothermal Nucleic Acid Amplification Tests
LAMP	Loop-mediated Isothermal Amplification
LOD	Limit of Detection
MB	Methylene blue
MERS-CoV	Middle East respiratory Syndrome Coronavirus
MNP	Magnetic Nanoparticle
mRNA	messenger RNA

NAATs	Nucleic Acid Amplification Techniques
NASBA	Nucleic Acid Sequence-based Amplification
NCBI	National Center for Biotechnology Information
NIH	National Institutes of Health
NTC	No Template Control
PC	Polycarbonate
PCB	Polychlorinated biphenyls
PCR	Polymerase Chain Reaction
pDNA	Plasmid Deoxynucleic Acid
pH	potential of Hydrogen
pKa	Acid dissociation constant
PMMA	Polymethylmethacrylate
POC	Point of Care
PSA	Prostate-specific antigen
qPCR	quantitative Polymerase Chain Reaction
qRT-PCR	quantitative real time Reverse Transcriptase- Polymerase Chain Reaction
RCA	Rolling Circle Amplification
RNA	Ribonucleic Acid
RPA	Recombinant Polymerase Amplification
RT-LAMP	Reverse Transcription loop-mediated isothermal amplification
SARS-CoV-2	Severe Acute Respiratory Syndrome-2 virus
SELEX	Systematic Evolution of Ligands by Exponential Enrichment

siRNA	Small interfering Ribonucleic Acid
SNP	Single Nucleotide Polymorphism
SPE	Screen-printed Electrode
STPP	Sodium Tripoly Phosphate
SWV	Square Wave Voltammetry
TAT	Turnaround time
TC	Target Control
TEOS	Tetraethoxysilane
TSB	Tryptic Soya Broth
USA	United States of America
UV	Ultraviolet
VTM	Viral Transmission Media
XRD	X-ray diffraction spectroscopy

LIST OF FIGURES

LIST OF SCHEMES

LIST OF TABLES

CHAPTER 1

THE CURRENT STATUS OF MOLECULAR DIAGNOSTICS WORLDWIDE FOR INFECTIOUS PATHOGEN DETECTION

1.1 The cause behind infectious disease

Infectious diseases have started to spread all over the world from ancient times when enhanced traffic between communities caused an increase in interaction between humans with animals favoring the transmission of pathogens [1]. Increased socialization and trade between provinces, and extended travel caused a high impact on the ecosystem due to increased population which increased the risk of spread of pathogens, named as an outbreak, endemic, and pandemic depending on the scale [2]-[3]. The words outbreak, epidemic, and pandemic refer to the incident of infection caused by a pathogen related to its infection rate and respective geographical containment [4]. An outbreak refers to the sudden increase of a health condition limited to a particular geographical region. An epidemic is a sudden increase of infection or health condition in a geographical region above the expected infection rate. A pandemic is a kind of epidemic that has spread among many countries. For the last few decades Zoonotic dissemination of pathogens from animal to human plays a key role in emerging infection which occurs newly in a particular area [5]. The chance of cross-species transmission of pathogens increased due to expanded interaction with animals, animal-based food, wet market, or animal farming. Climate change also plays a key factor in disease transmission (e.g., Dengue, Chikungunya, Zika, Japanese encephalitis) by disease-carrying vectors. Containment of vector-borne diseases usually needs the control of vectors. Moreover several infectious diseases spread to the expanded geographical territories which now pose major concerns fora significantly larger population [5]. This expansion of infectious pathogens is related to several factors e.g., drug resistance, resistance to pesticides, poor sanitization, global climate change, and as well as increased urbanization. In the twenty-first century, we are still fighting the old pathogens like the plague which have shaken society since the last few millenniums, and new pathogen like human immunodeficiency virus (HIV) and SARS-CoV-2 which both are the results of cross species transmission. Some other

infectious diseases (e.g., tuberculosis, malaria) have become endemic to many territories but still is a reason of concern to mankind. Others like influenza with a high rate of mutation have the possibilities of spreading globally. Meanwhile the drugs which were lifesaving to reduce the mortality of an infection in second half of the twentieth century, are now about to lose their effectiveness. This is due to the adaptability of microbial pathogens towards drugs termed as antimicrobial resistance (AMR). Table 1.1 describes the fatality of prominent outbreak happened since last century.

Table 1.1: The prominent outbreak from the last 100 years

Pathogen	**Area of outbreak**	**Fatality**	**Years active**	**Reference**
Spanish Flu (caused by influenza virus)	Whole worldwide	30-100 million deaths (Approx)	1918-1920	[6], [7]
Asian Flu (caused by a mutated version of the influenza virus)	Whole worldwide	1-2 million deaths (Approx)	1957-1958	[8]
HongKong Flu (caused by a mutated version of the influenza virus)	Whole worldwide	2 million deaths (Approx)	1968-1969	[8]
HIV/AIDS	Whole worldwide	0.15 million deaths annually (approx)	1960-present	[9]
Plague	India	100 deaths (approx)	1994	[10]
Cholera	Whole worldwide	0.15 million deaths annually	1961-present	[11]
Ebola	West Africa	11,000 deaths reported	2014-2016	[12]

Zika	America	Uncounted cases but 50 deaths reported	2015-present	[13]
SARS	China	1000 deaths reported	2002-2003	[14]
Swine Flu	Whole worldwide	0.3 million deaths	2009	[15]
Dengue	Whole worldwide	0.2 million deaths annually	2016-present	[16]
SARS-CoV-2	Whole worldwide	6.2 million deaths till April 2022	2019-present	[17]
Antimicrobial resistance death	Whole worldwide	1.27 million deaths annually	2010-present	[18]

Many vast arrays of infectious diseases were updated in the world health organization's blueprint of most critical and severe diseases for the future in 2018 which included Crimean-Congo haemorrhagic fever [19], Marburg virus disease [20], Middle East respiratory syndrome coronavirus (MERS-CoV) [21] where no vaccines are available till now. Fear of infection can lead to social isolation or the closure of schools, businesses, retail establishments, transportation, and public services, all of which disrupt economic and other socially valuable activities. Infectious diseases always have a great impact on social health as well as on economic health. We have seen in current SARS-CoV-2 pandemic scenario, fear of infection causes closing of schools, industries, commercial establishments, transportation and other valuable public services and results in economic disaster in a country. Under these circumstances, early proper diagnosis can help in reducing the fatality and containment of any infectious diseases.

1.2 The necessity of early detection of pathogen

Early-stage detection is essential for any infectious disease which can help save patient from future complications caused by the pathogen. The majority of infectious diseases cause minor complications if treated and diagnosed at the proper time. If undiagnosed, some of the infections e.g., pneumonia [22], HIV [23] can become life-threatening. Some virus-associated infection e.g., human papilloma virus is linked with life-threatening cervical cancer [24]. *Helicobacter sp* causes stomach cancer [25] or peptic ulcers [25] if not diagnosed at the proper time. Untreated Hepatitis B and C cause liver cancer [26]. Presently the regular evolution of microbes creates emerging infections that are occurring at a higher rate than two decades ago [27, p. 19]. Random mutations in the genome of pathogen results in immune escape from host immune machinery [28]. Antibiotic-resistant microbes are now posing a huge threat to social health worldwide. More than 2 million people get drug-resistant infections each year in the USA [29]. To avoid the future complications caused by infectious pathogens (bacteria, fungi, viruses), accurate and early detection of the pathogen is highly necessary. Undiagnosed patients can transmit the pathogen to other healthy people which can cause an outbreak, sometimes epidemic or pandemic. The diagnostic test manufacturers in charge of molecular diagnostics constantly strive by innovating new tools for rapid point of care diagnostics. But the conventional procedure or current gold standards for pathogen detection requires very costly instruments, a high-end centralized lab, and highly trained personnel which limits its application in the resource-constrained area.

1.3 Conventional ways of pathogen detection and their shortcomings

Nucleic acid extraction followed by the downstream detection by nucleic acid amplification tests is the gold standard for any kind of pathogen detection. This technique has been used regularly in medical and biomedical science as a starting point for any diagnostic procedure which includes the preconcentration of nucleic acids followed by downstream amplification (polymerase chain reaction). Immunology-based methods are also used for the detection of the pathogen, where antigen-specific to a membrane protein of pathogen is employed to capture the pathogen followed by secondary antibody-based detection (e.g., ELISA). Another common way of pathogen detection is plate culture method [30]. This method is based on the specific nutrient medium in which the target pathogen can only grow which confirms the visual identification of pathogen's

growth [31]. However, it takes 2-3 days for informative results about the specific pathogen detection. The long turnaround time limits its application to POC diagnostics [31]. Here we will be discussing the conventional ways of nucleic acid preconcentration from biological samples and their advantages and disadvantages and the same for the downstream gold standard amplification procedures.

1.4 The conventional ways of nucleic acid extraction and their limitations

The intracellular nucleic acid is mainly categorized as chromosomal or genomic DNA, plasmid and RNA which is the main target for any diagnostic course of action. Pre-concentration step involves the extraction of nucleic acid from biological sample or from pathogen by chemical precipitation or commercial kits and downstream readout involves the biomarker gene amplification by polymerase chain reaction or quantitative polymerase chain reaction. Chemical precipitation of nucleic acid is generally relies on the biological properties of cellular compartments to extract the desired molecular components preferably by extracting DNA or RNA depending on their intrinsic characteristics. Some common methods of chemically driven nucleic acid extraction are cesium chloride gradient centrifugation, guanidium-thiocyanate-phenol chloroform extraction, cetyltrimethyl ammonium bromide (CTAB) extraction, Chelex extraction, and alkaline extraction. Cesium chloride based methods are mainly based on the principle of buoyant density where ethidium bromide intercalated DNA is separated from other biomolecules by ultracentrifugation [32]. Guanidium thiocyanate- (GuSCN)-phenol-chloroform has been used for both DNA and RNA extraction [33]. Phenol chloroform method is used for both DNA and RNA extraction which involves salt and ethanol precipitation of DNA. Cetyltrimethylammonium bromide extraction method is basically used for plant samples and their parts, such as leaves, seeds, and grains. The working principle of CTAB involves the precipitation of nucleic acid in low ionic strength solution while protein stays in the solution. Chelex extraction of nucleic acid [34] involves the use of a chelating resin, which is commonly used in forensics for DNA extraction from various sources such as hair, blood stain cards, and buccal swabs. [35]. Alkaline precipitation is actually used for plasmid isolation where chromosomal DNA is denatured, while covalently bound plasmid stays as it is or quickly renatures. Table 1.2 summarizes the advantages and disadvantages of chemical based preconcentration methods.

Table 1.2: The advantages and shortcomings of chemical associated nucleic acid preconcentration from biological sample

Methods	Advantages	Disadvantages	Reference
Phenol Chloroform extraction	High purity nucleic acid	Time consuming, Presence of Phenol in elute cause interruption in PCR	[34]
GuSCN- Phenol Chloroform extraction	Rapid, High purity nucleic acid	Hazardous chemicals used. Presence of these chemical may inhibit downstream amplification	[34]
Alkaline Precipitation	Rapid, Accurate plasmid extraction	Fragments of genomic DNA present in elute, Medium purity	[36]
CsCl gradient EtBr-based ultracentrifugation	High purity and yield of nucleic acid	Laborious, expensive, and time-consuming	[37]
Chelex Extraction	Fast, simple, no hazardous chemical used	Low quality of nucleic acid	[38]
CTAB extraction	Nucleic acid extraction from cells which is hard to lyse.	Laborious, time-consuming; use of potentially hazardous chemicals	[39]

The second way of conventional nucleic acid preconcentration involves solid phase extraction which is the most efficient and commercially available nucleic acid extraction. This kind of extraction generally employs specific hydrophobic, ionic, polar properties of both solute and sorbent. The interaction between analyte and sorbent is the basic principles of this kind of technique [40, p. 15]. Also, the high cost of commercialized kits and instrument requirement for centrifuge column-based isolation, the field of molecular diagnosis still requires the development of low-cost and rapid DNA extraction techniques.

In Fig 1.1 and Fig 1.2, it is noticeable that for silica and cellulose based commercial spin column kits assay time and cost is inversely proportional. Thermo-Scientific purelink blood genomic DNA isolation kit's assay time is relatively low (30 minutes) than Himedia, Qiagen but assay cost is quite high -781 rupees /reaction for blood gDNA (Fig 1.1) and 620 rupees / reaction for bacterial gDNA (Fig 1.2).

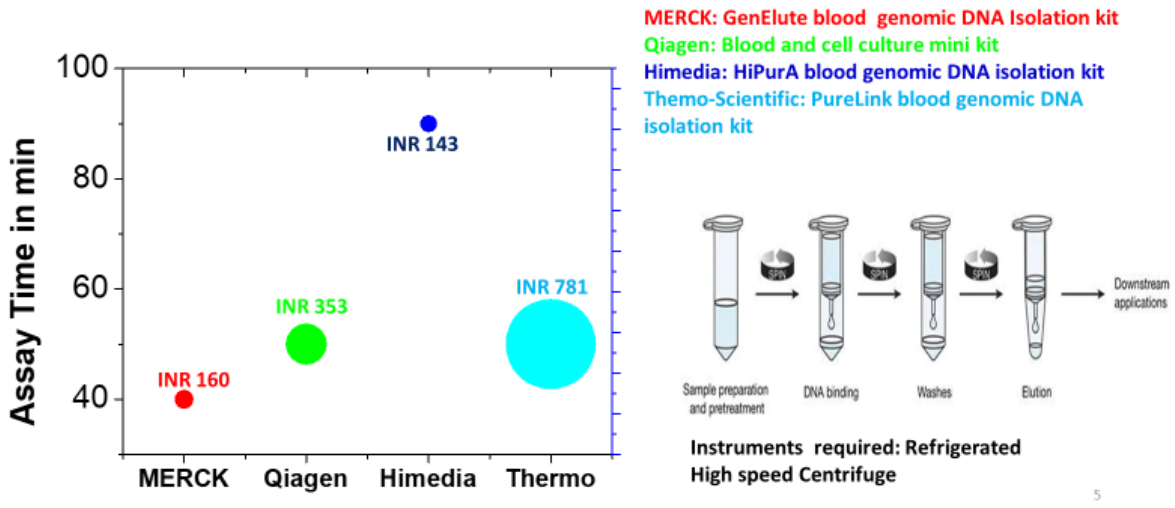

Fig 1.1: Comparison of cost & time of silica-based commercial spin-column kits for blood DNA extraction

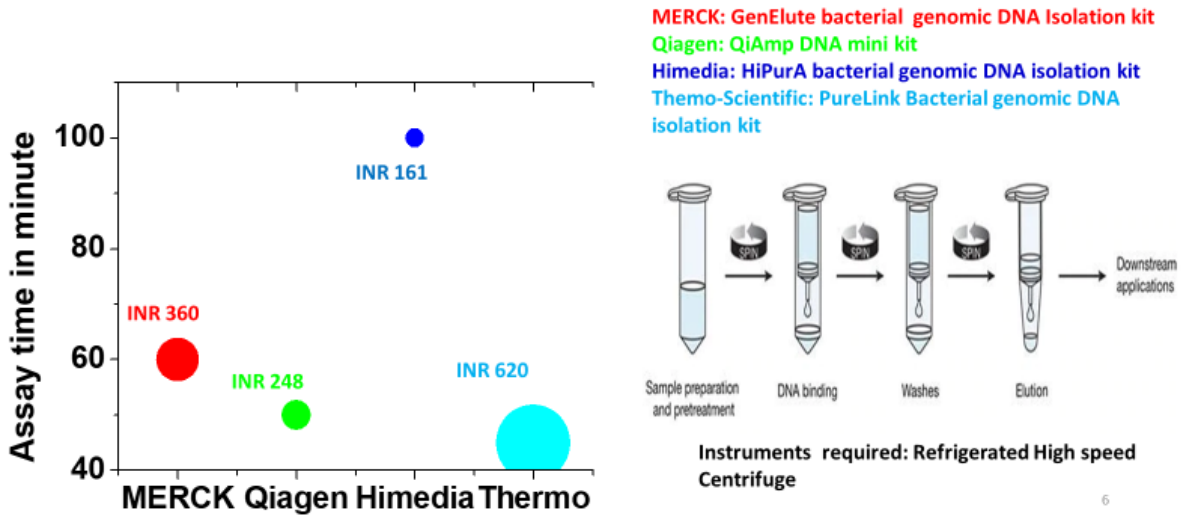

Fig 1.2: Comparison of cost and time of silica-based commercial spin-column kits for bacterial DNA extraction

In addition there is another technique used for DNA extraction is organic solvent based DNA extraction (Fig 1.3). This commercialization involves requirement of expensive chemicals, high end instruments which overall increase the cost of each reactions.

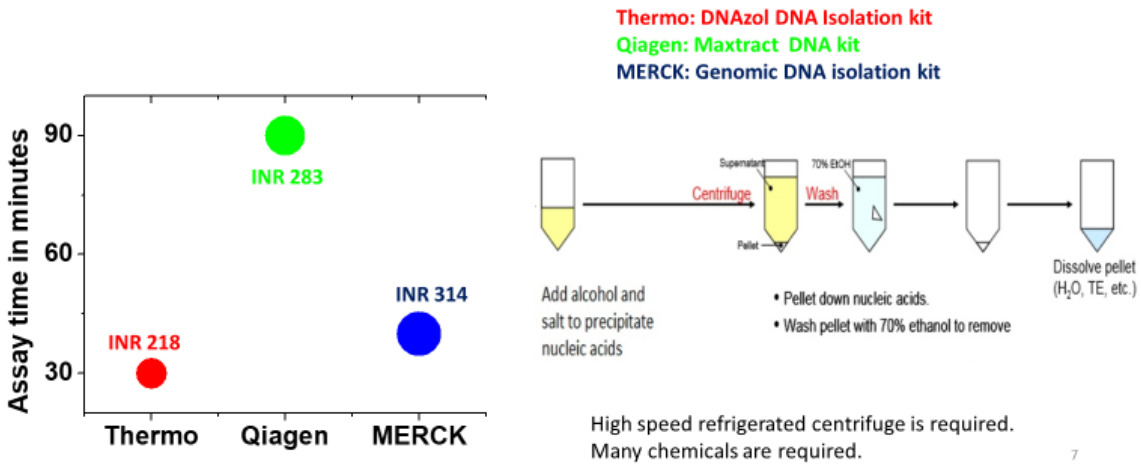

Fig 1.3: Comparison of cost and time of commercial DNAzol organic solvent-based DNA extraction

Most commonly used material for solid phase extraction is silica resin and silica glass particles. In 1979 it was discovered that silica-based compounds have better affinity for nucleic acid under increased salt and alkaline condition [41]. Silica membranes are generally used in a spin column as a resin or as glass particles for nucleic acid extraction [42]. There are different solid phase extractions has been reported for nucleic acid extraction which employs cellulose matrix. Cellulose is a glucose polymer which is hydroxylated and capable of introducing polar interaction with nucleic acid under specific chemical environment. Cellulose based paper devices are now widely used for fast and precise nucleic acid extraction but complex fabrication of the device, complicated extraction and engagement of hazardous chemicals (guanidium hydrochloride or sodium dodecyl sulphate) which interfere with the downstream amplification limits its application [43]. The conventional ways of nucleic acid extraction using spin column based kits (Fig 1.1, Fig 1.2) require costly instruments such as high speed refrigerated centrifuge for nucleic acid extraction which limits its application in resource-constrained area. The fabrication process of spin column is also complicated by the end users themselves. As an

example, in the ongoing pandemic times these spin columns got out of market as the demand of these spin columns overwhelmed the supply chain.

1.5 The conventional ways of signal amplification and their limitations

The polymerase chain reaction (PCR) and quantitative polymerase chain reaction has been widely used for the signal amplification process for detection of any infectious disease. Polymerase chain reaction uses a template DNA which is called as target and two sets of primers (forward primer and reverse primer) specific to the gene of the target DNA, nucleotides and a DNA polymerase enzyme to amplify the specific gene present in target [44]. Presence of pathogen thus can be detected by the amplicon size derived from agarose gel electrophoresis. To conduct polymerase chain reaction a thermal cycler is needed where DNA amplification occurs in three basic steps which are denaturation followed by primer annealing and extension. The thermal cyclers raises and lowers the temperature of the block or hole where tubes with reaction remain placed [45]. Multiplexing of PCR increases its capacity for detecting more than one target in one time [46]. Although this invention creates a new era in molecular biology field but these methods are time and resource-consuming, requiring post-PCR analysis and highly trained personnel. The most path breaking invention in PCR utilization was the discovery of real-time monitoring of DNA amplification based on fluorescence which is named as quantitative PCR or qPCR. qPCR employs a fluorescent dye SYBR-I which intercalates with double stranded DNA to establish fluorescence signal. Increase in amplicon numbers causes an increase in fluorescence after each cycle. TaqMan probe is also used to increase the specificity of the assay [47]. The TaqMan probe method relies on fluorescent labelled probe which hybridizes to specific region within target sequence. The probe contains a fluorescent probe (5’ end) and a quencher molecule (3’ end) which gives a fluorescence signal upon binding to target gene followed by the release of fluorophore through DNA polymerase exonuclease activity. PCR and qPCR is mainly used for medical diagnostics such as infectious disease detection, microRNA analysis, The qPCR has also used for detection of genetic inheritance in as well as detecting the upregulation or downregulation of specific gene products.

Although quantitative PCR possesses several advantages over conventional PCR, still this technology has some severe limitations. Costly instruments, high cost reagents, and requirement of highly trained manpower limit its application to rural area which is resource-constrained. Kits

are not readily available for all kinds of genes and disorders. PCR and qPCR also needs prior pure preconcentration of nucleic acid from biological sample. The presence of complex proteins such as heme and immunoglobulin in biological sample causes interruption in the amplification process [48]. Table 1.3 summarizes the conventional ways for signal amplification for infectious disease detection and their disadvantages.

Table 1.3: Disadvantages of conventional signal amplification methods

Methods	**Disadvantages**	**Reference**
Immunology based method	1. Complex assay and complex fabrication of device with antibodies. 2. Single end-point assays. 3. Multiplexing is not possible	[49], [50]
Count method for culturing colony	1. Requires selective plating, 2. pre-enrichment, 3. selective enrichment and identifications 4. 24 -72h to produce result	[49]
Polymerase chain reaction method	1. costly instruments (e.g.,- PCR or qPCR machine) 2. Common polymerase inhibitors (e.g.,- haemoglobin, lactoferrin present in biofluid.) 3. DNA extraction needed	[51]

1.6 Alternative ways for nucleic acid extraction and their limitations

Nucleic acid extraction by magnetic nanoparticles has become one of the emerging strategies in the field of biomedical engineering now days. This technique utilizes the

preconcentration/extraction of nucleic acid from complex biological sample by selective extraction through complementary hybridization techniques [52] or whole nucleic acid extraction [53]. From the last few decades extensive improvement has been done on surface modified magnetic nanoparticles for rapid whole nucleic acid extraction from pathogen [54]. The magnetic beads based nucleic acid extraction does not require centrifugation step which produce shear forces and fragmentation of nucleic acid and one of the main advantage of this procedure. It is sufficient to apply a magnet to the test tube containing the sample bound with surface modified magnetic beads to extract the desired nucleic acid. Nucleic acid extraction could also be possible from large batch sample from blood, plasma, culture [55]. The uniqueness of magnetic particles relies on the accumulation of an iron oxide core (typically Fe_3O_4) coated with charge based biomaterials. A versatile group of charge based functional groups can be modified on the surface of nanoparticles to increase its stability which can be used for many biomedical applications. Tables 1.4 – 1.8 have a comprehensive literature review of materials developed for DNA binding, which not only includes DNA isolation but sometimes for gene delivery. From the survey, we could conclude that iron oxide nanoparticles which have magnetic properties and its surface modified form have received a popular interest in molecular diagnostic field for rapid nucleic acid extraction. It is due their targeted gene delivery, due to their nucleic acid binding mechanism, low cytotoxicity and biocompatibility. Further chemical modification by amines, carboxylic acids, epoxy, and aldehydes could be usually used to conjugate biomolecules such as DNA, RNA and protein on the surface via electrostatic or covalent bonds. Table 4 describes the reported chitosan coated iron oxide nanoparticles, microparticles for efficient DNA binding from extracted DNA. Chitosan coated magnetic nanoparticles (MNP) are also used for magnetofection for its biocompatibility and it is also used for drug and gene delivery. Because of its biocompatibility and biodegradability, chitosan has been widely used as a coating material for MNPs. Chitosan coated MNP is known for its DNA binding capacity but very few reports are there where peoples utilizes chitosan's DNA binding capacity for direct nucleic acid extraction and detection. Table 1.4 is a selective list of chitosan based papers in application of DNA binding (detection and delivery).

Table 1.4: Chitosan coated iron oxide for nucleic acid binding and downstream applications

Type/Procedure of surface modification	**Types of nucleic acid extracted**	**Downstream application**	**Reference**
Co-precipitation of ferrous and ferric chlorides with ammonium hydroxide	Calf thymus DNA(DNA)	Cytotoxicity study	[56]
Co-precipitation of ferrous and ferric chlorides with ammonium hydroxide	Gram-positive bacterial DNA	Lysis of gram-positive bacteria	[57]
Precipitation of ferrous and ferric chlorides with ammonium hydroxide. The nanoparticles were then purified into the thiolation buffer N-hydroxy succinimide ester chemistry for surface modification	Plasmid DNA	Gene delivery	[58]
Co-precipitation of ferrous and ferric chlorides with ammonium hydroxide	Adenoviral DNA	Adenovirus infection study	[59]
Co-precipitation of ferrous and ferric chlorides with ammonium hydroxide followed by APS polymerization	salmon sperm DNA	PCR analysis and electrophoresis assays	.[60]
Co-precipitation of ferrous and ferric chlorides with ammonium hydroxide	siRNA	Gene delivery	[61]
Co-precipitation method of ferrous and ferric chlorides with ammonium hydroxide	biotinylated DNA aptamer sequence specific to the malathion	electrochemistry	[62]
Iron oxide microparticles were synthesized via a facile template-free hydrothermal method	Target DNA	Biosensors	[63]

followed by DNA immobilization using terephthalaldehyde			
Co-precipitation Sodium oleate chemistry	Plasmid DNA	Uptake assay of DNA. Gene transfer	[64]
Co-precipitation	plasmid DNA (pDNA)	fluorescence, MRI effectiveness, and desirable biocompatibility	[65]
Nano emulsion of PLGA, Chitosan and iron oxide nanoparticles	plasmid	Nucleic acid detection	**[66]**

The amine derivative coated iron oxide nanoparticles for DNA binding are described in the Table 1.5. Magnetofection, which is transfection mediated by magnetic nanoparticles (MNPs) in the presence of an external magnetic field, has sparked considerable interest in recent years. Different amine coatings or modifications on iron oxide nanoparticle surface increases its physical stability as well as make them compatible with various biological functions. Surprisingly, very less work is done in diagnostics field due to its highly complicated synthesis procedure.

Table 1.5: Amine derivative coated iron oxide nanoparticles for DNA binding capacity

Type of surface modification	**Types of nucleic acid extracted**	**Downstream application**	**Reference**
Galactosylated-carboxymethyl chitosan-magnetic iron oxide nanoparticles	Nude Mouse DNA	Transfection	[67]

Magnetic nanoparticles with chitosan-graft- poly(ethylenimine) (CHI-g-PEI) Co-precipitation	Mitochondrial DNA	Gene delivery	[68]
Molybdenum Schiff base complexes with a core-shell structure were immobilised on magnetic iron oxide nanoparticles for use as a new heterogeneous catalyst	Calf thymus DNA	molecular modelling study	[69]
Magnetic nanoparticles (MNPs) with Tween 20 and coated with oleic acid	genomic DNA (gDNA) and total RNA from prokaryote and eukaryote cells	PCR and electrophoresis	[70]
2',6'-dimethylcarbonylphenyl-10-sulfopropyl acridinium-9-carboxylate 4'-NHS ester (DMAE-NHS) is used for coating on magnetic nanoparticles.	p53 gene	DNA sensitivity or detection	[71]
Fabrication of polyaniline-molybdenum sulphate nanoflower architectures via hydrothermal route	Plasmid DNA	Sensor development	[72]
Cathodolumthin films with various concentrations of MNPs fabricated by the drop-casting method	Genomic DNA	Measurements of cathodoluminescence to better understand binding, dispersion, chemical identification/functional	[73]

		modes	

Chemical functionalization with amines, carboxylic acids, epoxy, and aldehydes is commonly used to covalently link proteins, enzymes, RNA, and DNA biomolecules to surfaces. Table 1.6 describes the reported works on silica-coated MNPs used for DNA extraction.

Table 1.6: Silica coated magnetic nanoparticles for DNA binding study

Type of surface modification	**Types of nucleic acid extracted**	**Downstream application**	**Reference**
Co-precipitiation of iron oxide followed by hydrolysis of tetraethoxysilane (TEOS) under alkaline conditions.	RNA from zika virus	PCR-based assay	[74]
Co-precipitiation of iron oxide followed by hydrolysis of tetraethoxysilane (TEOS) under alkaline condition	DNA hybridization	complementary DNA hybridization, leading to a decrease in signal intensity	[75]
Co-precipitiation of iron oxide followed by hydrolysis of tetraethoxysilane (TEOS) under alkaline condition	Genomic DNA	Detect the 5hmC in the genomic DNA of cancer tissue, which indicated that the immunosensor possesses potential applications in clinical detection.	[76]
Functionalized Fe_3O_4 nano-particle surface utilizing SiO_2 and TiO_2	plasmid DNA	Kit preparation	[77]

layer.			
Amino-rich silica-coated magnetic nanoparticles using hydrochloric acid treatment.	Genomic DNA	PCR based assay	[78]
The polymer of methyldopa (2-amino-3-(3,4-dihydroxyphenyl)-2-methyl acid, propanoic) (PMDP), magnetofluorescent PMDP-γ-Fe2O3 nanocrystal.	calf thymus DNA (ct-DNA)	PMDP-γ-Fe2O3 nanocrystal in bioanalytical chemistry and nanotechnology	[79]
Dendriplex-coated MNPs formed by generation 6 dendrimers at an N/P ratio of 10	plasmid DNA (pDNA)	Obtain nanohybrid systems suitable for nucleic acid therapy	[80]
polyaniline/maghemite nanocomposite (Pani/γ-Fe_2O_3 MNC)	double-stranded deoxyribonucleic acid (dsDNA)	DNA retrieval	[81]

It has been observed from the literature survey that most of the microdevices use chitosan for extensive DNA capturing. Chitosan has a free amine group that can be controlled based on pH change. As a result, chitosan has a similar DNA capturing capacity similar to commercial kits based on silica. Chitosan's cationic property contributes to its strong nucleic acid condensation ability, which is a popular therapeutic research topic. Table 1.7 describes where scientists have utilized chitosan's DNA binding property for nucleic acid extraction followed by downstream amplification. But very few reported works are there where chitosan's DNA binding property has been utilized for the downstream diagnostic application.

Table 1.7: Chitosan coated magnetic nanoparticles in analytical/molecular diagnostics

Types of Device/material	**Preparation of Device**	**Type of extracted nucleic acid**	**A device used in DNA extraction from complex biofluid/lysate?**	**Downstream application**	**Was there direct amplification ?**
1. γ-Fe_2O_3@Chitosan@Polyaniline hybrid (magnetic) [82]	Polymerization of aniline on the surface of the Fe3O4@Chi MNPs. Prep Time -48 hours	Genomic DNA from whole blood	Yes, gDNA from blood extracted	PCR	No
2. Microdevice for Nucleic Acid Amplification. [83]	Paper treated with O_2 plasma; Then immersed into 1% w/v chitosan Prep Time-30 hours	*Pure* genomic DNA	Yes, Chitosan filter paper-based	LAMP	No
3. Pipette-actuated capillary array comb with integrated DNA extraction [84]	Pipette-actuated capillary array comb with (poly(methyl methacrylate)) base embedded glass filter paper(chitosan) discs. Prep time-24 hours	*Pure* genomic DNA	Yes, PMMA based chitosan filter paper	LAMP	No

4. Two morphologies of nanoceria were synthesized.[85]	DNA probe was immobilized with CeO_2/chitosan modified electrode Prep time-24 hours	*C. perfringens* genomic DNA	No, Purchased	Electrochemistry	No
5. Reduced graphene oxide-nanoplatinum (rGO-nPt) electrode coating [86]	Nano platinum (not) layer electrodeposition in actuation of chitosan-aptamer nano brush borders Prep time-24 hours	*L. monocytogenes* genomic DNA	No	Electrochemistry	No
6. PDMS by the template-assisted soft lithography technique. [87]	10 mg/mL LSMO nanoparticles (magnetic) in deionized water was admixed with 0.5 mg/mL chitosan and kept overnight. Prep time-24 hours	*E. coli* genomic DNA	No isolated from the sample	PCR	No
7. Chitosan-coated magnetic microparticles. [88]	0.1% chitosan solution with magnetic microparticles and vortexed. Prep time-24 hours	Human genomic DNA	No, Kit	PCR	No

8. Cellulose-chitosan porous membrane. [89]	CS powder of 0.5, 1.0, 2.0, and 3.0 wt% was incubated in a mixture of a strong acid. Prep Time-24 hours	*E. coli* genomic DNA	Yes, Extraction based	PCR	No
9.Chitosan microparticles [90]	Chitosan microparticles were fabricated by creating aqueous chitosan droplets in oil. Prep time -24 hours	pUC19 plasmid DNA	No, Kit	PCR	Yes

From the reported work it can be seen that the existing device for nucleic acid extraction followed by detection by downstream nucleic acid amplification procedure facilitates a long and complex fabrication time (at least 12 – 15 h, if not longer).

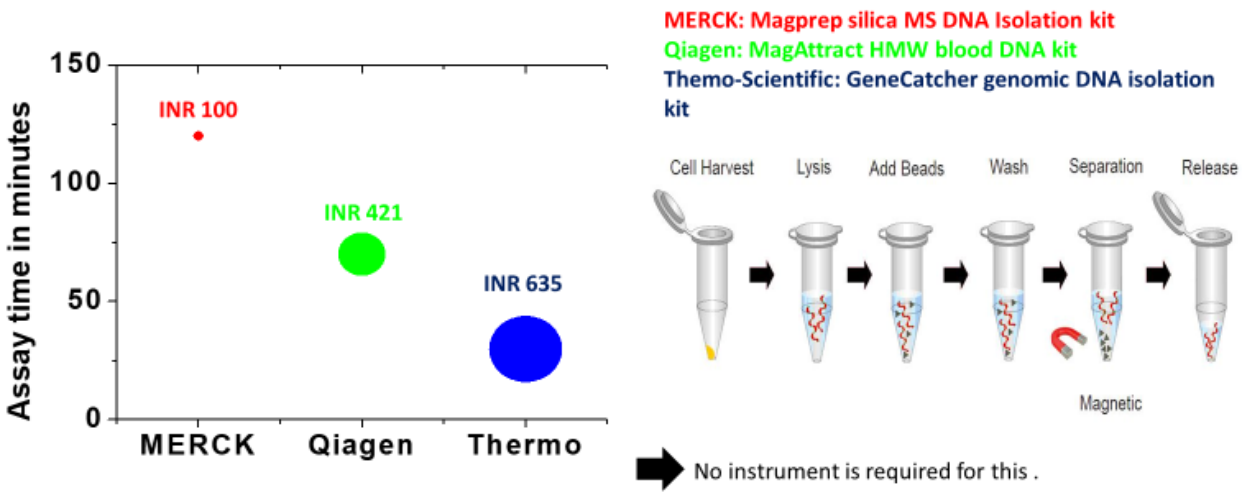

Fig 1.4: Comparison of cost & time of commercial magnetic beads-based assay for DNA extraction

Besides, due to the high cost of commercialized MNP and instrument requirement for centrifuge column-based isolation, the field of molecular diagnosis still requires the development of low-cost DNA binders. It has been noticed that very few commercial companies deal with direct amplification (no extraction at all or significantly less extraction time) kits with very high costs (Fig 1.4).

Table 1.8: Comparison of assay time and cost of commercial magnetic beads for one-step nucleic acid extraction plus amplification (direct amplification)

Company name	**Kit name**	**Total assay time**	**Cost/reaction(INR)**
Merck	SYBR® Green Extract-N-Amp™ Tissue PCR Kit	15 mins-extraction	222
Merck	Extract-N-Amp™ Blood PCR Kit	15 mins-extraction	204
Thermo Scientific	AmpFLSTR™ Identifiler™ Direct PCR Amplification Kit	No extraction is needed only lysis	3220

From the Data survey (Figure 1.4) from different commercial kits, it was clear that DNA extraction assay time and their respective kits' cost were inversely proportional for magnetic beads-based DNA extraction. This is the same trend that was noticed for conventional silica matrix-based spin columns. In addition, the potential presence of chaotropic chemicals in surface-modified magnetic beads in the final extracted nucleic acid solution interferes with its downstream amplification procedure [91].

Besides nucleic acid-based detection, there is a tremendous advancement has been made in nucleic acid-based pathogen detection, which employs aptamers instead of antigens in immunology-based detection. Aptamers, which originated from the systematic evolution of ligands by exponential enrichment (SELEX), are oligonucleotides that can bind to their target protein or nucleic acid with a high affinity comparable to that of the antibody [92]. Because of its low cost, amenability to chemical modifications, and increased stability, aptamers have become a

robust analytical candidate for highly sensitive detection, especially for bacteria present in food and environmental samples, and have shown desirable reliability [93]. Aptamer-based detections are fast and specific, and they can be used for detections that do not have any special requirements. An aptamer has a significant advantage over an antibody in that it can generate amplification signals that successfully increase detection sensitivity. Aptamer-based methods of pathogen detection can also distinguish between viable and non-viable pathogens, which are not possible for conventional nucleic acid extraction-based pathogen detection procedures.

As shown earlier, nucleic acid-based detection has several advantages over immunology-based methods in terms of sensitivity and specificity. However the time requirements and high-cost instruments limit its application on a broader spectrum in developing countries where centralized labs are not easily available in rural areas. Recent progress have been made on microfluidic chips, where all the extraction and amplification happen on a single chip carrying chambers [94]. The "lab on a chip" cartridges employ solid phase (silica matrices, cellulose matrix, magnetic beads) extraction of nucleic acid followed by nucleic acid amplification techniques. An extraordinary example of such a device is the commercialized rifampicin-resistant *Mycobacterium tuberculosis* detection by the platform GeneXpert MTB/RIF [95]. The procedure involves the initial lysis step of the pathogen by sonication followed by washing steps by rotors and advancement of the washed nucleic acid to the amplification chamber by a liquid pump [96]. Although point care diagnostics is possible in microfluidic chips, complex integration of devices and complicated sample preparation is the primary obstruction to these types of techniques by the end-users in the limited resource area. Besides, the commercial availability of these types of microdevices is still very little compared to conventional diagnostic kits [97]. Some commonly used molecular biology chemicals can interact with the plastic material in microfluidic chip cartridges, making them unstable and causing inefficient readouts [98]. The structural property of glassy polymers like thermo-stable polycarbonate (PC) and polymethylmethacrylate (PMMA) has been extensively studied in different chemicals to investigate their sustainability. So molecular diagnostic field still needs an upgrade in commonly and alternatively used nucleic acid extraction/preconcentration techniques.

1.7 Alternative ways of signal amplification other than conventional NAATs and their possible drawbacks

The main obstruction of the conventional nucleic acid amplification test is associated with the initial extraction of the pathogen nucleic acid followed by a costly instrument-assisted amplification procedure and data analysis. These steps are time-consuming and require highly trained personnel [99], especially when the gel associated analysis of nucleic acid is involved in data analysis. That's why recent progress has been seen in isothermal nucleic acid amplification procedures such as loop-mediated isothermal amplification (LAMP) [100], rolling circle amplification (RCA) [101], nucleic acid sequence-based amplification (NASBA) [102], recombination polymerase amplification (RPA), and toehold mediated strand displacement hybridization. These methods do not require a thermal cycler or any high-end instruments for signal amplification. The most common amplification method used extensively in clinical diagnostic is LAMP which was innovated in 2000 [100]. It requires 4-6 primers to amplify four different target nucleic acid segments and is well accepted in the biomedical field for its speed, sensitivity, and simplicity [103]. The LAMP amplification procedure generally happens at 60-66˚C, and the amplification takes a maximum of 1 hour to produce a signal which can be visually detected by turbidity. SYBR-I has been used widely in LAMP to quantify the amplification signal under a UV light [104], [104]. LAMP has been used widely to detect genetic mutation and infectious pathogens from food or water sample, especially in resource-constrained areas [105]. The products from LAMP show a ladder-like structure in agarose gel upon successful amplification of the target [106]. LAMP assays have been established to detect yeast [107], influenza virus [108], and *plasmodium sp* [109]. Many LAMP kits are commercialized for successful detection of verotoxin-producing *E. coli* [110], *Salmonella sp.* [111] ,and *campylobacter sp.* [112]. Scientists have integrated LAMP procedure in microfluidics strategy for rapid pathogen detection [113]. One drawback of LAMP is that it is highly prone to contamination, giving false-positive results. Hybridization of primers causes false positive amplification [114]. Experimentation of LAMP thus requires careful primer design, intensive care, and extreme asceptic techniques to prevent carryover contamination. A second limitation of LAMP is associated with multiplexing. Recently, scientists are trying to improve the efficiency

of loop-mediated isothermal amplification by introducing CRISPR/Cas9 technique with LAMP [115].

Another most common isothermal amplification technique is nucleic acid sequence-based amplification (NASBA). It is mainly used to detect RNA such as messenger RNA, ribosomal RNA, and genomic RNA [116], [117]. It is a transcription-based amplification procedure and self-sustained sequence replication procedure developed in 1990 [118]. The limitation of NASBA is associated with the need for an initial denaturation step (different temperatures for DNA and RNA). The amplification requires an additional thermolabile enzyme after the denaturation step. This amplification requires a 120-150 bp long sequence to amplify [117]**.** NASBA, like other isothermal amplification methods, has some drawbacks. One major drawback is the integrity of RNA isolated from the sample. The sensitive nature of RNA could lead to degradation, drastically reducing the assay performance. NASBA is also unlikely to amplify any target region less than 100bp and greater than 250 bp.

Another common isothermal amplification procedure is recombinant polymerase amplification (RPA), a dual nucleic acid probe-based method to amplify the product. The recombinase enzyme in the amplification process involves the DNA repair, recombination, and elongation. A thermal denaturation step is not required for this process as recombinant polymerase enzyme facilitates strand separation. After strand separation recombinase enzyme disengages from the DNA primer hybrid complex, and DNA polymerase starts the elongation process from the free 3' end. The displaced DNA has then conjugated with DNA binding proteins, and the new forms of dsDNA act as the template for another cycle of amplification. It is a one-tube reaction with real-time fluorescence monitoring at room temperature and it needs 30 minutes for amplification. RPA is commonly integrated with microfluidic devices for rapid detection of *Salmonella sp.* [119], *Listeria sp.* [120]and *Salmonella enterica* serotype *Enteritidis*[120], Group B streptococci [121], parasites (Giardia, Cryptosporidium, and Entamoeba) and fungus [122].

Another isothermal amplification procedures is rolling circle amplification (RCA), The principle of this kind of amplification is inspired by bacterial plasmid replication. Mainly three types of RCA are utilized for pathogen detection, which are a) linear RCA, b) hyper-branched RCA, c) multiply-primed RCA, d) circle-to-circle RCA, and e) primer regeneration RCA. RCA generally employs circular single-stranded DNA as a template [123]. The circular probe is usually designed

with partial complementarity with the target at the 5’ and 3’ end. This circular probe is known as a padlock probe. The probe becomes circularized with the help of ligase. After this complex formation target can be amplified with help of the Phi29 enzyme itself by making complementary copies of padlock probes or a second primer can also be added complementary to the padlock probe to increase the intensity of the amplification. Recently H5N1 influenza virus has been detected with hyper-branched rolling circle amplification with a detection limit of 9 fM [124]. Although rolling circle amplification is better than other isothermal amplification methods in terms of specificity and accuracy it has a lower detection limit than those of LAMP, RPA, and NASBA. It also needs an extra step for the circularization of padlock probe limiting its application in the clinical diagnostic field.

Another type of isothermal amplification technique is hybridization chain reaction (HCR) which was invented in 2004 [125]. Unlike other isothermal amplification methods, this reaction does not need enzymes to produce an amplification signal. The initiation of HCR needs a target molecule or initiator (I), which initiates the cross opening of one hairpin probe (H1) using a partially complementary initiator (I). Upon unfolding of H1 the other hairpin pin probe (H2) which again is partially complementary to H1 hybridizes with H1 and initiates a chain reaction at room temperature [125]. Finally, DNA polymers produce HCR nanowires until the amount of H1 and H2 in the reaction is exhausted. Scientists are now developing strategies to employ HCR in a wide array of diagnostics such as photoactivation [126], proximity-dependent initiation [127], etc. Very few clinical diagnostic studies have been reported that have utilized HCR for medical purposes. One drawback of this method is a low detection limit than other standard isothermal amplification methods.

1.8 Role of electrochemical analysis in molecular diagnostics

Electrochemical analysis has recently provided a wide array of quantitative methods for pathogen detection by analyzing a particular analyte, a protein or nucleic acid. An electrochemical biosensor is defined as a transducer of an electroactive species' oxidation (or reduction) reaction to an electrical current signal. The electrochemical activity of nucleic acid is not adequate for direct detection, requiring a redox indicator to be employed to achieve the purpose. The device senses the redox probe concentration and the variation in mass transfer to the working electrode. Since DNA has a strong affinity for redox probes, the binding significantly reduces the “free”

probe concentration in the electrolyte. Commonly used redox probes are transition metal complexes (e.g. ruthenium (Ru) complexes) and organic dyes (e.g. methylene blue (MB)). MB belongs to the thiazine class with the molecular formula $C_{16}H_{18}N_3SCl$ and can be employed as a redox probe Ruthenium hexamine was employed for the amplified detection of BRCA-1 mutant DNA [128], whereas MB was used for electrochemical monitoring of influenza virus RNA and quantitative detection of pathogenic DNA [129]-[130]. MB binds to the DNA electrostatically as well as intercalates into the DNA structure [131].

1.9 Summary and gap area

The above-mentioned conventional and alternative ways of pathogen detection need costly instruments for prior pathogen nucleic acid extraction and increase the time and cost of an assay. At present, the real-time polymerase chain reaction remains the gold standard for detecting any pathogen due to its accuracy and specificity. However, this approach is time-consuming, and it requires highly trained personnel and a highly equipped lab infrastructure which is a limiting factor in the resource-constrained area. These drawbacks of conventional detection procedures have increased the advancement of various isothermal nucleic acid amplification detection procedures. Despite their successes in reducing the burden of pathogen-causes diseases, the isothermal amplification techniques still have drawbacks. These include but are not limited to the requirement of prior extracted nucleic acid for downstream readouts. Therefore, our research area focuses on developing novel materials in combination with innovations in isothermal nucleic acid amplification techniques. This will enable us to fulfil the current research gap for

1. Rapid DNA extraction without using any high-cost instruments
2. It should be inexpensive compared to conventional methods
3. The extracted DNA should be amenable for downstream nucleic acid amplification or isothermal nucleic acid amplification
4. The workflow comprises direct amplification from the biological sample without using high-end instruments.
5. Detection of the viable pathogen using aptamers is less costly than conventional antigen-based detection.

CHAPTER 2

LIMITED-RESOURCE SUITABLE RAPID AND EASILY SYNTHESIZABLE CHITOSAN-COATED MAGNETIC PARTICLES FOR AMPLIFICATION-READY NUCLEIC ACID EXTRACTION

2.1 Abstract

Outbreaks such as SARS-CoV-2, Ebola, NIPAH are more prone to impact populations at rural, isolated areas. This is due to the inaccessibility to high-tech laboratories, time-consuming sample transport to distant diagnostic centres, and resulting delayed treatment leading to the unfortunate demise of many infected patients. However, it is time-consuming and instrument-intensive to extract the nucleic acid using silica or cellulose spin columns from any biological sample. In addition, the silica or cellulose-based spin column techniques utilize hazardous chemicals like guanidium thiocyanate for extraction, which has to be removed by multistep washing as it interferes with downstream nucleic acid amplification techniques (NAATs). On the other hand, conventional silica magnetic bead chemistry for nucleic acid extraction is instrument-free and rapid but depends on hazardous chemicals and ethanol desalting that may lower the sensitivity of downstream NAATs. Recent works on charge modulation chemistry-based material coating on magnetic beads may solve nucleic acid extraction problems. However, the availability and multistep synthesis of the particles still pose a problem in resource-constrained settings. To overcome this issue, we have investigated the nucleic acid capture ability of co-precipitation cured magnetic particles (CCCMP) and electrostatically conjugated chitosan-coated magnetic particles (ECCMP). These are preparable by minimally trained personnel without sophisticated instruments (i.e., only with hotplate magnetic stirrer) within 6 hours. We have also explored their suitability for clinically relevant sensitive downstream readouts, where low copies (100 – 1000) of *E. coli* or human genomic DNA from aqueous solution, crude cell lysate, and fetal bovine serum were extracted by them. The extracted DNA was then successfully detected using quantitative real-time loop-mediated isothermal amplification (LAMP) or real-time polymerase chain reaction (PCR). Despite the ease of synthesis, the prepared magnetic particle could still be

utilized in sensitive molecular diagnosis for a limited resource area. Parts of this chapter has been published in a peer-reviewed journal article [132].

2.2 Introduction

Nucleic acid extraction followed by amplification from biological samples is the main requirement for any nucleic acid-based molecular diagnostics application that explores genetic disease analysis, pathogen detection, SNP analysis, and bio warfare prevention. However, despite the high cost of commercialized MNP and instrument requirement for centrifuge column-based isolation, the field of molecular diagnosis still requires the development of low-cost and rapid DNA extraction techniques. The necessity of a highly equipped and power-intensive centralized lab and highly trained personnel for the conventional spin column-based nucleic acid extraction methods make it unsuitable for resource-limited areas. Recently, massive progress has happened in the lab-on-a-chip techniques for rapid pathogen detection. However, long and complicated fabrication of microdevices makes their utility difficult for the end-users themselves in resource-constrained areas. The application of charged polymer-coated magnetic nanoparticles for nucleic acid extraction is relatively instrument-free, less complicated, user friendly. Still, the extraction techniques by the nanoparticles rely on chaotropic salts and hazardous materials, limiting their application to downstream nucleic acid amplification tests (NAATs). Recent advances in several types of polyamine-coated magnetic nanoparticles that undergo salt-free nucleic acid extraction methods may offer a possible solution. Still, the multistep synthesis of polymer-coated magnetic nanoparticles is complex in the resource-constrained area. To address the gap, we attempted to develop instrument-free and novel chitosan and polyamine-coated magnetic nanoparticles which were coated by positively charged chitosan for isolating DNA from biological samples. Chitosan (CS) [(14)-2-amino-2-deoxy—D-glucan], a cationic polysaccharide derived from the deacetylation of chitin and composed of N-acetyl glucosamine (GlcNAc) and glucosamine (GlcN), has received widespread attention as a pharmaceutical excipient due to its unique properties such as biocompatibility, biodegradability, low As a result, it can be used in conjunction with magnetic (Fe3O4) nanoparticles.

In this work, we synthesized two types of chitosan-iron oxide magnetic particles, which can be prepared with minimally trained personnel with the help of only a magnetic stirrer within 6-8 hours. After characterizing them using FE-SEM, EDX, FT-IR spectroscopy, DLS-Zetasizer, and

XRD, the magnetic particles were subjected to DNA binding and isolation in a rapid (less than 30 min) magneto-extraction assay. Since the ultimate goal was biomedical detection without using high-cost instruments like refrigerated centrifuge and PCR, the isolated DNA was then characterized by loop-mediated isothermal amplification (LAMP) and further tested for its limit of detection (LOD). To explore the suitability of our magneto-extraction assay, clinically relevant 1000 and 100 copies (in the order of zeptomole) of *E. coli or* human genomic DNA from the aqueous sample, crude cell lysate, and complex biofluid (serum) were extracted. The elutions were subjected to real-time loop-mediated isothermal amplification (LAMP) or real-time PCR. The required optimization of the amplification procedure has been discussed in this chapter and reported [132]. Parts of this chapter has been published in a peer-reviewed journal article [132].

2.3 Results and Discussions

2.3.1 Characterization of magnetic particles

The main inspiration of this investigation is to employ magnetic particles for rapid nucleic acid extraction followed by downstream amplification for the resource-constrained area. To establish that such magnetic particles can be utilized for the sudden outbreak, we chose synthesis protocols that can be doable with a minimum setting with a large synthesis scale (0.1 gm) by minimally trained personnel. Chitosan is a biopolymer known for its pH-responsive nucleic acid capture efficiency. We have chosen chitosan as a coating material for the magnetic particle as it is biodegradable, cost-efficient, and readily available. We have opted for two synthesis protocols that have fulfilled the above-mentioned criteria and prepared co-precipitation cured chitosan magnetic particles (CCCMP) and electrostatically cross-linked chitosan magnetic particles (ECCMP). Surprisingly, we could not find any investigation in literature where such chitosan-coated magnetic particles have been employed for ultrasensitive detection of nucleic acids from crude cell lysate or complex biofluid. In the synthesis of CCCMP, chitosan in acetic acid was subjected to alkaline co-precipitation, where iron oxide nanoparticles were encapsulated in a chitosan polymer chain during synthesis. For ECCMP preparation, ionic cross linker sodium tripolyphosphate has been employed to entrap pre-synthesized ferrite magnetic nanoparticles in the chitosan polymer chain (scheme 2.1).

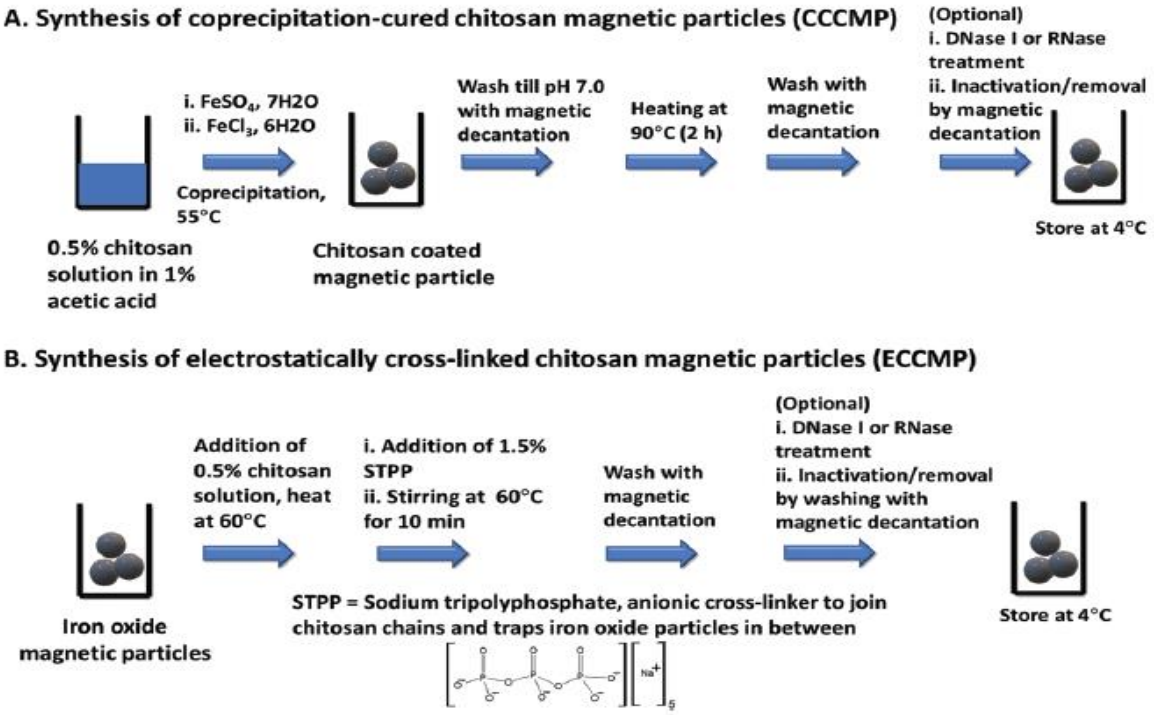

Scheme 2.1: Synthesis of chitosan-coated magnetic particles

The characterization of chitosan-coated magnetic particles and bare iron oxide magnetic nanoparticles was executed by scanning electron microscopy (FE-SEM), energy dispersive X-Ray diffraction for elemental analysis (EDX), and dynamic light scattering (DLS), Fourier transform infrared spectroscopy (FT-IR), zeta potential and XRD.FTIR was performed to confirm the functional groups on the surface of the synthetic materials. The spectra of bare iron-oxide MNP, CCCMP, and ECCMP were shown. FE-SEM images clearly showed an agglomerated spherical-shaped structure of three types of magnetic particles in the 500 nm range. From this data, we concluded that our synthesized magnetic particles are nanoparticles (Fig 2.1A-C). The crystal structure of Fe_3O_4 magnetic particles was characterized by XRD (Fig 2.1D), where all synthesized nanoparticles indicated diffraction peaks at 30.32° (220), 35.60° (311), 43.24° (400), 53.62°(422), 57.34° (511), and 62.83° (440) which are directly associated withFe_3O_4 as described in ICDD (international centre for diffraction data). The average diameter of the Fe_3O_4 nanoparticles was about 15.5 nm which was calculated by Debye-Scherrer's equation which is at peak (311), $2\theta = 35.60°$. The results indicated the crystalline structure of the iron oxide

nanoparticle core. EDX data shows the presence of carbon and nitrogen in CCCMP and ECCMP but absent in bare iron oxide nanoparticles (Fig 2.2).

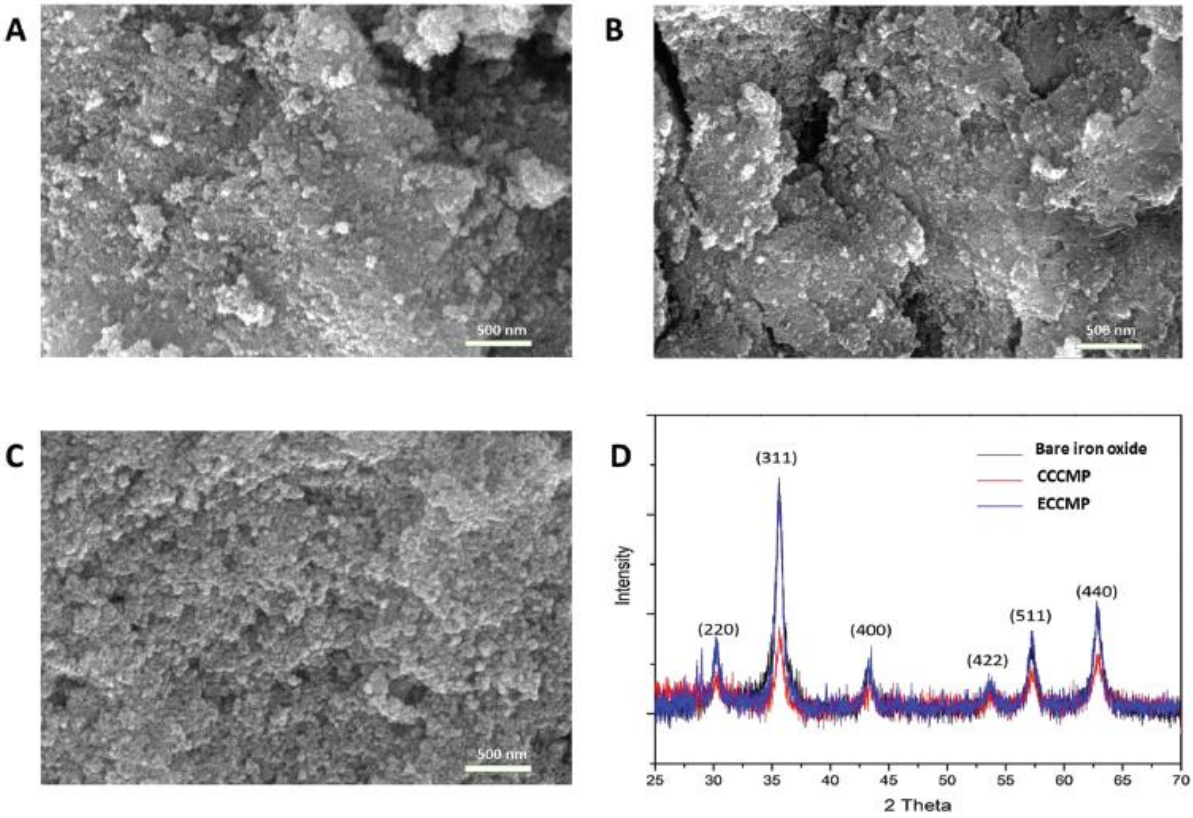

Fig 2.1 SEM and XRD images of chitosan-coated magnetic particles. A, SEM of bare iron oxide. B, SEM of CCCMP. C, SEM of ECCMP. D, XRD of bare iron oxide, CCCMP, and ECCMP

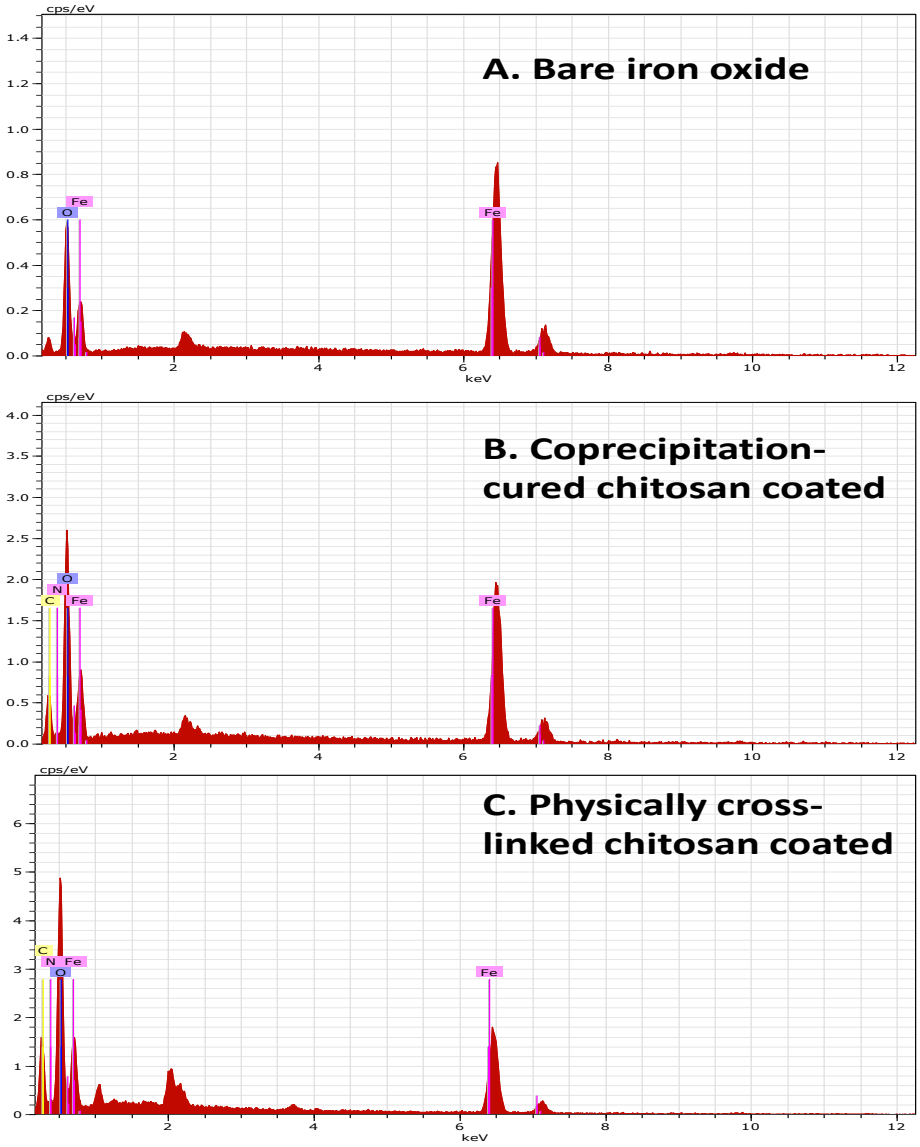

Fig 2.2 EDX characterization of A, bare iron oxide. B, CCCMP. C, ECCMP

The presence of two strong absorption bands of all materials in FT-IR at around 636 and 592 cm1 demonstrated the formation of magnetic nanoparticles. Furthermore, the band at 592 cm1 was identified as the Fe-O stretching vibration of spinel tetrahedral sites. 1100 cm^{-1} shows C-N stretching. The tetrahedral and octahedral absorption bands at 459 cm1 peak at 3400 cm1 due to the O-H stretching model adsorbed on the surface of the magnetic nanoparticles. In the case of chitosan-coated magnetic nanoparticles, the coating of chitosan is established by the appearance of the peak at 2922 cm^{-1}. This particular absorption was considered to be the stretching vibrations of –CH–in chitosan. The peak at 1641 cm^{-1} is relevant to the N–H vibration for the chitosan (Fig

2.3). Overall, the above-mentioned results indicated the successful coating of chitosan on iron oxide nanoparticles.

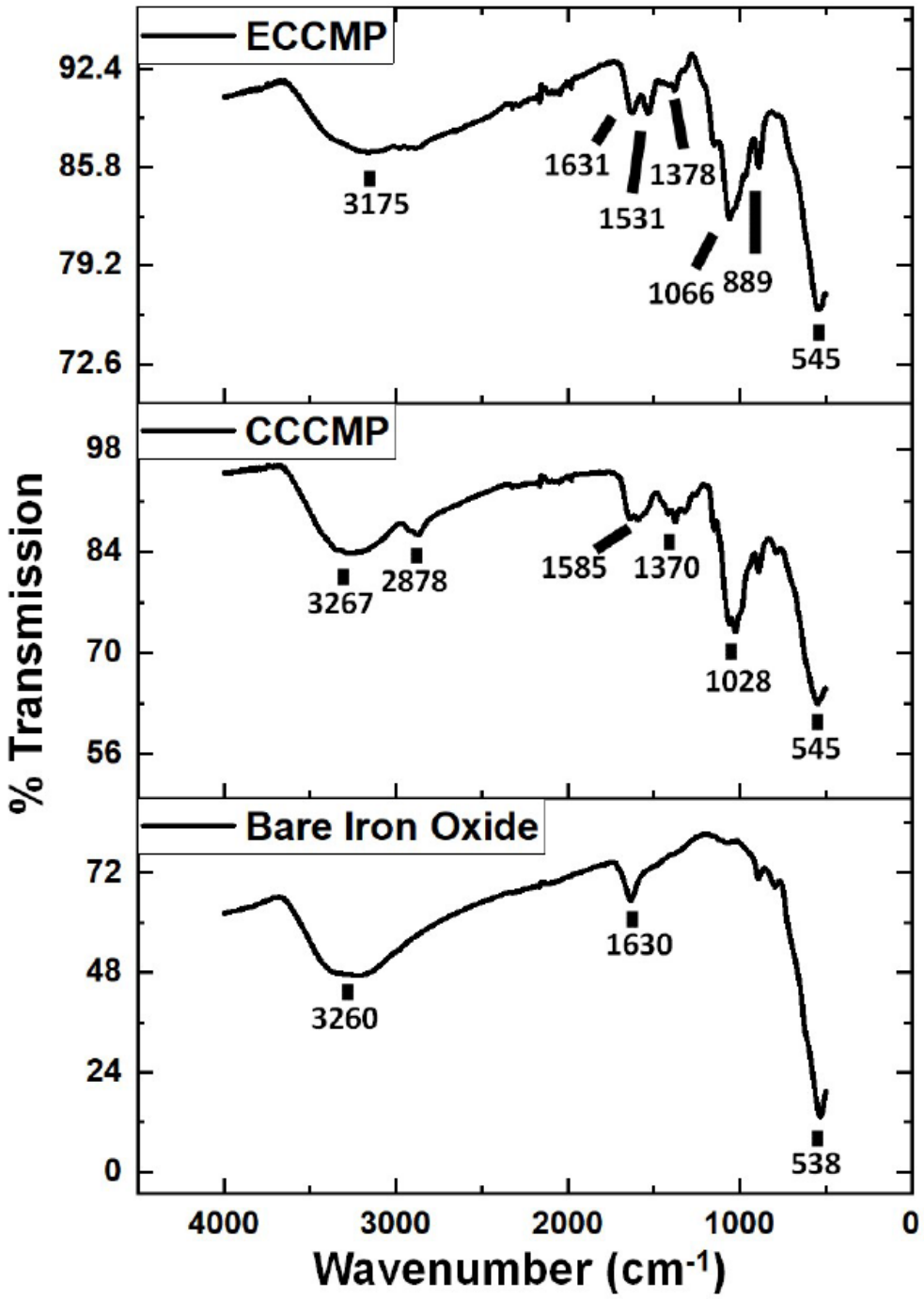

Fig 2.3 FT-IR characterization of ECCMP, CCCMP, and bare iron oxide

The DLS data suggests that the hydrodynamic size of bare iron oxide nanoparticles at pH-5.2 is 162 ± 24.18 nm (Table 2.1, Fig 2.4), which is expectedly higher than the crystalline size obtained from XRD. The hydrodynamic size of CCCMP and ECCMP has slightly increased from bare iron oxide nanoparticles, which again indicates the successful coating of chitosan. The zeta potential of CCCMP, ECCMP, and bare iron oxide has been carried out at pH-5.2 to examine their surface charge (Table 2.1) and their role in DNA binding.

Table 2.1 Hydrodynamic size and surface charge potential of synthesized chitosan-coated magnetic particles at pH-5.2

Name of the particles	**Hydrodynamic radius (nm)**	**Zeta potential (ζ)(mV) at pH 5.2**
CCCMP	253.5 ± 38.08	18.9 ± 1.63
ECCMP	275.0 ± 106.4	7.35 ± 1.36
Bare iron oxide	162 ± 24.18	−12.3 ± 1.63

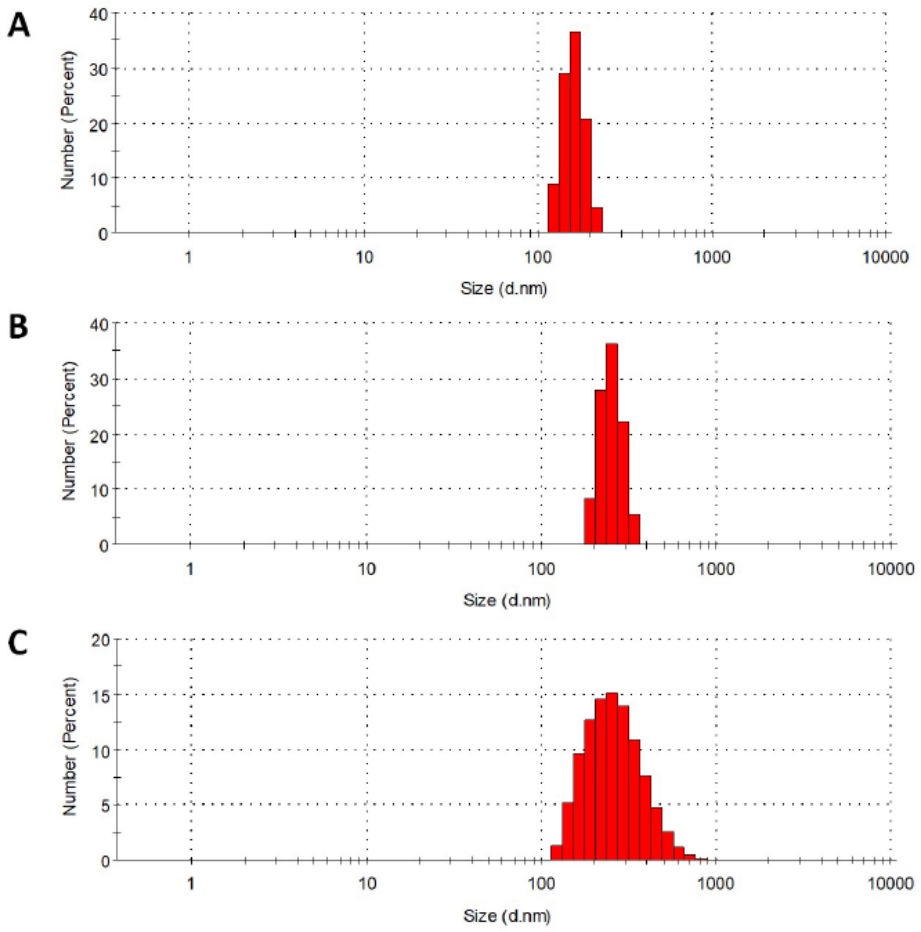

Fig 2.4: Dynamic light scattering (DLS) studies of magnetic particles. A, Bare iron oxide, B, CCCMP. C, ECCMP.

The bare iron oxide zeta potential is negative, which indicated no DNA binding capacity. For CCCMP and ECCMP, the zeta potential was positive, which again indicated the presence of the cationic protonated ammonium group. CCCMP showed higher zeta potential than ECCMP because of the presence of an anionic tripolyphosphate cross-linker

2.3.2 DNA binding study

Next, the nucleic acid binding capacity of synthesized magnetic particles was investigated. The CCCMP and ECCMP have chitosan as their coating material which has a free amine group with a pKa of 6.5 (approx) in an aqueous solution. Previous studies revealed that chitosan has pH-responsive charge switching behavior which relies on Henderson–Hasselbach equation ($pH = pK_a + \log_{10}([A^-]/[HA])$ which directly relates to the pH of the solution to a ratio of deprotonated (NH_2) to protonated (NH_3^+) form of chitosan backbone. As a result, chitosan-coated materials behave differently at different pH based on their pK_a which means chitosan-coated particles

acquire a positive backbone in a solution that has a pH less than its pK_a and become neutral in a solution where the pH is similar toor greater than its pK_a. It would therefore capture nucleic acid at a pH less than its pK_a and elutes nucleic acid at a pH greater than its pK_a. Many studies were reported where chitosan's charge switching behavior has been used for nucleic acid capture and extensive gene delivery. The 25-30 minutes magneto-capture assay (Scheme 2.2) was therefore formulated based on nucleic acid adsorption (capture) by the positively charged backbone of chitosan (CCCMP and ECCMP) coated particles under the influence of pH-5.2 (lesser than its pK_a) for 10 minutes. The magnetic property of CCCMP and ECCMP has been employed during the washing step which can be referred to as magnetic decantation (5 minutes). The desorption (elution) of captured nucleic acid was done using an elution buffer that has a pH of 8.5.

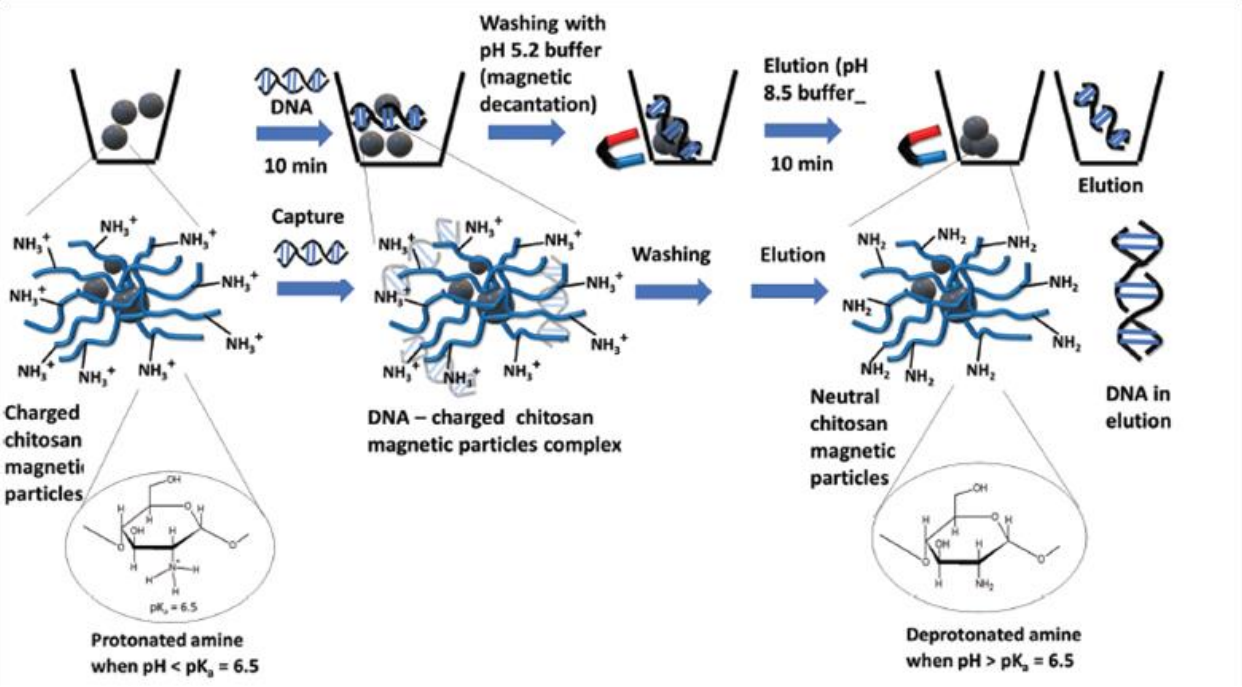

Scheme 2.2 30 min DNA magnetocapture procedure to extract (i.e., bind) DNA from solution, wash (to remove non-nucleic acid molecules), and then release ("elute") the same into solution. The procedure uses protonation–deprotonation-based charge switching of chitosan backbone amino groups

We have assessed three different conditions for nucleic acid capture and elution (Fig 2.5A). In the first condition, we carried out the whole magneto-capture of nucleic acid by passive mixing of nucleic acid by gentle finger tapping without using any instruments like a mechanical shaker (condition 1A, steps 1 and 3, Fig 2.5A). In the second condition, mechanical shaking (vortex)

was used in the capture step, followed by passive elution (condition 1B, steps 1 and 3, Fig 2.5A). In the third condition, mechanical shaking was used in the capture and elution step (condition 1C, steps 1 and 3, Fig 2.5A). A higher degree of nucleic acid capture was observed in mechanical shaking, but surprisingly it was not significantly higher than the passive nucleic acid capture. We were looking for method development for rapid nucleic acid capture for a resource-limited area, so we took condition one for nucleic acid capture for further studies. CCCMP showed a slightly higher nucleic acid adsorption (Fig 2.5B) than ECCMP (Fig 2.5C) due to a lesser degree of chitosan coating, which was evident in our zeta potential studies (Table 2.1). The 1-5 mg of wet CCCMP and ECCMP showed a linear genomic DNA extraction capability (capture and elution) from the aqueous sample with a mean extraction efficiency of 277.0 ± 21.2 and 233.3 ± 30.5 ng mg^{-1}, respectively (Fig 2.5D). Bare iron oxide magnetic particles showed a DNA capture ability of 11.2 ± 7.2 ng mg^{-1} (investigated for 5 mg bare iron oxide).

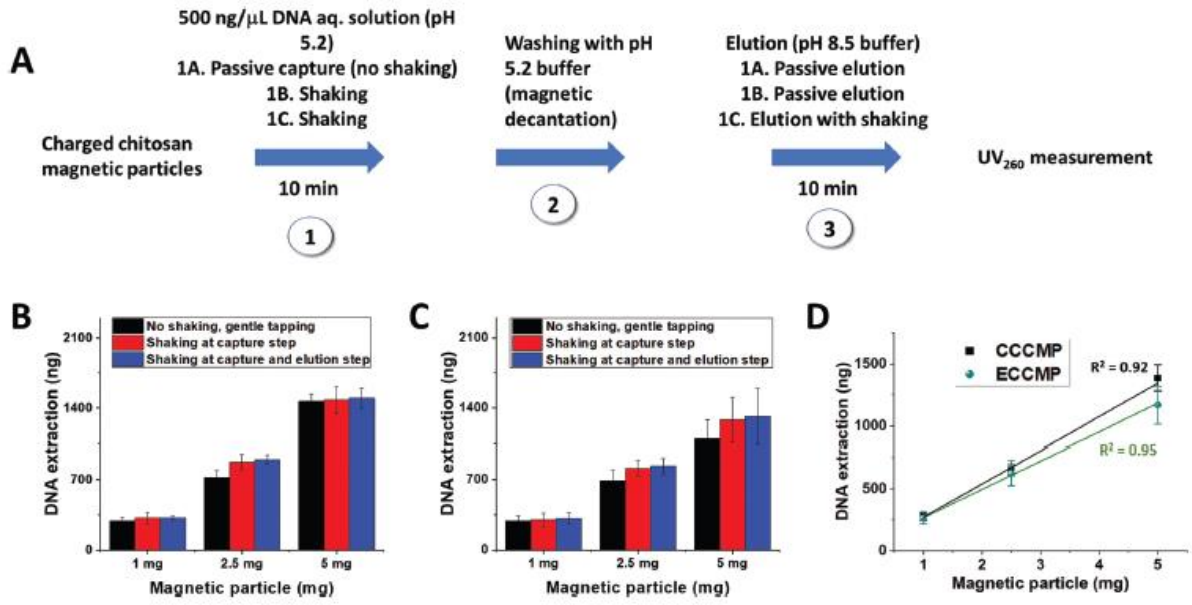

Fig 2.5: Quantification of the DNA capture and elution of 1, 2.5, and 5.0 mg of CCCMP and ECCMP. A, Experimental Scheme of magnetocapture followed by UV_{260} measurement. B, Magneto-capture by 1, 2.5, and 5.0 mg CCCMP. C, Magnetocapture by 1, 2.5, and 5.0 mg ECCMP. D, Linear fit of DNA extraction ability of 1, 2.5, and 5.0 mg magnetic particles. Error bars represent standard deviations (n = 3)

The higher level of DNA capture of CCCMP and ECCMP than bare iron oxide illustrates the importance of chitosan coating of magnetic particles. It also validated the DNA capture efficiency of CCCMP and ECCMP by instrument-free passive shaking (without using

mechanical shaking) without compromising the DNA capture ability. The higher zeta potential of CCCMP than ECCMP (Table 2.1) indicated a greater number of positively charged amino groups in magnetic particles. The higher number of the positively charged amino group increases the electrostatic interaction with the negatively charged phosphate backbone of DNA, which enhanced the adsorption capacity of CCCMP more than ECCMP.

2.3.3 Detection of magnetocaptured DNA using gel-based LAMP, colorimetric LAMP, and real-time LAMP

Detection by UV_{260} cannot quantify ultralow copies (hundreds or thousands of copies) of target nucleic acid nor detect the specific gene element inside the target. We needed nucleic acid amplification tests (NAATs) or instrument-free isothermal nucleic acid amplification tests (iNAATs) to quantify the particular gene element in the target nucleic acid captured by our chitosan-coated magnetic particles. NAATs can specify the gene target in a target nucleic acid, but the presence of polymerase inhibitors may cause attenuation of detection of extracted nucleic acid from clinical samples. An effective nucleic acid extraction with the separation from polymerase inhibitors followed by a downstream amplification test would be needed for near point of care diagnostics. The second aim of the study was thus to check the compliancy of magnetocapture extracted nucleic acid (CCCMP and ECCMP) to NAATs and iNAATs. To investigate this qualitatively, magneto-capture followed by loop-mediated isothermal amplification (LAMP) was performed on *E.coli* genomic DNA extracted from an aqueous solution and from crude cell lysate. Choosing LAMP over other isothermal amplification is due to its specificity, very high sensitivity, and compatibility with other downstream methods like turbidimetry, electrochemistry, colorimetry, surface plasmon resonance, and real-time fluorescence. To imitate the resource-constrained area settings, we opted to utilize our homemade mastermix over the commercial ones as the latter is not generally accessible in their real-time PCR counterpart. We used a reported LAMP primer of the *malB* gene of *E. coli* (Table 2), and we encountered a nonspecific amplification (Fig 2.6A) during agarose gel electrophoresis due to cross-contamination. While probing this non-specificity, we observed that at least two other papers encountered the same while using the same primer [133]. They removed the non-specificity by using betaine (inhibits primer dimer formation), absent in our homemade mastermix. In our case, the nonspecific amplification was mitigated by removing loop primers in

the LAMP reaction. Finally, we found a ladder-like structure in agarose gel electrophoresis which infers a successful LAMP reaction where no ladder-like structure was found in non-template control (Fig 2.6B).

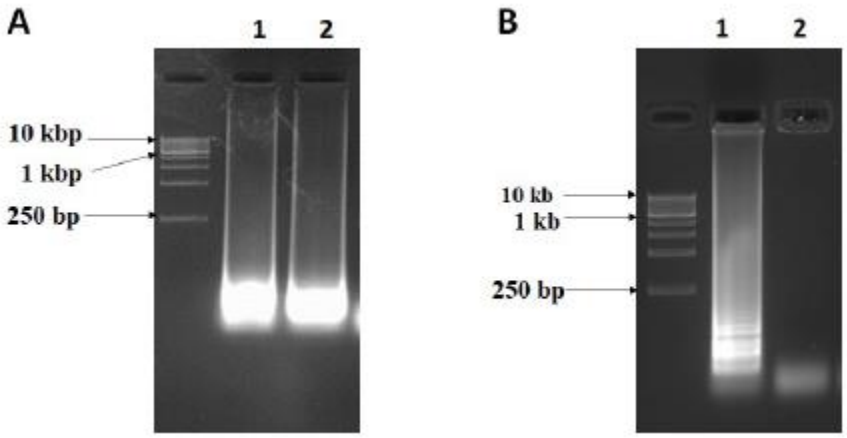

Fig 2.6: Loop-mediated isothermal amplification for detecting *malB* gene in *E. coli.* A, nonspecific amplification in the presence of loop primers was analyzed in 1.5% agarose gel. Lane 1, in presence of *E.coli* genomic DNA. Lane 2, in the absence of *E. coli* genomic DNA. B, amplification in the absence of loop primers analyzed in 1.5% agarose gel. Lane 1, in presence of *E. coli* genomic DNA. Lane 2, in the absence of *E. coli* genomic DNA. The leftmost lanes in both gels represent a 10 kb ladder

Without any other optimization, we checked for LAMP amplification of 10^9 copies of *E.coli* genomic DNA in an aqueous sample extracted by CCCMP and ECCMP (Fig 2.7A). The same was checked for heat lysed *E.coli* (where common polymerase inhibitors are present, which are expected to be removed by magnetic wash)and then subjected to magnetocapture by CCCMP and ECCMP. The elution obtained from both magnetocaptures was subjected to LAMP followed by gel electrophoresis (Fig 2.7A). The successful LAMP was observed for both cases (Fig 2.7B and Fig 2.7D). After that, we investigated for on-beads amplification before the elution step, which could reduce the assay time by 10 minutes. To examine this, we performed in situ LAMP where we subjected the DNA bound magnetic particles (following magnetic decantation wash but before pH 8.5 elution) to LAMP followed by agarose gel electrophoresis (Fig 2.7C and Fig 2.7E), where the ladder-like structure of characteristic LAMP amplicons was observed. Overall the whole assay established the amenability of magnetocaptured nucleic acid towards downstream amplification. Although the results of in situ amplification were quite promising, the aspect of this work would be pursued with a follow-up study.

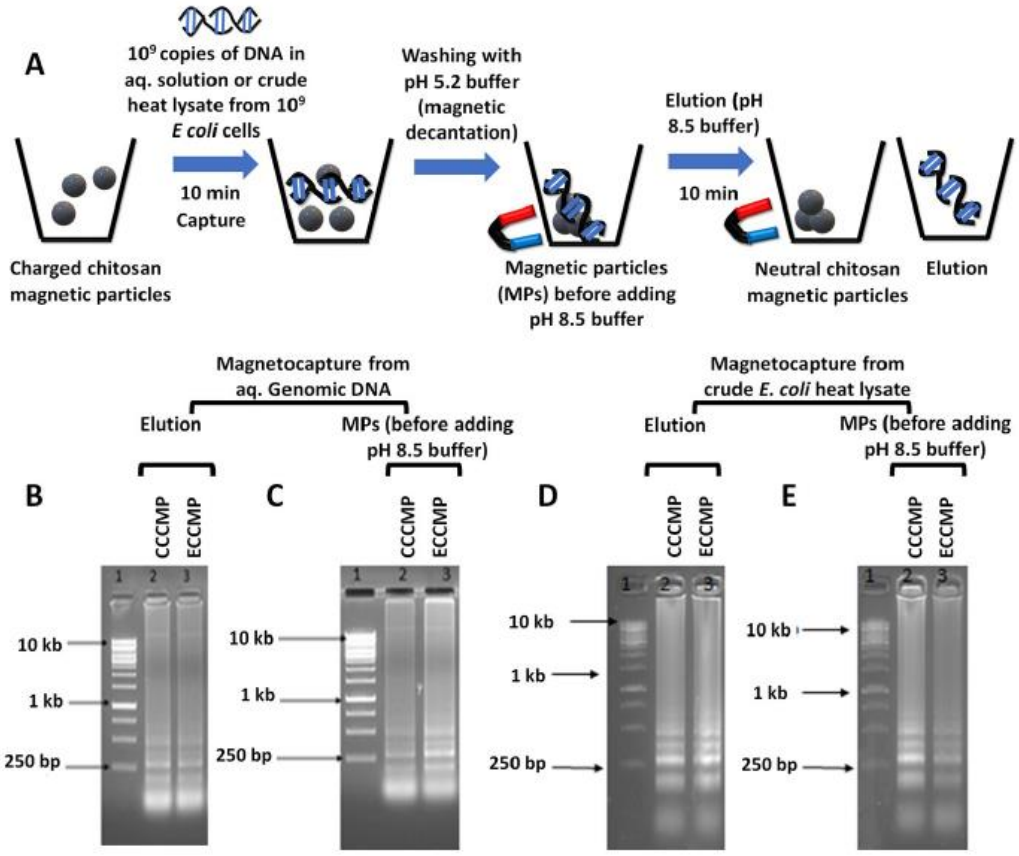

Fig 2.7: Magnetocapture, elution, and loop-mediated isothermal amplification (LAMP) on 10^9 copies of *E. coli* genomic DNA (gDNA) from aqueous solution or crude lysate. A, Scheme of magnetocapture assay. B, LAMP assay on pH 8.5 buffer elution from magnetocapture on gDNA in aqueous solution. C, LAMP assay on magnetic particles (MPs) itself after pH 5.2 buffer washing but before pH 8.5 buffer elution from magnetocapture on gDNA in aqueous solution. D, LAMP assay on pH 8.5 buffer elution from magnetocapture on crude lysate. E, LAMP assay on magnetic particles (MPs) itself after pH 5.2 buffer washing but before pH 8.5 buffer elution from magnetocapture on crude lysate. For crude lysate, 10^9 cells were heat treated (95˚C for 15 min) in lysis buffer (10 mM Tris-HCl, 1 mM EDTA, 1% Triton X-100, 0.5% Tween 20 pH 8) before magnetocapture. All experiments were analyzed in 2% agarose gel electrophoresis where the leftmost lanes represent a 10 kb ladder

While gel electrophoresis-based study can qualitatively confirm the amplification success, this readout method is not sensitive enough neither to detect low copy number nucleic acid nor a quantitative technique, which are both the main requirement in molecular diagnostic assays. Therefore, we opted for real-time LAMP to detect the analytical sensitivity of the whole assay using our homemade LAMP mastermix with the addition of SYBR-I. While establishing the

proof of concept, we first performed the entire assay with 10^6 copies of *E.coli* gDNA to check the difference of amplification in real-time fluorescence, which successfully distinguished the target from no template control (Fig 2.8A). However, the no template control-NTC (elutions from mock DNA binding assay) still produced fluorescence despite the reactions being devoid of loop primers. We deduced that the minor primer dimer formation might be the reason behind the significant fluorescence in NTC that can be inhibited by the initiation of reaction at a higher temperature. Therefore the standard LAMP protocol, which is 66˚C for 60 minutes, has been changed to a touch-down LAMP (Fig 2.8B) which attenuated the issue of high fluorescence of NTC by decreasing six fold.

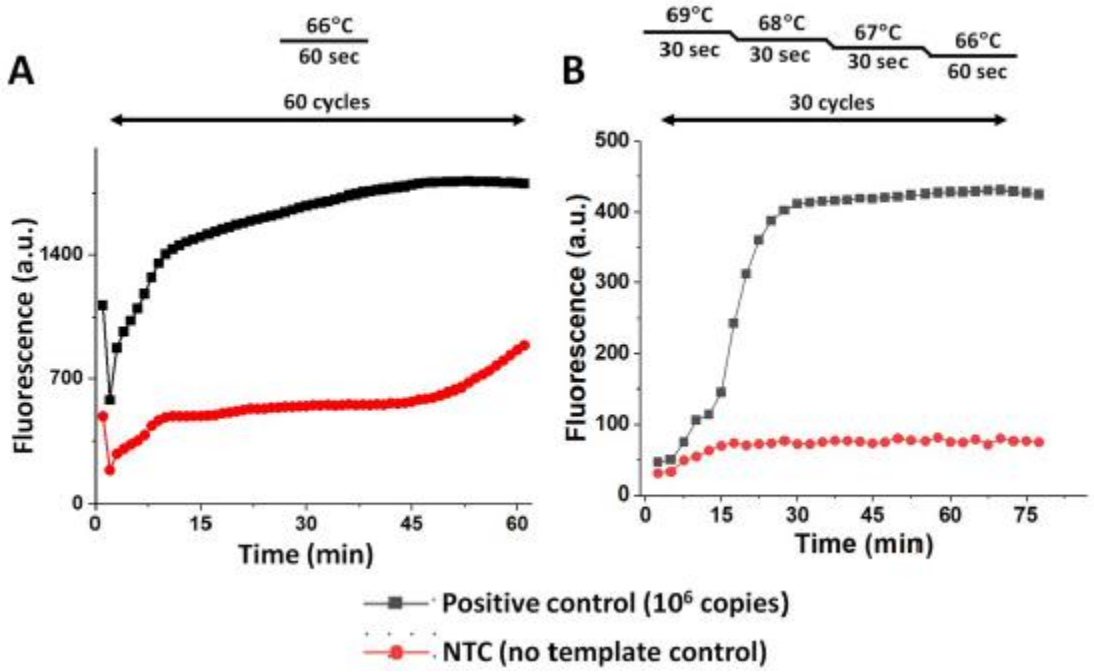

Fig 2.8: Comparison between real-time loop-mediated isothermal amplification (LAMP) (panel A) and touchdown real-time LAMP (panel B) along with respective temperature cycling information. In both cases, the fluorescence was monitored at the 66˚C step of the cycles. The experiments were conducted on 10^6 *E. coli* genomic DNA copies and with no template control (NTC)

Next, we subjected 10^1-10^5 copies of gDNA in an aqueous solution and heat lysed sample to magneto-extraction by CCCMP and ECCMP to analyze the limit of detection (LoD). The elution is investigated by follow-up real-time LAMP (Fig 2.9A). For CCCMP, the LoD was 10^2 copies for both aqueous solution and crude cell lysate (Fig 2.9B and Fig 2.9D with corresponding melt curve analysis in Fig 2.10A and Fig 2.10C). On the other hand, the LoD of ECCMP was 10^2

copies for crude cell lysate and 10^3 copies for aqueous gDNA solution (Fig 2.9C and Fig 2.9E with corresponding melt curve analysis in Fig 2.10B and Fig 2.10D).

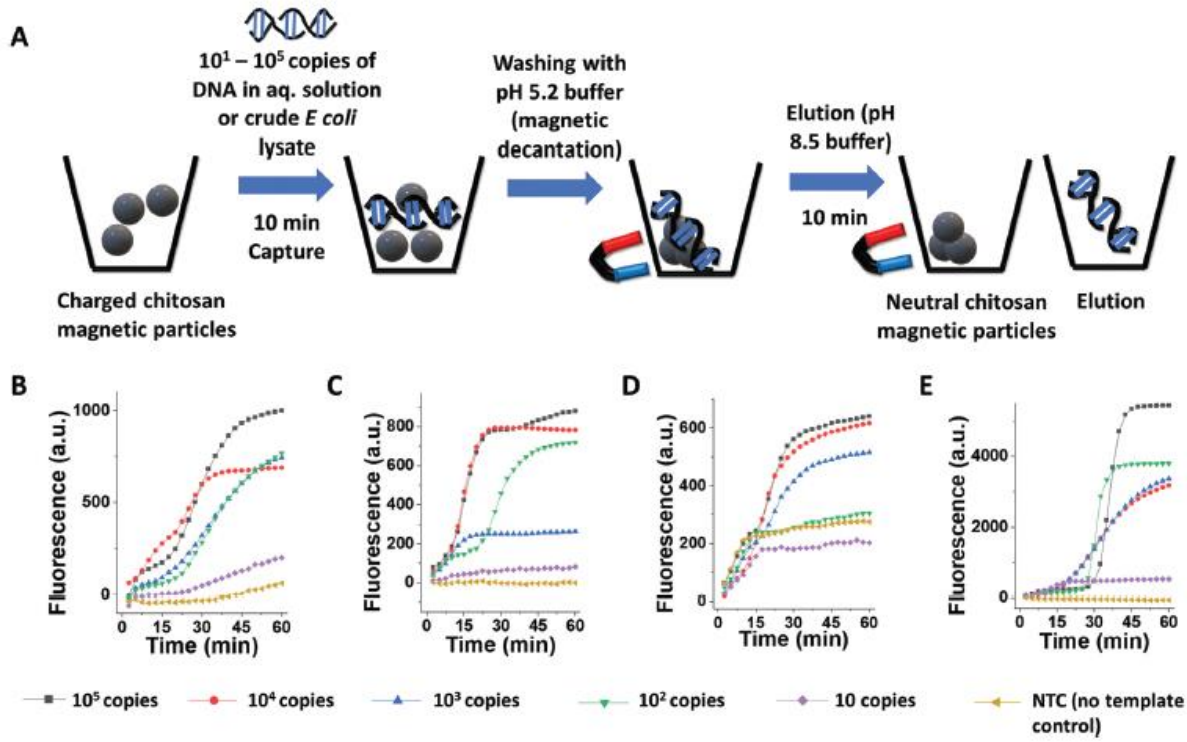

Fig 2.9: Limit of detection for magnetocapture, elution, and real-time LAMP for detecting nucleic acid (DNA) from aqueous solution or crude cell lysate. A, Scheme of magnetocapture assay. B, Elution from CCCMP magnetocapture assay on 10^1–10^5 copies of *E. coli* gDNA in aqueous solution subjected to real-time LAMP. C, Elution from CCCMP magnetocapture assay on 10^1–10^5 *E. coli* cells heat lysate subjected to real-time LAMP. D, Elution from ECCMP magnetocapture assay on 10^1–10^5 copies of *E. coli* gDNA in aqueous solution subjected to real-time LAMP. E, Elution from ECCMP magnetocapture assay on 10^1–10^5 *E. coli* cells heat lysate subjected to real-time LAMP

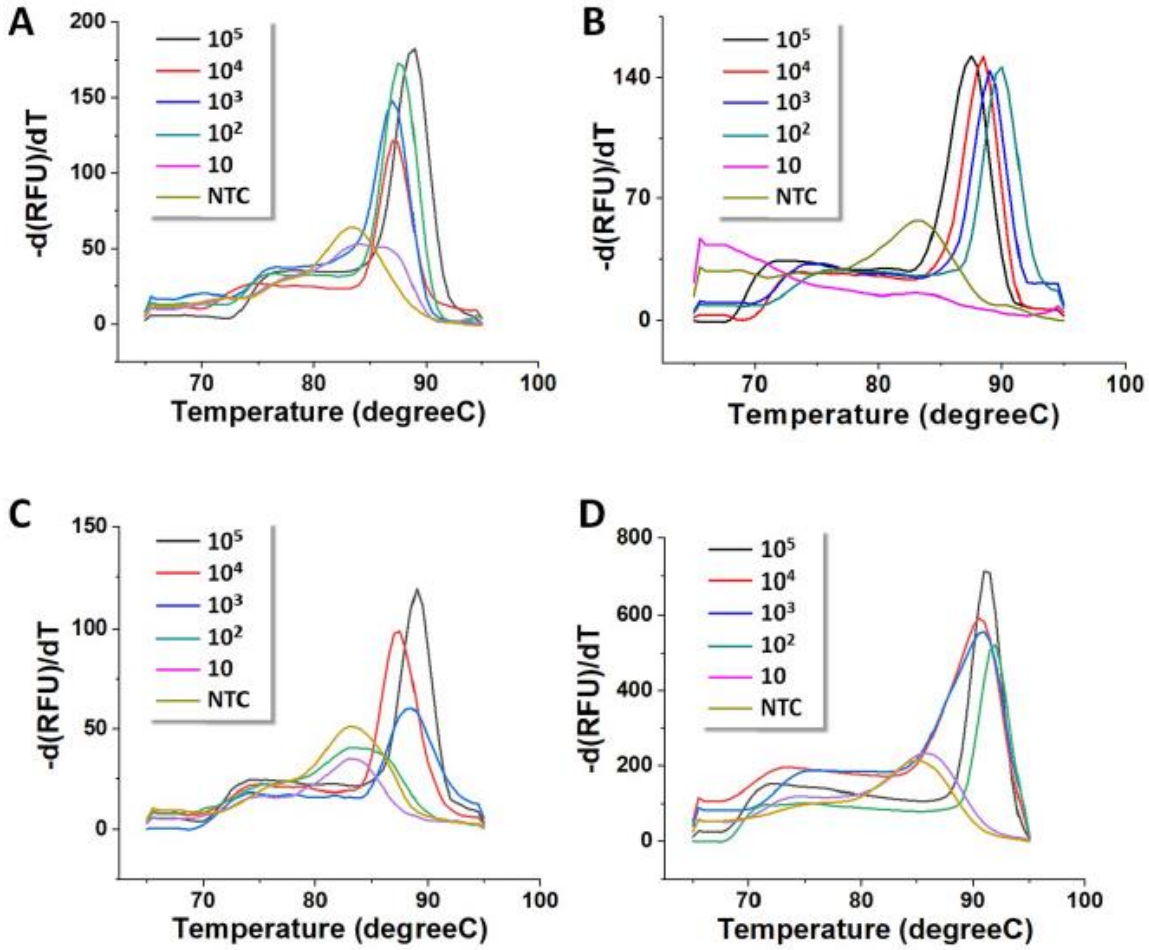

Fig 2.10: Derivative melt curve analysis for real-time LAMP experiments on the elution from magnetocapture performed on 10^1 – 10^5 copies of *E. coli* genomic DNA in aqueous solution or crude lysate. A real-time LAMP on elution from CCCMP magnetocapture on aqueous gDNA. B, real-time LAMP on elution from CCCMP magnetocapture on crude cell lysate. C, real-time LAMP on elution from ECCMP magnetocapture on aqueous gDNA. D, real-time LAMP on elution from ECCMP magnetocapture on crude cell lysate. For crude lysate, the cells were heat treated (95˚C for 15 min) in lysis buffer (10 mM Tris-HCl, 1 mM EDTA, 1% [v/v] Triton X100, 0.5% Tween-20, pH 8) before magnetocapture. NTC refers to no template control

Encouragingly, the LAMP assay could successfully distinguish between positive and negative results within 45 minutes which can be excellent criteria for the present pandemic scenario for SARS-CoV-2. The limitation of our assay is the cycle threshold value (C_t) varied considerably to procure a mean C_t value for low standard deviation. This observation could be attributed to homemade mastermix, use of touch down LAMP, and very less although detectable primer dimer

formation as seen in melt curve analysis. Altogether, the assay could detect very significant and clinically relevant copy numbers of nucleic acid from both aqueous and crude cell lysate.

Next, we investigated the elutions from both magnetocapture assays by CCCMP and ECCMP for colorimetric LAMP. The activity of polymerase release a number of protons which could drop a pH of a solution. Thus, if a pH indicator dye is present in the solution then the positive amplification could cause a color change. The proprietary warmstart LAMP mix employs the same principle of color change [134]. The pH change also relies on the reaction buffer (Tris-HCl) which provides a very low buffering capacity. We anticipated that this colorimetry integrated with our magneto-capture assay would offer a robust method in the molecular diagnostics field in terms of rapid nucleic acid extraction followed by visual detection. Therefore 2×10^1–10^6 copies of *E. coli* gDNA were magnetocaptured by CCCMP from an aqueous solution, and compatibility with colorimetry was investigated. After 10 minutes of reaction, the color change of different degree was observed (Fig 2.11, tube 1-6) where elutions from mock DNA binding assay and normal elution buffer gives no color change (Fig 2.11, tube 7 and 8 respectively). This indicated a successful LoD determination in the order of 10 copies by our magneto-capture assay followed by colorimetry.

Fig 2.11: Colorimetric LAMP assay using WarmStart LAMP Kit (NEB # E1700S) on magnetocapture extracted genomic DNA. DNA copies ranging from 2 x 10^1 – 10^6 copies in 25 µL 0.05 M MES buffer (pH 5.2) were used for magnetocapture using 2.5 mg CCCMP, and then eluted using 25 µL elution buffer (10 mM Tris-HCl (pH 8.5)). EB1 (tube 7) sample consisted of a CCCMP-mediated magnetocapture experiment without any genomic DNA that was eluted using elution buffer (a "mock" experiment), followed by colorimetric LAMP having the same reaction composition as above. EB2 (tube 8) sample contained the addition of 8 µL elution buffer (without any DNA from magnetocapture) to a colorimetric LAMP having the same reaction composition as above

For further optimization, we added the "neutralized" (i.e., by addition of elution buffer) magnetic particles from the "mock" magnetocapture to the warmstart amplification mix, which surprisingly gave a color change from pink to yellow after 10 minutes of initiation of the experiment (Fig 2.12, tube1). This result indicated that the color change might be due to the proton release of the amine group present in the chitosan backbone of our magnetic particles. For further analysis, we captured 10^6 copies of gDNA from the aqueous sample by CCCMP and eluted them in neutral pH (water). Then we investigated the colorimetry with our magnetic particles and the elution obtained from the experiment where a visible "pink to yellow" color changes was observed (Fig 2.12, tube 2, 3) after 10 minutes of the starting of the experiment. This again hinted towards of our hypothesis of chitosan proton release during the reaction. LAMP on a mock study (where water was used instead of gDNA in the capture step) by CCCMP was done where neutralized elution buffer after the elution step was checked for colorimetric readout, which also gave a color change (Fig 2.12, tube 4). The experiments thus confirmed the amine group present in the chitosan backbone of CCCMP itself caused pH reduction, which gave false-positive results. Another hypothesis was that the chitosan amine group might not have fully neutralized with 10 mM Tris-HCl buffer pH-8.5 (elution buffer), so an increase in the concentration of elution buffer might get rid of the false positive.

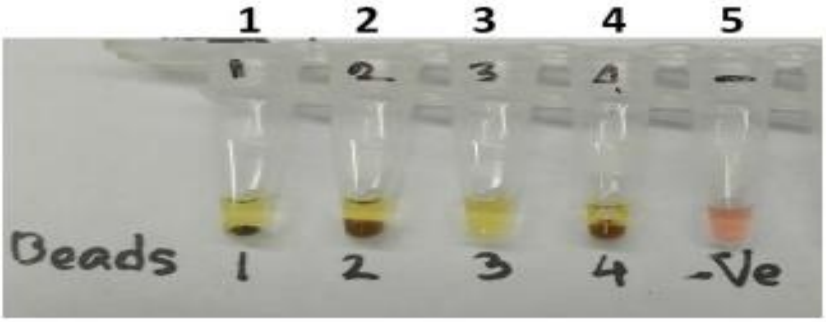

Fig 2.12: Colorimetric LAMP assay using WarmStart LAMP Kit (NEB # E1700S) on magnetocapture extracted gDNA and "neutralized" magnetic particles. In tube 1, a mock CCCMP magnetocapture experiment using 2.5 mg CCCMP and 25 µL 0.05 M MES pH 5.2 was conducted but in the absence of any genomic DNA.For tube 2, 10^6 copies of *E. coli* genomic DNA in 25 µL 0.05 M MES pH 5.2 buffers were subjected to 2.5 mg CCCMP magnetocapture. In tube 3, 8 µL elution from the magnetocapture experiment described for tube 2 was subjected to a 20 µL colorimetric LAMP as discussed above. In tube 4, an identical magnetocapture experiment as described for tube 1 was performed but was not subjected to elution.

For further optimization, we increased the elution buffer concentration from 10 mM to 25 mM pH-8.5 without changing the capture and washing step of the DNA binding assay, and the whole magnetocapture from 10^1-10^6 copies by CCCMP was repeated, followed by colorimetry. Only elution obtained from 10^6 copies showed colour change. Possibly, tris buffer at 25 mM was too concentrated for its pH to be altered by LAMP proton release (Fig 2.12, tubes 1–6). The experiments hinted toward a possible correlation between chitosan and elution buffer which include a possible role of neutralization kinetics.

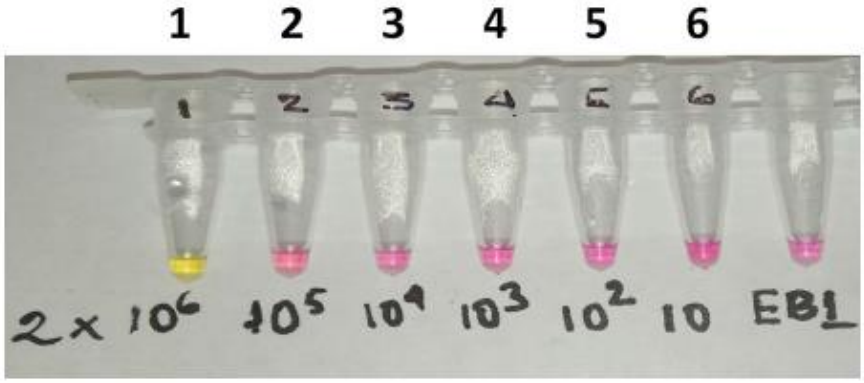

Fig 2.13: Colorimetric LAMP assay using WarmStart LAMP Kit (NEB # E1700S) on magnetocapture extracted gDNA. The follow-up 20 µL colorimetric LAMP reaction in tubes 1 – 6 then consisted of 10 µL 2X proprietary LAMP colorimetric mastermix, 8 µL elution, and 2 µL, 10X *E. coli* LAMP primer mix (without loop primers). EB1 (tube 7) sample consisted of a CCCMP mediated magnetocapture experiment without any genomic DNA (a "mock" experiment) that was eluted using 25 mM Tris-HCl pH 8.5 elution buffer, followed by colorimetric LAMP having the samereaction composition as above

We felt that more optimization was needed to establish the correlation between elution buffer and proton release of a chitosan amine group. This may involve investigating the capture time and elution time and degree of concentration of elution buffer for extra proton neutralization to integrate our magneto capture assay with colorimetry. No further experiments were conducted and would be pursued as a part of future studies.

2.3.4 Detection of magnetocaptured DNA using real-time PCR

The real-time PCR assay is the gold standard for the NAAT amplification procedure for its high specificity and sensitivity toward specific gene target detection. However, the target nucleic acid in clinical samples is generally present in complex biofluid like urine, cough, swab, and serum-containing PCR inhibitors, which has the potential to inhibit the polymerase activity. The

conventional spin column-based nucleic acid extraction involves a high-speed centrifuge which is mostly unavailable in the resource-constrained area. We hypothesized that CCCMP and ECCMP-based magneto-extraction could be compatible with downstream real-time PCR as we established the analytical sensitivity of the whole magnetocapture assay coupled with LAMP previously. Unlike the homemade amplification mix we used for real-time LAMP, here we used a commercial real-time PCR mastermix due to their availability. We opted for serum as the complex biofluid of choice due to the presence of immunoglobulin and hemoglobin which is a well-known PCR inhibitor[135]. Additionally, the serum is the main component of the viral transport medium (VTM) commonly being used in SARS-CoV-2 detection[136]. To investigate the inhibitory effect of serum, 10^2-10^4 copies of MCF-7 (breast cancer cell line) genomic DNA was spiked with 50% fetal bovine serum (FBS), and a real-time PCR experiment was performed, which clearly shows no amplification in all of the copies (Fig 2.14). An assay succeeding in the extraction of amplification-compatible nuclei acid from serum would therefore be helpful in real-life clinical assays involving SARS-CoV-2 detection.

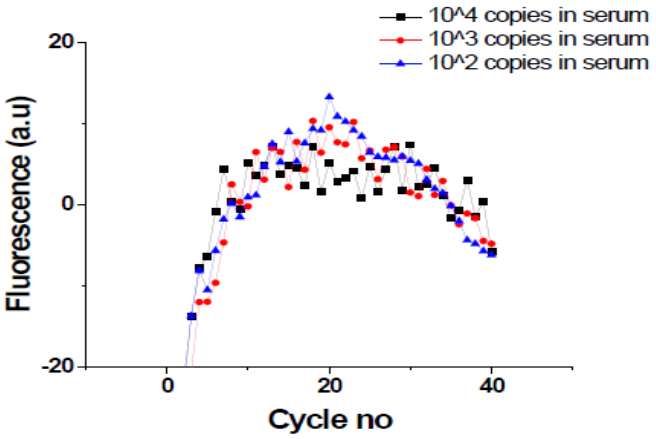

Fig 2.14: Real-time PCR amplification of human genomic DNA in the presence of 50% fetal bovine serum

Before performing the magnetic particles-based extraction assay with DNA spiked in serum, their compatibility with real-time PCR was checked with their ability to capture 10^2–10^4 copies of genomic DNA from an aqueous solution (Fig 2.15A). When compared for cycle threshold (C_t) values, there was an increase between the identical copies of pure genomic DNA beforehand after

magnetocapture from aqueous solution (Fig 2.15B and Fig 2.15C, melt curve analysis in Fig 2.16A-E).

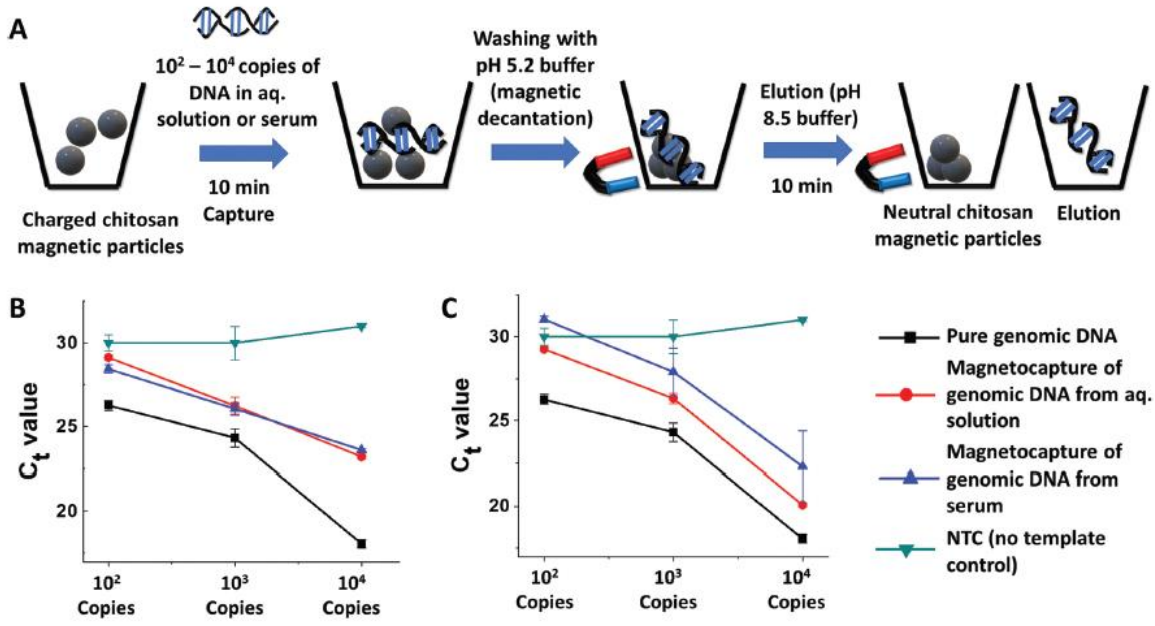

Fig 2.15: Limit of detection for magnetocapture, elution, and real-time PCR for detecting nucleic acid (DNA) from aqueous solution or fetal bovine serum. A, Scheme of magnetocapture assay. B, Cycle threshold (Ct) values for CCCMP magnetocapture followed by real-time PCR on 10^2–10^4copies of human genomic DNA in aqueous solution or serum. C, Cycle threshold (Ct) values for CCCMP magnetocapture followed by real-time PCR on 10^2–10^4copies of human genomic DNA in aqueous solution or serum. The same dataset for pure genomic DNA and no template control (NTC) has been plotted in both cases. Error bars represent standard deviation (n = 3)

The increase in the C_t value could be attributed to the reduction in analytical sensitivity from the loss of some DNA during the magnetic decantation steps or from the failure to collect all bound DNA during elution. Next, we tried to extract 10^2–10^4 copies of genomic DNA spiked with serum, and the resulting elution was subjected to real-time PCR. The result indicates that both CCCMP and ECCMP magnetocapture were able to restore real-time PCR amplification, although with a slight further increase of C_t value (Fig 2.15B and Fig 2.15C, melt curve analysis in Fig 2.16A-E). The rise in C_t value is due to the multiple magnetic decantations during the washing step. The magnetocapture with follow-up real-time PCR together had an LoD in the order of 10^2 copies for CCCMP and 10^3 copies for ECCMP for both aqueous and serum samples.

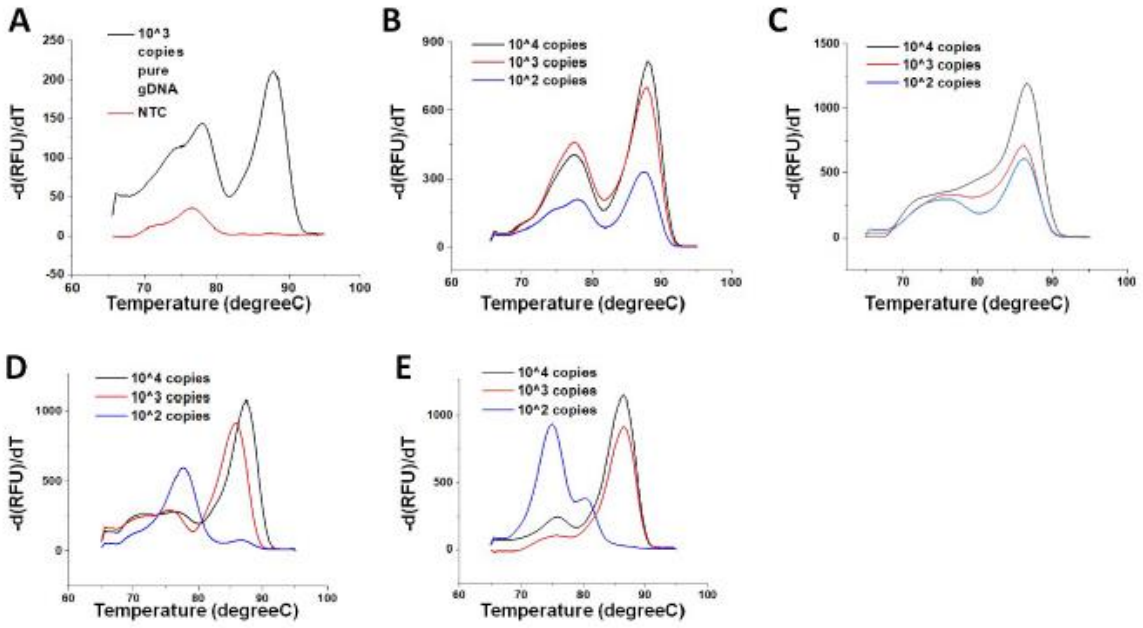

Fig 2.16: Real-time PCR melt curve analysis for magnetocapture experiments on 10^2–10^4copies of human genomic DNA in aqueous solution and serum. A, melt curve analysis for pure genomic DNA (10^3 copies) and no template control (NTC). B, melt curve analysis for CCCMP magnetocapture followed by real-time PCR on 10^2–10^4copies of genomic DNA from the aqueous sample. C, CCCMP magnetocapture followed by real-time PCR on 10^2–10^4copies of genomic DNA from serum. D, ECCMP magnetocapture followed by real-time PCR on 10^2–10^4copies of genomic DNA from the aqueous sample. E, ECCMP magnetocapture followed by real-time PCR on 10^2 – 10^4 copies of genomic DNA

Therefore, they were sufficiently sensitive to detect a clinically relevant low copy number of target nucleic acid in aqueous and from complex biofluid. Interestingly, the LoD from the magnetocapture in combination with real-time PCR was similar to that for magnetocapture with follow-up real-time LAMP reactions, validating the reproducibility of the methods.

2.4 Conclusion

In this work, we evaluated the application of two chitosan-coated magnetic particles for the extraction of amplification-ready nucleic acid from complex biofluids for application in limited-resource settings. The magnetic particles are preparable within 6–8 h by minimally trained personnel using only a water bath and magnetic stirrer using commonly available inexpensive chemicals. The resulting CCCMP and ECCMP particles showed a surface charge-dependent

DNA extraction capacity in the order of 233–277 ng μL^{-1}. The particles were able to capture and physically separate genomic DNA from aqueous solutions, crude cell lysate, and fetal bovine serum without any mechanized shaking, mixing, or stirring. The extraction assay was completed within 30 min, purifying nucleic acid that can be detected using NAATs/iNAATs such as real-time LAMP and real-time PCR. Within a combined 1.5–2 h turnaround time, the magnetocapture method in combination with real-time LAMP was able to extract and detect 10^2–10^3copies (i.e., in the order of zeptomole) of genomic DNA. This was performed reproducibly from both aqueous solution and crude cell lysate. In combination with real-time PCR assays, the magnetocapture methods were able to extract and detect 10^2–10^3 copies of spiked human genomic DNA in 50% fetal bovine serum with few-cycle threshold values (C_t values) higher than that of pure genomic DNA. Assays involving the CCCMP consistently demonstrated slightly higher analytical sensitivity than ECCMP, which could be due to the marginally higher DNA binding capacity of the former. To the best of our knowledge, this work is the first to report the application of coprecipitation synthesized or electrostatically cross-linked chitosan-coated iron oxide magnetic particles to demonstrate their application in nucleic acid magnetocapture from cell lysate and complex biofluid. It is also probably the first report about the compatibility of the low copies of extracted nucleic acid with both real-time LAMP and real-time PCR. The compatibility of the magnetocapture methods with real-time LAMP and real-time PCR highlighted the potential application of the method with rapid pathogen detection, biowarfare prevention, cell-free nucleic acid detection, genetic disease identification, mutation screening, and digital PCR. Overall, the study eliminates the necessity for sophisticated instruments for magnetic particle synthesis and then demonstrates the utility of high-efficiency magnetocapture of the clinically relevant low copy of nucleic acids. Altogether, we anticipate that this study would help expand NAAT applications in limited-resource settings and democratize nucleic acid-based diagnosis.

2.5 Materials and Methods

2.5.1 Materials

$FeCl_3 \cdot 6H_2O$ (#GRM165), $FeSO_4$,$7H_2O$ (#TCE119), 2X real-time SYBR mastermix (#MBT074) were purchased from HiMedia. Chitosan (medium molecular weight, #18824) and the rest of the chemicals were purchased from SRL Chemicals unless mentioned

otherwise. Bst 2.0 enzyme, dNTP mix were procured from New England Biolab, USA. Fetal bovine serum was procured from Sigma Aldrich and was heat-inactivated prior to usage. MCF-7 genomic DNA was a gift from Prof. Subhabrata Sen's lab at Department of Chemistry, Shiv Nadar University, India. Thermo MultiSkan Go plate reader was used to estimate DNA concentrations using UV260. The BioRad CFX Maestro or Connect instrument was used for real-time LAMP and PCR experiments.. Gel and colorimetric LAMP experiments were carried out at the Eppendorf master cycler.

2.5.2 Synthesis of coprecipitation-cured chitosan-coated magnetic nanoparticles (CCCMP)

The synthesis was carried out as described elsewhere with slight modification[137]. The process was carried out in a 50 mL conical flask. 5 mL of 2 M $FeCl_3 \cdot 6H_2O$ (HiMedia) (2.7 gm in 5 mL) and 5 mL of 1.5 M $FeSO_4$,$7H_2O$ (HiMedia) (2.1 gm in 5 mL). The procedure started with mixing of 293 μL of $FeSO_4$,$7H_2O$ (final concentration 0.04 M) and 440 μL $FeCl_3 \cdot 6H_2O$ (final concentration 0.08 M) with preheated (50°C) 9.3 mL 1% medium molecular weight chitosan in 1% acetic acid (total reaction mixture volume-10 mL). The dosing of 4 mL of the aqueous ammonia at 200 μL/min was started with constant stirring. After that reaction mixture was kept at 50°C for the next 20 minutes. The resulting magnetic particles were then subjected to magnetic decantation-mediated washing with deionized water with the help of a permanent magnet until pH increased to 7, resuspension to 10 mL water, followed by continuous stirring for two hours at 90°C ("curing"). The particles were then washed 5 times with 10 mL 0.05 M MES buffer each (in each step incubated with MES buffer for 10 minutes) and finally, 5 times washed with 10 mL autoclaved water each using magnetic decantation. The magnetic particles (MPs) were stored in water at 4°C after the concentration (mg/mL) was calculated.

2.5.3 Preparation of bare iron oxide magnetic particles

The bare iron oxide particles were prepared using alkaline co-precipitation methods from $FeCl_3$ and $FeSO_4$ exactly as described above except the use of chitosan solution and without the follow-up curing step (heating at 90°C for 2 h). The magnetic particles (MPs) were stored in water at 4°C after the concentration (mg/mL) was calculated.

2.5.4 Synthesis of electrostatically cross-linked chitosan magnetic particles (ECCMP)

The electrostatically cross-linked chitosan coated iron oxide particles were adopted as previously reported with the following modification [138]. 9 mL of 1% chitosan in 1% acetic acid was mixed with 1 mL 0.5 mg/ml bare iron oxide magnetic particles in a vial in a preheated water bath at 60°C for 10 mins. The vial was placed on the magnetic stirrer (700 r.p.m) and added with 1.5 mL of sodium tripolyphosphate (STPP) solution (stock concentration 0.5% in water) with continuous stirring. The reaction was carried out for 10 mins. Then the reaction mixture was washed with 10 mL of autoclaved water each 10 times. The magnetic particles (MPs) were stored in water at 4°C after the concentration (mg/mL) was calculated.

2.5.5 Characterization and sample preparation of magnetic particles for FE-SEM, EDX, FT-IR, DLS, Zeta Sizer and XRD

Morphology and size of the CCCMP, ECCMP, and bare iron oxide were determined by field emission scanning electron microscopy (FE-SEM, Sigma-Carl Zeiss). The presence of elements in all types of magnetic particles was identified using energy-dispersive X-ray spectroscopy (EDX) attached with FE-SEM. X-ray diffraction spectroscopic (XRD) analysis was carried out for the determination of the crystalline structure of prepared magnetic particles. Fourier transform infrared spectra (FT-IR) of the samples were recorded on an FTIR spectrometer (Perkin Elmer) from 500 to 4000 cm^{-1}.

Dynamic light scattering (DLS) was employed to determine the hydrodynamic diameter and zeta potential of chitosan coated iron oxide nanoparticles dissolved in MiliQ water at 25 ± 0.1 °C. For hydrodynamic diameter determinations, a backscattering detection angle of 173° was employed. The ζ-potential was estimated using the Smoluchowski equation from the laser Doppler electrophoretic mobility measurement at 25 ± 0.1 °C.

2.5.6 Genomic DNA isolation from *E. coli*

E. coli DH5α strain was cultured on tryptic soya broth (TSB) at 37°C for 12 – 15 h. 10 mL of culture were pelleted down at 4000 r.p.m for 5 minutes and the pellet is resuspended in 1 mL of lysis buffer (10 mM Tris-HCl, 0.1 M NaCl, 5 mM EDTA, 0.5% [w/v] sodium dodecyl sulfate, Proteinase K (100 ng/mL), pH 7.8). The cell suspension was incubated at

37°C, 1 mL of 10M ammonium acetate is added, and centrifuged at 12000 r.p.m at 4°C. The supernatant fluid was placed in a new sterile tube. Following that, cold isopropanol was added to the supernatant to a final concentration of 50% and kept at 20 °C for 20 minutes. The solution was then centrifuged at 12000 r.p.m., and the supernatant was discarded. The pellet is dissolved with 1 mL of cold 70% ethanol, centrifuged at 12000 r.p.m, and the supernatant was discarded. DNA template was air-dried and dissolved in 50 μL sterile distilled water and stored at −20 °C until PCR amplification.

2.5.7 Cell lysate preparation from bacterial culture

E.coli DH5α strain was cultured on tryptic soy broth (TSB) at 37 °C for 12 h. 25 μL of culture containing 10^9 cells was mixed with 25 μL of 2X lysis buffer (20 mM Tris-HCl, 2 mM EDTA, 2% [v/v] Triton X100, 1.0% Tween-20, pH-8). For the limit of detection assays, the cell suspension was serially diluted to 10^1 – 10^5 cells/50 μL using 1X lysis buffer. The cell suspension was incubated at 95°C for 15 minutes and neutralized with 50 μL of 0.05 M MES buffer pH-5.2 before magnetocapture experiments.

2.5.8 UV_{260} quantification of DNA binding capacity of CCCMP, ECCMP, and bare iron oxide with pure genomic DNA

1.0, 2.5, or 5.0 mg of wet CCCMP, ECCMP, or bare iron oxide was taken from storage and the supernatant was removed by magnetic decantation. 100 μL 0.05 M MES buffer (pH - 5.2) was added and incubated for 10 mins (charging step) on the benchtop with occasional finger tapping. The supernatant was removed by magnetic decantation. The magnetic particles were then incubated with 50 μL 500 ng/μL *E. coli* genomic DNA solution in 0.05 M MES buffer (pH - 5.2) on the benchtop with occasional finger tapping or vortex-enabled shaking. The supernatant was separated from magnetic particles by magnetic decantation. The particles were washed by resuspension once by addition of 50 μL 0.05 M MES buffer (pH - 5.2) and the supernatant was separated from magnetic particles by magnetic decantation. The particles were incubated with 10, 25, or 50 μL of elution buffer 10 mM Tris HCl-pH-8.5 (for 1.0, 2.5, or 5.0 mg magnetic particles, respectively) on a benchtop with occasional finger tapping or vortex-enabled shaking. The eluent (supernatant) was separated from magnetic particles using magnetic decantation

and quantified with UV_{260} in a Thermo MultiSkan Go plate reader nanodrop. Assuming a linear correlation of DNA adsorption for 1.0, 2.5 or 5.0 mg magnetic particles, eluted DNA (in ng) was plotted against weight (in mg) of magnetic particles and a linear fitting was applied. The slope of the linear fit was calculated as the amount of DNA captured and eluted per mg of wet magnetic particles.

2.5.9 DNA binding assay with CCCMP, ECCMP with pure genomic DNA, and crude cell lysate

2.5 mg of wet CCCMP or ECCMP was taken from storage and the supernatant was removed by magnetic decantation. 100 μL 0.05 M MES buffer (pH -5.2) was added and incubated for 10 mins (Charging step) on the benchtop with occasional finger tapping. The supernatant was removed by the magnet. Next, 25 μL MES 0.05 M pH 5.2 solution containing 10^1 – 10^5 copies of *E. coli* gDNA (in case of genomic DNA) or 100 μL of neutralized (above) heat lysate from 10^1 – 10^5 cells (in case of crude lysate) was added to the particles and incubated for 10 mins on the benchtop with occasional finger tapping. The supernatant was separated from magnetic particles by magnetic decantation. The particles were washed by resuspension twice by addition of 25 μL 0.05 M MES buffer (pH 5.2) each time and the supernatant was separated from magnetic particles by magnetic decantation. 25 μL elution buffer (10 mM Tris HCl, pH 8.5) was added and incubated for 10 mins on the benchtop with occasional finger tapping. The supernatant was collected as elution and subjected to NAAT procedure as described below. The magnetic particles left out are called beads and resuspended in 25 μL autoclaved water and stored in 4°C.

2.5.10 LAMP with elution and beads obtained from DNA binding assay

The LAMP reaction was conducted with the elution and beads obtained from DNA magnetocapture assay with 10^9 copies of gDNA or heat lysate from 10^9 cells. The final LAMP reaction (total 25 μL) contained the primer pairs in the following final concentrations: 0.2 μM outer primers, and 1.6 μM forward and backward inner primers. The loop primers, when utilized were used at final concentrations at 0.8 μL. The reaction mix also contained 2.5 μL of 10× Bst 2.0 DNA polymerase reaction buffer [1× containing 20 mM Tris-HCl, 50 mM KCl, 10 mM $(NH_4)_2SO_4$, 2 mM $MgSO_4$, 0.1% Tween-20, pH

8.8], 1.4 mM dNTPs, 1 μL of an 8 U/μL concentration of Bst 2.0 DNA polymerase, 6 mM $MgSO_4$ and 5 μL of elution as template. In the case of beads, 5 μL of beads resuspended in autoclaved water is used as the template. In case of no template control, 5 μL of autoclaved water is used instead of beads or elution obtained from DNA binding assay.

2.5.11 Real-time LAMP to determine LoD for detection of bacterial genomic DNA from the aqueous and crude lysate

Elutions from magnetocapture experiments performed on $10^1 – 10^5$ copies of aqueous *E. coli* gDNA solutions or heat lysate from $10^1 – 10^5$*E. coli* cells were subjected to real-time LAMP experiments. The final LAMP reaction (total 25 μL) contained 0.2 μM outer primers, 1.6 μM forward inner primers, 2.5 μL of 10× Bst 2.0 DNA polymerase reaction buffer [1× containing 20 mM Tris-HCl, 50 mM KCl, 10 mM $(NH_4)_2SO_4$, 2 mM $MgSO_4$, 0.1% Tween 20, pH-8.8], 2.5 μL SYBR I (final concentration 1X diluted from 10,000X), 1.4 mM dNTPs, 1 μL of an 8 U/μL concentration of Bst DNA polymerase (New England Biolabs), 6 mM $MgSO_4$ (2 μL) and 5 μL of elution as template. Real-time LAMP was set at the following settings for each cycle; 69°C for 30 s, 68°C for 30 s, 67°C for 30 s, 66°C for 60 s with fluorescence monitoring at the last step. The cycles were repeated 30 times in a CFX Maestro or CFX connect real-time PCR machine (BioRad). This was immediately followed by the default standard melt curve analysis protocol present in the instrument, where the temperature was gradually increased from 65°C to 95°C every 5 s by 0.5°C. Alongside, the fluorescence was recorded at each temperature increment step.

2.5.12 DNA extraction with CCCMP, ECCMP with mammalian genomic DNA from aqueous solution and complex biofluid

The magnetocapture extraction-amplification assay was tested for detecting human genomic DNA sample (obtained from MCF-7 cells) spiked in aqueous solution or 50% (final) heat-inactivated fetal bovine serum (FBS) samples. In each case, the assay was performed on 10^4 copies, 10^3 copies, or 10^2 copies present in 25 μL solution. The aqueous solution or the serum was added with 25 μL 0.1 M MES pH 5.2 buffer. The DNA was captured using 2.5 mg of either CCCMP or ECCMP by 10 min benchtop incubation with occasional finger tapping. Following two successive washing with 25 μL 0.05 M MES pH

5.2, the bound DNA was eluted in 25 μL 10 mM Tris-HCl buffer pH 8.5. 5μL of the elution was subjected to real-time PCR.

2.5.13 Real-time PCR to determine LoD for detection of human genomic DNA from the aqueous sample and complex biofluid

In each case, the assay was performed in 25 μL solution, where the template was the 5 μL elution from the magnetocapture of 10^4, 10^3, 10^2 copies of MCF-7 genomic DNA. The elution was added with 2X proprietary real-time PCR mix (12.5 μL), forward and reverse primer (final concentration 0.4 μM, *actin B* gene), and molecular grade water. PCR was set at the following settings: 95°C for 180 s, then 39 cycles of 95°C for 10 s, 55°C for 10 s, and 72°C for 30 s, where the last step consisted of fluorescence monitoring. This was followed by the default program of melt curve analysis where the temperature was gradually increased from 65°C to 95°C every 5 s by 0.5°C. Alongside, the fluorescence was recorded at each temperature increment step.

CHAPTER 3

EVALUATION OF INDIRECT SEQUENCE-SPECIFIC MAGNETO-EXTRACTION-AIDED LAMP FOR FLUORESCENCE AND ELECTROCHEMICAL SARS-COV-2 NUCLEIC ACID DETECTION

3.1 Abstract

Since the beginning of the SARS-CoV-2 pandemic, nucleic acid amplification test (NAAT), such as quantitative real-time reverse transcriptase PCR (qRT-PCR), has remained the primary intervention for diagnostics and containment of SARS-CoV-2. Despite its remarkable clinical and analytical specificity and sensitivity, qRT-PCR necessitates pure nucleic acid-free of polymerase inhibitors (from complex biological matrices) as its substrate. Similarly, isothermal NAATs (iNAATs), despite their advantage over qRT-PCR in terms of thermal cycler independence, still require pure nucleic acid as a template. In turn, the requirement of pure nucleic acid warrants the use of spin-column mediated extraction with centralized high-speed centrifuges. Additionally, utilization of centralized real-time fluorescence readout and the use of sequence-specific molecular probes like TaqMan further prevent their deployment in decentralized locations. In order to circumvent these disadvantages, we have envisioned a sample-to-answer workflow comprising indirect sequence-specific magneto-extraction (also referred to as magnetocapture, magneto-preconcentration, or magneto-enrichment) followed by in situ fluorescence or electrochemical LAMP. Using SARS-CoV-2 nucleic acid as the analyte, this study compared the analytical effectiveness of indirect and direct sequence-specific magneto-extraction followed by LAMP. Since contamination carryover may affect the efficacy of sequence-specific indirect magnetocapture, its performance in the presence of excess host nucleic acid or serum was probed. Through these experiments, we have established a comprehensive limited resource-adoptable and highly specific nucleic acid detection method with a limit of detection of 2.5 copies/µL. Its advantage lies in the flexibility of using centralized real-time SYBR-based fluorescence LAMP or portable electrochemical LAMP as the readout. Simultaneously, the performance with

magneto-capture aided fluorescence and electrochemical LAMP readouts were weighed against each other in terms of analytical sensitivity, specificity, and turnaround time. Additionally, the analytical efficacy of the magnetocapture-LAMP workflow was also checked against that of LAMP using pure nucleic acid as a template. Besides being the first report utilizing electrochemical LAMP to detect SARS-CoV-2 nucleic acid, this would probably be the first study to assess the comparative analytical of magnetic preconcentration combined with in situ fluorescence and electrochemical LAMP. It is perhaps also the first study (to the best of our knowledge) to compare the analytical efficacy of a sequence-specific magnetic target enrichment-LAMP (fluorescence and electrochemical) to that of a LAMP assay using pure nucleic acid as a template. Parts of this chapter is now undergoing peer-review and is available as a pre-print [139].

3.2 Introduction

The upsurge of novel coronavirus disease (COVID-19), caused by the severe acute respiratory syndrome-2 virus (SARS–CoV-2), has led to 510 million infections and 6.2 million deaths (as of April 26, 2022) [140]. The SARS-CoV-2 RNA could be detected via the quantitative reverse transcription-polymerase chain reaction (qRT-PCR), a high specificity and sensitivity method, using molecular targets present in their genome [141]. Despite the availability of several commercial qRT-PCR kits, however, it has several disadvantages. It requires a spin-column mediated pure nucleic acid extraction from the biological samples. This increases the overall turnaround time (TAT), cost, and need for a high-speed centrifuge present in a centralized lab.

Additionally, a separate reverse transcription step is often required as few existing kits integrate the reverse transcription with the real-time PCR step. Single-step qRT-PCR has lower sensitivity than two-step assays [3, 4]. The multi-step assays necessitate the recruitment of a trained workforce to conduct them. Furthermore, the possible presence of host nucleic acid requires a sequence-selective TaqMan probe, adding to the cost.

Thermal-cycler-independent isothermal nucleic acid amplification techniques (iNAATs) such as reverse transcription loop-mediated isothermal amplification (RT-LAMP) have been deployed in one-step SARS-CoV-2 detection using colorimetric as well fluorescence readouts [144]–[146]. Besides, a LAMP amplicon could also be quantified by end-point electrochemical detection

[147]. Besides quantitative readouts in the centralized laboratory, the latter feature could be utilized for near-point-of-care (near-POC) diagnostics in a resource-limited area [147]. Most LAMP assays require prior RNA extraction from viral transmission media (VTM) despite such advantages. Few studies have bypassed or integrated nucleic acid extraction with downstream in situ LAMP or other NAATs [148, p. 2]. Rather than using direct amplification from clinical or simulated samples, most LAMP-based bioanalytical methods utilized pre-extracted nucleic acid or in situ purifications. On the other hand, NAATs using non-extracted nucleic acid as a template significantly reduced the specificity and sensitivity for SARS-CoV-2 detection. They may not work at all with SYBR-based qRT-PCR [149]. The clinical sensitivity and specificity of reverse transcription LAMP(RT-LAMP) decrease significantly when non-extracted RNA has been used as a template(sensitivity reducing from 97% to 71% and specificity from 100% to 47%, for pre-extracted and non-extracted RNA templates, respectively) [150]. In another study, direct colorimetric LAMP using non-extracted RNA from saliva samples generated false positive readouts [151]. Similarly, direct colorimetric RT-LAMP on the untreated clinical sample detected SARS-CoV-2 only when the viral copy number was above 3000 copies/μL. With RNase inactivation or combined RNase inactivation and extraction, the analytical sensitivity improved to 25 copies/μL and 2.5 copies/μL, respectively [152]. Besides, SARS-CoV-2 detection has surprisingly not been conducted yet using electrochemical LAMP readouts, despite their utility in the near-POC settings.

A sequence-specific magnetic preconcentration is advantageous due to its minimal equipment necessity, the scope of in situ amplification, lesser TAT, and reduced cost [153], [154], [155]. Due to its selectivity of target nucleic acid, it would (in principle) eradicate the need for TaqMan-like sequence-selective reporters in the downstream NAAT. In combination with electrochemistry-mediated readout, such assays would be advantageous in near-POC diagnostics in limited-resource settings. The sequence-specific capture could be direct or indirect. In the direct capture, a magnetic bead-immobilized sequence-specific probe exploits complementarity to extract target nucleic acid [155]. The indirect magneto-enrichment utilizes a sequence-specific probe to first bind to the target of interest before magnetic bead immobilization. However, due to the absence of a blocking step, it could become susceptible to carryover contamination [156]. Despite the potential advantage and utility of sequence-specific magneto-enrichment, a

comprehensive literature search of magnetic extraction methods combined with LAMP tabulated in Table 3.1 yielded only four direct magneto-enrichment studies (entries 20, 23, 43, 46) [155], [157]–[159]. All four utilized a microfluidic setup, requiring costly flow-controller equipment. The rest predominantly are either whole nucleic acid extraction(includes all SARS-CoV-2 detections, entries 7, 10, 14, 24, 35, 48, [160]–[162], [163, p.], [164], [165]), or immune magnetic capture-lysis. Surprisingly, none of the studies utilized electrochemical readout despite promising potential in limited resource detection or indirect sequence-specific magneto-enrichment. Therefore, the modality of an indirect magneto-enrichment of pathogen nucleic acid from a complex biofluid or host nucleic acid-containing sample with downstream LAMP, either with fluorescence or electrochemical readout, remains unexplored.

Table 3.1: List of studies in NCBI PubMed that integrate magnetocapture and LAMP. NA stands for not applicable

Entry No	**Method of detection**	**Analyte**	**Type of magneto-extraction (whole nucleic acid, sequence-specific, immunocapture)** **In situ amplification**	**If sequence-specific capture, direct or indirect?**	**LoD, Readout**	**Detection from Complex Biofluid or host genomic DNA containing sample**	**Detection from host genomic DNA containing sample**
1	Antibody-assisted sandwich assay formation on target analyte, followed by the heat-mediated release of LAMP template, then real-time LAMP [166]	P-glycoprotein	Immunocapture No	NA	5 fg/mL (35.4 aM) Real-time fluorescence	Not performed	No

2	Orthogonal biotinylated and digoxigenin modified primers for multiplexed LAMP amplification of dengue and chikungunya viral nucleic acid, followed by selective immobilization on streptavidin or anti-digoxigenin coated magnetic beads and then naked eye detection [167]	Dengue and chikungunya viral nucleic acid	NA NA	Sequence-specific capture of the amplicon was utilized Direct	51.6 ng/μL	Not performed	No
3	Magnetic bead-based extraction of *Yersinia pestis* genomic DNA (gDNA) from simulated lung, spleen, and liver samples followed by LAMP [168]	*Yersinia pestis* gDNA	Whole nucleic acid extraction No	NA	2.3 – 23 CFU for pure gDNA 10^4 – 10^6 CFU for simulated samples Turbidimetry or colorimetry (calcein)	simulated lung, spleen, and liver samples	Yes
4	LAMP Amplicons inserted with fluorescein were immobilized using a biotinylated probe on a streptavidin magnetic bead. The probe was	Leptospira gDNA	Sequence-specific NA	Direct, against the amplicon	80 genome copies/25 μL (3.2 copies/μL) Visual, colorimetric	NA	NA

	complementary to the amplicon. Anti-fluorescein horse-radish peroxidase was utilized for TMB based colorimetric readout [169]						
5	Immuno-magnetic capture of *Shigella* from the sample, followed by lysis, and then real-time LAMP [170]	Shigella	Immunocapture No	NA	8.7 CFU/mL Real-time fluorescence	From milk and clinical stool sample	
6	Immuno-magnetic capture of *Salmonella* from the sample, followed by lysis, and then real-time LAMP [171]	*Salmonella*	Immunocapture No	NA	5 CFU/mL Real-time fluorescence	From meat samples	
7	A comparison of RT-PCR and RT-LAMP for clinical samples: RT-PCR used extracted RNA using a spin-column based protocol while LAMP used a proprietary magnetic bead-based RNA extraction (MicrosensDx RapiPrep®) [160]	SARS-CoV-2 RNA, *ORF1ab*	Proprietary No	Proprietary	Not provided, but commented as equivalent to RT-PCR Proprietary	From clinical sample	Yes (likely)
8	A LF primer immobilized on a	pre-extracted *Helicobacter*	Sequence-specific	Direct	40 CFU/mL	NA	NA

	magnetic bead was utilized for LAMP on pre-extracted *Helicobacter pylori* gDNA. The LAMP also used a biotinylated BF primer incorporating the biotin tag into it. The LAMP was then colorimetrically detected using a neutravidin-HRP and ABTS assay [172]	*pylori* gDNA	No	Against amplicon	colorimetric		
9	Pre-extracted viral RNA was subjected to LAMP containing a biotinylated primer. Next, the amplicon was immobilized on streptavidin magnetic beads and detected using a magnetic readout [173]	Pre-extracted Newcastle disease virus RNA	Sequence-specific No	Direct Against amplicon	10 aM (6 copies/μL) Optomagnetic readout	NA (LAMP on pre-extracted RNA used)	NA
10	Magnetic bead-based SARS-CoV-2 viral RNA extracts were subjected to RT-LAMP and RT-PCR for Comparison [161]	SARS-CoV-2 viral RNA extracts	Whole nucleic acid extraction No	NA	4.23 copies/reaction (for LAMP assay only, not for the entire method) Real-time fluorescence	Yes, clinical sample. Pre-extracted RNA from the clinical sample used.	Yes (likely)

11	Immuno-magnetic capture of *Escherichia coli* O157:H7 from the sample, followed by lysis, and then real-time LAMP [174]	*Escherichia coli* O157:H7	Immunocapture No	NA	18 CFU/mL Turbidimetry	Yes, from meat samples	
12	Magneto-extraction followed by real-time LAMP [175]	*Agrilus planipennis* species	Sequence-specific No	Direct Against amplicon	0.1 ng of gDNA/rection Visual (SYBR Green I), Lateral flow dipstick	Yes	
13	Detection of LAMP amplicons by complementary probes immobilized on magnetic beads followed by chemiluminescence detection [176]	Avian influenza virus RNA (in vitro transcribed)	Sequence-specific No	Direct Against amplicon	1000 copies/mL Chemiluminescence	NA	NA
14	SiO_2 magnetic bead-based whole SARS-CoV-2 RNA extraction followed by RT-LAMP [162]	SARS-CoV-2 RNA	Whole nucleic acid extraction No	NA	LOD for LAMP not performed Real-time fluorescence and pH change colorimetry	Yes	
15	Immuno-magnetic capture of *Salmonella* from the sample, separation of viable	*Salmonella*	Immunocapture 	NA	14 CFU/mL Turbidimetry	Yes (meat sample)	

	bacteria, followed by lysis, and then real-time LAMP [177]		No				
16	Magnetic extraction of the whole gDNA for *Helicobacter pylori* followed by LAMP [178]	*Helicobacter pylori*	Whole nucleic acid extraction No	NA	100 fg Gel-based	Yes	
17	Methylated gene was detected using anti-methyl antibody followed by LAMP [179]	Methylated Septin9 gene	Immunocapture No	NA	0.02 ng/μL Colorimetry	Yes	
18	A microfluidic platform enabling magnetic RNA extraction followed by LAMP [180]	Zika virus	Whole nucleic acid extraction Yes	NA	100 copies/mL Colorimetry	Yes	
19	Oligonucleotides bearing Zika virus sequence were subjected to LAMP containing a biotinylated primer. Next, the amplicon was immobilized on streptavidin magnetic beads and detected using an AC susceptibility readout [173]	Zika virus	Sequence-specific No	Direct Against amplicon	1 aM (0.6 copies/μL) AC susceptibility measurement	NA (pre-synthesized oligonucleotide used)	
20	Microfluidic sequence-specific	nervous necrosis virus	Sequence-	Direct	10 fg (measured with cDNA).	Proof-of-concept	

	magnetocapture of nervous necrosis virus RNA followed by RT-LAMP [155]	RNA	specific Yes	 Against target nucleic acid	LOD not performed with tissue sample Gel electrophoresis	demonstrated using an infected fish tissue sample	
21	SiO_2 based purification of RNA followed by RT-LAMP [181]	Potato virus Y RNA	Whole nucleic acid extraction No	NA	Not determined Real-time fluorescence	From plant tissue sample	
22	Microfluidic chip having whole gDNA extraction from *Salmonella* followed by on-chip real-time LAMP [182]	*Salmonella*	Whole nucleic acid extraction Yes	NA	50 cells Real-time fluorescence	From spiked meat samples	No
23	Microfluidic sequence-specific magnetocapture of *Staphylococcus aureus* gDNA followed by real-time LAMP [157]	*Staphylococcus aureus*	Sequence-specific Yes	Yes Against target nucleic acid	10 fg/μL 10 CFU/mL (for clinical sample) Spectroscopy (260 nm)	From spiked food and serum samples	No
24	Extraction of SARS-CoV-2 from saliva using magnetic bead followed by RT-LAMP [163]	SARS-CoV-2 RNA	Whole nucleic acid extraction Yes	NA	3.7 copies/μL Colorimetric	Yes (saliva)	Yes (likely)
25	Magnetic bead assisted microfluidic	*Mycobacterium tuberculosis*	Whole nucleic acid extraction	NA	10 bacteria	Yes (sputum)	Yes (likel

	droplet technology for *Mycobacterium tuberculosis* gDNA detection [183]	gDNA	Yes		Naked eye fluorescence readout		y)
26	LAMP amplicon was further subjected to hybridization chain reaction using a magnetic bead-immobilized hairpin, followed by flow cytometric or glucometer readout [184]	Norovirus genome synthetic template	Sequence-specific Yes	Direct Against amplicon	30 copies Flow cytometric or glucometer readout	NA	NA
28	Immunomagnetic capture of *Salmonellaenterica* followed by LAMP [185]	*Salmonella enterica*	Immunocapture No	NA	14 CFU/mL Visual (colorimetric)	Yes (blood sample)	Yes (likely)
29	Magnetic bead-based whole RNA extraction followed by RT-LAMP [186]	Prunus necrotic ringspot virus	Whole nucleic acid extraction No	NA	Not determined Visual (colorimetric) and gel electrophoresis	Yes (plant tissue)	Yes (likely)
30	Immunomagnetic capture of bacteria followed by lysis and LAMP [187]	*Salmonella typhi*	Immunocapture No	NA	5 CFU/mL Fluorescence	Yes (blood samples)	Yes (likely)
31	Immunomagnetic capture of bacteria	tdh (+) *V. parahaemolyti*	Immunocapture	NA	Not determined	Yes (food sample)	Yes (likel

	followed by lysis and LAMP [188]	*cus*	No		Real-time fluorescence		y)
32	Magnetic cartridge-based preconcentration of target nucleic acid followed by LAMP [189]	*S. pneumoniae*, *B. pertussis*, and *L. pneumoniae*	Whole nucleic acid extraction Yes	NA	10 copies/reaction Real-time fluorescence	Yes (sputum)	Yes (likely)
33	Microfluidic immunomagnetic (aptamer-assisted) capture of bacteria and virus, lysis, followed by LAMP [190]	Influenza A (H1N1) virus and methicillin-resistant *Staphylococcus aureus*	Immunocapture No	NA	3.2×10^{-3} hemagglutinating units (HAU) per reaction and 30 colony-forming units (CFU) per reaction Colorimetric detection	No	No
34	Centrifugal microfluidic device for SiO_2 magnetic bead-based total nucleic acid extraction followed by LAMP [191]	dengue virus (different serotypes), chikungunya virus, *Plasmodium falciparum*, *Salmonella enterica* Typhi, *Salmonella enterica* Paratyphi A, and *Streptococcus*	Whole nucleic acid extraction Yes	NA	10^2 - 10^3 copies/reaction Fluorescence readout	Yes (serum, blood, stool)	Yes (likely)

		pneumonia					
35	Magnetic preconcentration of target nucleic acid followed by LAMP [164, p. 2]	SARS-CoV-2	Whole nucleic acid extraction No	NA	25 copies Visual fluorescence readout	Yes (mock clinical samples)	Yes (likely)
36	Microfluidic SiO2 based whole DNA extraction followed by LAMP [192]	*Escherichia coli, Proteus mirabilis, Salmonella typhimurium* and *Staphylococcus aureus*	Whole nucleic acid extraction Yes	NA	1 – 10 CFU/μL Real-time fluorescence	No	No
37	Immunomagnetic capture of bacteria followed by lysis and LAMP [193]	Vibrio parahaemolyticus	Immunocapture No	NA	1.9 – 0.19CFU/g Real-time fluorescence	Yes (spiked oyster)	Yes (likely)
38	Immunomagnetic capture of bacteria followed by lysis and LAMP [194]	Salmonella	Immunocapture No	NA	5 CFU/mL Visual fluorescence readout	Yes (food sample)	No
39	Microfluidic immunomagnetic capture of bacteria followed by lysis and LAMP [195]	Salmonella	Immunocapture) Yes	NA	2 Cells/μL Acoustic readout	Yes (food sample)	No
40	Magnetic bead-based	Influenza A	Whole nucleic	NA	100 copies	Yes (throat	Yes

	whole nucleic acid extraction followed by LAMP [196]	virus subtypes (H1N1, H3N2, H5N1, and H7N9), influenza B virus, and human adenoviruses	acid extraction Yes		Colorimetry	swabs)	(likely)
41	Microfluidic magnetic bead-based whole DNA extraction followed by LAMP [197]	SARS-CoV-2 and *Klebsiella pneumonia, Pseudomonas aeruginosa*, and *Stenotrophomonas maltophilia*	Whole nucleic acid extraction No	NA	2.5 copies/μL Real-time Fluorescence	No	Yes
42	Microfluidic magnetic bead-based whole RNA extraction followed by LAMP [198]	HIV RNA	Whole nucleic acid extraction No	NA	10^3 viral particles/mL Lateral flow dipstick assay	Yes (blood and saliva)	Yes (likely)
43	Microfluidic magnetic bead-based sequence-specific RNA extraction followed by LAMP [158]	CymMV, 155 the Odontoglossum ringspot virus (ORSV), the Capsicum 156 chlorosis virus (CaCV) and the Tomato spotted wild	Sequence-specific Yes	Direct Against target nucleic acid	25 fg Turbidimetric (optical fiber-based)	Yes (plant sample)	Yes (likely)

		virus 157 (TSWV)					
44	Microfluidic immunomagnetic capture of bacteria followed by lysis and LAMP [199]	*E. coli* and *Salmonella*	Immunocapture No	NA	10^5 CFU/mL Real-time fluorescence	Yes (spiked sample)	No
45	Capillary microfluidic system for whole DNA extraction followed by integrated LAMP [200]	*Chlamydia trachomatis* and *Neisseria gonorrhoea*	Whole nucleic acid extraction Yes	NA	2.5 copies/μL Visual fluorescence readout	Yes	Yes (likely)
46	Sequence-specific magnetic capture, followed by droplet encapsulation and LAMP [159]	Hepatitis C Virus sequence in plasma	Sequence-specific Yes	Yes Against target nucleic acid	300 copies/reaction Flow cytometry	Yes (spiked plasma)	No
47	Microfluidic magnetic bead-based whole DNA extraction followed by LAMP [201]	*Xylella fastidiosa*	Whole nucleic acid extraction Not described)	NA	500 copies Colorimetry	Yes (plant sample)	Yes (likely)
48	Centrifugal microfluidic magnetic extraction of the whole RNA followed by LAMP [165]	SARS-CoV-2	Whole nucleic acid extraction No	NA	20 copies Colorimetry	Yes (spiked sample)	No

49	Sequence-specific capture of LAMP amplicon followed by electrochemistry [202]	HPV DNA	Sequence-specific No	Direct Against amplicon	0.6 ng Amperometry	NA	NA

This work aims to establish a minimally instrument-intensive sample-to-answer workflow for selectively extracting target nucleic acid from samples containing complex biofluid and host nucleic acid, followed by an iNAAT assay. With this goal, the performance of an indirect sequence-specific magneto-extraction followed by fluorescence (SYBR-based) and electrochemical LAMP was probed. The experiment used SARS-CoV-2 *RdRp* plasmid DNA and RNA as analytes. In doing so, the effectiveness of direct and indirect sequence-specific magneto-extraction using quantitative real-time LAMP (qLAMP) was investigated. Their performance in a real-life-mimicking scenario was compared by detecting SARS-CoV-2 *RdRp* plasmid DNA from samples containing excess human genomic DNA (hgDNA) and serum. The superior one, the indirect magneto-extraction, was then integrated with electrochemical end-point LAMP (eLAMP) to detect SARS-CoV-2 nucleic acid from the real-life-simulating hgDNA serum-spiked samples. In these experiments, we have not only established a flexible (compatible with fluorescence and electrochemical readout) yet sensitive pathogen nucleic acid detection method, but also analyzed the effect of potential contaminants from serum and hgDNA on the performance of direct and indirect magnetocapture combined with downstream LAMP. Parts of this chapter is now undergoing peer-review and is available as a pre-print [139].

3.3 Results and discussions

3.3.1 Use of plasmid constructs containing SARS-CoV-2 RdRp gene and selection of LAMP primers

The resource-constrained area lacks the infrastructure of a highly equipped BSL-3 laboratory for viral nucleic acid extraction followed by downstream applications. According to the guidelines of NIH for SARS-CoV-2 research, in vitro expression of partial viral RNA or protein obtained from

any plasmid construct results in non-infectious products, which could be investigated further in BSL-2 containment [203]. Likewise, bacteria containing the plasmid construct could also be examined in BSL-1 containment as such cultures, or frozen glycerol stocks are non-contagious. Accordingly, in this study, we employed a plasmid (plasmid #14567, https://www.addgene.org/145671/) containing RNA-dependent RNA polymerase gene (RdRp) and in vitro transcribed RNA for the investigation of our sequence-specific nucleic acid capture followed by electrochemical readout based diagnostics. Three sets of reported LAMP primers (Table 3.2) were used to optimize the successful real-time LAMP using the RdRp gene-containing plasmid, where we tried to explore the ability of real-time LAMP to distinguish between 10^3 copies of plasmid in aqueous solution from NTC (no template control).

Table 3.2: Sequences of LAMP primers

Primer set name	Sequence Information (5'-3')
Primer set 1 [204]	F3: TGCTTCAGTCAGCTGATG B3: TTAAATTGTCATCTTCGTCCTT FIP: TCAGTACTAGTGCCTGTGCCCACAATCGTTTTTAAACGGGT BIP: TCGTATACAGGGCTTTTGACATCTATCTTGGAAGCGACAACAA Loop F: CTGCACTTACACCGCAA Loop B: GTAGCTGGTTTTGCTAAATTCC
Primer set 2 [205, p. 2]	F3: CGA TAA GTA TGT CCG CAA TT B3: GCT TCA GAC ATA AAA ACA TTG T FIP: ATG CGT AAA ACT CAT TCA CAA AGT CCA ACA CAGACT TTA TGA GTG TC BIP: TGA TAC TCT CTG ACG ATG CTG TTT AAA GTT CTTTAT GCT AGC CAC Loop F: TGT GTC AAC ATC TCT ATT TCT ATA G Loop B: TCA ATA GCA CTT ATG CAT CTC AAG G
Primer set 3 [206, p. 2]	F3: TCACCTTATGGGTTGGGA

	B3: CAGTTGTGGCATCTCCTG FIP: CGTTGTATGTTTGCGAGCAAGATTTTGAGCCATGCCTAACATGC BIP: GTGCTCAAGTATTGAGTGAAATGGTTTTTATGAGGTTCCACCTGGTT Loop F: ACAAGTGAGGCCATAATTCTAAG Loop B: GTGTGGCGGTTCACTATATGTT

While all the primers were successfully differentiated 10^3 copies of positive template control from NTC, the primer set 2 displayed the highest ΔC_t (C_t value refers to the cycle threshold value) between template control and non-template control among all the primers. Accordingly, we investigated further experiments using primer set 2 (Fig 3.1A and Fig 3.1B). The LoD study was performed using 10^1-10^4 copies of plasmid using primer set 2 to scrutinize the analytical sensitivity of real-time LAMP, which detects as low as 10 copies/reaction (Fig 3.2).

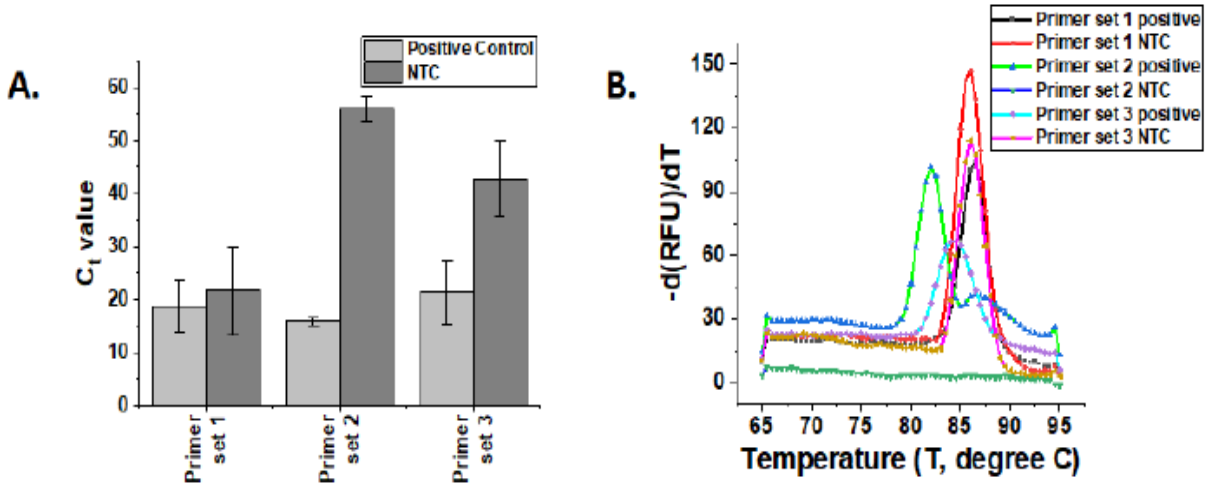

Fig 3.1: Initial screening and melt curve analysis of LAMP primer sets against RdRp gene. A, Ct value difference of three primer sets (Table 3) which involves 10^3 copies as positive control or NTC as a reaction. B, Melt curve analysis with the amplicons formed during real-time LAMP

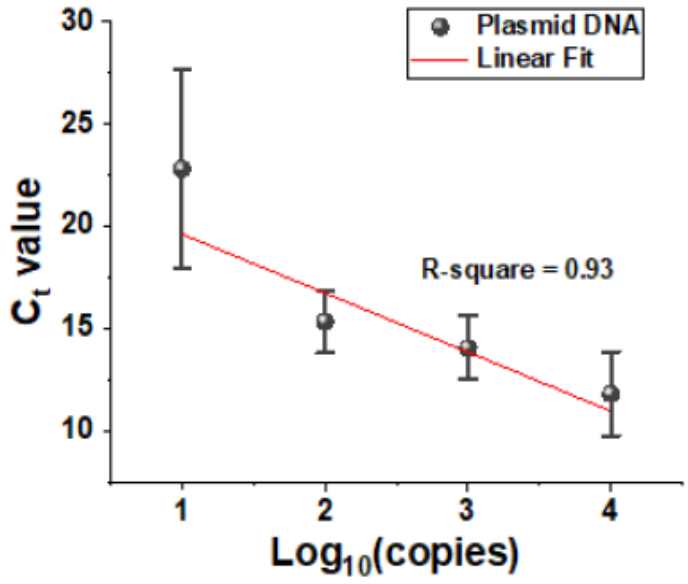

Fig 3.2: LoD determination of RdRp gene-containing plasmid (10^1-10^4copies/reaction) by real-time LAMP using primer set 2 (Table 3.2). (The Ct value of NTC in this reaction is 59.7±0.6 for this reaction, Error bars denote standard deviation (n=3)

3.3.2 Methodology of sequence-specific magnetocapture of SARS-CoV-2 RdRp plasmid followed by detection using qLAMP

We used two types of in vitro sequence-specific magnetocapture assay on a solid support- direct magneto capture (Scheme 3.1) and indirect magneto capture (Scheme 3.2) with the clinically significant 1000 and 100 copies of plasmid in aqueous solution. For direct magnetocapture, 5' biotinylated oligonucleotides (b*) complementary to RdRp gene (b) were employed firstly to immobilize with streptavidin-coated magnetic nanoparticles. This was followed by annealing with target plasmid (b c*) to investigate the performance of on beads downstream readout capability by real-time LAMP. For the indirect magneto capture, 5' biotinylated oligonucleotides were annealed with a target (b c*) to form the binary complex followed by attachment of streptavidin-coated MNP. The next steps are the same for both of the sequence-specific magnetocapture studies. Using magnetic decantation wash, any polymerase inhibitors, non-target nucleic acid can be physically separated from the magnetic bead-bound binary complex. The complex immobilized in magnetic nanoparticles or solid support added itself into the

amplification mix (in situ amplification). The total extraction assay time for direct and indirect sequence-specific magnetocapture is 60 minutes and 30 minutes. Next, we assessed the on-beads (in situ) amplification for direct and indirect magneto extraction studies with 10^3-10^2 copies of the plasmid to investigate the effectiveness of the magnetocapture (Fig 3.3A). Non-template control (NTC) assays were carried out with a blank sample's direct and indirect sequence-specific magnetocapture.

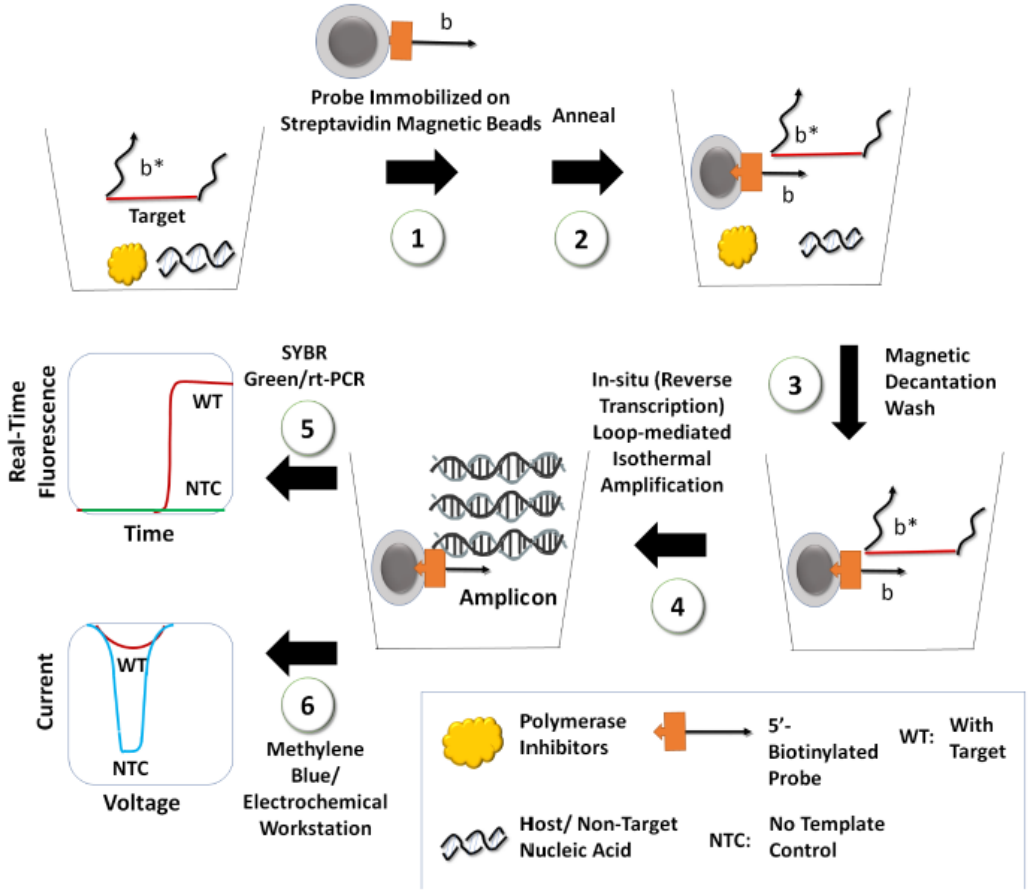

Scheme 3.1: Direct sequence-specific magnetocapture of nucleic acid by immobilizing the biotinylated probe on streptavidin-coated magnetic nanoparticles (step 1) followed by annealing of the target which contains host genomic DNA or common polymerase inhibitors present in the clinical sample (step 2). After magnetic decantation and wash (Steps 3 and 4), magnetic beads bound target was used for downstream fluorescence-based and electrochemical in situ LAMP-based readouts (steps 5 and 6)

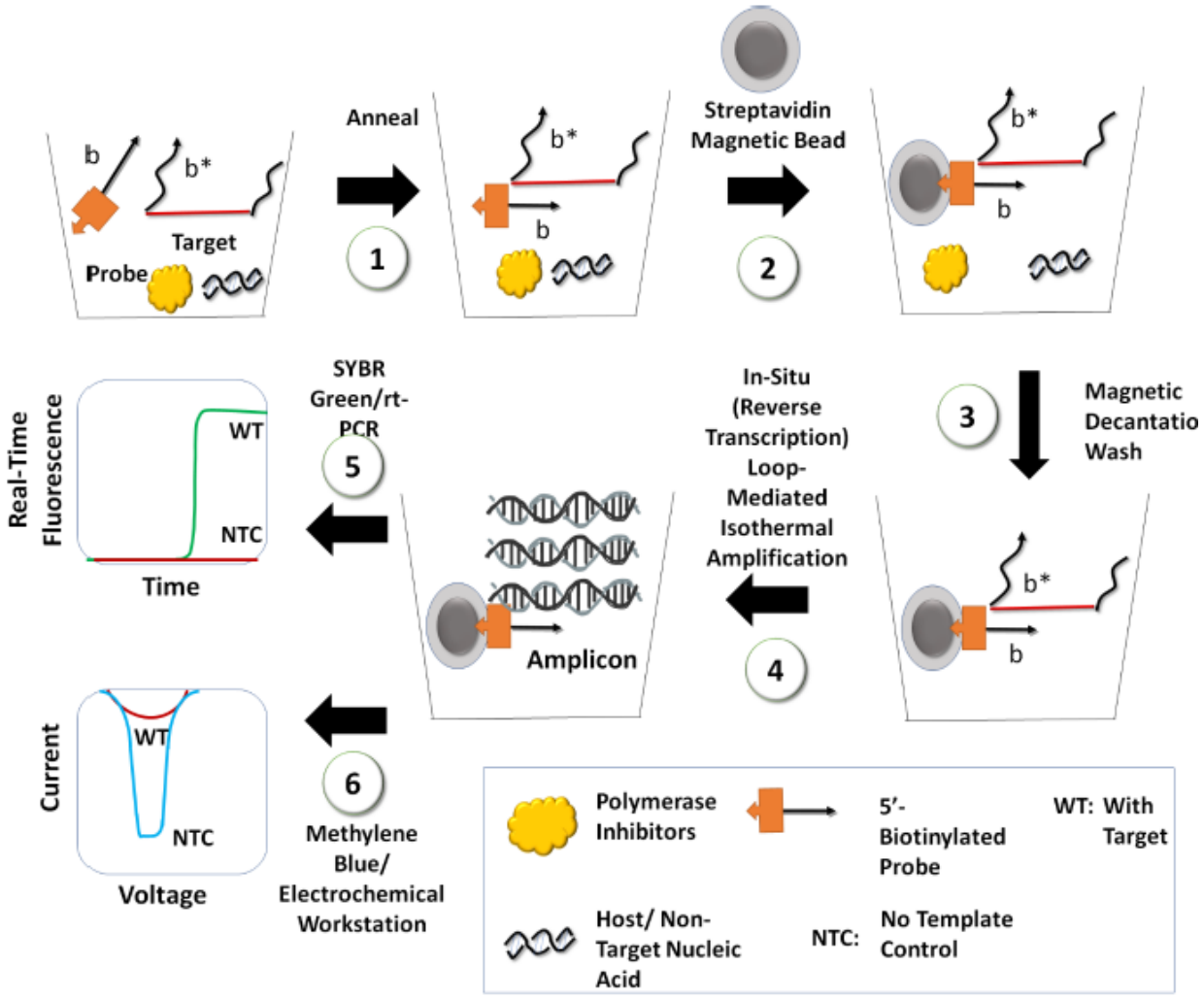

Scheme 3.2: Indirect sequence-specific magneto capture of nucleic acid by annealing the biotinylated probe with the target containing host genomic DNA or common polymerase inhibitors present in the clinical sample (step 1) followed by immobilization streptavidin-coated magnetic nanoparticles (step2). After magnetic decantation and wash (Steps 3 and 4), magnetic beads bound target was used for downstream fluorescence-based and electrochemical in situ LAMP-based readouts (steps 5 and 6)

In the case of direct magneto capture followed by in situ amplification, 100 and 100 copies of plasmid DNA (in an aqueous sample) which contains the RdRp gene was detected at a cycle threshold value of 51±1.4 and 43.1±2.7, respectively (Fig 3.3B, amplification curve analysis in Fig 3.4A) The positive control was amplified at a cycle threshold value of 13.8±4.9. On the other hand, while doing in situ amplification using indirect magneto capture, 100 copies and 1000 copies of plasmid DNA which contains the RdRp gene, was amplified at a cycle threshold value

of 25.3±12.1 and 18.1±5.3, respectively (Fig 3.3B, amplification curve analysis in Fig 3.4B). Though 100 and 1000 copies of DNA in the aqueous sample were successfully detected with the two magneto extraction method, a significant difference was found between the cycle threshold values obtained from direct and indirect magneto-extraction. Therefore, indirect magneto-extraction was used for the downstream studies.

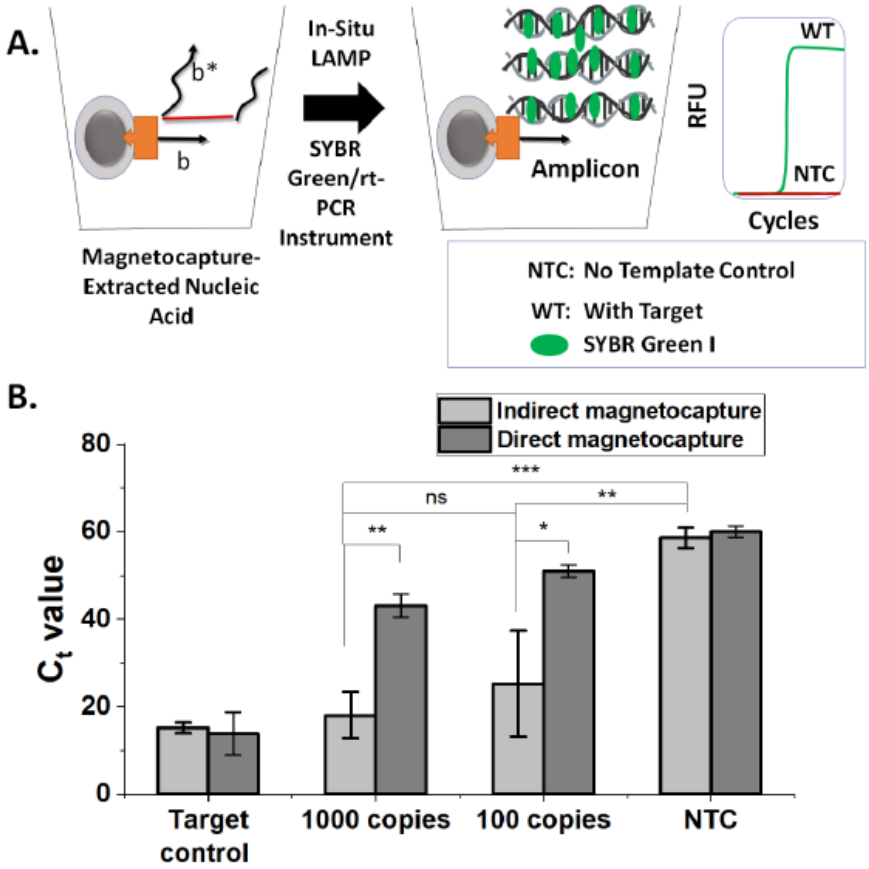

Fig 3.3: Comparison of sequence-specific direct and indirect magnetocapture followed by real-time LAMP to quantify 100 and 1000 copies of SARS-CoV-2 gene (RdRp) containing plasmid in aqueous solution. A, Scheme of the assay. B, Comparison of the Ct value (cycle threshold) for sequence-specific indirect and direct magnetocapture of 100 and 1000 copies of SARS-CoV-2 plasmid obtained from real-time LAMP. Error bars represent standard deviation (n=3). *P ≤ 0.05, **P ≤ 0.01, ***P ≤ 0.001, ****P ≤ 0.0001

In the sequence-specific indirect magneto capture, the free biotinylated probe had a higher chance of annealing with the target than the magnetic beads immobilized Biotinylated probe employed for direct magneto capture. In previous studies also indirect magnetocapture showed better efficiency in terms of annealing with the target. Besides that, indirect magnetocapture is a much

faster and simpler procedure than the direct method as the former does not require the blocking step of magnetic particles to avoid nonspecific binding during the magnetocapture assay. Despite these advantages of indirect magneto capture, this method has some probability to carryover contamination during insufficient washing, which causes nonspecific or false-negative amplification. We tried to explore the efficiency of direct and indirect magnetocapture efficiency in further studies where target plasmid DNA was spiked with host genomic DNA or serum in an aqueous sample.

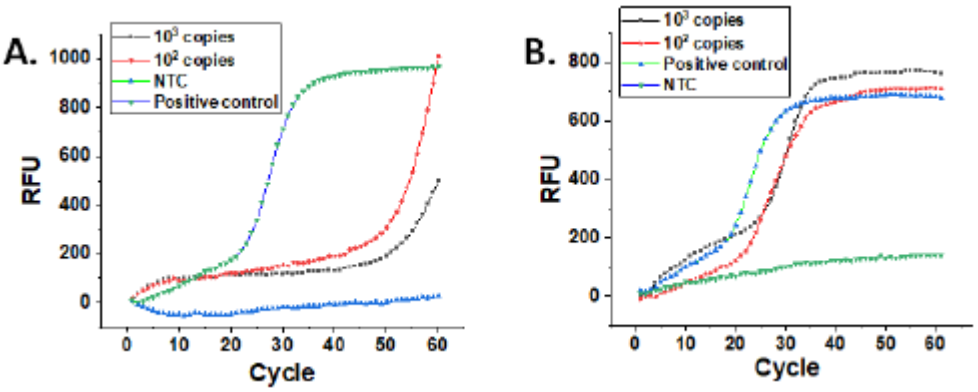

Fig 3.4: Real-time LAMP amplification profile of sequence-specific direct and indirect magnetocapture. A, Amplification curve of direct magnetocapture of RdRp gene-containing plasmid (100 and 1000 copies in 40 µL). B, Amplification curve of direct magnetocapture of RdRp gene-containing plasmid (100 and 1000 copies in 40 µL)

3.3.3 Detection of SARS-CoV-2 RdRp plasmid DNA from gDNA- and serum-spiked samples

Target nucleic acid in clinical samples often presents with different matrices like serum, swab, sputum, and saliva which contains various polymerase inhibitors. The presence of these polymerase inhibitors in the clinical sample interferes with the downstream amplification procedure. The serum is also part of viral transport media (VTM). So the main aim was to investigate the effectiveness of direct and indirect sequence-specific magnetocapture followed by in situ amplification with the 1000 and 100 copies (both in 40 µL) of RdRp gene-containing plasmid in presence of human genomic DNA and the presence of 10% fetal bovine serum. Non-template control assay also includes the presence of human gDNA and serum in the initial step followed by in-situ amplification. In each case, the assay was performed on 100 and 1000 copies of plasmid DNA present in 40 µL solution to determine the analytical sensitivity of the assay.

The annealed target with 5’ biotinylated oligonucleotides was captured with streptavidin-coated MNP, followed by in-situ amplification (Fig 3.5A). As expected, the pure plasmid DNA (positive control) had the lowest C_t values. The C_t value magnitude of 100 and 1000 copies of plasmid in the human genomic spiked sample (Fig 3.5B, amplification plot in Fig 3.6A, melt curve analysis in Fig 3.6C) and serum spiked sample (Fig 3.5C, amplification plot in Fig 3.6B, melt curve analysis in Fig 3.6D) are slightly higher for both direct and indirect sequence-specific magnetocapture. The detection limit of the target gene was 2.5 copies/μL for both host genomic DNA spiked and serum spiked samples. At the same time, the turnaround time for capture integrated with amplification was 1 hour.

The slightly higher C_t value might be attributed to the minute amount of polymerase inhibitor present in the sample. More washes during magnetic decantation (step 4, scheme 3.1, and scheme 3.2) might eliminate the polymerase inhibitors, thus lowering the C_t value. As demonstrated for plasmid DNA in the aqueous sample, the C_t value of the direct magnetocaptured target is higher than the indirect magnetocaptured target. These experiments validate the supremacy of indirect sequence-specific magnetocapture over direct sequence-specific magnetocapture in terms of target binding followed by in situ real-time LAMP amplification for detecting 1000 and 100 copies of RdRp gene-containing plasmid (detection limit 2.5 copies/μL, 4.1 aM).

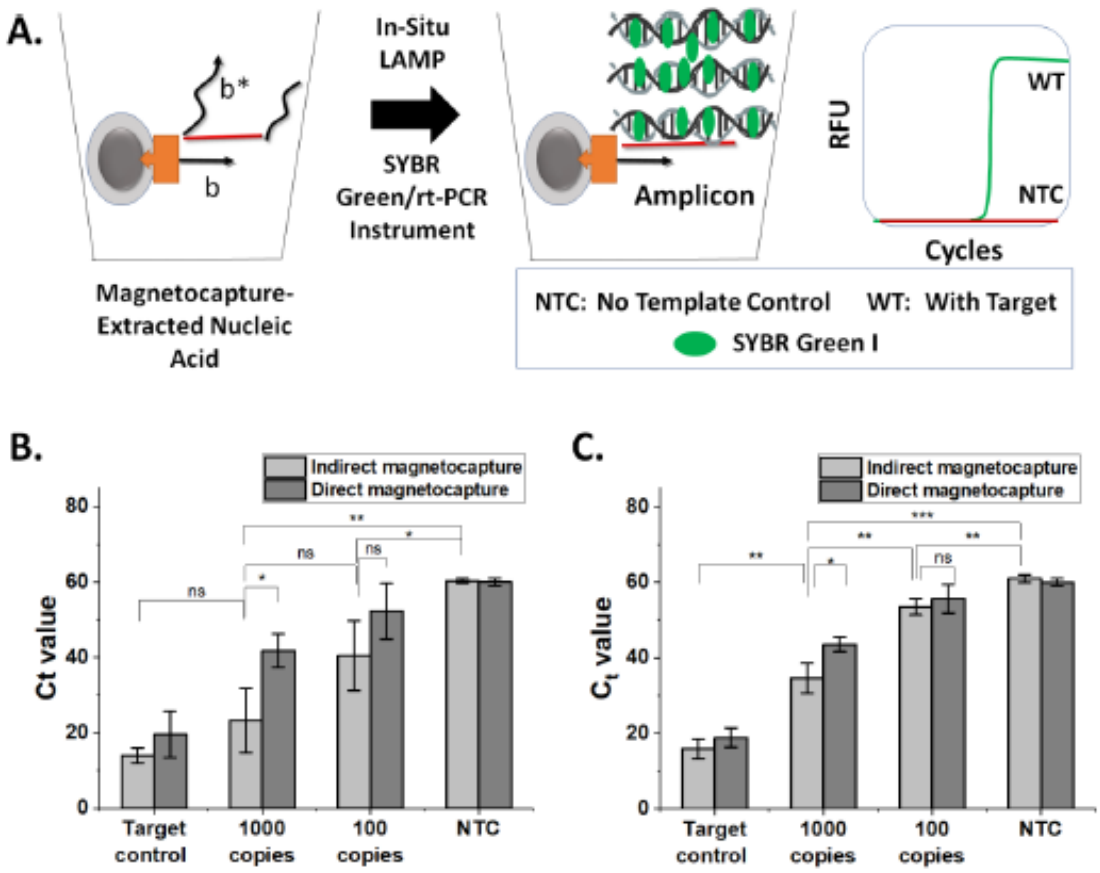

Fig 3.5: In-situ real-time LAMP amplification of magnetocaptured target nucleic acid in the presence of excess host genomic DNA and with the serum to investigate the assay's sensitivity. A, Scheme of the assay. B, In-situ real-time LAMP amplification of magnetocaptured target nucleic acid in the presence of excess host genomic DNA to investigate the assay's sensitivity**.** C, In-situ real-time LAMP amplification of magnetocaptured target nucleic acid in the presence of complex biofluid. For both of the cases, successful beads amplification was seen. This assay can detect as low as 2.5 copies /µL for both cases

3.3.4 Detection of SARS-CoV-2 RdRp RNA spiked with hgDNA and serum

The 5′- and 3′-terminal fragments contained the T7 RNA polymerase promoter upstream of the target plasmid (Fig 3.7A) at the 3′ end and the restriction endonuclease cleavage site SnaB-I downstream of the poly (A) sequence, To determine the analytical sensitivity of our approach we used in-vitro transcription assay using T7 RNA polymerase promoter. Firstly the target plasmid was digested with the SnaB-I enzyme (Fig 3.7B). Then the linearized plasmid was used as a template for in-vitro transcription (Fig 3.7D). Complementary DNA (cDNA) was made from the resulting RNA (Fig 3.7C) to obtain the actual RNA concentration for further experiments from

the qPCR standard curve employed with the target plasmid. RdRp gene-specific qPCR primers were used for obtaining the standard curve with the 10^1-10^6 copies of the target plasmid. 400 fold diluted cDNA was used as unknown and sought to have a $10^{5.55}$ copy number while calculating from the standard curve (Fig 3.7C). We deduced the concentration of in vitro transcribed mRNA from that data, which sought to have a concentration of 10^8 copies/µL. The limit of the detection study was investigated by q-LAMP with primer set 2 (Table 3.3), and the sensitivity of LAMP with in-vitro transcribed RNA is less than 10 copy/µL (Fig 3.8).

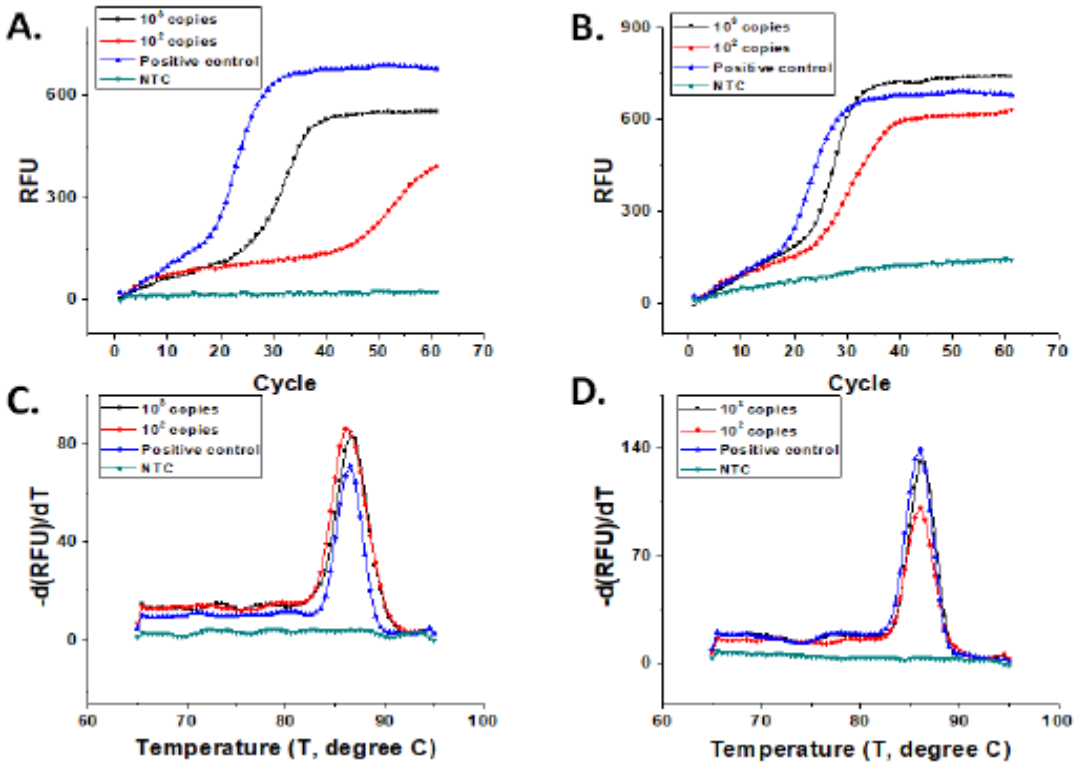

Fig 3.6: A, Amplification plot of in situ amplification of SARS-CoV-2 plasmid spiked with excess host genomic DNA. B, Amplification plot of in situ amplification of SARS-CoV-2 plasmid spiked with 10% fetal bovine serum (FBS). C, Melt curve analysis for a limit of detection study using SARS-CoV-2 plasmid spiked with human genomic DNA. From the melt curve peak, it can be deduced that the assay can sense as low as 100 copies in 40 µL which means 2.5 copies/µL. D, Melting curve analysis for the limit of detection study using SARS-CoV-2 plasmid spiked with 10% fetal bovine serum (FBS), a PCR inhibitor. This solid phase support assisted in situ LAMP amplification for this scenario and also can detect as low as 2.5 copies/ µL

Table 3.3: qPCR primers of RdRp gene

Primer name	**Sequence (5'-3')**
RdRp Forward Primer	ACACAATGGCAGACCTCGTC
RdRp Reverse Primer	CAAAGCTTGGCGTACACGTT

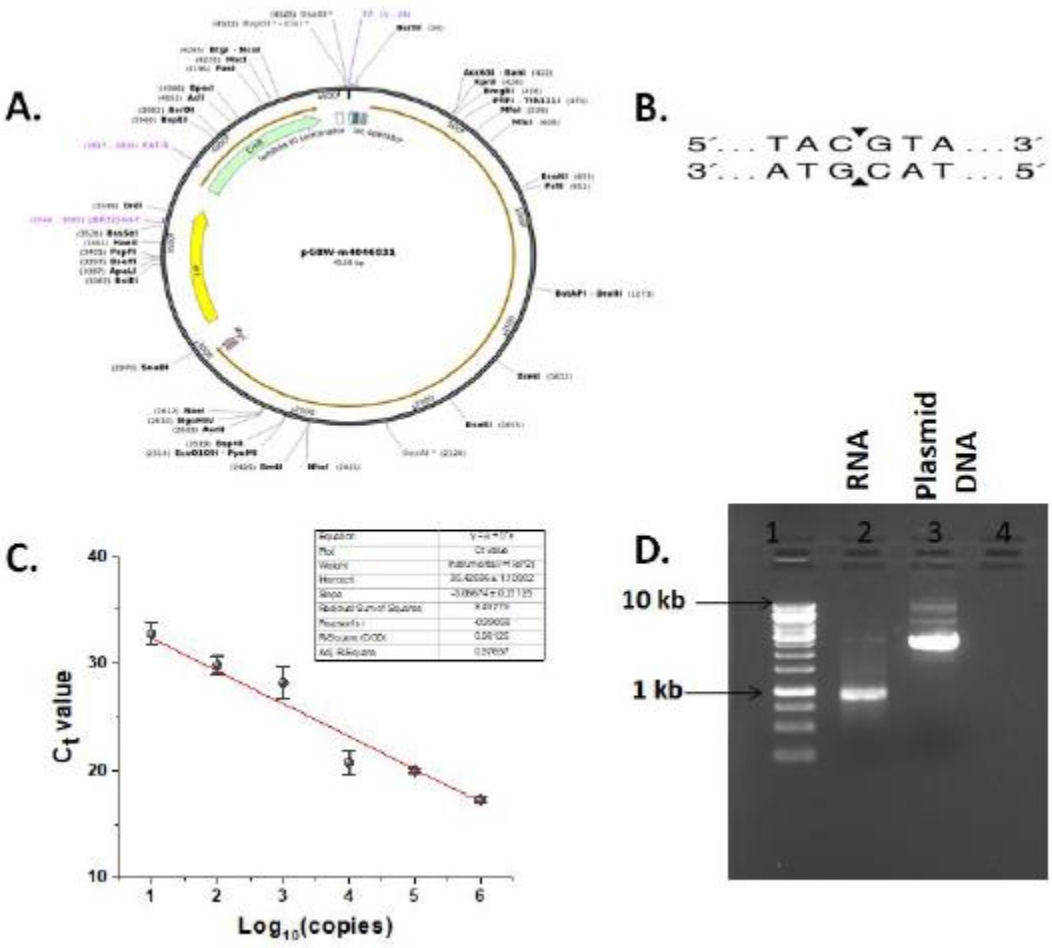

Fig 3.7: RdRp gene in vitro transcription and quantification. A, SARS-CoV-2 plasmid map (https://www.addgene.org/145671/). B, SnaB-I cutting site. C, In-vitro transcribed mRNA quantification by qPCR. D, Gel for in-vitro transcribed RNA

We further investigated whether the magnetic bead-mediated sequence-specific capture followed by in situ amplification could be utilized for detecting clinically relevant concentrations of RNA containing the RdRp gene of SARS-CoV-2.

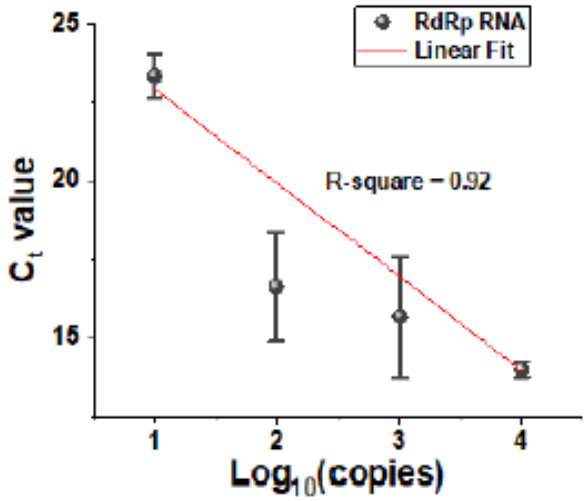

Fig 3.8: Limit of Detection of RNA by quantitative real-time reverse transcription LAMP (qRT-LAMP) using pure RNA as a template for concentrations 10^1-10^4 copies/reaction

The detection of in vitro transcribed RNA carrying the RdRp gene of SARS-CoV-2 was investigated for magnetocapture, followed by one step amplification procedure. Similar to indirect capture of SARS-CoV-2 plasmid DNA, 100 – 1000 copies of RNA present in 40 µL aqueous media, human genomic DNA spiked aqueous solution, or serum-spiked sample was annealed with the 5' biotinylated probe oligonucleotide and then immobilized on streptavidin magnetic beads (Fig 3.9A). Following washing (for removal of inhibitor and non-target nucleic acid), the beads were subjected to in situ qRT-LAMP where one strep reverse transcriptase LAMP was employed for amplification. For the magnetocapture of the aqueous RNA sample, 100 and 1000 copies of target RNA were detected with a cycle threshold value of 45.1±8.1 and 32.4±4.1, respectively (Fig 3.9B, amplification and melt curve analysis at Fig 3.10A and 3.10C respectively). 1000 copies of non-magneto captured RNA were used as positive template control, which showed a cycle threshold value of 9.3±2.3, while non-template control showed a cycle threshold value of more than 60.

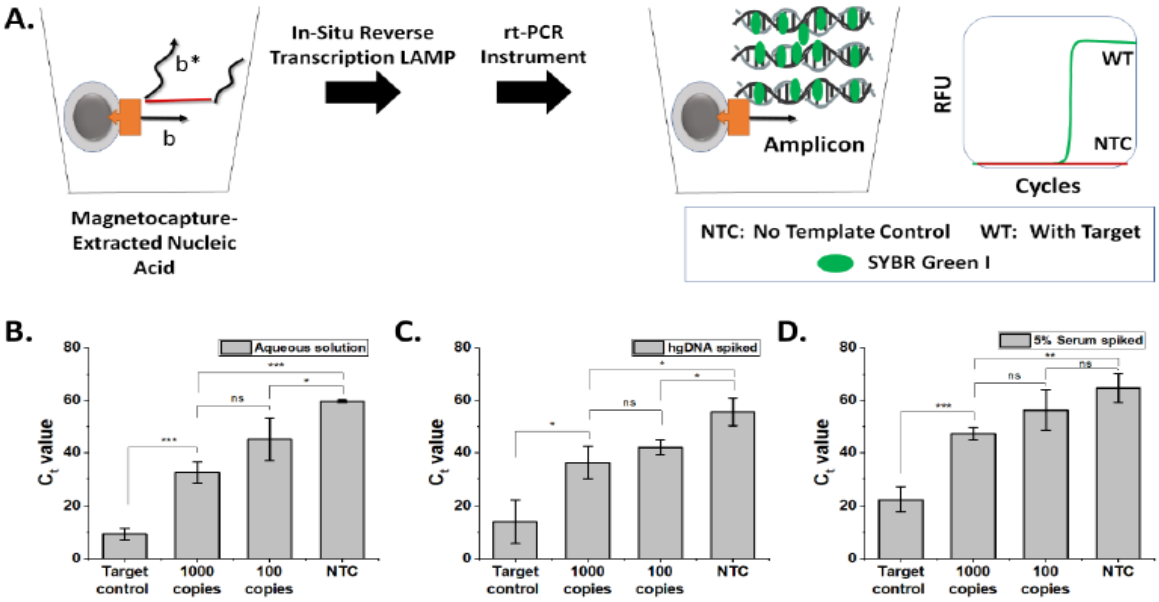

Fig 3.9: Detection of clinically significant copy numbers of SARS-CoV-2 RNA in an aqueous sample, spiked with host genomic DNA (1 ng) and PCR inhibitors (5% serum) using indirect magneto capture by qRT-LAMP. **A**, Scheme of the assay. **B,** Determination of LoD of target RNA by in-situ reverse transcriptase LAMP (containing SARS-CoV2 RdRp gene) in an aqueous sample. **C**, In-situ reverse transcriptase LAMP amplification of magnetocaptured target nucleic acid in presence of excess host genomic DNA to investigate the assay's sensitivity. **D**, In-situ reverse transcriptase LAMP amplification of magnetocaptured target nucleic acid in the presence of complex biofluid (mimicking clinical sample)

Next, we investigated the detection of RNA present in the serum-spiked sample. This assay was highly important as the 5% serum spiked aqueous sample resembled the composition of the nasopharyngeal swabs sample transporting VTM used in SARS-CoV-2 diagnosis. The assay efficacy and turnaround time would be predictive of those used in actual clinical sample detection. In this assay, however, we detected little or no amplification from the magnetocapture of RNA from a 5% serum spiked solution. (Fig 3.11).

From the previous reported scientific reports, we found that RNA has a half-life of 15 seconds in the presence of serum. So, the analytical sensitivity dropped to 2000 fold lower than pre-extracted RNA from the clinical sample (reference). As RNase present in serum may cause RNA degradation, used RNAse inhibitor and 25mM EDTA to check the effect of those to protect RNA against serum. We found that prior incubation of RNAase inhibitor with serum followed by addition of RNA in 25 mM EDTA has a better RNA protection (reference)

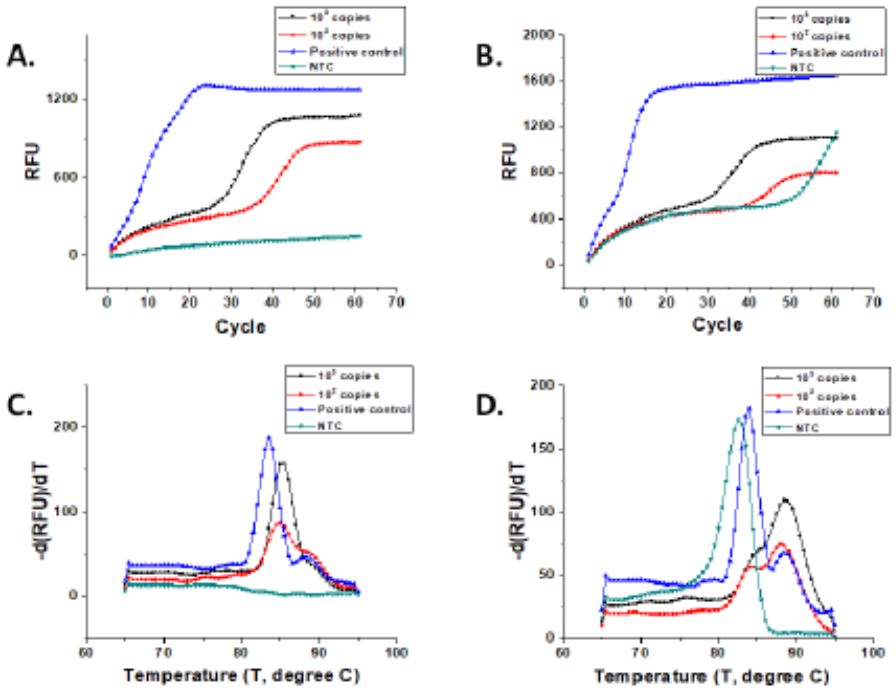

Fig 3.10: Amplification and melt curve analysis of 100 and 1000 copies of in-vitro transcribed RNA present in an aqueous sample and excess host genomic DNA (1 ng). **A**, Amplification plot of in vitro transcribed mRNA (from SARS-CoV2 RdRp gene-containing plasmid) in an aqueous solution. **B**, Amplification plot of in vitro transcribed mRNA in the presence of excess host genomic DNA. **C**, Melt curve analysis for the limit of detection study using mRNA (transcribed from SARS-CoV2 plasmid) in an aqueous solution. From the melt curve peak, it can be deduced that the assay can sense as low as 100 copies in 40 µL which means 2.5 copies/µL. **D**, Melt curve analysis for the limit of detection study using mRNA (transcribed from SARS-CoV2 plasmid) spiked with human genomic DNA

With the stated optimization and same magnetocapture method described above, we assessed the efficacy of the magnetocapture-amplification to detect 100 and 1000 copies of RNA in a 40 µL RNA-EDTA-serum mixture. The cycle threshold value was relatively higher than (100 and 1000 copies of RNA in 40 µL aqueous solution in the presence of 5% serum amplified at a C_t value of 56.2±7.7 and 47.3±2.2 respectively, Fig 3.9D, amplification and melt curve plot in Fig 3.12) the cycle threshold value obtained from RNA in aqueous solution and spiked with excess host genomic DNA.

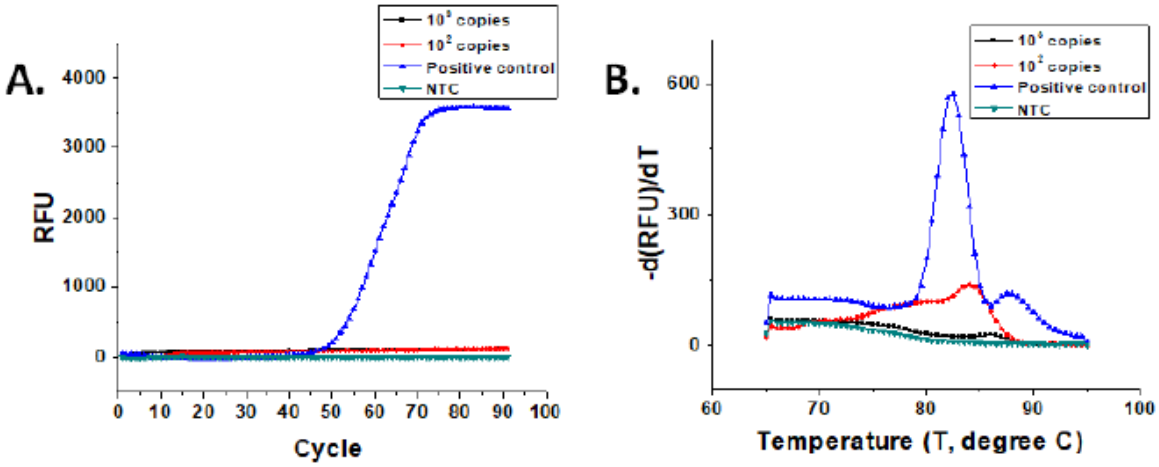

Fig 3.11: qRT-LAMP amplification profiles and melt curve analysis of indirect sequence-specific magnetocapture of SARS-CoV-2 RdRp RNA from aqueous solution spiked with serum (5% v/v). **A**, Representative amplification profile of indirect magnetocapture of SARS-CoV-2 RdRp RNA (1000 and 100 copies in 40 µL) in the serum-spiked aqueous sample followed by in situ qRT-LAMP. **B,** Melt curve analysis for qRT-LAMP assays

The higher C_t value in the presence of serum is probably due to the degradation of target RNA in the presence of serum which causes a slightly longer assay turnaround time (2 hours).

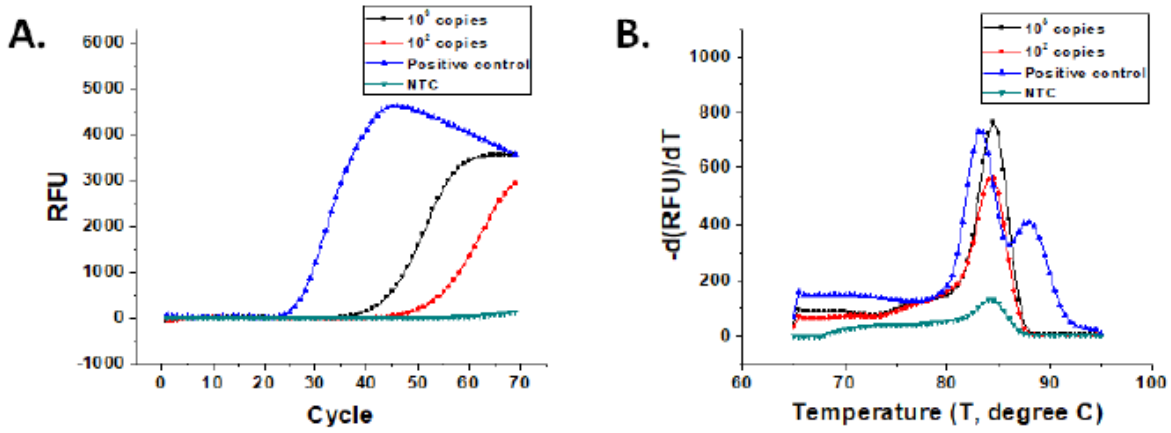

Fig 3.12: A, Amplification plot of a limit of detection studies (in-situ LAMP) with in-vitro transcribed mRNA(1000 and 100 copies) in 25mM EDTA spiked with 5% serum (generally used in VTM). B, Melting curve analysis of in-situ LAMP with in-vitro transcribed mRNA(1000 and 100 copies) in 25mM EDTA spiked with 5% serum

3.3.5 Detection of SARS-CoV-2 plasmid DNA and RNA using sequence-specific indirect magneto-extraction and electrochemical LAMP

Next, we examined the detection of 100 and 1000 copies of RdRp plasmid DNA or RNA using the indirect magneto-extraction integrated LAMP with end-point electrochemical readout. Electrochemical detection of NAATs is advantageous as it facilitates nucleic acid-sensing without bulky instruments like real-time PCR. However, the performance of such electrochemical NAAT sensing systems should also match their gold standard fluorescence-based real-time PCR instrument counterparts. With this objective, we investigated whether the proposed sequence-specific indirect magneto-extraction is amenable to downstream electrochemical end-point LAMP (eLAMP) or electrochemical reverse transcription end-point LAMP (eRT-LAMP) readout on a commercial screen-printed electrode. The methylene blue reagent was utilized as the electron mediator due to its superiority over other electrochemical NAAT redox mediators such as sodium molybdate or osmium tetroxide. Similarly, square wave voltammetry (SWV) was applied due to its proven greater sensitivity thanks to minimal capacitive and background currents. In principle, the presence of an amplicon would prevent the methylene blue-mediated electron transfer to the electrode, thereby reducing the current signal (Fig 3.13A).

Additionally, an increasingly greater amount of template copies in the reaction would generate a higher amount of amplicon. This would trap more methylene blue and cause a successively lesser current transfer to the electrode, generating a gradually lower signal. The same results could alternatively be observed through the increasing magnitude of the signal % change ($S(I) = (I_0 - I_1) \times 100/I_0$). Here, I_0 and I_1 were the current signals generated from samples corresponding to the NTC and target containing samples, respectively. The S(I) thus represented the relative change in the current signal compared to the NTC samples.

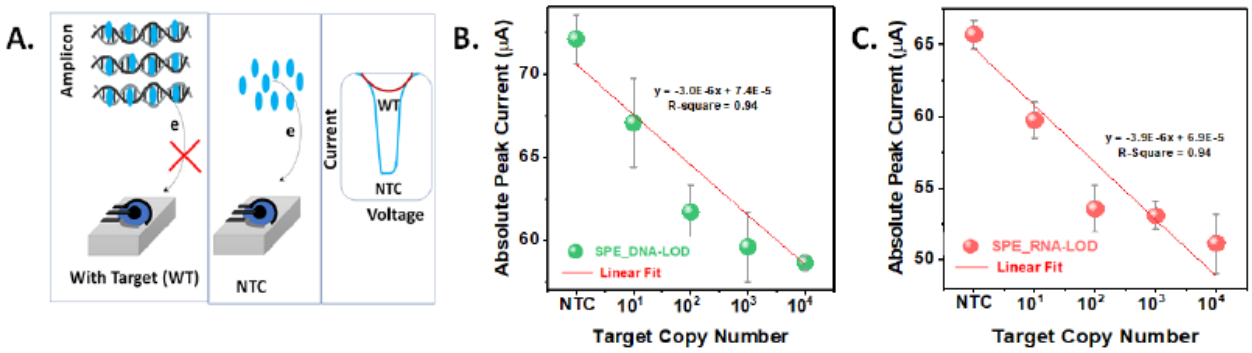

Fig 3.13: Electrochemical LAMP studies were conducted on pure 10^1 – 10^4 copies of nucleic acid (without magnetocapture). **A,** Mechanism of amplicon-mediated methylene blue sequestration and subsequent reduction of current. **B,** LoD for eLAMP on pure 10^1 – 10^4 copies SARS-CoV-2 RdRp plasmid DNA/reaction. **C,** LoD for eRT-LAMP on pure 10^1 – 10^4 copies SARS-CoV-2 RdRp RNA. NTC assays comprised of eLAMP or eRT-LAMP without any template nucleic acid addition

Accordingly, eLAMP or eRT-LAMP assay involving pure (i.e., without magnetocapture) 10^1 – 10^4 copies of DNA and RNA showed a gradually decreasing peak current signal that was progressively lower than the negative template control or NTC (Fig 3.13B and Fig 3.13C). The Comparison of peak current signal with NTC was thus utilized to assess the detectability of the target nucleic acid. Similarly, the signal % change also demonstrated a gradual increase in S(I) with increasing concentrations (Fig 3.14). In the magneto-extraction assisted amplification as well, the eLAMP current signal for 10^2 – 10^3 copies was compared with NTC assays performed with a target nucleic acid-free magneto-extraction. A current signal difference of 100 – 1000 copies of nucleic acid compared to NTC would reflect the sensing approach's effectiveness. Besides NTC, an internal target control (TC) comprising of an eLAMP (or eRT-LAMP as relevant) with pure (i.e., without magnetocapture) 10^3 copies of plasmid or RNA (as applicable) was included in each assay.

The significant difference in peak current signal for magneto-extraction of target plasmid from aqueous, hgDNA spiked, and serum spiked samples validated the compatibility of indirect magneto-extraction with eLAMP (Fig 3.15B and Fig 3.15C). The peak current signal difference between NTC and 100 – 1000 copies of plasmid reproducibly remained in 15 – 25 µA. (approximately 30 – 50% in signal % change, Fig 3.16A).

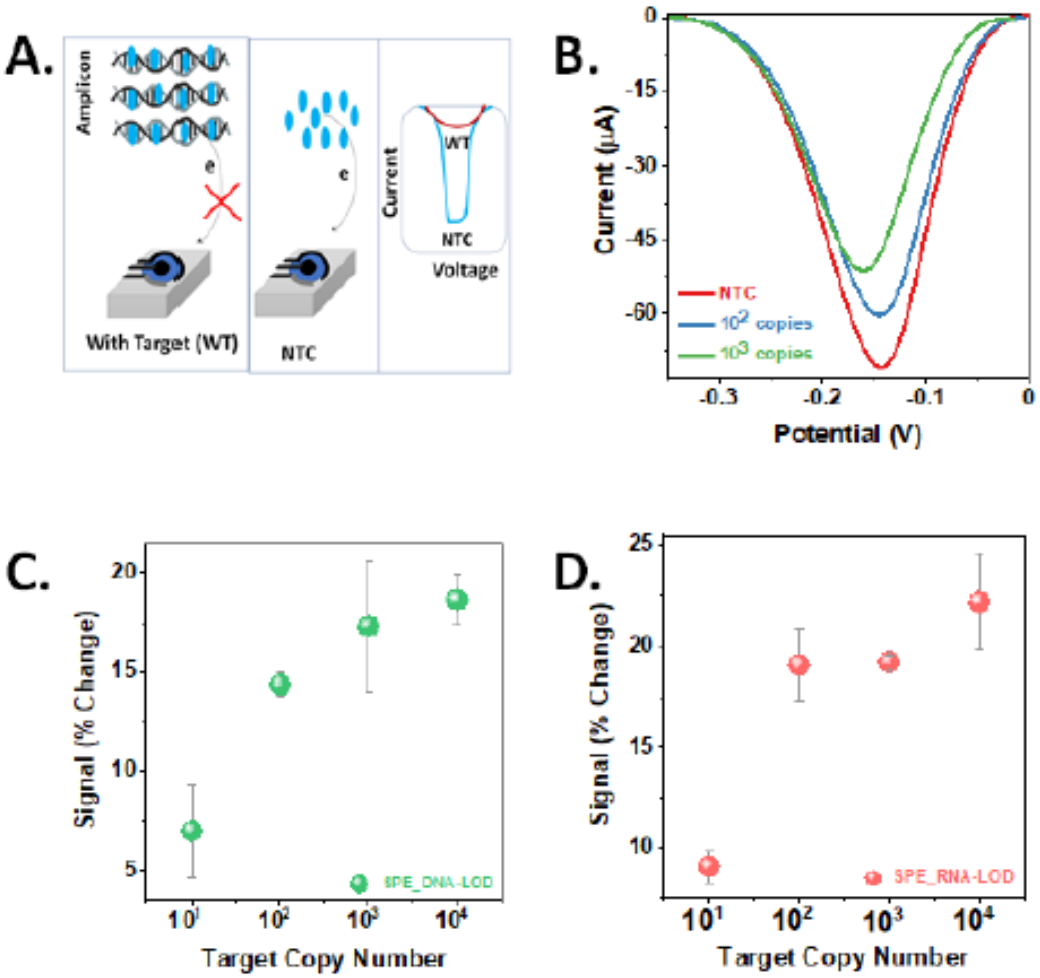

Fig 3.14: Representative electrochemical LAMP and LoD for eLAMP or eRT-LAMP amplification involving using pure SARS-CoV-2 RdRp plasmid DNA or RNA as the template. **A**, Mechanism of amplicon-mediated methylene blue sequestration and subsequent reduction of current. **B,** Representative current profile of eRT-LAMP detection of 10^2 - 10^3 copies of pure RdRp RNA and NTC using SWV. **C,** LoD for eLAMP on pure 10^1 – 10^4 copies SARS-CoV-2 RdRp plasmid DNA/reaction using signal % change. B, LoD for eRT-LAMP of pure 10^1 – 10^4 copies SARS-CoV-2 RdRp RNA/reaction using signal % change

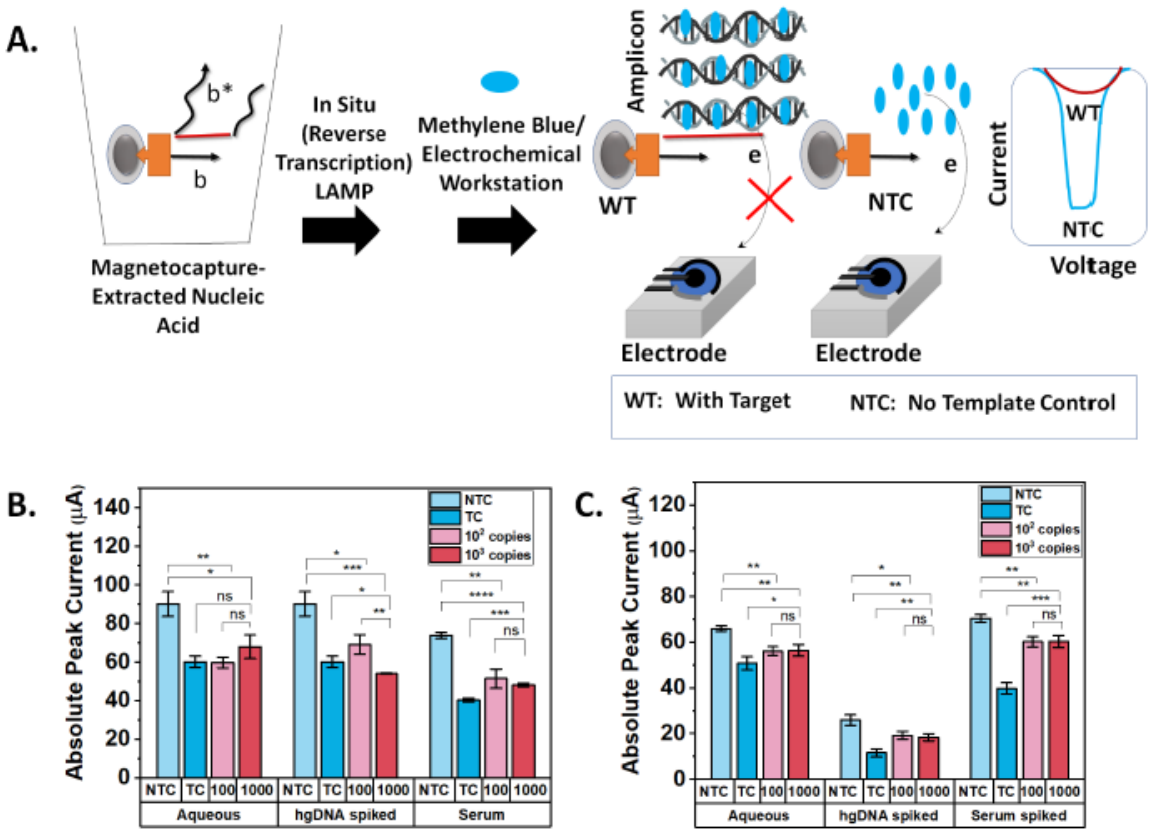

Fig 3.15: Indirect sequence-specific magnetocapture of 100 and 1000 copies of SARS-CoV-2 RdRp plasmid DNA and RNA from aqueous media, or aqueous sample spiked with hgDNA (1 ng), or serum followed by in situ electrochemical end-point (reverse transcription) LAMP (eLAMP or eRT-LAMP). **A,** Scheme of in situ eLAMP with magnetocaptured 100 and 1000 copies of SARS-CoV-2 RdRp plasmid DNA or RNA. **B,** Indirect magnetocapture of 100 and 1000 copies of SARS-CoV-2 RdRp plasmid DNA from aqueous solution or aqueous sample spiked with hgDNA (1 ng), or serum (10%, v/v) followed by in situ eLAMP. **C,** Indirect magnetocapture of 100 and 1000 copies of SARS-CoV- 2 RdRp RNA from aqueous solution or aqueous sample spiked with hgDNA (1 ng), or serum (5%, v/v) followed by in situ eRT-LAMP. Target control (TC) eLAMP or eRT-LAMP experiments were performed with 10^3 RdRp DNA or RNA copies, respectively (without any magnetocapture). NTC assays comprised magnetocapture experiments carried out without any target DNA or RNA followed by eLAMP or eRT-LAMP, respectively. Error bars represent standard deviation (n = 3). *P ≤ 0.05, **P ≤ 0.01, ***P ≤ 0.001, ****P ≤ 0.0001

Although the detection of 100 copies of plasmid was expected to produce a higher current signal than 1000 copies, the signal difference between the detection of magneto-extracted 100 and 1000 copies themselves was not statistically significant. Similarly, for the RdRp RNA magneto-extraction-amplification, a lesser, albeit still statistically significant, current difference (7 – 10 μA) was observed compared to their respective NTCs. This lesser difference in current compared

to NTC (12 – 30% in terms of signal % change, Fig 3.16B) was probably due to partial RNA degradation, resulting in a lesser amplicon generation. It led to a higher quantity of free methylene blue mediator in the solution, causing reduced current difference with NTC. Similar to plasmid DNA magneto-extraction, RNA detection could also not differentiate between 100 – 1000 copies of magneto-extracted RNA. While the experiments thus validated the magneto-extraction amplification assays for both plasmid DNA and RNA, they could not distinguish between magnetocaptured 100 – 1000 copies of nucleic acid, an aspect to be improved in future developments (please see below for rationalization).

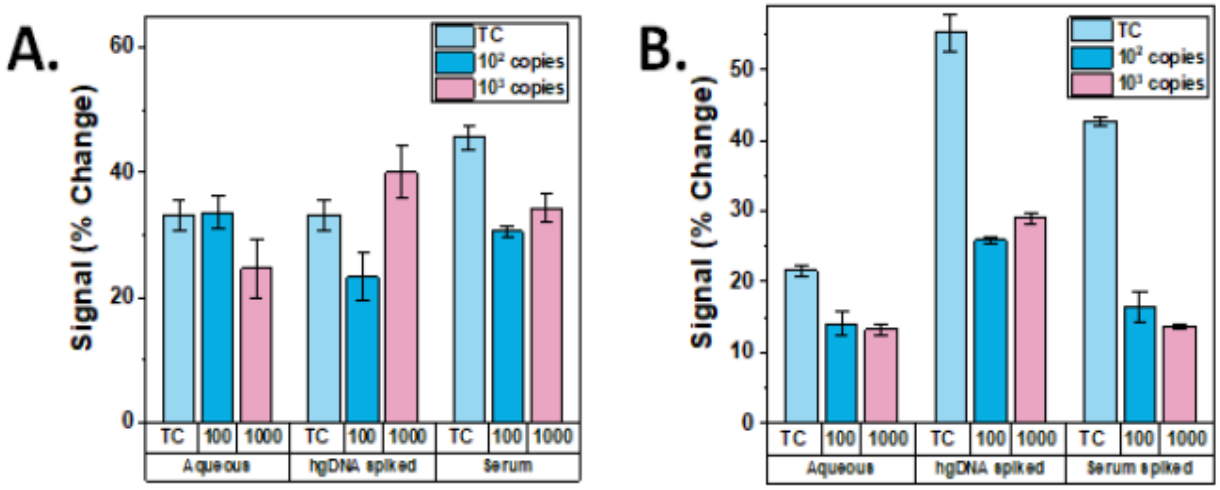

Fig 3.16: Signal % change-based analysis of indirect sequence-specific magnetocapture efficiency for extracting 100 and 1000 copies of SARS-CoV-2 *RdRp* plasmid DNA and RNA from aqueous media, aqueous sample spiked with hgDNA (1 ng), or serum followed by in situ electrochemical end-point (reverse transcription) LAMP (eLAMP or eRT-LAMP). AnIndirect magnetocapture of 100 and 1000 copies of SARS-CoV-2 *RdRp* plasmid DNA from aqueous solution or aqueous sample spiked with hgDNA (1 ng), or serum (10%, v/v) followed by in situ eLAMP. B, Indirect magnetocapture of 100 and 1000 copies of SARS-CoV-2 *RdRp* RNA from aqueous solution or aqueous sample spiked with hgDNA (1 ng), or serum (5%, v/v) followed by in situ eRT-LAMP. Error bars represent standard deviation (n = 3)

The assay performance for rescuing and detecting target nucleic acid from aqueous, hgDNA spiked, and serum spiked samples was equivalent to that of the real-time fluorescence readout. Both provided detections for at least 2.5 copies/ µL targets. Overall, the indirect magneto-enrichment followed by eLAMP thus successfully detected clinically relevant concentration (2.5

copies/µL or 4.1 aM) of target SARS-CoV-2 nucleic acid with a sample-to-answer turnaround time of 2 h.

3.4 Conclusion

This work addressed several critical issues currently concerning the NAAT molecular diagnosis: the requirement of RNA extraction to remove polymerase inhibitors, the use of TaqMan probe for specificity, thermal cycling, and the necessity of a centralized real-time PCR machine. While isothermal amplification such as LAMP partially addresses some of these challenges, their optimal performance is dependent on the presence of pure nucleic acid as a template. Therefore, using the pure nucleic acid template, LAMP cannot overcome the need for an instrument-intensive nucleic acid extraction step in the workflow. It also does not address the need for sequence-recognizing reporter molecular beacon-like probes for specificity.

This work is presumably the first study demonstrating an electrochemical LAMP (eLAMP) involving pure SARS-CoV-2 nucleic acid. It is also novel in proving the superiority of indirect sequence-specific magneto-preconcentration (followed by in situ LAMP) over direct magneto-preconcentration in nucleic acid NAAT biosensing. It is the first to do so with LAMP as the downstream NAAT. In addition, the developed assay would probably be the first to demonstrate its effectiveness in magneto-extracting and then detecting SARS-CoV-2 nucleic acid mixed with real life-simulating sample involving the field application-friendly electrochemical readout.

This study is probably the first to quantitatively evaluate the role of hgDNA and serum-based polymerase inhibitors on sequence-specific direct and indirect magneto-extraction and downstream NAAT. It also compared magnetic preconcentration-assisted electrochemical LAMP with that of a magnetocapture combined with a real-time fluorescence LAMP. The process conclusively demonstrated their equivalent analytical sensitivity, which enhanced the operational flexibility of the overall workflow. Furthermore, it quantitatively compared (for the first time in published literature, to the best of our knowledge) the sequence-specific magneto- extraction-LAMP assay with that of LAMP using the pure nucleic acid template. Doing so demonstrated that the former has a similar or superior performance to the latter in detecting clinically relevant 100 copies of target nucleic acid in terms of turnaround time and assay cost. The study is general and could be extended to detect non-SARS-CoV-2 pathogens as well. Similarly, the indirect

sequence-specific magnetic enrichment could also be integrated with other NAATs. Overall, our assay provided a sensitive, low-cost, near-point-of-care, sample-to-answer, and non-instrument-intensive method for detecting pathogen nucleic acid.

3.5Materials and Methods

3.5.1 Materials

Escherichia coli str. K-12 substr. MG1655 plasmid construct with RNA dependent RNA polymerase (*RdRp*) gene with T7 RNA polymerase promoter (4538 bp) was purchased from Addgene (plasmid #14567, https://www.addgene.org/145671/)**.** The Bst 2.0 polymerase, RTx enzyme, dNTP, and SnaBI were procured from NEB, USA. The SYBR I (10,000X concentrated) was purchased from Invitrogen, USA. Molecular biology grade water was purchased from HiMedia, India. The RNase inhibitor was purchased from Takara. Streptavidin-coated magnetic beads were purchased from Sigma-Aldrich (# 11641778001) or Invitrogen (Dynabeads M-280). 5′-biotinylated probe having the b sequence (5'-[BIO]-AAA AAA AAA ACG AGC AAG AAC AAG TGA GGC CAT AAT TC, HPLC purified) was purchased from Sigma-Aldrich. Primer oligonucleotides (desalting purified) were purchased from Eurofins or Sigma-Aldrich, India.

3.5.2 LAMP reaction and primer optimization using real-time fluorescence readout

A real-time quantitative LAMP (qLAMP) experiment was performed on 10^3 copies of ORF1ab containing a plasmid with three sets of primers. The final LAMP reaction (20 µl) contained the three primer pairs in the following final concentrations: 0.2 µM outer primers, and 1.6 µM forward and backward inner primers, 0.8 µM forward and back loop primers (for primer sets 1 and 3) [207], [208]. For primer set 2, 0.4 µM outer primers, 0.332 µM forward and backward inner primer, 1 µM forward loop primers, and 0.4 µM back loop primers were utilized in final concentration [209]. The reaction mixture also contained 2.0 µL of 10× Bst 2.0 DNA polymerase reaction buffer [1× containing 20 mM Tris-HCl, 50 mM KCl, 10 mM $(NH_4)_2SO_4$,2 mM $MgSO_4$, 0.1% Tween-20, pH 8.8], 1.4 mM dNTPs, 2.0 µLSYBR I (final concentration 1X diluted from 10,000X stock), 0.5 µLof an 8 U µl concentration of Bst 2.0 DNA polymerase, 6 mM $MgSO_4$ and 1 µl template (alternatively, 2 µL magnetic bead for magnetocapture assays). For quantitative real-time reverse transcription LAMP (qRT-LAMP), 7U (0.25 µL) of reverse transcriptase RTx

(NEB) was additionally added to the above. The qLAMP (or qRT-LAMP) reaction was set at the following settings for each cycle with a fluorescence monitoring step, 65˚C for 1 minute for primer set 1, 64˚C for 1 minute for primer set 2, 60˚C for 1 minute for primer set 3 followed by thermal melting analysis step. The cycles were repeated 60 times (unless otherwise stated) in a CFX Maestro or CFX Connect real-time PCR (rt-PCR) machine (BioRad).

3.5.3 Electrochemical LAMP (eLAMP) assays

For eLAMP or eRT-LAMP using the pure nucleic acid template, the assay was performed on 10^1 – 10^5 copies of nucleic acid (*RdRp* plasmid DNA or *RdRp* RNA)/25 µL of reaction. For magnetocapture followed by eLAMP or eRT-LAMP assays, 2 µL magnetic beads containing immobilized target nucleic acid were added to 25 µL electrochemical LAMP reaction having a composition as described below. A 25 µL eLAMP or eRT-LAMP reaction comprised of 2.5 µL of 10× Bst 2.0 DNA polymerase reaction buffer [1× containing 20 mM Tris-HCl, 50 mM KCl, 10 mM $(NH_4)_2SO_4$, 2 mM $MgSO_4$, 0.1% Tween-20, pH 8.8], 1.4 mM dNTPs, 0.4 µM outer primers, 0.332 µM forward and backward inner primer, 1 µM forward loop primers, 0.4 µM back loop primers (primer set 2), 0.5 µL Bst 2.0 polymerase, and 50 µM methylene blue.During magnetocapture followed by eLAMP or eRT-LAMP, 1000 copies of non-magnetocaptured plasmid DNA or RNA was used as the positive control. For eRT-LAMP, 7 U of reverse transcriptase (RTx) was also used for 25 µL of reaction. The assays were set at the following settings for each cycle, 64˚C for 1 minute for 60 cycles followed by heat inactivation at 80˚C for 20 minutes in a thermal cycler (Eppendorf). The resultant LAMP amplicons were electrochemically analyzed.

3.5.4 Method of plasmid digestion & in vitro transcription

1 µg target plasmid was linearized with 1 µL SnaBI enzyme (10 U/µL) and 1X NEB CutSmart buffer (50 mM Potassium Acetate, 20 mM Tris-acetate, 10 mM Magnesium Acetate, 100 µg/ml BSA pH 7.9 at 25°C) by incubating at 37^0C for 1 hour (final volume 50 µL). Next, the digestion was stopped by an additional enzyme inactivation step (80^0C for 20 mins). Next, 4 µL of the digested sample was loaded into 2% agarose gel to check the linearized product. 1 µg of digested plasmid was then added with 1X NTP buffer mix (NEB), 2 µL of T7 RNA polymerase in 20 µL reaction, and incubated at 37^0C for 2 hours. The resultant RNA product was cleaned with

Monarch® RNA Cleanup Kit (NEB) as per the manufacturer's instruction. Briefly, 100 µL of RNA clean-up binding buffer was added to the 50 µL sample obtained from the reaction. 150 µL of pure ethanol is added to the mixture and loaded into the column provided in the kit. After centrifugation at 13000 rpm for 1 minute, the column is again washed with 500 µL wash buffer and finally, the product was eluted in 50 µL nuclease-free water.

3.5.5 Method of RNA quantification by qPCR

cDNA was synthesized using the PrimeScript 1st strand cDNA Synthesis Kit (Takara) as per the manufacturer's instruction. Briefly, 1 µg RNA was mixed with 0.4 µL random hexamers, 1 mM dNTP mixture, and snap cooled (65^0C for 5 minutes followed by incubation in ice for 5 minutes, final volume 10 µL). Then, cDNA was synthesized with 1X prime script buffer, 100 U of reverse transcriptase, and template RNA primer mixture and was incubated at 30^0C for 10 minutes followed by 50^0C for 30 minutes (final volume 20 µL total). Parallelly a standard curve for copy numbers vs C_t value was generated by qPCR on plasmid DNA. The qPCR was performed to determine the cDNA concentration and analyzed using a CFX Maestro (BioRad) with SYBR Green Real-Time PCR Master Mix Plus (HiMedia) followed by thermal melting analysis. The primers were designed against the *RdRp* gene of the plasmid (Eurofins, please see sequences in Table S3). The cDNA was diluted 1/400 fold and subjected to qPCR to determine its concentration.

3.5.6 Direct sequence-specific magnetocapture followed by in situ LAMP

0.1 µM 5′-biotinylated probe oligonucleotide (having a b sequence) was first immobilized on the 10-µg streptavidin-coated magnetic nanoparticles for 20 minutes incubation. After incubation with wash-binding buffer (5 mM Tris-HCl, 0.5 mM EDTA, 1 M NaCl, pH 7.5) the biotinylated probe bound streptavidin-coated MNP was blocked with 1% BSA for 20 minutes. After three times of washing with wash-binding buffer, the probe-MNP complex was incubated (15 min, using vortex enabled mild shaking) with snap-cooled (65°C 5 min followed by cooling in ice for 5 min) 100 or 1000 copies of target plasmid carrying the *RdRp* gene (containing a b* sequence) in 40 µL 50 mM NaCl solution. For magnetocapture from hgDNA spiked sample, the plasmid was instead present in 40 µL 50 mM NaCl solution containing 1 ng MCF-7 extracted hgDNA and then subjected to magnetocapture as described. Similarly, for serum spiked samples, the plasmid

was instead present in 40 µL 50 mM NaCl solution containing 10% (v/v, for DNA capture) serum. For the negative control (NTC), water is used instead of plasmid during the magnetocapture. After three successive washes using magnetic decantation with 200 µL wash-binding buffer, the target nucleic acid bound MNP was resuspended in 10 µLnuclease-free water. 2 µL beads are used for 20 µL in situ qLAMP reactions as described above.

3.5.7 Indirect sequence-specific magnetocapture followed by in situ LAMP

In this method, 0.1 µM 5′-biotinylated probe oligonucleotides having b sequence were first annealed with 100 or 1000 copies of target plasmid or *RdRp* RNA copies in 40 µL 50 mM NaCl solution by heating at 65^0C (2 minutes), followed by ice (5 min) and then 15 min benchtop incubation at room temperature. For magnetocapture from hgDNA spiked sample, the plasmid or RNA was instead present in 40 µL 50 mM NaCl solution containing 1 ng MCF-7 extracted hgDNA and then subjected to magnetocapture as described. Similarly, for serum spiked samples, the plasmid or RNA was instead present in 40 µL 50 mM NaCl solution containing 10% (v/v, for DNA capture) or 5% (v/v, for RNA capture) serum (with or without the addition of RNase inhibitor and EDTA, see Supporting Information Section 8) and then subjected to magnetocapture as described (please see below for the protocol of RNA magnetocapture from RNase and EDTA treated serum). This step generates the plasmid (or RNA)-probe binary complex which is then followed by 15 min incubation (using vortex enabled mild shaking) with 10 µg streptavidin-coated MNP at room temperature. For the negative control (NTC), the magnetocapture was performed with the same solution but lacking the target nucleic acid. After three times washes with wash-binding buffer using magnetic decantation the target nucleic acid bound MNP has resuspended in 10 µl nuclease-free water. 2 µL beads were used for 20 µL in situ qLAMP/eLAMP as described above.

3.5.8 Method of magnetocapture of 100 and 1000 copies of in-vitro transcribed RNA from 5% serum spiked solution

6.6% fetal bovine serum (Gibco), 1.0 µL of RNase inhibitor, and 25 mM EDTA (final) are incubated together at 37˚C for 1 h to a final volume of 30µL. 100 and 1000 copies of RNA in an aqueous solution (final volume 10µL) was heated up to 65˚Cfor 2 minutes followed by immediate addition of preincubated EDTA-serum mixture (above) and 0.1 µM (final

concentration) of 5′-biotinylated probe oligonucleotides (sequence b) to a final volume of 40 µL and then cooled in ice. The rest of the magnetocapture procedure was identical to as described for indirect magnetocapture in the main manuscript.

3.5.9 Method of Electrochemical measurement

The samples were tested electrochemically using commercially purchased screen-printed electrodes (SPE) with carbon, carbon, and silver as working, counter, and quasi-reference electrodes, respectively. The electroanalytical study was performed via square-wave voltammetry (SWV) using Metrohm Autolab PGSTAT302N potentiostat/galvanostat. The voltage was swept from a range of 0 to -1 V for 5 consecutive cycles and the current was recorded simultaneously. All the electroanalytical data presented are averaged over 4 cycles, excluding the first cycle since an intense current was observed in the first cycle due to electric double layer (EDL) charging of the electrode. The percent signal change (S(I)) was calculated using this formula,

$$S(I) = \frac{I_0 - I_1}{I_0} * 100\ \%$$

Where I_0 and I_1 were the current signals generated from samples corresponding to the NTC and target containing samples, respectively.

CHAPTER 4

USE OF MAGNETIC BEAD DECORATED APTAMER COUPLED CATALYTIC DNA NANOWIRES FOR VIABLE BACTERIA DETECTION

4.1 Abstract

Proper detection and identification of infectious pathogens are crucial for human health and food safety. Current molecular assays for molecular diagnostic require high-end instruments and centralized labs, limiting their application to resource-limited areas. Aptamers are single stranded DNA or RNA molecules that can be used as binders to particular targets selected from a vast library and have the ability to bind with different non-nucleic acid targets. The unique character of the aptamer is that it binds with viable cells with a high affinity. This work utilized aptamer's binding affinity to capture viable *Staphylococcus aureus* from a biological sample. Firstly, we employed streptavidin coated magnetic nanoparticles to conjugate with biotinylated aptamers followed by pathogen capture from biological sample. After pathogen capture, we utilized a secondary aptamer with a pre-assembled hybridization chain reaction nanowire (DNAzyme is a part of nanowire which has catalytic activity in presence of hemin). ABTS, H_2O_2 chemistry was used to accomplish the colorimetry based readout where we have successfully detected 10^6 copies of *Staphylococcus aureus* from a biological sample.

4.2 Introduction

Immunoassays could also be used to detect the viable pathogen. However, those methods are still limited by the high cost and instability of antibodies, which play an important role in pathogen recognition. Aptamers were created through the systematic evolution of ligands via exponential enrichment (SELEX)[210], re oligonucleotides that can bind to various targets with high affinity, comparable to antibodies. Aptamers have proven to be a powerful tool for highly sensitive detection, particularly of bacteria in environmental and food samples, due to their high stability, low cost, and accessibility to chemical modification. Aptamer-based detections are low-cost, fast, and reliable, and they can be easily modified to meet specific needs. In comparison to an antibody, an additional advantage of an aptamer is that it can be

coupled with a DNA replication using the aptamer as a primer, generating amplified signals that would significantly enhance the detection sensitivity. When conjugated with a magnetic bead, the aptamer-based methods can be used to physically separate an analyte from complex biofluids, therefore improving detection efficiency. Table 4.1 will describe the conventional ways for aptamer magnetic bead-based pathogen/analyte detection from biological samples.

Table 4.1: Aptamer magnetic beads-based Hybridization chain reaction for pathogen detection

Reference	**Target type**	**Samples used (clinical etc.)**	**Limit of detection (LoD)**	**Brief description of the method**
[211]	hepatic carcinoma	Isolated HepG2 cells	100 cells	• An antibody as the recognition element • Antibody was used to capture the exosome. • Probe 1 consisted of aptamer sequence and trigger sequence
[212]	Heavy metal ions, antibiotics, and estrogen residues	Food	1.76×10^{-4}nM (kanamycin), 1.18×10^{-4}nM (17β-estradiol), and 1.29×10^{-4}nM (lead ion)	• A micro-fluidic chip (MC)-with magnetic encoded aptamer probes • Aptamer hybrid chains were first used to selectively capture multiple targets, followed by generating single-stranded primers. • This initiates HCR
[213]	Determination of the antibiotic kanamycin (Kana)	Food	0.45 $pg \cdot mL^{-1}$	• Dual signal amplification is accomplished by making use of double Y-shaped aptamer DNA. • In addition to Kana, the Y-shaped aptamer probe captures Kana which releases two single-stranded DNAs.

				• These trigger target recycling and HCR between the two bars simultaneously.
[214]	Polychlorinated biphenyls (PCB)	Water	0.0035 ng/mL	• Two hairpins (H1 and H2) were first designed according to the partial complementary sequence (cDNA) of the PCB • The cDNA was detached from the magnetic microspheres (MMPs). • FRET has been used to calculate the energy
[215]	Prostate-specific antigen (PSA)	Blood	0.001-100ng/mL	The assay mainly involved in • Anchor DNA-conjugated magnetic bead (MB-aDNA), • PSA aptamer/trigger DNA (Apt-DNA) which triggers the initiation of chain reaction.
[216]	Adenosine detection	Urine	2.0×10^{-7}mol/L	• The recognition probe was divided into two parts: Apt-1, which included an adenosine aptamer and toehold domain, and Apt-2, which included another adenosine aptamer and branch migration domain. • Apt-1 was immobilised on a streptavidin-magnetic nanobead (streptavidin-MBs) and served as an enrichment and separation agent.
[217]	Thrombin	Blood	15.0 pM	• In the presence of target TB, the aptamer was taken away from the aptasensor, • The free P-DNA immediately triggered HCR to spontaneously form DNA.

Since nucleic acid amplification-based detection has shortcomings, such as prior nucleic acid extraction, and differentiation between viable and non-viable cells, there has been increasing focus on whole-cell extraction and identification from biofluid with the use of aptamers and magnetic nanoparticles. In this chapter, we have developed a sandwich aptamer assay which has been employed for *Staphylococcus aureus* capture from a biological sample. The downstream readout has been associated with DNAzyme incorporated hybridization chain reaction (HCR) nanowire coupled colorimetry. HCR is an enzyme-free method that enables the sequence-selective self-assembly of partially complementary metastable hairpin oligonucleotide [217], [218]. Depending on the desired readout, the hairpins could be decorated with catalytic moieties or reporter probes.

4.3 Results and discussions

4.3.1 Working scheme and principle of the assay

We used the sandwich aptamer method to detect live pathogens from biological samples. Firstly, biotinylated aptamers will bond with streptavidin-coated magnetic nanoparticles described in scheme 4.1. While incubation with a biological fluid, this conjugated aptamer will then recognize the specific pathogen, e.g., -*Staphylococcus aureus* (SA) in this case. After washing off residual and non-bound components of the biological fluid, pre-assembled HCR nanowires with a secondary aptamer will come and initiate the binding and create a sandwich aptamer in which cells are entrapped. We will investigate the colorimetry after three to four successive magnetic decantations washing with wash buffer. The complementary DNAzyme sequence is part of the H1 probe. Hemin DNAzymes generate green color upon incubation with 2,2'-azino-bis (3-ethylbenzothiazoline-6-sulfonic acid) (ABTS) and H_2O_2. Thus, colorimetric readouts can be generated in a specific manner.

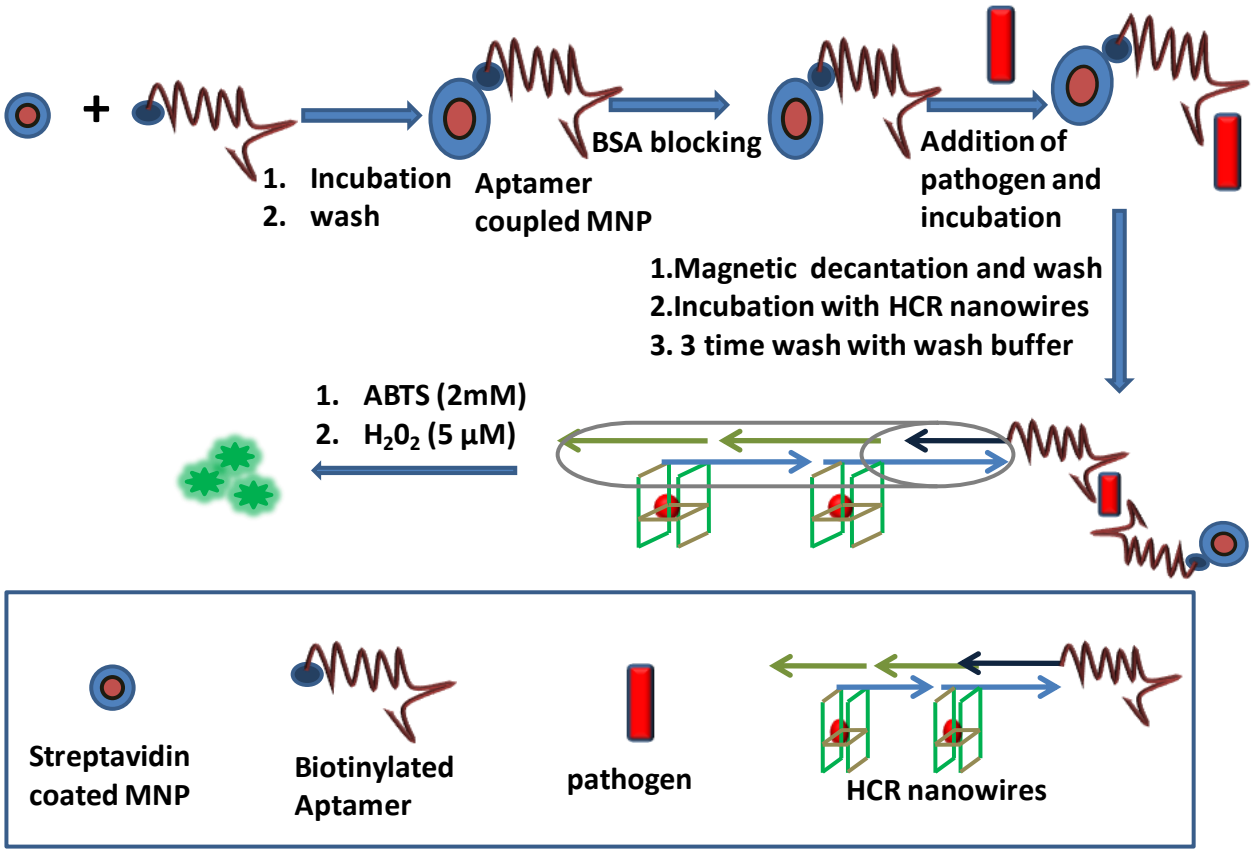

Scheme 4.1: Aptamer-magnetic beads-based hybridization chain reaction for pathogen detection

4.3.2 Aptamer initiator analysis

In this assay, S*taphylococcus aureus* aptamer has been selected from a published journal and the initiator has been selected based on the non-availability of the sequence in either the host (human) or pathogen species [219]. The initiator sequence has been verified for its absence in humans, or pathogens have been checked by nucleotide blast. The presence of minimal secondary structure of the initiator sequence at its 3' end of aptamer has been probed by NUPACK and UNAfold to get its secondary structure. If the initiator sequence is found to form a secondary structure with the aptamer, then the initiator sequence has been shuffled to obtain a fresh initiator to avoid the unwanted secondary structures. After confirming a non-identity match from nucleotide blast again, the structures have been folded via UNAfold again. This process continued until a proper aptamer initiator structure was found.

4.3.3 Design of hairpin probes by NUPACK for HCR

The target has been selected by conjugating aptamer and initiator, and the hairpin 1 has been designed on NUPACK on partial complementarity and introducing loop with random repeat sequence. After designing hairpins 1 and 2, we have checked the structure in UNAfold and

IDT oligo analyzer to check its secondary structure. After that, DNAzyme sequence has been added to the 3' end of hairpin 1 followed by investigating its NUPACK simulation presence of secondary structure. We have gone for a simulation with our designed aptamer initiator, hairpin 1-DNAzyme and 2 to probe the occurrence of hybridization chain reaction (Fig 4.1, Table 4.2).

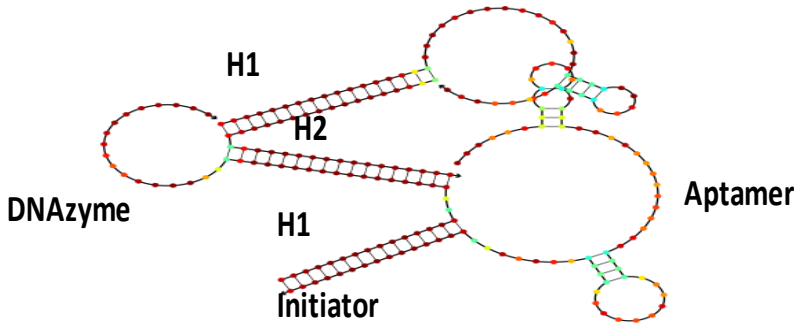

Fig 4.1: Simulation of hybridization chain reaction with aptamer-initiator and hairpin probes (H1 and H2)

Table 4.2: DNA sequences used in this study

Aptamer sequence	**5'-3'-initiator sequence**	**H1 and H2 sequences without DNAzyme (5'-3')**	**H1 and H2 sequences with DNAzyme (5'-3')**
ATACCAGCTTATTCAATTAGCAACATGAGGGGGATAGAGGGGGTGGGTTCTCTCGGCT	i21: CTTAGTACGGCTCGCAAC	H1-i21-GTTGCGAGCCGTACTAAGTTTAATTAGTACGGCT H2-i21-TTAGTACGGCTCGCAACAGCCGTACTAATTAAAC	H1-i21 (H1Dzyme-i21)-GTTGCGAGCCGTACTAAGTTTAATTAGTACGGCT*CTGGGAGGAGGAGGA* H2-i21-TTAGTACGGCTCGCAACAGCCGTACTAATTAAAC
	i22: CTGTATCTTAGTACGGCTCGCAAC	H1-i22-GTTGCGAGCCGTACTAAGATACAGAACGACCTGTATCTTAGTACGGCT H2-i22-	H1-i22(H1Dzyme-i22)-GTTGCGAGCCGTACTAAGATACAGAACGACCTGTATCTTAGTACGGCT*CTGGG*

		CTGTATCTTAGTA CGGCTCGCAACAG CCGTACTAAGATA CAGGTCGTT	*AGGG AGGG AGGG A* H2-i22- CTGTATCTTAGTA CGGCTCGCAACA GCCGTACTAAGAT ACAGGTCGTT

Table 4.3: Buffer compositions used in this study

Buffer name	**Compositions**
Colorimetric buffer	Tris-HCl buffer (25 mM, pH 7.6) containing 150 mM NaCl, 20 mM KCl, 0.03% Triton X-100, and 1% DMSO
New colorimetric buffer	Tris-HCl buffer (25 mM, pH 7.6) containing 0.5M NaCl, 20 mM KCl, 0.03% Triton X-100, and 1% DMSO
Hybridization chain reaction buffer (HCR buffer)	0.5 M sodium phosphate, 0.5 M sodium chloride
KTD buffer	20 mM KCl, 0.03% Triton X-100, and 1% DMSO
Ten_{100} buffer	10 mM Tris-HCl, 1 mM EDTA, 100 mM NaCl pH-7.5
Ten_{100o} buffer	10 mM Tris-HCl, 1 mM EDTA, 1M NaCl pH-7.5

4.3.4 Verifying aptamer binding to bacteria

Whether *Staphylococcus aureus* (SA) is bound to the aptamer has been investigated with selective media plate assay. Biotinylated aptamer bound streptavidin-coated magnetic nanoparticles were applied to a biofluid containing SA and incubated for 30 mins. After that, frequent magnetic decantation wash has been applied the remove unbound bacteria in the biofluid. Then the SA-bound aptamer-MNP has been plated in mannitol sugar agar where only SA can grow. Fig 4.2 shows that with an increase in magnetic nanoparticles quantity, the amount of bacteria attachment has increased proportionally.

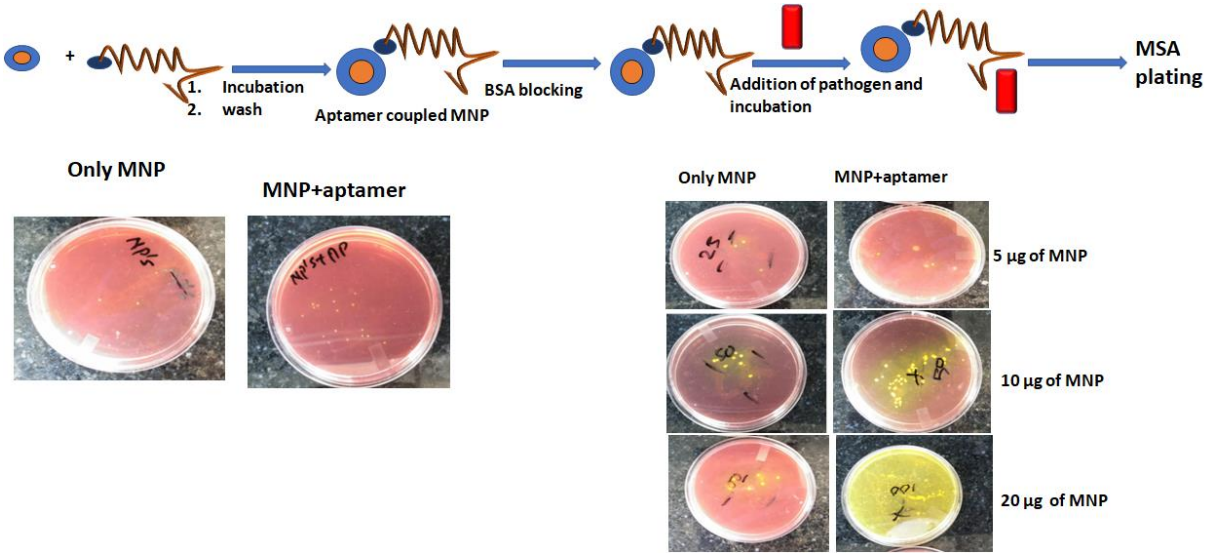

Fig 4.2: The biotin-coated aptamer is bound to streptavidin-coated MNP, and the bacteria binding with aptamer is directly proportional to the amount of MNPs

4.3.5 Optimization of colorimetry with DNAzyme sequence

The DNAzyme oligonucleotide (EAD2) is a reported DNAzyme [8] that has been widely used for optimizing colorimetry with a hybridization chain reaction. The G-quadruplex structure has been formed in the presence of potassium ions in the colorimetric buffer. The hemin has been intercalated into it to make a horseradish peroxidase (HRP) analog. While in the presence of K+, Oligo EAD2 folds into a parallel G-quadruplex (Fig 4.3A), It can bind with hemin to form a hemin-G-quadruplex DNAzyme that can catalyse the oxidation-reduction reaction between ABTS and H_2O_2. The green color developed based on the oxidation of ABTS in the presence of hydrogen peroxide to produce the colored radical cation ($ABTS^{\bullet+}$). Fig 4.3C shows a proper intense green color development upon incubation with ABTS & H_2O_2 when DNAzyme oligo has been initially denatured at 95˚C for 5 minutes followed by ice incubation for 5 minutes (snap-cooled). Non-snap-cooled oligo has given a less intense color than the snap cooled sample, probably for improper folding of G-quadruplex (Fig 4.3B).

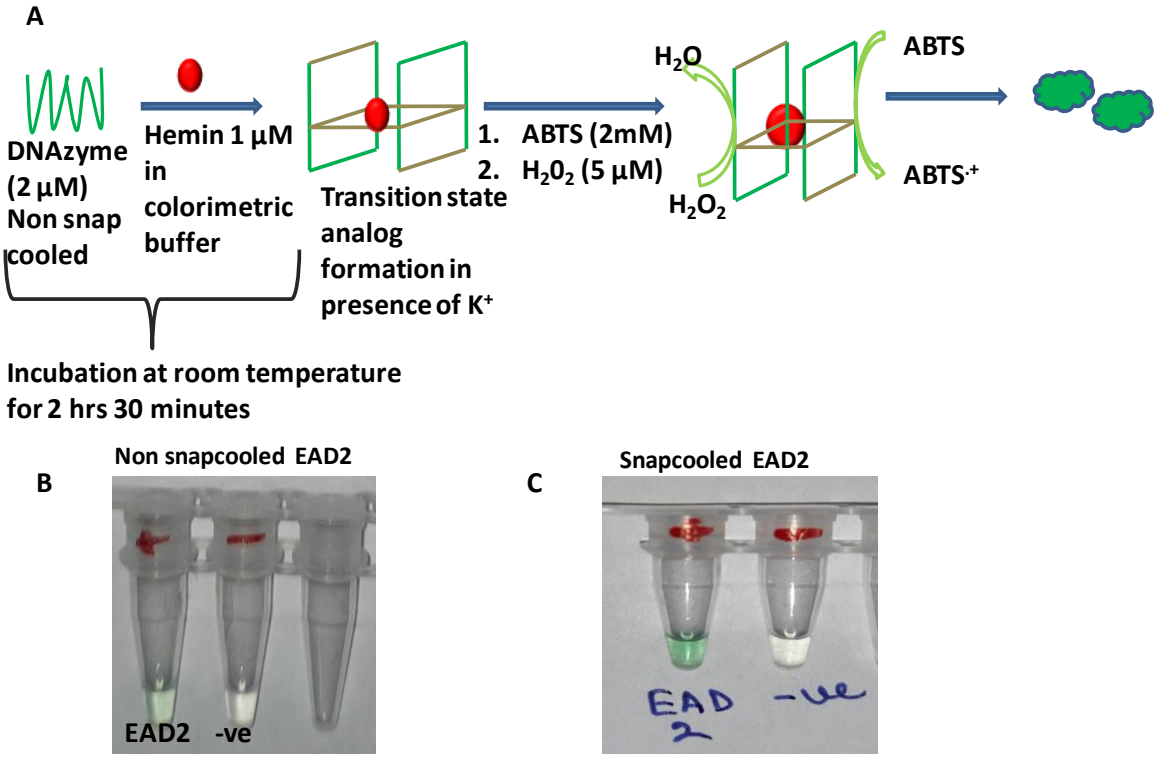

Fig 4.3: A, Scheme of colorimetry with DNAzyme sequence (EAD2). B, Non-snap-cooled EAD2. C, Snap-cooled EAD2

4.3.6 Colorimetry optimization with H1-DNAzyme

H1-DNAzyme i21 (H1-i21) and H1-DNAzyme i22 (H1-i22) have been investigated for colorimetry in the colorimetric buffer to see their compatibility for color development. Fig 4.4B shows a proper color has been intensified upon quadruplex formation of both DNAzymes followed by the incubation with ABTS and H_2O_2.

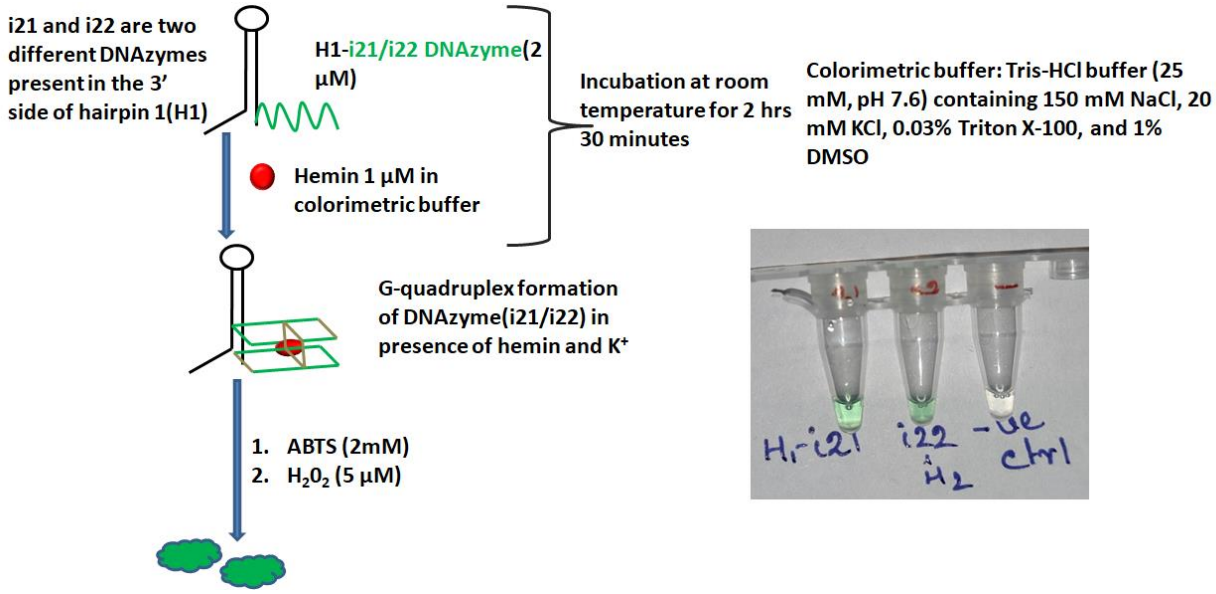

Fig 4.4: A, Scheme of the experiment with hairpin probe 1 DNAzyme sequence. B, color development of each hairpin 1 DNAzyme sequence

4.3.7 Compatibility check of H1 DNAzymes with HCR compatible buffer

Next, hairpin1-DNAzyme-i21 (H1-i21) and Hairpin1-DNAzyme-i22 (H1-i22) have been investigated for colorimetry in new colorimetric buffer with higher salt concentration (0.5 M NaCl) to see its compatibility for the color development. This high salt buffer is suitable for further downstream applications like hybridization chain reaction (HCR). Fig 4.5 shows a proper color has been generated upon quadruplex formation of H1-i21 DNAzymes (2nd tube) followed by the incubation with ABTS and H_2O_2. No color formation was seen for H1-i22 DNAzyme (3rd tube). Henceforth, we used only aptamer-initiator i21 for further study.

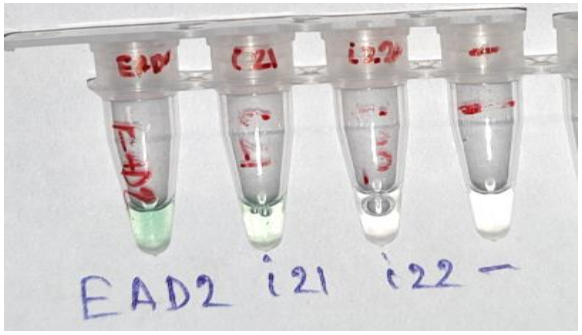

Fig 4.5: Color development in new colorimetric buffer with higher salt concentration

4.3.8 Amplification and colorimetry optimization by HCR with hemin incubated H1-i21

Next, we investigated whether hemin-incubated H1-i21-DNAzyme (H1Dzyme-i21) would participate in HCR with aptamer-initiator-i21 and H2 in the new colorimetric buffer. In this case, the hemin has already been incorporated into the G-quadruplex structure of H1Dzyme-i21 before incubation with the aptamer-initiator-i21 and H2 (Fig 4.6A). Negative control has been taken where water has been used in place of the aptamer initiator. Surprisingly, non-specific amplification occurred in the case of negative control and was visible in gel electrophoresis. (Fig 4.6B). This could be due to distortion of the metastable secondary structure of hairpin 1 while incubating with hemin. This quadruplex formation may open up the hairpin structure of H1 due to less thermodynamic stability, leading to the initiation of HCR without aptamer. Color has not been developed for both positive (with aptamer initiator) and negative control (without aptamer) (Fig 4.6C).

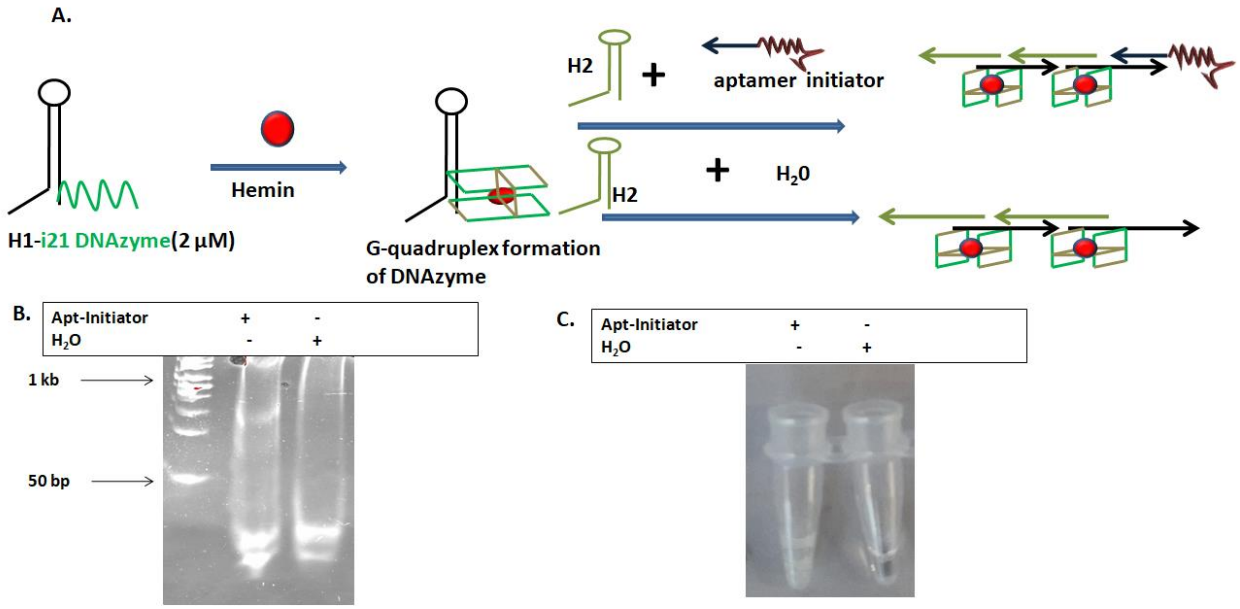

Fig 4.6: A, Scheme of the work. B, Gel electrophoresis (lane 1 is ladder, lane 2 is HCR with aptamer and lane 3 is HCR without aptamer). C, Colorimetry (tube 1 is with aptamer and tube 2 is without aptamer)

4.3.9 Amplification optimization by HCR with non-hemin incubated H1-i21.

Next, we investigated whether the H1DNAzyme-i21 would initiate HCR with H2 and aptamer initiator i21 in the new colorimetric buffer. In this case, we removed the hemin incubation step since it led to non-specific amplification (above). H1Dzyme-i21 (2 µM) in new colorimetric buffer (with high salt concentration), aptamer–initiator (2 µM) and hairpin 2 (H2) (2 µM) have been incubated together and further investigated for amplification and

colorimetry (Fig 4.7A). Negative control has been taken where water has been used in place of the aptamer initiator. Surprisingly, in this case as well, non-specific amplification occurred in the case of negative control (Fig 4.7B). Although the hemin is absent, the presence of the K^+ ion may have induced G-quadruplex formation distorting the metastable secondary structure of hairpin 1 using the colorimetric buffer. This quadruplex formation may open up the hairpin structure of H1 due to less thermodynamic stability, which leads to the initiation of HCR without aptamer.

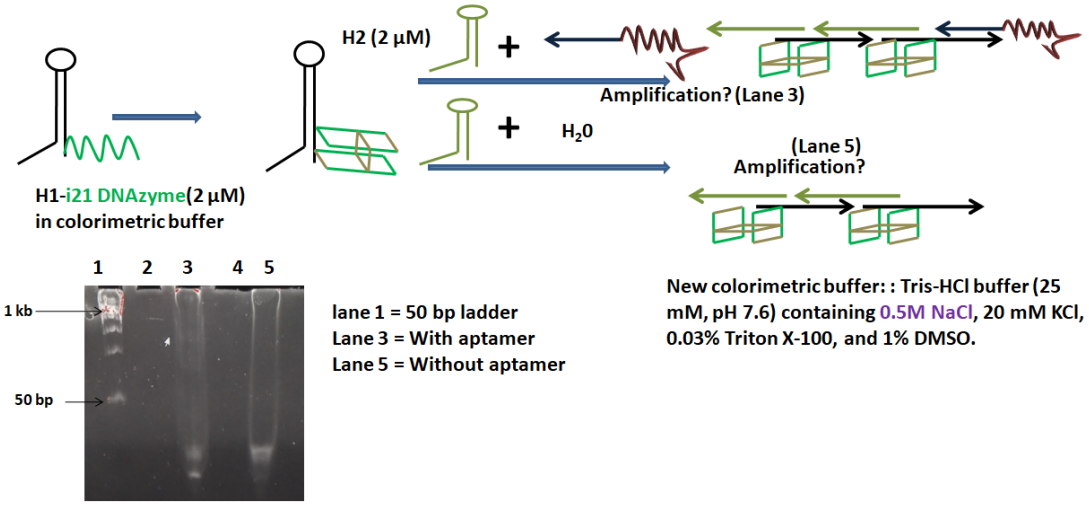

Fig 4.7: A, Scheme of the assay. B, Gel electrophoresis (lane 1 is ladder, lane 3 is HCR with aptamer and lane 5 is HCR without aptamer)

4.3.10 Amplification optimization by HCR in HCR buffer without formation of G-quadruplex

Since the presence of hemin and K^+ could lead to non-specific amplification, we next attempted the G-quadruplex formation after the self-assembled product formation. Hairpin 1-DNAzyme-i21 (H1Dzyme-i21), H2, and aptamer-initiator-i21 have been investigated for amplification in sodium phosphate-sodium chloride buffer (HCR buffer) to investigate without quadruplex formation of DNAzyme the occurrence of hybridization chain reaction (the Scheme is described in Fig 4.7A). Negative control has been taken where water has been used in place of the aptamer initiator. Fig 4.8B shows there is a clear amplification in the positive control (lane 2), whereas in negative control, there is no amplification visible (lane 4). The previous non-specific amplification possibly originated from the distorted ion of H1 secondary structure due to the formation of the G-quadruplex. This, in turn, led to the hybridization of H2 with H1 causing non-specific amplification.

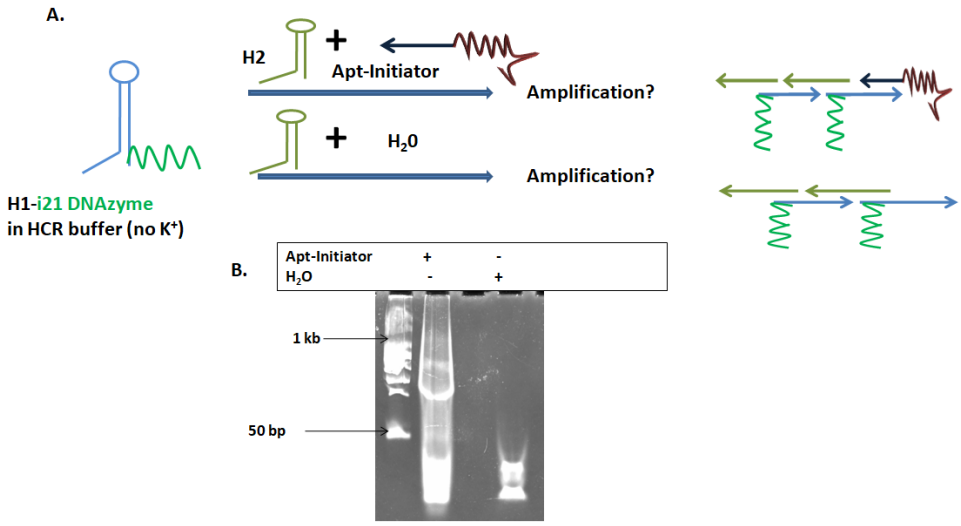

Fig 4.8: A, Scheme of the assay. B, Gel electrophoresis

4.3.11 Synthesis of HCR nanowires and optimization of colorimetry

Preassembled HCR product is incubated with hemin in KTD buffer (20 mM KCl, 0.03% Triton X-100, and 1% DMSO). Hemin and K^+ in the buffer are necessary for the formation of G-quadruplex (DNAzyme part of H1) where hemin intercalated into the G-quadruplex structure (Fig 12A), and upon incubation with ABTS and H_2O_2 green color developed (Fig 4.9B). This G-quadruplex-hemin decorated HCR product with aptamer is termed as catalytic HCR DNA nanowires and would be used for further bacterial detection through sandwich aptamer assay (Scheme 1).

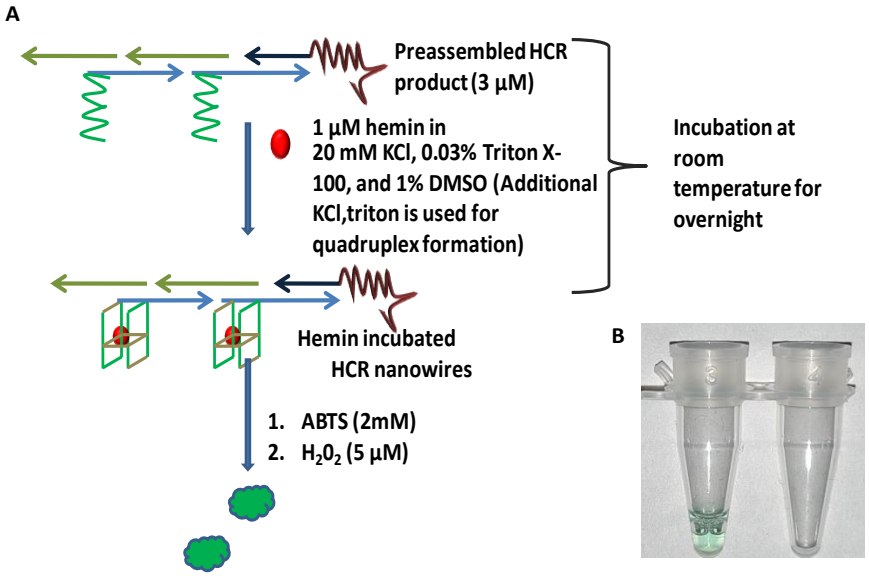

Fig 4.9: A, Scheme of the assay B, Colorimetry with HCR nanowires

4.3.12 Colorimetry with Preassembled HCR products for *Staphylococcus aureus* (SA) detection

The assay was used in the determination to investigate its applicability to bacteria detection of 10^6 copies of *Staphylococcus aureus* (SA). Biotinylated aptamer bound streptavidin-coated magnetic nanoparticles were applied to biofluid containing SA and were incubated for 30 mins. Next, magnetic decantation wash was used in the removal of unbound bacteria. Then preassembled HCR nanowires with secondary aptamer have bound to the bacteria to make the cell entrapped between two aptamers. After washing, ABTS and H_2O_2 have been added, and there is a clear green color developed in the positive control (Fig 4.10B). In the negative control, water has been used in place of the bacteria.

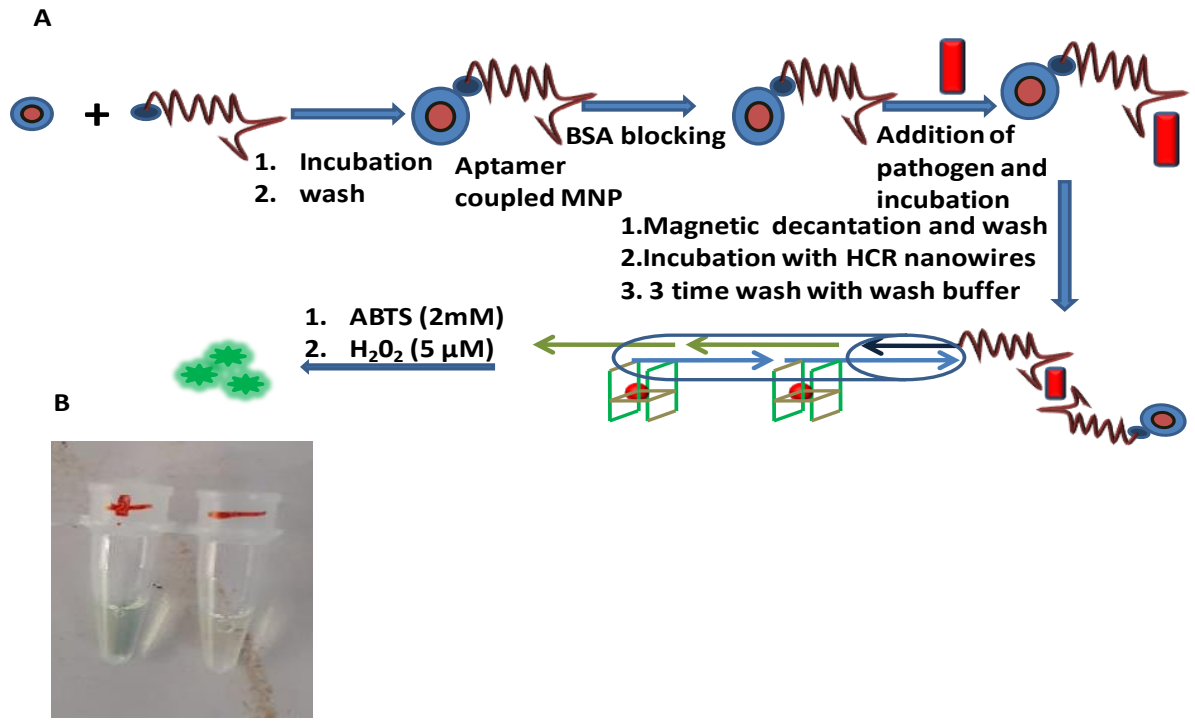

Fig 4.10: A, Scheme of the sandwich aptamer assay. B, Colorimetry with sandwich aptamer assay to determine 10^6 copies of *Staphylococcus aureus*

4.3.13 ABTS and H_2O_2 concentration determination based on ABTS.

We observed very faint color was produced while working with 10^6 copies of *Staphylococcus aureus* and color persistence was less than 2 minutes. So, we tried to increase the intensity of color by increasing the ABTS concentration to improve the color persistence. We attempted to investigate the color change (%) with respect to hemin while EAD2 was used as positive control. The colorimetric study was done in presence of hemin while different concentrations

(8 mM, 10 mM, 12 mM, 15 mM) of ABTS was used in the colorimetric reaction. We observed that the increase of ABTS concentration increased the color persistence for longer time as well as it generated more intense color which we were able to quantify by fluorescence plate reader at 420 nm (Fig 4.12).

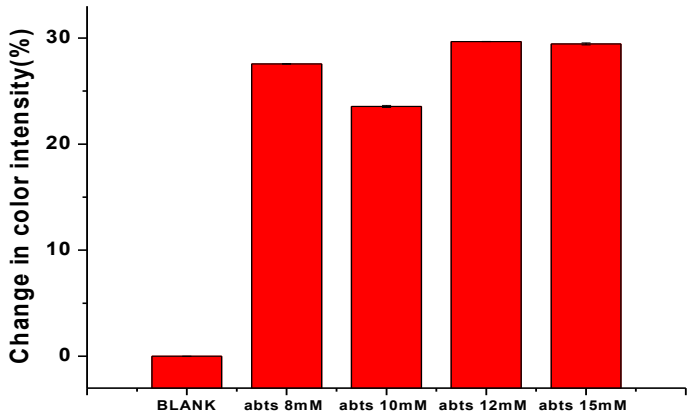

Fig 4.11: Increased ABTS concentration gives a more intense color. 15 mM ABTS in colorimetric reaction buffer gave the highest intensity as well as more than 15 minutes of color persistence

4.4 Conclusion

In this objective we tried to develop alternative methods for costly antibody-based pathogen detection method with the help of aptamer. Aptamer mediated pathogen detection does not need any high end instrument for viable pathogen capture. We have used the sandwich aptamer assay method for capturing live pathogens from biological samples followed by enzyme free hybridization chain reaction to detect SA. A novel colorimetric strategy was developed to accomplish the experiment where we have manipulated the buffer condition and employed pre-assembled HCR nanowires for successful pathogen detection. In future we will be trying to detect circulatory tumor cell by this method for early cancer diagnosis.

4.5 Materials and Methods

4.5.1 Instrumentation and reagents

DNAzyme sequences were synthesized and purified by Merck (India). They were dissolved in colorimetric buffer (Table 4.3), heated to 95 ˚C for 5 min, cooled quickly in ice, and then stored at 4 ˚C. Hairpin 1with DNAzyme (H1-DNAzyme), H2, and aptamer initiator were ordered from Eurofins (India). They were dissolved in TE buffer, heated to 95 ˚C for 5 min, cooled quickly in ice, and then stored at 4˚C. A hemin stock solution (10 mM) was prepared in DMSO and stored in the dark at -20˚C. ABTS was purchased from SRL. ABTS and H_2O_2 working solutions were freshly prepared with 0.15 M citrate phosphate buffer (pH 5.5). Hemin working solutions were freshly prepared with colorimetric buffer.

4.5.2 DNAzyme experiments with naked DNAzyme and hairpin

The activities of the G4/Hemin DNAzymes were determined in reactions that contained colorimetric buffer, 2 μM DNAzyme, ABTS (2 mM) and H_2O_2 (5 μM). Each reaction was started by adding hemin to DNAzyme sequence and incubation for 2 hours at room temperature, followed by the addition of ABTS and H_2O_2, and a change of color has been observed in 5 minutes.

4.5.3 Aptamer bacteria binding assay

200 μg of streptavidin-coated MNP (Sigma) is washed with TEN_{100} buffer (10 mM Tris-HCl, 1 mM EDTA, 100 mM NaCl pH-7.5). 5 pmoles of biotinylated primary aptamer heated to 95˚C for 5 min, cooled quickly in ice, and added to the MNP and incubated for 30 minutes. For negative control, water is used in place of biotinylated aptamer. After 2 times magnetic decantation wash with TEN_{100} buffer blocking with 200 μL 1% BSA has been accomplished by incubating BSA for 30 minutes. After 2 times magnetic decantation with TEN_{1000} buffer (10 mM Tris-HCl, 1 mM EDTA, 1 M NaCl pH-7.5). 10^6 copies of *Staphylococcus aureus* in 100 μL TEN_{1000} buffer has been incubated with aptamer conjugated MNP for 30 minutes. After consecutive washing with TEN_{1000}buffer, the MNPs have been plated on a mannitol sugar agar plate.

4.5.4 HCR nanowire formation with G-quadruplex

Aptamer-initiator, H1-DNAzyme, H2 (3 μM final concentration for each) has been added to a final volume of 30 μL in sodium phosphate sodium chloride (HCR buffer) and incubated at room temperature for 2 hours. Hemin (1 μM final) is added to the HCR mix with additional potassium-containing KTD buffer (Table 4.3), overnight. By the addition of ABTS (2 mM) and H_2O_2 (5 μM), a change of color has been observed in 5 minutes.

4.5.5 Bacterial detection by sandwich aptamer assay followed by colorimetry

200 μg of streptavidin-coated MNP (Sigma) is washed with TEN_{100} buffer (10 mM Tris-HCl, 1 mM EDTA, 100 mM NaCl pH-7.5). 5 picomoles of biotinylated primary aptamer heated to 95 ˚C for 5 min, cooled quickly in ice, and added to the MNP and incubated for 30 minutes. For negative control, water is used in place of Biotinylated aptamer. After 3 times magnetic decantation with TEN_{100} buffer blocking with 100 μL 1% BSA has been accomplished by incubating BSA for 30 minutes. After 2 times magnetic decantation with TEN_{1000} buffer (10 mM Tris-HCl, 1 mM EDTA, 1M NaCl pH-7.5) 10^6 copies of *Staphylococcus aureus* in TEN_{1000} buffer has been incubated with aptamer conjugated MNP for 30 minutes. After consecutive washing with TEN_{1000} buffer HCR nanowires with quadruplex structure (1 μM) are incubated with the bacteria attached MNPs. After 3 times of washing with 1X HCR, KTD buffer ABTS (2 mM) and H_2O_2 (5 μM), are added.]

CHAPTER 5

CONCLUSION

5.1 Introduction

In this chapter, we will discuss the overview of the research, key findings and future prospects of our research. In the chapter 1, we have discussed our primary goal of study and then fill the research gap in the field of rapid nucleic acid extraction followed by detection in resource-limited settings. This chapter will also show the accomplishment of our research goals, as well as their future prospects and limitations.

5.2 Overview and Conclusion

5.2.1 Chitosan coated MNP for instrument-free nucleic acid extraction followed by amplification

Our first objective (chapter 2) explores the activity of two types of easily synthesizable chitosan coated magnetic nanoparticles for rapid nucleic acid extraction from complex biofluid followed by downstream isothermal amplification. Our primary focus in that objective was to establish an assay which can be achievable in resource-constrained settings. Our studies have primarily used medium molecular weight chitosan, a polymer with an average 120,000 Da molecular weight. It has an amine (NH_2) group with a pK_a of 6.5 and acquires a pH-controlled positive charge. Since DNA was negatively charged, the positively charged chitosan can be employed to capture DNA at a certain pH (when pH $<pK_a$). Then after increasing the pH (when pH $>pK_a$), this captured DNA can be released. We tested the extracted nucleic acid's compatibility with downstream NAATs such as real-time LAMP, colorimetric LAMP, and real-time PCR. In the process, we established the overall method's analytical sensitivity, which is clinically relevant 100 copies.

Our experiments reported a decreasing DNA extraction capacity as a function of zeta potential, which controlled the sensitivity of downstream NAAT/iNAAT assays. Previous studies involving DLS measurement and molecular tweezers have indicated a possible role of cooperative effect on chitosan-DNA binding. On the other hand, a permanent positive charge on chitosan magnetic particles was found to benefit DNA binding and in situ NAAT. Our colorimetric LAMP experiment also hinted at a role of chitosan deprotonation kinetics that may, in principle, affect DNA extraction efficiency. Future studies would therefore comprise

of in-depth investigations for correlating chitosan coating on nanoparticles with DNA binding capacity, optimizations to improve the stability of magnetic particles beyond 2 weeks, the kinetics of chitosan- DNA electrostatic complexation, experimenting with buffer conditions for colorimetric LAMP readout, and obtaining C_t values for real-time LAMP. We would also be exploring the ability of magnetic particles to extract RNA, associated reverse transcription, and TaqMan probe-based detection. We also noted but chose not to examine the possibility of "in situ" (on bead/on-particle) amplification for LAMP experiments which would minimize the extraction timing by at least 10 min. The experimental optimization for "in situ" optimization would also be taken up in future studies.

5.2.2 Evaluation of indirect sequence-specific magneto-extraction-aided LAMP for fluorescence and electrochemical SARS-CoV-2 nucleic acid detection

In our second objective (chapter 3), we have circumvented the necessity of pure nucleic acid templates, and thermal cycling in NAAT and iNAAT methods by exploring indirect sequence-specific magneto-extracted assisted LAMP. The proposed assay successfully demonstrated proof-of-concept detection of clinically relevant 100 – 1000 copies (equivalent to 2.5 – 25 copies/μL) SARS-CoV-2 *RdRp* plasmid DNA and RNA from aqueous, human genomic DNA (hgDNA) spiked, and serum spiked VTM-simulating samples. The proposed assay has a comparable performance when compared with RT-LAMP performed on RNase treated and silica-bead extracted RNA template and qRT-PCR (both reporting limit of detection at 2.5 copies/μL). When assessed for cost benefits, the cost of the raw materials in our method was INR 224 or $3.04 per assay (involving all commercial reagents) with TAT in 2 – 2.5 h. In comparison, the spin-column or magnetic bead-based RNA detection kits (inclusive of extraction and amplification module) would cost $6 – 11/sample with TAT (sample-to-answer) ranging from 4 h to 1 day. This implied that our integrated indirect magnetocapture amplification would be more inexpensive than existing RNA extraction and qRT-PCR kits despite the faster and limited-resource-friendly detection. With in-house prepared magnetic beads and enzymes, the assay cost could be expected to go down even further. Given the general nature of detection and low assay cost, this method would also be able to sense any target pathogen nucleic acid and is therefore expected to see broader applications in the future. We are currently optimizing its applicability with clinical samples, lateral flow assay readouts, and a microfluidic set-up.

5.2.3 Magnetic nanoparticle associated sandwich aptamer assay followed by hybridization chain reaction for *Staphylococcus aureus* detection

Our third objective (chapter 4) describes our attempt to perform a modified sandwich aptamer assay. The aptamer was coupled with streptavidin coated magnetic nanoparticles bound with aptamer for detecting the live pathogen from a biological sample by an enzyme free detection method hybridization chain reaction (HCR) coupled with colorimetry. By this technique, we have overcome shortcomings of the nucleic acid detection method (inability to differentiate viable from non-viable cells) in a very cost-effective and time-saving manner. By this assay, we have detected up to 10^6 copies of *Staphylococcus aureus* by colorimetric readouts. In future we can use this assay for the detection of antibiotic resistance in bacterial culture.

5.3 Conclusion

From all of our research objectives we explored about conventional and alternative ways of molecular diagnostics. We have overcome the non-specificity issue with isothermal amplification as well as we have standardized indirect sequence-specific magneto–extraction of the pathogen nucleic acid from biological sample. We have established several strategies for improving commercial magnetic beads based on nucleic acid extraction in terms of cost and time. We have demonstrated clinically relevant analytical sensitivity for our proposed research work. But there is still scope for improvement in terms of specificity for all of our established methods. In future, we would thus be exploring the ability of our established methods to extract RNA, associated reverse transcription, and TaqMan probe-based detection.

REFERENCES

[1] A. P. Dobson and E. R. Carper, “Infectious Diseases and Human Population History: Throughout history the establishment of disease has been a side effect of the growth of civilization,” BioScience, vol. 46, no. 2, pp. 115–126, Feb. 1996, doi: 10.2307/1312814.

[2] J. F. Lindahl and D. Grace, “The consequences of human actions on risks for infectious diseases: a review,” Infect Ecol Epidemiol, vol. 5, p. 30048, 2015, doi: 10.3402/iee.v5.30048.

[3] J. Piret and G. Boivin, “Pandemics Throughout History,” Front Microbiol, vol. 11, p. 631736, 2020, doi: 10.3389/fmicb.2020.631736.

[4] D. Grennan, “What Is a Pandemic?,” JAMA, vol. 321, no. 9, p. 910, Mar. 2019, doi: 10.1001/jama.2019.0700.

[5] D. M. Morens, G. K. Folkers, and A. S. Fauci, “The challenge of emerging and re-emerging infectious diseases,” Nature, vol. 430, no. 6996, pp. 242–249, Jul. 2004, doi: 10.1038/nature02759.

[6] K. D. Patterson and G. F. Pyle, “The geography and mortality of the 1918 influenza pandemic,” Bull Hist Med, vol. 65, no. 1, pp. 4–21, 1991.

[7] J. K. Taubenberger and D. M. Morens, “1918 Influenza: the mother of all pandemics,” Emerg Infect Dis, vol. 12, no. 1, pp. 15–22, Jan. 2006, doi: 10.3201/eid1201.050979.

[8] P. R. Saunders-Hastings and D. Krewski, “Reviewing the History of Pandemic Influenza: Understanding Patterns of Emergence and Transmission,” Pathogens, vol. 5, no. 4, p. E66, Dec. 2016, doi: 10.3390/pathogens5040066.

[9] T. Zhu, B. T. Korber, A. J. Nahmias, E. Hooper, P. M. Sharp, and D. D. Ho, “An African HIV-1 sequence from 1959 and implications for the origin of the epidemic,” Nature, vol. 391, no. 6667, Art. no. 6667, Feb. 1998, doi: 10.1038/35400.

[10] P. M. Arguin, A. W. Navin, S. F. Steele, L. H. Weld, and P. E. Kozarsky, “Health Communication during SARS,” Emerg Infect Dis, vol. 10, no. 2, pp. 377–380, Feb. 2004, doi: 10.3201/eid1002.030812.

[11] A. Camacho et al., “Cholera epidemic in Yemen, 2016-18: an analysis of surveillance data,” Lancet Glob Health, vol. 6, no. 6, pp. e680–e690, Jun. 2018, doi: 10.1016/S2214-109X(18)30230-4.

[12] “2014-2016 Ebola Outbreak in West Africa | History | Ebola (Ebola Virus Disease) | CDC,” Mar. 17, 2020. https://www.cdc.gov/vhf/ebola/history/2014-2016-outbreak/index.html (accessed May 16, 2022).

[13] R. Lowe et al., “The Zika Virus Epidemic in Brazil: From Discovery to Future Implications,” Int J Environ Res Public Health, vol. 15, no. 1, p. 96, Jan. 2018, doi: 10.3390/ijerph15010096.

[14] S. J. Olsen et al., “Transmission of the severe acute respiratory syndrome on aircraft,” N Engl J Med, vol. 349, no. 25, pp. 2416–2422, Dec. 2003, doi: 10.1056/NEJMoa031349.

[15] F. S. Dawood et al., “Estimated global mortality associated with the first 12 months of 2009 pandemic influenza A H1N1 virus circulation: a modelling study,” Lancet Infect Dis, vol. 12, no. 9, pp. 687–695, Sep. 2012, doi: 10.1016/S1473-3099(12)70121-4.

[16] “GBD Results Tool | GHDx.” https://ghdx.healthdata.org/gbd-results-tool (accessed Apr. 28, 2022).

[17] “COVID-19 Map,” Johns Hopkins Coronavirus Resource Center. https://coronavirus.jhu.edu/map.html (accessed Jan. 06, 2022).

[18] Antimicrobial Resistance Collaborators, “Global burden of bacterial antimicrobial resistance in 2019: a systematic analysis,” Lancet, vol. 399, no. 10325, pp. 629–655, Feb. 2022, doi: 10.1016/S0140-6736(21)02724-0.

[19] “Crimean-Congo haemorrhagic fever.” https://www.who.int/news-room/fact-sheets/detail/crimean-congo-haemorrhagic-fever (accessed Apr. 29, 2022).

[20] “Marburg virus disease.” https://www.who.int/news-room/fact-sheets/detail/marburg-virus-disease (accessed Apr. 29, 2022).

[21] “Priority diseases,” CEPI. https://cepi.net/research_dev/priority-diseases/ (accessed Apr. 29, 2022).

[22] J. T. Mattila, M. J. Fine, A. H. Limper, P. R. Murray, B. B. Chen, and P. L. Lin, “Pneumonia. Treatment and diagnosis,” Ann Am Thorac Soc, vol. 11 Suppl 4, pp. S189-192, Aug. 2014, doi: 10.1513/AnnalsATS.201401-027PL.

[23] M. Ramos-E-Silva, P. Secchin, and B. Trope, “The life-threatening eruption in HIV and immunosuppression,” Clin Dermatol, vol. 38, no. 1, pp. 52–62, Feb. 2020, doi: 10.1016/j.clindermatol.2019.10.014.

[24] I. Aleksioska-Papestiev, V. Chibisheva, M. Micevska, and G. Dimitrov, “Prevalence of Specific Types of Human Papiloma Virus in Cervical Intraepithelial Lesions and Cervical Cancer in Macedonian Women,” Med Arch, vol. 72, no. 1, pp. 26–30, Feb. 2018, doi: 10.5455/medarh.2018.72.26-30.

[25] L. E. Wroblewski and R. M. Peek, “Helicobacter pylori, Cancer, and the Gastric Microbiota,” Adv Exp Med Biol, vol. 908, pp. 393–408, 2016, doi: 10.1007/978-3-319-41388-4_19.

[26] M. Ringelhan, J. A. McKeating, and U. Protzer, “Viral hepatitis and liver cancer,” Philos Trans R Soc Lond B Biol Sci, vol. 372, no. 1732, p. 20160274, Oct. 2017, doi: 10.1098/rstb.2016.0274.

[27] D. M. Morens and A. S. Fauci, “Emerging Pandemic Diseases: How We Got to COVID-19,” Cell, vol. 182, no. 5, pp. 1077–1092, Sep. 2020, doi: 10.1016/j.cell.2020.08.021.

[28] J. D. Ernst, “Antigenic Variation and Immune Escape in the MTBC,” Adv Exp Med Biol, vol. 1019, pp. 171–190, 2017, doi: 10.1007/978-3-319-64371-7_9.

[29] CDC, “Antibiotic Resistance Threatens Everyone,” Centers for Disease Control and Prevention, Mar. 17, 2022. https://www.cdc.gov/drugresistance/index.html (accessed Apr. 29, 2022).

[30] A. J. Cross, E. Haworth, and R. C. Spencer, “A re-evaluation of the pour plate blood culture method for the detection of Candida and other septicaemias,” J Hosp Infect, vol. 7, no. 1, pp. 74–77, Jan. 1986, doi: 10.1016/0195-6701(86)90029-0.

[31] G. López-Campos, J. V. Martínez-Suárez, M. Aguado-Urda, and V. López-Alonso, Microarray Detection and Characterization of Bacterial Foodborne Pathogens. Boston, MA: Springer US, 2012. doi: 10.1007/978-1-4614-3250-0.

[32] S. M. Carr and O. M. Griffith, “Rapid isolation of animal mitochondrial DNA in a small fixed-angle rotor at ultrahigh speed,” Biochem Genet, vol. 25, no. 5–6, pp. 385–390, Jun. 1987, doi: 10.1007/BF00554547.

[33] P. Chomczynski and N. Sacchi, “Single-Step Method Of RNA Isolation By Acid Guanidinium Thiocyanate-Phenol-Chlorform Extraction,” Analytical biochemistry, vol. 162, pp. 156–9, May 1987, doi: 10.1006/abio.1987.9999.

[34] K. Nath, J. W. Sarosy, J. Hahn, and C. J. Di Como, “Effects of ethidium bromide and SYBR® Green I on different polymerase chain reaction systems,” Journal of Biochemical and Biophysical Methods, vol. 42, no. 1–2, pp. 15–29, Jan. 2000, doi: 10.1016/S0165-022X(99)00033-0.

[35] P. S. Walsh, D. A. Metzger, and R. Higushi, “Chelex 100 as a medium for simple extraction of DNA for PCR-based typing from forensic material. BioTechniques 10(4): 506-13 (April 1991),” Biotechniques, vol. 54, no. 3, pp. 134–139, Mar. 2013, doi: 10.2144/000114018.

[36] A. Ullrich et al., “Rat Insulin Genes: Construction of Plasmids Containing the Coding Sequences,” Science, vol. 196, no. 4296, pp. 1313–1319, Jun. 1977, doi: 10.1126/science.325648.

[37] L. Meng and L. Feldman, “A rapid TRIzol-based two-step method for DNA-free RNA extraction from Arabidopsis siliques and dry seeds,” Biotechnol J, vol. 5, no. 2, pp. 183–186, Feb. 2010, doi: 10.1002/biot.200900211.

[38] M. J. Murnane and S. W. Tam, “Isolation and characterization of RNA from snap-frozen tissues and cultured cells,” The Journal of Nutritional Biochemistry, vol. 3, no. 5, pp. 251–260, May 1992, doi: 10.1016/0955-2863(92)90047-M.

[39] M. M. Burrell, Enzymes of Molecular Biology, vol. 16. New Jersey: Humana Press, 1993. doi: 10.1385/0896032345.

[40] “Polish Journal of Environmental Studies - Issue 5/2006 vol. 15.” http://www.pjoes.com/Issue-5-2006,3808 (accessed Apr. 29, 2022).

[41] B. Vogelstein and D. Gillespie, “Preparative and analytical purification of DNA from agarose,” Proc Natl Acad Sci U S A, vol. 76, no. 2, pp. 615–619, Feb. 1979, doi: 10.1073/pnas.76.2.615.

[42] V. V. Padhye, C. York, and A. Burkiewicz, “Nucleic acid purification on silica gel and glass mixtures,” US5658548A, Aug. 19, 1997 Accessed: May 16, 2022. [Online]. Available: https://patents.google.com/patent/US5658548A/en

[43] E. Milne et al., “Buccal DNA collection: comparison of buccal swabs with FTA cards,” Cancer Epidemiol Biomarkers Prev, vol. 15, no. 4, pp. 816–819, Apr. 2006, doi: 10.1158/1055-9965.EPI-05-0753.

[44] K. B. Mullis, “The unusual origin of the polymerase chain reaction,” Sci Am, vol. 262, no. 4, pp. 56–61, 64–65, Apr. 1990, doi: 10.1038/scientificamerican0490-56.

[45] H. U. Weier and J. W. Gray, “A programmable system to perform the polymerase chain reaction,” DNA, vol. 7, no. 6, pp. 441–447, Aug. 1988, doi: 10.1089/dna.1.1988.7.441.

[46] M. Gaňová, H. Zhang, H. Zhu, M. Korabečná, and P. Neužil, “Multiplexed digital polymerase chain reaction as a powerful diagnostic tool,” Biosens Bioelectron, vol. 181, p. 113155, Jun. 2021, doi: 10.1016/j.bios.2021.113155.

[47] Y. Wang et al., “Development of a TaqMan-based real-time assay for the specific detection of canine astrovirus,” J Virol Methods, vol. 296, p. 114247, Oct. 2021, doi: 10.1016/j.jviromet.2021.114247.

[48] M. Sidstedt et al., “Inhibition mechanisms of hemoglobin, immunoglobulin G, and whole blood in digital and real-time PCR,” Anal Bioanal Chem, vol. 410, no. 10, pp. 2569–2583, 2018, doi: 10.1007/s00216-018-0931-z.

[49] K. Kivirand and T. Rinken, “Introductory Chapter: Why Do We Need Rapid Detection of Pathogens?,” in Biosensing Technologies for the Detection of Pathogens - A Prospective Way for Rapid Analysis, T. Rinken and K. Kivirand, Eds. InTech, 2018. doi: 10.5772/intechopen.74670.

[50] “The Trouble with ELISA,” Intellicyt. https://intellicyt.com/articles/the-trouble-with-elisa/ (accessed Apr. 29, 2022).

[51] H. Zhang et al., “Determination of Advantages and Limitations of qPCR Duplexing in a Single Fluorescent Channel,” ACS Omega, vol. 6, no. 34, pp. 22292–22300, Aug. 2021, doi: 10.1021/acsomega.1c02971.

[52] M. J. Archer, B. Lin, Z. Wang, and D. A. Stenger, “Magnetic bead-based solid phase for selective extraction of genomic DNA,” Anal Biochem, vol. 355, no. 2, pp. 285–297, Aug. 2006, doi: 10.1016/j.ab.2006.05.005.

[53] J. Kang, Y. Li, Y. Zhao, Y. Wang, C. Ma, and C. Shi, “Nucleic acid extraction without electrical equipment via magnetic nanoparticles in Pasteur pipettes for pathogen detection,” Anal Biochem, vol. 635, p. 114445, Dec. 2021, doi: 10.1016/j.ab.2021.114445.

[54] S. M. Azimi, G. Nixon, J. Ahern, and W. Balachandran, “A magnetic bead-based DNA extraction and purification microfluidic device,” Microfluid Nanofluid, vol. 11, no. 2, pp. 157–165, Aug. 2011, doi: 10.1007/s10404-011-0782-9.

[55] S. Berensmeier, “Magnetic particles for the separation and purification of nucleic acids,” Appl Microbiol Biotechnol, vol. 73, no. 3, pp. 495–504, Dec. 2006, doi: 10.1007/s00253-006-0675-0.

[56] Z. Sohrabijam, M. Saeidifar, and A. Zamanian, “Enhancement of magnetofection efficiency using chitosan coated superparamagnetic iron oxide nanoparticles and calf thymus DNA,” Colloids Surf B Biointerfaces, vol. 152, pp. 169–175, Apr. 2017, doi: 10.1016/j.colsurfb.2017.01.028.

[57] M. Mukherjee and S. De, “Investigation of antifouling and disinfection potential of chitosan coated iron oxide-PAN hollow fiber membrane using Gram-positive and Gram-negative bacteria,” Mater Sci Eng C Mater Biol Appl, vol. 75, pp. 133–148, Jun. 2017, doi: 10.1016/j.msec.2017.02.039.

[58] F. M. Kievit et al., “PEI-PEG-Chitosan Copolymer Coated Iron Oxide Nanoparticles for Safe Gene Delivery: synthesis, complexation, and transfection,” Adv Funct Mater, vol. 19, no. 14, pp. 2244–2251, Jul. 2009, doi: 10.1002/adfm.200801844.

[59] S. R. Bhattarai et al., “Laboratory formulated magnetic nanoparticles for enhancement of viral gene expression in suspension cell line,” J. Virol. Methods, vol. 147, no. 2, pp. 213–218, Feb. 2008, doi: 10.1016/j.jviromet.2007.08.028.

[60] B. G. Maciel, R. J. da Silva, A. E. Chávez-Guajardo, J. C. Medina-Llamas, J. J. Alcaraz-Espinoza, and C. P. de Melo, “Magnetic extraction and purification of DNA from whole human blood using a γ-Fe2O3@Chitosan@Polyaniline hybrid nanocomposite,” Carbohydr Polym, vol. 197, pp. 100–108, Oct. 2018, doi: 10.1016/j.carbpol.2018.05.034.

[61] M. Abdelrahman et al., “siRNA delivery system based on magnetic nanovectors: Characterization and stability evaluation,” Eur J Pharm Sci, vol. 106, pp. 287–293, Aug. 2017, doi: 10.1016/j.ejps.2017.05.062.

[62] N. Prabhakar, H. Thakur, A. Bharti, and N. Kaur, “Chitosan-iron oxide nanocomposite based electrochemical aptasensor for determination of malathion,” Anal. Chim. Acta, vol. 939, pp. 108–116, Oct. 2016, doi: 10.1016/j.aca.2016.08.015.

[63] B. Xu, D. Zheng, W. Qiu, F. Gao, S. Jiang, and Q. Wang, “An ultrasensitive DNA biosensor based on covalent immobilization of probe DNA on fern leaf-like α-Fe2O3 and chitosan Hybrid film using terephthalaldehyde as arm-linker,” Biosens Bioelectron, vol. 72, pp. 175–181, Oct. 2015, doi: 10.1016/j.bios.2015.05.015.

[64] S. Hsu, T.-T. Ho, and T.-C. Tseng, “Nanoparticle uptake and gene transfer efficiency for MSCs on chitosan and chitosan-hyaluronan substrates,” Biomaterials, vol. 33, no. 14, pp. 3639–3650, May 2012, doi: 10.1016/j.biomaterials.2012.02.005.

[65] W. Wang, X. Jiang, and K. Chen, “Lanthanide-doped chitosan nanospheres as cell nuclei illuminator and fluorescent nonviral vector for plasmid DNA delivery,” Dalton Trans, vol. 41, no. 2, pp. 490–497, Jan. 2012, doi: 10.1039/c1dt11200g.

[66] C. M. Pandey, A. Sharma, G. Sumana, I. Tiwari, and B. D. Malhotra, “Cationic poly(lactic-co-glycolic acid) iron oxide microspheres for nucleic acid detection,” Nanoscale, vol. 5, no. 9, pp. 3800–3807, May 2013, doi: 10.1039/c3nr34355c.

[67] W.-J. Xue et al., “Asialoglycoprotein receptor-magnetic dual targeting nanoparticles for delivery of RASSF1A to hepatocellular carcinoma,” Sci Rep, vol. 6, p. 22149, Feb. 2016, doi: 10.1038/srep22149.

[68] Y.-K. Kim et al., “PK11195-chitosan-graft-polyethylenimine-modified SPION as a mitochondria-targeting gene carrier,” J Drug Target, vol. 24, no. 5, pp. 457–467, 2016, doi: 10.3109/1061186X.2015.1087527.

[69] J. Rakhtshah, B. Shaabani, S. Salehzadeh, and N. Hosseinpour Moghadam, “Synthesis of 1-(α-aminoalkyl)-2-naphthol and α-aminonitrile derivatives with molybdenum Schiff base complex covalently bonded on silica-coated magnetic nanoparticles and DNA interaction study of one type of derivatives using computational and spectroscopic methods,” Bioorg. Chem., vol. 85, pp. 420–430, Apr. 2019, doi: 10.1016/j.bioorg.2019.01.022.

[70] S. Ghahari, S. Ghahari, and G. A. Nematzadeh, “Magnetic nano fluids for isolation of genomic DNA and total RNA from various prokaryote and eukaryote cells,” J. Chromatogr. B Analyt. Technol. Biomed. Life Sci., vol. 1102–1103, pp. 125–134, Dec. 2018, doi: 10.1016/j.jchromb.2018.10.006.

[71] L. Wang, M. Yao, X. Fang, and X. Yao, “Novel Competitive Chemiluminescence DNA Assay Based on Fe3O4@SiO2@Au-Functionalized Magnetic Nanoparticles for Sensitive Detection of p53 Tumor Suppressor Gene,” Appl. Biochem. Biotechnol., vol. 187, no. 1, pp. 152–162, Jan. 2019, doi: 10.1007/s12010-018-2808-1.

[72] A. Soni, C. M. Pandey, M. K. Pandey, and G. Sumana, “Highly efficient Polyaniline-MoS2 hybrid nanostructures based biosensor for cancer biomarker detection,” Anal Chim Acta, vol. 1055, pp. 26–35, May 2019, doi: 10.1016/j.aca.2018.12.033.

[73] M. R. Kesama et al., “Magneto-optical and thermal characteristics of magnetite nanoparticle-embedded DNA and CTMA-DNA thin films,” Nanotechnology, vol. 29, no. 46, p. 465703, Nov. 2018, doi: 10.1088/1361-6528/aade31.

[74] A. H. F. Lee, S. F. Gessert, Y. Chen, N. V. Sergeev, and B. Haghiri, “Preparation of iron oxide silica particles for Zika viral RNA extraction,” Heliyon, vol. 4, no. 3, p. e00572, Mar. 2018, doi: 10.1016/j.heliyon.2018.e00572.

[75] E. E. Bedford, S. Boujday, C.-M. Pradier, and F. X. Gu, “Spiky gold shells on magnetic particles for DNA biosensors,” Talanta, vol. 182, pp. 259–266, May 2018, doi: 10.1016/j.talanta.2018.01.094.

[76] W. Jiang, L. Wu, J. Duan, H. Yin, and S. Ai, “Ultrasensitive electrochemiluminescence immunosensor for 5-hydroxymethylcytosine detection based on Fe3O4@SiO2 nanoparticles and PAMAM dendrimers,” Biosens Bioelectron, vol. 99, pp. 660–666, Jan. 2018, doi: 10.1016/j.bios.2017.08.023.

[77] H. Rahnama, A. Sattarzadeh, F. Kazemi, N. Ahmadi, F. Sanjarian, and Z. Zand, “Comparative study of three magnetic nano-particles (FeSO4, FeSO4/SiO2, FeSO4/SiO2/TiO2) in plasmid DNA extraction,” Anal. Biochem., vol. 513, pp. 68–76, 15 2016, doi: 10.1016/j.ab.2016.08.029.

[78] Y. Bai et al., “Synthesis of amino-rich silica-coated magnetic nanoparticles for the efficient capture of DNA for PCR,” Colloids Surf B Biointerfaces, vol. 145, pp. 257–266, Sep. 2016, doi: 10.1016/j.colsurfb.2016.05.003.

[79] M. Toprak, “Fluorescence study on the interaction of human serum albumin with Butein in liposomes,” Spectrochim Acta A Mol Biomol Spectrosc, vol. 154, pp. 108–113, Feb. 2016, doi: 10.1016/j.saa.2015.10.023.

[80] S. Xiao, R. Castro, J. Rodrigues, X. Shi, and H. Tomás, “PAMAM Dendrimer/pDNA Functionalized-Magnetic Iron Oxide Nanoparticles for Gene Delivery,” J Biomed Nanotechnol, vol. 11, no. 8, pp. 1370–1384, Aug. 2015, doi: 10.1166/jbn.2015.2101.

[81] J. C. Medina-Llamas, A. E. Chávez-Guajardo, C. A. S. Andrade, K. G. B. Alves, and C. P. de Melo, “Use of magnetic polyaniline/maghemite nanocomposite for DNA retrieval from aqueous solutions,” J Colloid Interface Sci, vol. 434, pp. 167–174, Nov. 2014, doi: 10.1016/j.jcis.2014.08.002.

[82] R. Priyadarshi, null Sauraj, B. Kumar, and Y. S. Negi, “Chitosan film incorporated with citric acid and glycerol as an active packaging material for extension of green chilli shelf life,” Carbohydr Polym, vol. 195, pp. 329–338, Sep. 2018, doi: 10.1016/j.carbpol.2018.04.089.

[83] P. T. Trieu and N. Y. Lee, “Paper-Based All-in-One Origami Microdevice for Nucleic Acid Amplification Testing for Rapid Colorimetric Identification of Live Cells for Point-of-Care Testing,” Anal. Chem., vol. 91, no. 17, pp. 11013–11022, Sep. 2019, doi: 10.1021/acs.analchem.9b01263.

[84] T. Nguyen, S. Zoëga Andreasen, A. Wolff, and D. Duong Bang, “From Lab on a Chip to Point of Care Devices: The Role of Open Source Microcontrollers,” Micromachines (Basel), vol. 9, no. 8, p. 403, Aug. 2018, doi: 10.3390/mi9080403.

[85] X. Qian et al., “Ultrasensitive Electrochemical Detection of Clostridium perfringens DNA Based Morphology-Dependent DNA Adsorption Properties of CeO_2 Nanorods in Dairy Products,” Sensors (Basel), vol. 18, no. 6, p. E1878, Jun. 2018, doi: 10.3390/s18061878.

[86] K. D. Hills, D. A. Oliveira, N. D. Cavallaro, C. L. Gomes, and E. S. McLamore, “Actuation of chitosan-aptamer nanobrush borders for pathogen sensing,” Analyst, vol. 143, no. 7, pp. 1650–1661, Mar. 2018, doi: 10.1039/C7AN02039B.

[87] V. Kamat, S. Pandey, K. Paknikar, and D. Bodas, “A facile one-step method for cell lysis and DNA extraction of waterborne pathogens using a microchip,” Biosensors and Bioelectronics, vol. 99, pp. 62–69, Jan. 2018, doi: 10.1016/j.bios.2017.07.040.

[88] I. A. Nanayakkara, W. Cao, and I. M. White, “Simplifying Nucleic Acid Amplification from Whole Blood with Direct Polymerase Chain Reaction on Chitosan Microparticles,” Anal. Chem., vol. 89, no. 6, pp. 3773–3779, Mar. 2017, doi: 10.1021/acs.analchem.7b00274.

[89] S. Chumwangwapee, A. Chingsungnoen, and S. Siri, “A plasma modified cellulose-chitosan porous membrane allows efficient DNA binding and provides antibacterial properties: A step towards developing a new DNA collecting card,” Forensic Science International: Genetics, vol. 25, pp. 19–25, Nov. 2016, doi: 10.1016/j.fsigen.2016.07.020.

[90] K. R. Pandit, I. A. Nanayakkara, W. Cao, S. R. Raghavan, and I. M. White, “Capture and Direct Amplification of DNA on Chitosan Microparticles in a Single PCR-Optimal Solution,” Anal. Chem., vol. 87, no. 21, pp. 11022–11029, Nov. 2015, doi: 10.1021/acs.analchem.5b03006.

[91] M. Franzreb, M. Siemann-Herzberg, T. J. Hobley, and O. R. T. Thomas, “Protein purification using magnetic adsorbent particles,” Appl Microbiol Biotechnol, vol. 70, no. 5, pp. 505–516, May 2006, doi: 10.1007/s00253-006-0344-3.

[92] C. Kolm et al., “DNA aptamers against bacterial cells can be efficiently selected by a SELEX process using state-of-the art qPCR and ultra-deep sequencing,” Sci Rep, vol. 10, no. 1, p. 20917, Dec. 2020, doi: 10.1038/s41598-020-77221-9.

[93] M. Y. Song, D. Nguyen, S. W. Hong, and B. C. Kim, “Broadly reactive aptamers targeting bacteria belonging to different genera using a sequential toggle cell-SELEX,” Sci Rep, vol. 7, p. 43641, Mar. 2017, doi: 10.1038/srep43641.

[94] M. G. Mauk, C. Liu, M. Sadik, and H. H. Bau, “Microfluidic Devices for Nucleic Acid (NA) Isolation, Isothermal NA Amplification, and Real-Time Detection,” in Mobile Health Technologies, vol. 1256, A. Rasooly and K. E. Herold, Eds. New York, NY: Springer New York, 2015, pp. 15–40. doi: 10.1007/978-1-4939-2172-0_2.

[95] C. C. Boehme et al., “Rapid Molecular Detection of Tuberculosis and Rifampin Resistance,” N Engl J Med, vol. 363, no. 11, pp. 1005–1015, Sep. 2010, doi: 10.1056/NEJMoa0907847.

[96] M. A. Dineva, L. Mahilum-Tapay, and H. Lee, “Sample preparation: a challenge in the development of point-of-care nucleic acid-based assays for resource-limited settings,” Analyst, vol. 132, no. 12, p. 1193, 2007, doi: 10.1039/b705672a.

[97] F. Cui, M. Rhee, A. Singh, and A. Tripathi, “Microfluidic Sample Preparation for Medical Diagnostics,” Annu. Rev. Biomed. Eng., vol. 17, no. 1, pp. 267–286, Dec. 2015, doi: 10.1146/annurev-bioeng-071114-040538.

[98] V. Busin, B. Wells, M. Kersaudy-Kerhoas, W. Shu, and S. T. G. Burgess, “Opportunities and challenges for the application of microfluidic technologies in point-of-care veterinary diagnostics,” Molecular and Cellular Probes, vol. 30, no. 5, pp. 331–341, Oct. 2016, doi: 10.1016/j.mcp.2016.07.004.

[99] A. M. Caliendo et al., “Better Tests, Better Care: Improved Diagnostics for Infectious Diseases,” Clinical Infectious Diseases, vol. 57, no. suppl 3, pp. S139–S170, Dec. 2013, doi: 10.1093/cid/cit578.

[100] T. Notomi, “Loop-mediated isothermal amplification of DNA,” Nucleic Acids Research, vol. 28, no. 12, pp. 63e–663, Jun. 2000, doi: 10.1093/nar/28.12.e63.

[101] G. T. Walker, M. S. Fraiser, J. L. Schram, M. C. Little, J. G. Nadeau, and D. P. Malinowski, “Strand displacement amplification—an isothermal, in vitro DNA amplification technique,” Nucl Acids Res, vol. 20, no. 7, pp. 1691–1696, 1992, doi: 10.1093/nar/20.7.1691.

[102] J. Compton, “Nucleic acid sequence-based amplification,” Nature, vol. 350, no. 6313, pp. 91–92, Mar. 1991, doi: 10.1038/350091a0.

[103] A. B. Nurul Najian, E. A. R. Engku Nur Syafirah, N. Ismail, M. Mohamed, and C. Y. Yean, “Development of multiplex loop mediated isothermal amplification (m-LAMP) label-based gold nanoparticles lateral flow dipstick biosensor for detection of pathogenic Leptospira,” Analytica Chimica Acta, vol. 903, pp. 142–148, Jan. 2016, doi: 10.1016/j.aca.2015.11.015.

[104] Y. Mori, M. Kitao, N. Tomita, and T. Notomi, “Real-time turbidimetry of LAMP reaction for quantifying template DNA,” Journal of Biochemical and Biophysical Methods, vol. 59, no. 2, pp. 145–157, May 2004, doi: 10.1016/j.jbbm.2003.12.005.

[105] T. Notomi, Y. Mori, N. Tomita, and H. Kanda, “Loop-mediated isothermal amplification (LAMP): principle, features, and future prospects,” J Microbiol, vol. 53, no. 1, pp. 1–5, Jan. 2015, doi: 10.1007/s12275-015-4656-9.

[106] J. Abdullah et al., “Rapid detection of Salmonella Typhi by loop-mediated isothermal amplification (LAMP) method,” Braz J Microbiol, vol. 45, no. 4, pp. 1385–1391, 2014, doi: 10.1590/s1517-83822014000400032.

[107] K. Kasahara, H. Ishikawa, S. Sato, Y. Shimakawa, and K. Watanabe, “Development of multiplex loop-mediated isothermal amplification assays to detect medically important yeasts in dairy products,” FEMS Microbiol Lett, vol. 357, no. 2, pp. 208–216, Aug. 2014, doi: 10.1111/1574-6968.12512.

[108] J. Mahony, S. Chong, D. Bulir, A. Ruyter, K. Mwawasi, and D. Waltho, “Multiplex loop-mediated isothermal amplification (M-LAMP) assay for the detection of influenza A/H1, A/H3 and influenza B can provide a specimen-to-result diagnosis in 40 min with single genome copy sensitivity,” J Clin Virol, vol. 58, no. 1, pp. 127–131, Sep. 2013, doi: 10.1016/j.jcv.2013.06.006.

[109] N. W. Lucchi et al., “Real-time fluorescence loop mediated isothermal amplification for the diagnosis of malaria,” PLoS One, vol. 5, no. 10, p. e13733, Oct. 2010, doi: 10.1371/journal.pone.0013733.

[110] Y. Hara-Kudo et al., “Detection of Verotoxigenic Escherichia coli O157 and O26 in food by plating methods and LAMP method: a collaborative study,” Int J Food Microbiol, vol. 122, no. 1–2, pp. 156–161, Feb. 2008, doi: 10.1016/j.ijfoodmicro.2007.11.078.

[111] M. Okamura et al., “Loop-mediated isothermal amplification for the rapid, sensitive, and specific detection of the O9 group of Salmonella in chickens,” Vet Microbiol, vol. 132, no. 1–2, pp. 197–204, Nov. 2008, doi: 10.1016/j.vetmic.2008.04.029.

[112] W. Yamazaki et al., “Development and evaluation of a loop-mediated isothermal amplification assay for rapid and simple detection of Campylobacter jejuni and Campylobacter coli,” J Med Microbiol, vol. 57, no. Pt 4, pp. 444–451, Apr. 2008, doi: 10.1099/jmm.0.47688-0.

[113] Y. Hataoka, L. Zhang, Y. Mori, N. Tomita, T. Notomi, and Y. Baba, “Analysis of specific gene by integration of isothermal amplification and electrophoresis on poly(methyl methacrylate) microchips,” Anal Chem, vol. 76, no. 13, pp. 3689–3693, Jul. 2004, doi: 10.1021/ac035032u.

[114] M. R. Watts et al., “A loop-mediated isothermal amplification (LAMP) assay for Strongyloides stercoralis in stool that uses a visual detection method with SYTO-82 fluorescent dye,” Am J Trop Med Hyg, vol. 90, no. 2, pp. 306–311, Feb. 2014, doi: 10.4269/ajtmh.13-0583.

[115] Y. Bao et al., “CUT-LAMP: Contamination-Free Loop-Mediated Isothermal Amplification Based on the CRISPR/Cas9 Cleavage,” ACS Sens, vol. 5, no. 4, pp. 1082–1091, Apr. 2020, doi: 10.1021/acssensors.0c00034.

[116] J. Li and J. Macdonald, “Advances in isothermal amplification: novel strategies inspired by biological processes,” Biosensors and Bioelectronics, vol. 64, pp. 196–211, Feb. 2015, doi: 10.1016/j.bios.2014.08.069.

[117] B. Deiman, P. van Aarle, and P. Sillekens, “Characteristics and applications of nucleic acid sequence-based amplification (NASBA),” Mol Biotechnol, vol. 20, no. 2, pp. 163–179, Feb. 2002, doi: 10.1385/MB:20:2:163.

[118] J. C. Guatelli, K. M. Whitfield, D. Y. Kwoh, K. J. Barringer, D. D. Richman, and T. R. Gingeras, “Isothermal, in vitro amplification of nucleic acids by a multienzyme reaction modeled after retroviral replication.,” Proc. Natl. Acad. Sci. U.S.A., vol. 87, no. 5, pp. 1874–1878, Mar. 1990, doi: 10.1073/pnas.87.5.1874.

[119] S. Santiago-Felipe, L. A. Tortajada-Genaro, S. Morais, R. Puchades, and Á. Maquieira, “Isothermal DNA amplification strategies for duplex microorganism detection,” Food Chemistry, vol. 174, pp. 509–515, May 2015, doi: 10.1016/j.foodchem.2014.11.080.

[120] H. Liu, X. Du, Y.-X. Zang, P. Li, and S. Wang, “SERS-Based Lateral Flow Strip Biosensor for Simultaneous Detection of Listeria monocytogenes and Salmonella enterica Serotype Enteritidis,” J. Agric. Food Chem., vol. 65, no. 47, pp. 10290–10299, Nov. 2017, doi: 10.1021/acs.jafc.7b03957.

[121] R. K. Daher, G. Stewart, M. Boissinot, and M. G. Bergeron, “Isothermal recombinase polymerase amplification assay applied to the detection of group B streptococci in vaginal/anal samples,” Clin Chem, vol. 60, no. 4, pp. 660–666, Apr. 2014, doi: 10.1373/clinchem.2013.213504.

[122] H. Y. Lau, Y. Wang, E. J. H. Wee, J. R. Botella, and M. Trau, “Field Demonstration of a Multiplexed Point-of-Care Diagnostic Platform for Plant Pathogens,” Anal Chem, vol. 88, no. 16, pp. 8074–8081, Aug. 2016, doi: 10.1021/acs.analchem.6b01551.

[123] L. M. Zanoli and G. Spoto, “Isothermal amplification methods for the detection of nucleic acids in microfluidic devices,” Biosensors (Basel), vol. 3, no. 1, pp. 18–43, Mar. 2013, doi: 10.3390/bios3010018.

[124] S. V. Hamidi, H. Ghourchian, and G. Tavoosidana, “Real-time detection of H5N1 influenza virus through hyperbranched rolling circle amplification,” Analyst, vol. 140, no. 5, pp. 1502–1509, Mar. 2015, doi: 10.1039/c4an01954g.

[125] R. M. Dirks and N. A. Pierce, “Triggered amplification by hybridization chain reaction,” Proc Natl Acad Sci U S A, vol. 101, no. 43, pp. 15275–15278, Oct. 2004, doi: 10.1073/pnas.0407024101.

[126] F. Huang, M. You, D. Han, X. Xiong, H. Liang, and W. Tan, “DNA branch migration reactions through photocontrollable toehold formation,” J Am Chem Soc, vol. 135, no. 21, pp. 7967–7973, May 2013, doi: 10.1021/ja4018495.

[127] B. Koos et al., “Proximity-dependent initiation of hybridization chain reaction,” Nat Commun, vol. 6, p. 7294, Jun. 2015, doi: 10.1038/ncomms8294.

[128] J. Zhang, S. Song, L. Wang, D. Pan, and C. Fan, “A gold nanoparticle-based chronocoulometric DNA sensor for amplified detection of DNA,” Nat Protoc, vol. 2, no. 11, pp. 2888–2895, 2007, doi: 10.1038/nprot.2007.419.

[129] N. Nagatani et al., “Semi-real time electrochemical monitoring for influenza virus RNA by reverse transcription loop-mediated isothermal amplification using a USB powered portable potentiostat,” Analyst, vol. 136, no. 24, pp. 5143–5150, Dec. 2011, doi: 10.1039/c1an15638a.

[130] K. Hsieh, A. S. Patterson, B. S. Ferguson, K. W. Plaxco, and H. T. Soh, “Rapid, sensitive, and quantitative detection of pathogenic DNA at the point of care through microfluidic electrochemical quantitative loop-mediated isothermal amplification,” Angew Chem Int Ed Engl, vol. 51, no. 20, pp. 4896–4900, May 2012, doi: 10.1002/anie.201109115.

[131] “Intercalative Stacking: A Critical Feature of DNA Charge-Transport Electrochemistry | The Journal of Physical Chemistry B.” https://pubs.acs.org/doi/10.1021/jp030753i (accessed May 04, 2022).

[132] S. Tripathy et al., “Limited-resource preparable chitosan magnetic particles for extracting amplification-ready nucleic acid from complex biofluids,” Analyst, vol. 147, no. 1, pp. 165–177, Dec. 2021, doi: 10.1039/d1an01150b.

[133] J. T. Connelly, J. P. Rolland, and G. M. Whitesides, “‘Paper Machine’ for Molecular Diagnostics,” Anal Chem, vol. 87, no. 15, pp. 7595–7601, Aug. 2015, doi: 10.1021/acs.analchem.5b00411.

[134] A. Morgan, D. Babu, B. Reiz, R. Whittal, L. Y. K. Suh, and A. G. Siraki, “Caution for the routine use of phenol red - It is more than just a pH indicator,” Chem Biol Interact, vol. 310, p. 108739, Sep. 2019, doi: 10.1016/j.cbi.2019.108739.

[135] W. A. Al-Soud, L. J. Jönsson, and P. Rådström, “Identification and characterization of immunoglobulin G in blood as a major inhibitor of diagnostic PCR,” J Clin Microbiol, vol. 38, no. 1, pp. 345–350, Jan. 2000, doi: 10.1128/JCM.38.1.345-350.2000.

[136] “Criticality of In-House Preparation of Viral Transport Medium in Times of Shortage During COVID-19 Pandemic - PubMed.” https://pubmed.ncbi.nlm.nih.gov/33225352/ (accessed May 04, 2022).

[137] T. Ahn, J. H. Kim, H.-M. Yang, J. W. Lee, and J.-D. Kim, “Formation Pathways of Magnetite Nanoparticles by Coprecipitation Method,” J. Phys. Chem. C, vol. 116, no. 10, pp. 6069–6076, doi: 10.1021/jp211843g.

[138] V. Zamora-Mora, M. Fernández-Gutiérrez, J. San Román, G. Goya, R. Hernández, and C. Mijangos, “Magnetic core-shell chitosan nanoparticles: rheological characterization and hyperthermia application,” Carbohydr Polym, vol. 102, pp. 691–698, Feb. 2014, doi: 10.1016/j.carbpol.2013.10.101.

[139] S. Tripathy, T. Agarkar, A. Talukdar, M. Sengupta, A. Kumar, and S. Ghosh, “A Comparative Evaluation of Indirect Sequence-Specific Magnetoextraction-aided Fluorescence and Electrochemical LAMP with SARS-CoV-2 Nucleic Acid as the Analyte,” Feb. 2022, doi: 10.26434/chemrxiv-2022-x2qxq.

[140] “Johns Hopkins Coronavirus Resource Center: Home,” Johns Hopkins Coronavirus Resource Center. https://coronavirus.jhu.edu/ (accessed Jan. 24, 2022).

[141] Q. Diagnostics, “FDA instructions on detectimg SARS-CoV-2 RNA with real-time RT-PCR.” FDA. [Online]. Available: https://www.fda.gov/media/136231/download

[142] M. J. Wacker and M. P. Godard, “Analysis of One-Step and Two-Step Real-Time RT-PCR Using SuperScript III,” J Biomol Tech, vol. 16, no. 3, pp. 266–271, Sep. 2005.

[143] “RT-PCR: One step vs. two step | IDT,” Integrated DNA Technologies. https://sg.idtdna.com/pages/support/faqs/what-are-the-advantages-and-disadvantages-of-one-step-vs.-two-step-rt-pcr (accessed Dec. 04, 2021).

[144] V. L. Dao Thi et al., “A colorimetric RT-LAMP assay and LAMP-sequencing for detecting SARS-CoV-2 RNA in clinical samples,” Sci Transl Med, vol. 12, no. 556, p. eabc7075, Aug. 2020, doi: 10.1126/scitranslmed.abc7075.

[145] J. P. Broughton et al., “CRISPR-Cas12-based detection of SARS-CoV-2,” Nat Biotechnol, vol. 38, no. 7, pp. 870–874, Jul. 2020, doi: 10.1038/s41587-020-0513-4.

[146] L. Yu et al., “Rapid Detection of COVID-19 Coronavirus Using a Reverse Transcriptional Loop-Mediated Isothermal Amplification (RT-LAMP) Diagnostic Platform,” Clin Chem, doi: 10.1093/clinchem/hvaa102.

[147] N. Y. Jayanath, L. T. Nguyen, T. T. Vu, and L. D. Tran, “Development of a portable electrochemical loop mediated isothermal amplification (LAMP) device for detection of hepatitis B virus,” RSC Adv., vol. 8, no. 61, pp. 34954–34959, Oct. 2018, doi: 10.1039/C8RA07235C.

[148] A. Ganguli et al., “Rapid isothermal amplification and portable detection system for SARS-CoV-2,” Proc Natl Acad Sci U S A, vol. 117, no. 37, pp. 22727–22735, Sep. 2020, doi: 10.1073/pnas.2014739117.

[149] J. D. Pearson et al., “Comparison of SARS-CoV-2 indirect and direct RT-qPCR detection methods,” Virol J, vol. 18, no. 1, p. 99, May 2021, doi: 10.1186/s12985-021-01574-4.

[150] K. Taki et al., “SARS-CoV-2 detection by fluorescence loop-mediated isothermal amplification with and without RNA extraction,” Journal of Infection and Chemotherapy, vol. 27, no. 2, pp. 410–412, Feb. 2021, doi: 10.1016/j.jiac.2020.10.029.

[151] L. Mautner et al., “Rapid point-of-care detection of SARS-CoV-2 using reverse transcription loop-mediated isothermal amplification (RT-LAMP),” Virology Journal, vol. 17, no. 1, p. 160, Oct. 2020, doi: 10.1186/s12985-020-01435-6.

[152] M. N. Anahtar et al., “Clinical Assessment and Validation of a Rapid and Sensitive SARS-CoV-2 Test Using Reverse Transcription Loop-Mediated Isothermal Amplification Without the Need for RNA Extraction,” Open Forum Infectious Diseases, vol. 8, no. 2, p. ofaa631, Feb. 2021, doi: 10.1093/ofid/ofaa631.

[153] P. Oberacker et al., “Bio-On-Magnetic-Beads (BOMB): Open platform for high-throughput nucleic acid extraction and manipulation,” PLoS Biol, vol. 17, no. 1, p. e3000107, Jan. 2019, doi: 10.1371/journal.pbio.3000107.

[154] S. Tripathy et al., “Limited-resource preparable chitosan magnetic particles for extracting amplification-ready nucleic acid from complex biofluids,” Analyst, vol. 147, no. 1, pp. 165–177, Dec. 2021, doi: 10.1039/d1an01150b.

[155] C.-H. Wang, K.-Y. Lien, T.-Y. Wang, T.-Y. Chen, and G.-B. Lee, “An integrated microfluidic loop-mediated-isothermal-amplification system for rapid sample pre-treatment and detection of viruses.,” Biosens Bioelectron, vol. 26, no. 5, pp. 2045–2052, Jan. 2011, doi: 10.1016/j.bios.2010.08.083.

[156] S. P. Tsai et al., “Nucleic acid capture assay, a new method for direct quantitation of nucleic acids,” Nucleic Acids Res, vol. 31, no. 6, p. e25, Mar. 2003.

[157] C.-H. Wang, K.-Y. Lien, J.-J. Wu, and G.-B. Lee, “A magnetic bead-based assay for the rapid detection of methicillin-resistant Staphylococcus aureus by using a microfluidic system with integrated loop-mediated isothermal amplification.,” Lab Chip, vol. 11, no. 8, pp. 1521–1531, Apr. 2011, doi: 10.1039/c0lc00430h.

[158] C.-L. Lin et al., “A microfluidic system integrated with buried optical fibers for detection of Phalaenopsis orchid pathogens.,” Biosens Bioelectron, vol. 63, pp. 572–579, Jan. 2015, doi: 10.1016/j.bios.2014.08.013.

[159] J. Chen, X. Xu, Z. Huang, Y. Luo, L. Tang, and J.-H. Jiang, “BEAMing LAMP: single-molecule capture and on-bead isothermal amplification for digital detection of hepatitis C virus in plasma.,” Chem Commun (Camb), vol. 54, no. 3, pp. 291–294, Jan. 2018, doi: 10.1039/c7cc08403j.

[160] M. F. Österdahl et al., “Detecting SARS-CoV-2 at point of care: preliminary data comparing loop-mediated isothermal amplification (LAMP) to polymerase chain reaction (PCR).,” BMC Infect Dis, vol. 20, no. 1, p. 783, Oct. 2020, doi: 10.1186/s12879-020-05484-8.

[161] X. Hu et al., “Development and Clinical Application of a Rapid and Sensitive Loop-Mediated Isothermal Amplification Test for SARS-CoV-2 Infection.,” mSphere, vol. 5, no. 4, Aug. 2020, doi: 10.1128/mSphere.00808-20.

[162] S. Klein et al., “SARS-CoV-2 RNA Extraction Using Magnetic Beads for Rapid Large-Scale Testing by RT-qPCR and RT-LAMP.,” Viruses, vol. 12, no. 8, Aug. 2020, doi: 10.3390/v12080863.

[163] A. D. Yu et al., “Development of a Saliva-Optimized RT-LAMP Assay for SARS-CoV-2.,” J Biomol Tech, vol. 32, no. 3, pp. 102–113, Sep. 2021, doi: 10.7171/jbt.21-3203-005.

[164] A. Bektaş et al., “Accessible LAMP-Enabled Rapid Test (ALERT) for Detecting SARS-CoV-2.,” Viruses, vol. 13, no. 5, Apr. 2021, doi: 10.3390/v13050742.

[165] L. M. Dignan, M. S. Woolf, C. J. Tomley, A. Q. Nauman, and J. P. Landers, “Multiplexed Centrifugal Microfluidic System for Dynamic Solid-Phase Purification of Polynucleic Acids Direct from Buccal Swabs.,” Anal Chem, vol. 93, no. 19, pp. 7300–7309, May 2021, doi: 10.1021/acs.analchem.1c00842.

[166] H. Cao et al., “Magnetic-Immuno-Loop-Mediated Isothermal Amplification Based on DNA Encapsulating Liposome for the Ultrasensitive Detection of P-glycoprotein.,” Sci Rep, vol. 7, no. 1, p. 9312, Aug. 2017, doi: 10.1038/s41598-017-10133-3.

[167] S. Kumar, S. Sharma, S. Kumari, V. Pande, D. Savargaonkar, and A. R. Anvikar, “Magnetic Multiplex Loop Mediated Isothermal Amplification (MM-LAMP) technique for simultaneous detection of dengue and chikungunya virus.,” J Virol Methods, vol. 300, p. 114407, Feb. 2022, doi: 10.1016/j.jviromet.2021.114407.

[168] N. Feng et al., “Yersinia pestis detection by loop-mediated isothermal amplification combined with magnetic bead capture of DNA.,” Braz J Microbiol, vol. 49, no. 1, pp. 128–137, Mar. 2018, doi: 10.1016/j.bjm.2017.03.014.

[169] A. B. Nurul Najian, P. C. Foo, N. Ismail, L. Kim-Fatt, and C. Y. Yean, "Probe-specific loop-mediated isothermal amplification magnetogenosensor assay for rapid and specific detection of pathogenic Leptospira.," Mol Cell Probes, vol. 44, pp. 63–68, Apr. 2019, doi: 10.1016/j.mcp.2019.03.001.

[170] L. Zhang et al., "Detection of Shigella in Milk and Clinical Samples by Magnetic Immunocaptured-Loop-Mediated Isothermal Amplification Assay," Frontiers in Microbiology, vol. 9, 2018, doi: 10.3389/fmicb.2018.00094.

[171] Yan Bi, "A Novel SDS Rinse and Immunomagnetic Beads Separation Combined with Real-Time Loop-Mediated Isothermal Amplification for Rapid and Sensitive Detection of Salmonella in Ready-to-Eat Duck Meat," Food analytical methods, vol. v. 13, no. 5, pp. 1166–1175, May 2020, doi: 10.1007/s12161-020-01735-1.

[172] K. Bangpanwimon, P. Mittraparp-Arthorn, K. Srinitiwarawong, and N. Tansila, "Non-Invasive Colorimetric Magneto Loop-Mediated Isothermal Amplification (CM-LAMP) Method for Helicobacter pylori Detection.," J Microbiol Biotechnol, vol. 31, no. 4, pp. 501–509, Apr. 2021, doi: 10.4014/jmb.2101.01008.

[173] B. Tian et al., "Rapid Newcastle Disease Virus Detection Based on Loop-Mediated Isothermal Amplification and Optomagnetic Readout," ACS Sensors, vol. 1, no. 10, pp. 1228–1234, 2016, doi: 10.1021/acssensors.6b00379.

[174] Y. Qin et al., "Rapid and Specific Detection of Escherichia coli O157:H7 in Ground Beef Using Immunomagnetic Separation Combined with Loop-Mediated Isothermal Amplification," Pol. J. Food Nutr. Sci., vol. 68, no. 2, pp. 115–123, 2018, doi: 10.1515/pjfns-2017-0014.

[175] G. Kyei-Poku, D. Gauthier, and G. Quan, "Development of a Loop-Mediated Isothermal Amplification Assay as an Early-Warning Tool for Detecting Emerald Ash Borer (Coleoptera: Buprestidae) Incursions," Journal of Economic Entomology, vol. 113, no. 5, pp. 2480–2494, Jul. 2020, doi: 10.1093/jee/toaa135.

[176] J. Wang et al., "Rapid and Sensitive Detection of RNA Viruses Based on Reverse Transcription Loop-Mediated Isothermal Amplification, Magnetic Nanoparticles, and Chemiluminescence.," J Biomed Nanotechnol, vol. 12, no. 4, pp. 710–716, Apr. 2016, doi: 10.1166/jbn.2016.2244.

[177] S. Wang, N. Liu, L. Zheng, G. Cai, and J. Lin, "A lab-on-chip device for the sample-in-result-out detection of viable Salmonella using loop-mediated isothermal amplification and real-time turbidity monitoring.," Lab Chip, vol. 20, no. 13, pp. 2296–2305, Jun. 2020, doi: 10.1039/d0lc00290a.

[178] Y. Zheng, J. Wu, Y. Yang, M. Liu, and D. Li, "Rapid Detected and Diagnostic Assessment Vacuolating Cytotoxin A (vacA) Gene of Helicobacter pylori by Loop-Mediated Isothermal Amplification (LAMP).," J Nanosci Nanotechnol, vol. 20, no. 3, pp. 1478–1485, Mar. 2020, doi: 10.1166/jnn.2020.17354.

[179] Q. Lin, X. Fang, H. Chen, W. Weng, B. Liu, and J. Kong, "Dual-modality loop-mediated isothermal amplification for pretreatment-free detection of Septin9 methylated DNA in colorectal cancer.," Mikrochim Acta, vol. 188, no. 9, p. 307, Aug. 2021, doi: 10.1007/s00604-021-04979-8.

[180] S. Sharma, M. A. Kabir, and W. Asghar, “Lab-on-a-Chip Zika Detection With Reverse Transcription Loop-Mediated Isothermal Amplification-Based Assay for Point-of-Care Settings.,” Arch Pathol Lab Med, vol. 144, no. 11, pp. 1335–1343, Nov. 2020, doi: 10.5858/arpa.2019-0667-OA.

[181] K. Treder et al., “Optimization of a magnetic capture RT-LAMP assay for fast and real-time detection of potato virus Y and differentiation of N and O serotypes.,” Arch Virol, vol. 163, no. 2, pp. 447–458, Feb. 2018, doi: 10.1007/s00705-017-3635-3.

[182] Y. Sun, T. L. Quyen, T. Q. Hung, W. H. Chin, A. Wolff, and D. D. Bang, “A lab-on-a-chip system with integrated sample preparation and loop-mediated isothermal amplification for rapid and quantitative detection of Salmonella spp. in food samples.,” Lab Chip, vol. 15, no. 8, pp. 1898–1904, Apr. 2015, doi: 10.1039/c4lc01459f.

[183] D. Liu, G. Liang, Q. Zhang, and B. Chen, “Detection of Mycobacterium tuberculosis using a capillary-array microsystem with integrated DNA extraction, loop-mediated isothermal amplification, and fluorescence detection.,” Anal Chem, vol. 85, no. 9, pp. 4698–4704, May 2013, doi: 10.1021/ac400412m.

[184] Q. Dong et al., “A signal-flexible gene diagnostic strategy coupling loop-mediated isothermal amplification with hybridization chain reaction.,” Anal Chim Acta, vol. 1079, pp. 171–179, Nov. 2019, doi: 10.1016/j.aca.2019.06.048.

[185] A. C. Vinayaka, M. Golabi, T. L. Q. Than, A. Wolff, and D. D. Bang, “Point-of-care diagnosis of invasive non-typhoidal Salmonella enterica in bloodstream infections using immunomagnetic capture and loop-mediated isothermal amplification.,” N Biotechnol, vol. 66, pp. 1–7, Jan. 2022, doi: 10.1016/j.nbt.2021.08.003.

[186] X. Zong et al., “Rapid detection of Prunus necrotic ringspot virus using magnetic nanoparticle-assisted reverse transcription loop-mediated isothermal amplification.,” J Virol Methods, vol. 208, pp. 85–89, Nov. 2014, doi: 10.1016/j.jviromet.2014.07.033.

[187] A. Kaur, A. Kapil, R. Elangovan, S. Jha, and D. Kalyanasundaram, “Highly-sensitive detection of Salmonella typhi in clinical blood samples by magnetic nanoparticle-based enrichment and in-situ measurement of isothermal amplification of nucleic acids.,” PLoS One, vol. 13, no. 3, p. e0194817, 2018, doi: 10.1371/journal.pone.0194817.

[188] N. Tanaka et al., “Most-probable-number loop-mediated isothermal amplification-based procedure enhanced with K antigen-specific immunomagnetic separation for quantifying tdh(+) Vibrio parahaemolyticus in molluscan Shellfish.,” J Food Prot, vol. 77, no. 7, pp. 1078–1085, Jul. 2014, doi: 10.4315/0362-028X.JFP-13-536.

[189] T. Yonekawa et al., “Fully Automated Molecular Diagnostic System ‘Simprova’ for Simultaneous Testing of Multiple Items.,” Sci Rep, vol. 10, no. 1, p. 5409, Mar. 2020, doi: 10.1038/s41598-020-62109-5.

[190] Y.-D. Ma et al., “A sample-to-answer, portable platform for rapid detection of pathogens with a smartphone interface.,” Lab Chip, vol. 19, no. 22, pp. 3804–3814, Nov. 2019, doi: 10.1039/c9lc00797k.

[191] S. Hin et al., “Fully automated point-of-care differential diagnosis of acute febrile illness.,” PLoS Negl Trop Dis, vol. 15, no. 2, p. e0009177, Feb. 2021, doi: 10.1371/journal.pntd.0009177.

[192] N. Li, Y. Lu, J. Cheng, and Y. Xu, “A self-contained and fully integrated fluidic cassette system for multiplex nucleic acid detection of bacteriuria.,” Lab Chip, vol. 20, no. 2, pp. 384–393, Jan. 2020, doi: 10.1039/c9lc00994a.

[193] J. Zeng et al., “Rapid detection of Vibrio parahaemolyticus in raw oysters using immunomagnetic separation combined with loop-mediated isothermal amplification.,” Int J Food Microbiol, vol. 174, pp. 123–128, Mar. 2014, doi: 10.1016/j.ijfoodmicro.2014.01.004.

[194] L. Zhang et al., “Development of a rapid, one-step-visual method to detect Salmonella based on IC-LAMP method.,” Iran J Vet Res, vol. 21, no. 1, pp. 20–25, Winter 2020.

[195] G. Papadakis et al., “Micro-nano-bio acoustic system for the detection of foodborne pathogens in real samples.,” Biosens Bioelectron, vol. 111, pp. 52–58, Jul. 2018, doi: 10.1016/j.bios.2018.03.056.

[196] R. Wang et al., “Rapid detection of multiple respiratory viruses based on microfluidic isothermal amplification and a real-time colorimetric method.,” Lab Chip, vol. 18, no. 22, pp. 3507–3515, Nov. 2018, doi: 10.1039/c8lc00841h.

[197] N. Li et al., “Multiplexed detection of respiratory pathogens with a portable analyzer in a ‘raw-sample-in and answer-out’ manner.,” Microsyst Nanoeng, vol. 7, p. 94, 2021, doi: 10.1038/s41378-021-00321-7.

[198] Z. Chen et al., “A Rapid, Self-confirming Assay for HIV: Simultaneous Detection of Anti-HIV Antibodies and Viral RNA.,” J AIDS Clin Res, vol. 7, no. 1, Jan. 2016, doi: 10.4172/2155-6113.1000540.

[199] N. Sandetskaya et al., “An integrated versatile lab-on-a-chip platform for the isolation and nucleic acid-based detection of pathogens.,” Future Sci OA, vol. 3, no. 2, p. FSO177, Jun. 2017, doi: 10.4155/fsoa-2016-0088.

[200] G. Xu, H. Zhao, J. M. Cooper, and J. Reboud, “A capillary-based multiplexed isothermal nucleic acid-based test for sexually transmitted diseases in patients.,” Chem Commun (Camb), vol. 52, no. 82, pp. 12187–12190, Oct. 2016, doi: 10.1039/c6cc05679b.

[201] S. J. Harper, L. I. Ward, and G. R. G. Clover, “Development of LAMP and real-time PCR methods for the rapid detection of Xylella fastidiosa for quarantine and field applications.,” Phytopathology, vol. 100, no. 12, pp. 1282–1288, Dec. 2010, doi: 10.1094/PHYTO-06-10-0168.

[202] M. Bartosik, L. Jirakova, M. Anton, B. Vojtesek, and R. Hrstka, “Genomagnetic LAMP-based electrochemical test for determination of high-risk HPV16 and HPV18 in clinical samples.,” Anal Chim Acta, vol. 1042, pp. 37–43, Dec. 2018, doi: 10.1016/j.aca.2018.08.020.

[203] X. Xie et al., “Engineering SARS-CoV-2 using a reverse genetic system,” Nat Protoc, vol. 16, no. 3, Art. no. 3, Mar. 2021, doi: 10.1038/s41596-021-00491-8.

[204] M. El-Tholoth, H. H. Bau, and J. Song, “A Single and Two-Stage, Closed-Tube, Molecular Test for the 2019 Novel Coronavirus (COVID-19) at Home, Clinic, and Points of Entry,” ChemRxiv, Feb. 2020, doi: 10.26434/chemrxiv.11860137.

[205] K. Nawattanapaiboon et al., “Colorimetric reverse transcription loop-mediated isothermal amplification (RT-LAMP) as a visual diagnostic platform for the detection of the emerging coronavirus SARS-CoV-2,” Analyst, vol. 146, no. 2, pp. 471–477, Jan. 2021, doi: 10.1039/d0an01775b.

[206] W. S. Jang et al., “Development of a multiplex Loop-Mediated Isothermal Amplification (LAMP) assay for on-site diagnosis of SARS CoV-2,” PLoS One, vol. 16, no. 3, p. e0248042, 2021, doi: 10.1371/journal.pone.0248042.

[207] M. El-Tholoth, H. H. Bau, and J. Song, “A Single and Two-Stage, Closed-Tube, Molecular Test for the 2019 Novel Coronavirus (COVID-19) at Home, Clinic, and Points of Entry,” ChemRxiv, Feb. 2020, doi: 10.26434/chemrxiv.11860137.

[208] K. Nawattanapaiboon et al., “Colorimetric reverse transcription loop-mediated isothermal amplification (RT-LAMP) as a visual diagnostic platform for the detection of the emerging coronavirus SARS-CoV-2,” Analyst, vol. 146, no. 2, pp. 471–477, Jan. 2021, doi: 10.1039/d0an01775b.

[209] W. S. Jang et al., “Development of a multiplex Loop-Mediated Isothermal Amplification (LAMP) assay for on-site diagnosis of SARS CoV-2,” PLoS One, vol. 16, no. 3, p. e0248042, 2021, doi: 10.1371/journal.pone.0248042.

[210] C. Chai, Z. Xie, and E. Grotewold, “SELEX (Systematic Evolution of Ligands by EXponential Enrichment), as a powerful tool for deciphering the protein-DNA interaction space,” Methods Mol Biol, vol. 754, pp. 249–258, 2011, doi: 10.1007/978-1-61779-154-3_14.

[211] L. Shi, L. Ba, Y. Xiong, and G. Peng, “A hybridization chain reaction based assay for fluorometric determination of exosomes using magnetic nanoparticles and both aptamers and antibody as recognition elements,” Mikrochim Acta, vol. 186, no. 12, p. 796, Nov. 2019, doi: 10.1007/s00604-019-3823-9.

[212] X. Chen et al., “Microfluidic Chip for Multiplex Detection of Trace Chemical Contaminants Based on Magnetic Encoded Aptamer Probes and Multibranched DNA Nanostructures as Signal Tags,” ACS Sens, vol. 4, no. 8, pp. 2131–2139, Aug. 2019, doi: 10.1021/acssensors.9b00963.

[213] K. Zhang et al., “A fluorometric aptamer method for kanamycin by applying a dual amplification strategy and using double Y-shaped DNA probes on a gold bar and on magnetite nanoparticles,” Microchimica Acta, vol. 186, Jan. 2019, doi: 10.1007/s00604-018-3207-6.

[214] Y. Wang et al., “Upconversion Fluorescent Aptasensor for Polychlorinated Biphenyls Detection Based on Nicking Endonuclease and Hybridization Chain Reaction Dual-Amplification Strategy,” Anal Chem, vol. 90, no. 16, pp. 9936–9942, Aug. 2018, doi: 10.1021/acs.analchem.8b02159.

[215] Q. Zhou, Y. Lin, K. Zhang, M. Li, and D. Tang, “Reduced graphene oxide/BiFeO3 nanohybrids-based signal-on photoelectrochemical sensing system for prostate-specific antigen

detection coupling with magnetic microfluidic device," Biosens Bioelectron, vol. 101, pp. 146–152, Mar. 2018, doi: 10.1016/j.bios.2017.10.027.

[216] C. Feng, Z. Hou, W. Jiang, L. Sang, and L. Wang, "Binding induced colocalization activated hybridization chain reaction on the surface of magnetic nanobead for sensitive detection of adenosine," Biosens Bioelectron, vol. 86, pp. 966–970, Dec. 2016, doi: 10.1016/j.bios.2016.07.108.

[217] Y. Zhang, W. Ren, H. Q. Luo, and N. B. Li, "Label-free cascade amplification strategy for sensitive visual detection of thrombin based on target-triggered hybridization chain reaction-mediated in situ generation of DNAzymes and Pt nanochains," Biosens Bioelectron, vol. 80, pp. 463–470, Jun. 2016, doi: 10.1016/j.bios.2016.02.016.

[218] R. M. Dirks and N. A. Pierce, "Triggered amplification by hybridization chain reaction," Proc Natl Acad Sci U S A, vol. 101, no. 43, pp. 15275–15278, Oct. 2004, doi: 10.1073/pnas.0407024101.

[219] R. Stoltenburg, P. Krafčiková, V. Víglaský, and B. Strehlitz, "G-quadruplex aptamer targeting Protein A and its capability to detect Staphylococcus aureus demonstrated by ELONA," Sci Rep, vol. 6, p. 33812, Sep. 2016, doi: 10.1038/srep33812.

[220] S. Bhattarai, B. K. Sharma, N. Subedi, S. Ranabhat, and M. P. Baral, "Burden of Serious Bacterial Infections and Multidrug-Resistant Organisms in an Adult Population of Nepal: A Comparative Analysis of Minimally Invasive Tissue Sampling Informed Mortality Surveillance of Community and Hospital Deaths," Clin Infect Dis, vol. 73, no. Suppl_5, pp. S415–S421, Dec. 2021, doi: 10.1093/cid/ciab773.

[221] S. Bustin, R. Mueller, G. Shipley, and T. Nolan, "COVID-19 and Diagnostic Testing for SARS-CoV-2 by RT-qPCR-Facts and Fallacies," Int J Mol Sci, vol. 22, no. 5, p. 2459, Feb. 2021, doi: 10.3390/ijms22052459.

[222] "Methods for Rapid Detection of Foodborne Pathogens: An Overview." https://scialert.net/abstract/?doi=ajft.2011.87.102 (accessed Mar. 17, 2022).

[223] X. Zhao, C.-W. Lin, J. Wang, and D. H. Oh, "Advances in rapid detection methods for foodborne pathogens," J Microbiol Biotechnol, vol. 24, no. 3, pp. 297–312, Mar. 2014, doi: 10.4014/jmb.1310.10013.

[224] A. M. B. Vidal and W. R. Catapani, "Enzyme-linked immunosorbent assay (ELISA) immunoassaying versus microscopy: advantages and drawbacks for diagnosing giardiasis," Sao Paulo Med J, vol. 123, no. 6, pp. 282–285, Nov. 2005, doi: 10.1590/s1516-31802005000600006.

[225] D. White et al., "Forensic Analysis by Comprehensive Rapid Detection of Pathogens and Contamination Concentrated in Biofilms in Drinking Water Systems for Water Resource Protection and Management," Environmental Forensics - ENVIRON FORENSICS, vol. 4, pp. 63–74, Mar. 2003, doi: 10.1080/15275920303481.

[226] C. Schrader, A. Schielke, L. Ellerbroek, and R. Johne, "PCR inhibitors - occurrence, properties and removal," J Appl Microbiol, vol. 113, no. 5, pp. 1014–1026, Nov. 2012, doi: 10.1111/j.1365-2672.2012.05384.x.

[227] L. El Bali, A. Diman, A. Bernard, N. H. C. Roosens, and S. C. J. De Keersmaecker, "Comparative study of seven commercial kits for human DNA extraction from urine samples suitable

for DNA biomarker-based public health studies," J Biomol Tech, vol. 25, no. 4, pp. 96–110, Dec. 2014, doi: 10.7171/jbt.14-2504-002.

[228] C. F. Anticona Huaynate et al., "Diagnostics barriers and innovations in rural areas: insights from junior medical doctors on the frontlines of rural care in Peru," BMC Health Serv Res, vol. 15, p. 454, Oct. 2015, doi: 10.1186/s12913-015-1114-7.

[229] C. Tang et al., "Application of magnetic nanoparticles in nucleic acid detection," J Nanobiotechnology, vol. 18, no. 1, p. 62, Apr. 2020, doi: 10.1186/s12951-020-00613-6.

[230] L. Yi, Y. Huang, T. Wu, and J. Wu, "A magnetic nanoparticles-based method for DNA extraction from the saliva of stroke patients," Neural Regen Res, vol. 8, no. 32, pp. 3036–3046, Nov. 2013, doi: 10.3969/j.issn.1673-5374.2013.32.007.

[231] D. Kami, S. Takeda, Y. Itakura, S. Gojo, M. Watanabe, and M. Toyoda, "Application of magnetic nanoparticles to gene delivery," Int J Mol Sci, vol. 12, no. 6, pp. 3705–3722, 2011, doi: 10.3390/ijms12063705.

[232] L. Maldonado-Camargo, M. Unni, and C. Rinaldi, "Magnetic Characterization of Iron Oxide Nanoparticles for Biomedical Applications," Methods Mol Biol, vol. 1570, pp. 47–71, 2017, doi: 10.1007/978-1-4939-6840-4_4.

[233] D. Ling and T. Hyeon, "Chemical design of biocompatible iron oxide nanoparticles for medical applications," Small, vol. 9, no. 9–10, pp. 1450–1466, May 2013, doi: 10.1002/smll.201202111.

[234] H. Wei, Y. Hu, J. Wang, X. Gao, X. Qian, and M. Tang, "Superparamagnetic Iron Oxide Nanoparticles: Cytotoxicity, Metabolism, and Cellular Behavior in Biomedicine Applications," Int J Nanomedicine, vol. 16, pp. 6097–6113, 2021, doi: 10.2147/IJN.S321984.

[235] Q. Feng, Y. Liu, J. Huang, K. Chen, J. Huang, and K. Xiao, "Uptake, distribution, clearance, and toxicity of iron oxide nanoparticles with different sizes and coatings," Sci Rep, vol. 8, no. 1, p. 2082, Feb. 2018, doi: 10.1038/s41598-018-19628-z.

[236] F. M. Kievit et al., "PEI-PEG-Chitosan Copolymer Coated Iron Oxide Nanoparticles for Safe Gene Delivery: synthesis, complexation, and transfection," Adv Funct Mater, vol. 19, no. 14, pp. 2244–2251, Jul. 2009, doi: 10.1002/adfm.200801844.

[237] E. Torres-Chavolla and E. C. Alocilja, "Nanoparticle based DNA biosensor for tuberculosis detection using thermophilic helicase-dependent isothermal amplification," Biosens Bioelectron, vol. 26, no. 11, pp. 4614–4618, Jul. 2011, doi: 10.1016/j.bios.2011.04.055.

[238] Y. Bai et al., "Synthesis of amino-rich silica-coated magnetic nanoparticles for the efficient capture of DNA for PCR," Colloids Surf B Biointerfaces, vol. 145, pp. 257–266, Sep. 2016, doi: 10.1016/j.colsurfb.2016.05.003.

[239] "DNA aptamers against bacterial cells can be efficiently selected by a SELEX process using state-of-the art qPCR and ultra-deep sequencing - PubMed." https://pubmed.ncbi.nlm.nih.gov/33262379/ (accessed Mar. 17, 2022).

[240] M. Y. Song, D. Nguyen, S. W. Hong, and B. C. Kim, “Broadly reactive aptamers targeting bacteria belonging to different genera using a sequential toggle cell-SELEX,” Sci Rep, vol. 7, p. 43641, Mar. 2017, doi: 10.1038/srep43641.

[241] “Point-of-care diagnostics for infectious diseases: From methods to devices - PubMed.” https://pubmed.ncbi.nlm.nih.gov/33584847/ (accessed Mar. 17, 2022).

[242] Y. Cao et al., “Development of a real-time fluorescence loop-mediated isothermal amplification assay for rapid and quantitative detection of Ustilago maydis,” Sci Rep, vol. 7, no. 1, p. 13394, 17 2017, doi: 10.1038/s41598-017-13881-4.

LIST OF PUBLICATIONS AND PATENTS

Journal Publications:

1. *Limited-resource preparable chitosan magnetic particles for extracting amplification-ready nucleic acid from complex biofluids*. **Sayantan Tripathy**, Ashish Kumar Chalana, Arunansu Talukdar, P. V. Rajesh, Abhijit Saha, Goutam Pramanik* and Souradyuti Ghosh *, Analyst, RSC, 2022,147, 165-177 . [IF-4.6, Q1]

2. *Oxygen Vacancy Modulated MnO2 Bi-Electrode System for Attomole-Level Pathogen Nucleic Acid Sequence Detection*. Tanvi Agarkar, Vandana Kuttappan Nair, **Sayantan Tripathy**, Vipin Chawla, Souradyuti Ghosh, Ashvani Kumar*. Electrochimica acta, Volume 407, 1 March 2022, 139876 Elsevier, (just accepted) [IF-6.9, Q1]

3. *Magnetic beads-based sequence specific nucleic acid extraction coupled with electrochemical loop mediated isothermal amplification for rapid detection of SARS-CoV-2*. **Sayantan Tripathy**, Tanvi Agarkar, Ashvani Kumar, Mrittika Sengupta, Arunansu Talukdar, Souradyuti Ghosh* Sensors and Actuators B,Chemical Elsevier.[IF-7.3,Q1] (under revision)

4. *Titanium Oxide-Vanadium Oxide nanocompositebased solid state dual-electrode sensor for nucleic acid detection*. Tanvi Agarkar[#], **Sayantan Tripathy**[#], Ashvani Kumar, Mrittika Sengupta, Arunansu Talukdar, Souradyuti Ghosh*. Under review at ACS Analytical Chemistry [IF-6.9,Q1] ([#], joint 1st author)

5. *Aptamer-magnetic beads-based Hybridization chain reaction for pathogen detection based on colorimetric readouts in resource limited area*. **Sayantan Tripathy**, Arunansu Talukdar, and Souradyuti Ghosh * (manuscript prepared)

Patents:

1. Souradyuti Ghosh, Ashvani Kumar, Mrittika Sengupta, Arunansu Talukdar, Heera Singh Gariya, Shrawan Kumar, Vandana K Nair, **Sayantan Tripathy**, Tanvi Agarkar. *Methods for identification of charged biopolymer*. (Indian patent application, 2021, filing number 202111037358)

2. **Sayantan Tripathy**, Souradyuti Ghosh. *A method for nucleic acid extraction using coated magnetic particles and detection thereof*. (Indian patent application, 2021, filing number 202111004691).

Conference:

- Presented a poster titled "*Ultrasensitive Detection of Nucleic Acid using Limited Resource Synthesizable Chitosan Magnetic Particles Combined with Downstream Real-Time Amplification*" at conference in 2nd Virtual International symposium of RSC chemical biology and bioorganic group in University of Nottingham, United Kingdom, 2021.

Synopsis on

Surface Modified Magnetic particles in Combination with Isothermal Nucleic Acid Amplification for Rapid Pathogen Detection

Submitted by

Sayantan Tripathy (E18SOE801)

Ph.D. Scholar

Supervised by Dr. Souradyuti Ghosh

Department of Chemistry

School of Engineering and Applied Sciences

Bennett University

Greater Noida, UP-201310

A dissertation submitted to Bennett University in conformity with the requirements for the degree of Doctor of Philosophy

1. Introduction:

Diseases caused by microbial pathogens pose a big warning to social health. They have escalated at an alarming rate since past few decades[1]. Among the most common predominant pathogenic bacteria, Salmonella sp, *Escherichia coli*, *Staphylococcus aureus*, *Listeria monocytogenes,* and *Vibrio parahaemolyticus* are some of the most frequently reported pathogens. From the initiation of the SARS-CoV-2 pandemic, nucleic acid amplification tests (NAATs) like polymerase chain reaction (PCR). quantitative real-time reverse transcriptase PCR (qRT-PCR) has persisted the major detection techniques for sensing and restriction of SARS-CoV-2[2]. Requirement of prior extracted nucleic acid, high end instruments and highly trained personnel make the above mentioned NAATs not compatible with the resource limited area. Therefore, originating vigorous methods for fast and accurate detection of pathogen is required. Conventional, plate counting method utilizes a selective nutrient medium specific to pathogen of interest which is applied to identification of that particular pathogen[3] [4]. Despite the fact that the method is authenticate, specific and accurate, its prolonged procedure (18-24 h) and laborious methods obstructing of advancing it to the POC (point-of-care) detection[5]. Immunology based methods could be used for the detection of the pathogen, but the uncertainty of antibodies and high cost which play a vital role in pathogen identification limits its application[5]. Alternatively, pathogen genomic DNA extracted from clinical sample was an essential tool for identification of genetic variation, mutation analysis or DNA biomarkers[6]. DNA isolation in molecular diagnosis was necessary as biofluids contain PCR inhibitors like hemoglobin, albumin, or lactoferrin that can contaminate the template DNA and can affect downstream analysis[7]. Commercially available tools for nucleic acid extraction are cellulose-based technologies, silica-based technologies, or anion exchange technologies[8], However, all of the above methods involve refrigerated centrifuge, which is mostly unavailable except at centralized lab, therefore increasing the assay cost and time. It can be noted that the requirement of costly instruments and highly trained technicians hampering their extensive applications[9]. Therefore, the field of molecular diagnosis has recently seen the tremendous development of smart polymeric and nanomaterials for rapid DNA isolation. Among these, magnetic nanoparticles modified with DNA binding material can provide mostly instrument-free rapid DNA isolation[10] [11]. Fe_3O_4 nanoparticles (NPs), the commonly used magnetic nanoparticles as well as its conjugates are now the main attention in the biomedical field, specifically for targeted drug/gene delivery systems[12], due to their outstanding

magnetism[13], biocompatibility[14], comparatively low toxicity[15], biodegradability, and other features[16]. Bare iron oxide nanoparticles were easy to agglomerate and oxidize, and for this reason this types of nanoparticles were subjected to different biomaterial coating for targeted drug/gene delivery. Scientists have used calf thymus DNA[17], plasmid DNA[18] for gene delivery or they have used iron oxide as an aptasensor. There were several amines and cellulose, silica was used for coating magnetic nanoparticles for gene delivery and biosensing, such as detection of DNA hybridization using Au/Fe_3O_4[19], nanoparticle-based DNA biosensor[20], Amine based silica-coated magnetic nanoparticles are generally used for systematic capture of DNA for PCR[21], and gene transfer. It was observed from the literature survey that most of the micro device use chitosan for extensive DNA capturing as chitosan was biocompatible. Chitosan has a free amine group that can be controlled based on pH change and chitosan has a similar DNA capturing capacity like other commercial kits based on silica, cellulose but nucleic acid based extraction has limitation to differentiate between viable and non viable pathogen.

Immunoassays or antigen based methods could also be used for the identification of the viable pathogen, but high cost and uncertainty of antibodies limits its application. Aptamers, originated by systematic evolution of ligands by exponential enrichment are oligonucleotides which can bind to their target protein or nucleic acid with high affinity comparable to that of the antibody[22]. Because of its low cost, and amenability to chemical modifications, high stability, aptamers have become a strong analytical procedure for highly sensitive detection, especially for bacteria present in food and environmental samples, and have shown desirable reliability[23]. The aptamer-based detections are rapid and specific and can be used for detections without special requirements. In comparison to an antibody, the great advantage of an aptamer is that it can replicate itself, generating the amplification signals which successfully enhance the detection sensitivity.

Importance of our work and Research gap:

However, due to the difficulty of conjugation techniques with MNP with published DNA binding materials, few of them have been commercialized. Also, the high cost of commercialized MNP and instrument requirement for centrifuge column-based isolation, the field of molecular diagnosis still requires the development of low-cost DNA binders.

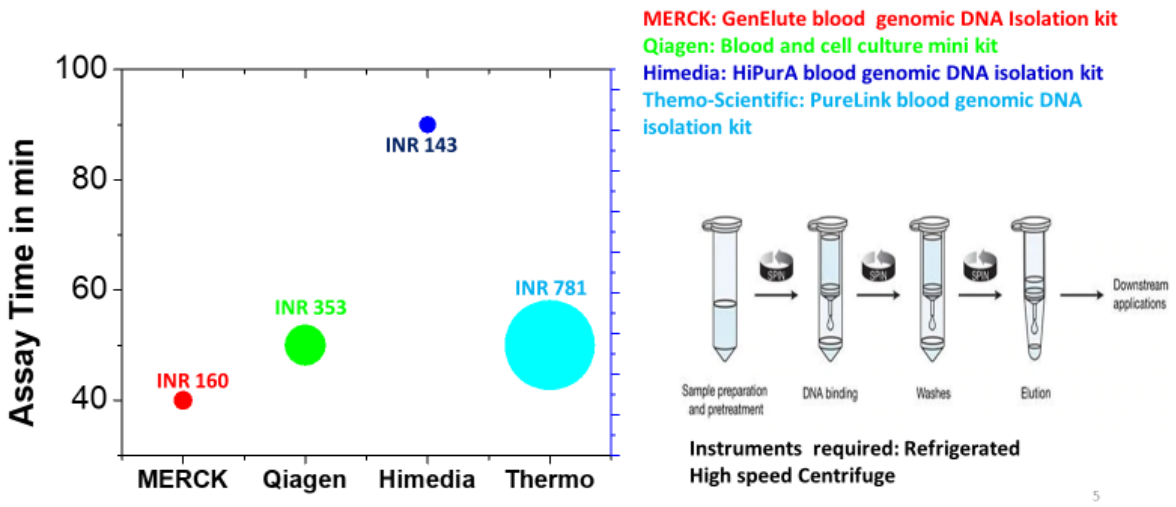

Fig 1: Comparison of cost & time of silica-based commercial spin-column kits for Blood DNA extraction

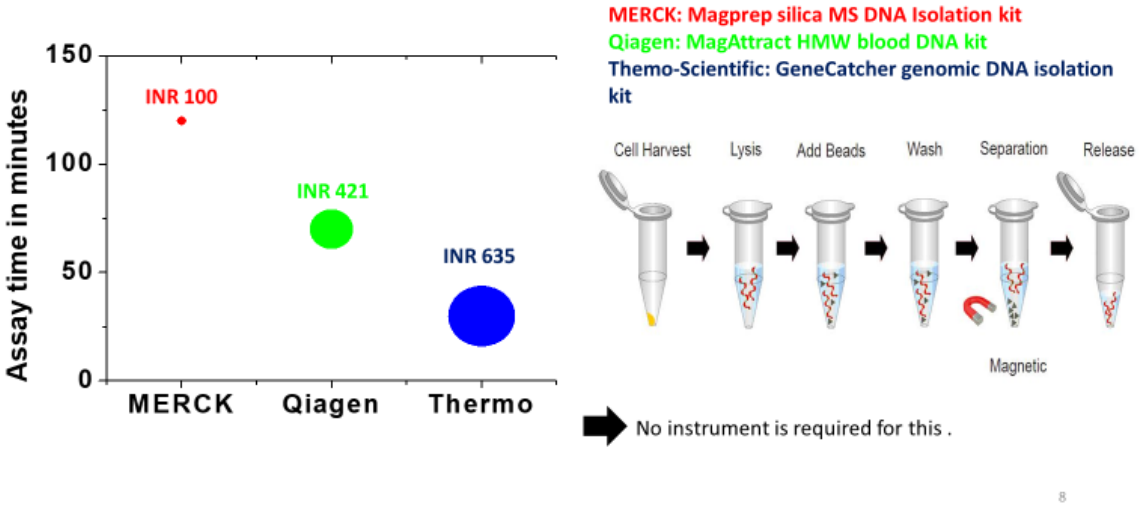

Fig 2: Comparison of cost & time of commercial magnetic beads-based assay for DNA extraction

It has been noticed that very few commercial companies deal with direct amplification (no extraction or very less extraction time) kits with very high cost.

Table 1: Comparison of assay time and cost of commercial magnetic beads for nucleic acid extraction plus amplification

Company name	Kit name	Total assay time	Cost/reaction(INR)
Merck	SYBR® Green Extract-N-Amp™ Tissue PCR Kit	15 mins-extraction	222
Merck	Extract-N-Amp™ Blood PCR Kit	15 mins-extraction	204
Thermo Scientific	AmpFLSTR™ Identifiler™ Direct PCR Amplification Kit	No extraction is needed only lysis	3220

From the Data survey (Figure 1-2, Table 1) from different commercial kits, it was clear that DNA extraction assay time and their respective kit's cost were inversely proportional. The conventional ways of nucleic acid extraction using spin column based kits (Figure 1) requires costly instruments such as high speed refrigerated centrifuge for nucleic acid extraction which limits its application in resource constrained area. The fabrication process of spin column is also complicated by the end users themselves. As an example for recent pandemic times these spin columns got out of market as the demand of these spin columns overwhelms the supply chain.

Magnetic beads based extraction overcomes the needs of costly instruments and highly trained personnel during nucleic acid amplification but high cost (Table 1) and less on beads amplification limits their application for point of care sample analysis. Despite the advancements on silica or carboxyl-based magnetic beads based nucleic acid extraction and widespread application; it has some shortcomings e.g-utilizing of chaotropic salts and ethanol for separating polymerase inhibitors which affects in their downstream application procedure. Additionally, very less magnetic beads that have been reported for nucleic acid extraction is yet to be commercialized.

At present, real time polymerase chain reaction is gold standard of detection of any pathogen due to its accuracy and specificity. However this approach is time consuming and it requires highly trained personnel and highly equipped lab infrastructure which is a limiting factor in resource constrained area. This drawbacks of conventional detection procedure has increased the advancement of various isothermal nucleic acid amplification detection procedures (iNAATs)[24].

2. Aims and Objectives:

Our research area focuses on the development of nanomaterials which will enable to fulfill the current research gap for

1. Rapid DNA extraction without using any high-cost instruments
2. Inexpensive compare to conventional methods
3. If the extracted DNA was applicable for downstream nucleic acid amplification or isothermal nucleic acid amplification
4. Direct amplification from biological sample without using any high end instruments.
5. Detection of viable pathogen using aptamers which is less costly than conventional antigen based detection.

The objectives of our research work with their context are stated below

Objective 1: Charge switching magnetic particle based rapid DNA extraction and downstream amplification.

Context of objective 1:

- Rapid DNA extraction for resource limited area.
- Fast and non-instrument intensive to preparation
- High-end instrument free technique.
- Should be inexpensive.
- Extracted DNA suitable for downstream readouts. (NAATs & iNAATs)

Objective 2: Magnetic beads based sequence specific nucleic acid extraction of SARS-CoV-2 coupled with in situ electrochemical LAMP.

Context of objective 2

- Alternative of highly expensive antigen based detection.
- Sequence specific capture of target nucleic acid increases the specificity of the whole assay.
- Limited resource area friendly.
- High end infrastructure is not needed.
- Less sample to answer time.

Objective 3: Aptamer-magnetic beads based Hybridization chain reaction for pathogen detection.

Context of objective 3

- Alternative of highly expensive antigen based detection.
- Differentiate between viable and nonviable pathogen.

3. Research Methodology:

4.1 Working principle of chitosan coated iron oxide nanoparticles:

Chitosan was a product of deacetylated chitin which has biocompatible and biodegradable characteristics. In our studies, we have primarily used medium molecular weight chitosan, which was a polymer with an average 120,000 Da molecular weight. It has an amine (NH_2) group which has a pKa of 6.5, which has a charge controlled behavior. This protonation deprotonation behaviour of chitosan can be calculated by the Henderson–Hasselbalch equation, pH = pKa + log([A-]/[HA]). Since DNA was negatively charged, the positively charged chitosan can,

therefore, be employed for capturing DNA at a certain pH (when pH <pKa). Then after increasing the pH (when pH >pKa), this captured DNA can be released (scheme1).

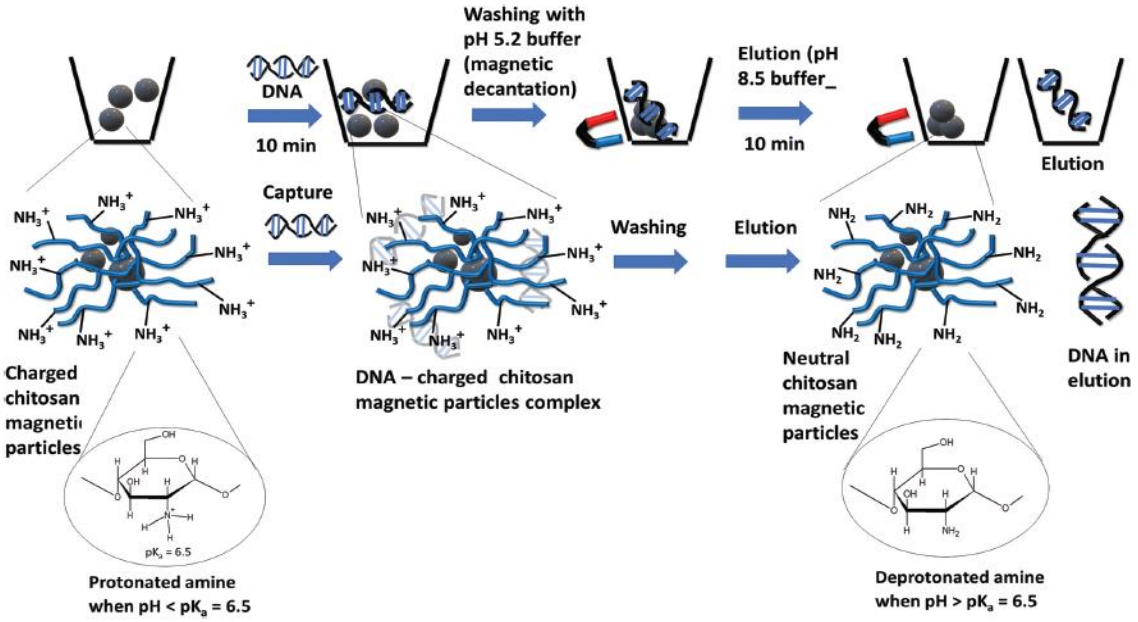

Scheme 1: Chitosan coated magnetic particles based DNA extraction

4.2 Strategy to evaluate the assay is amenable to downstream amplification:

One type of Chitosan coated magnetic nanoparticles was synthesized by coprecipitation with an additional curing step (CCCMP) and the second type of magnetic nanoparticles coated with chitosan was synthesized with a physical cross linker called sodium tri polyphosphate (ECCMP) and the resultant dried magnetic nanoparticles was characterized with FE-SEM, EDX, FT-IR, XRD, DLS, Zetasizer. DNA binding assay was used for elution from chitosan coated MNPs using genomic DNA .The eluted DNA was subjected to UV_{260} to find out the DNA binding capacity of magnetic nanoparticles. The eluted nucleic acid is in the clinical concentration, i.e., 10^4 copies/mL or lower it was impossible to detect the same in UV. The usual practice is therefore to amplify the extracted nucleic acid using primers specific to a gene of that species. If it is amplified then it can be concluded that the nucleic acid originated from the organism of interest. So, the eluted DNA was subjected to

LAMP which is known for its specificity. Limit of Detection refers to what is the lowest concentration of analyte that can be detected in an assay.

Two independent sets of assays was performed, one with the aqueous genomic DNA concentration and second with the serially diluted cell lysate. Both the experiments was performed with both types of magnetic nanoparticles. The amplification reaction was performed with SYBR-I fluorescent dye and reaction progress was tracked with qPCR machine. Real-time LAMP was conducted using methods reported[25]. The extraction amplification assay was checked for human genomic DNA sample with aqueous solution and with fetal bovine serum (FBS) spiked solution. FBS has its own PCR inhibitory properties. Compatability was checked whether our chitosan –MNP can rule out the PCR inhibitors from clinical sample or not and eluted DNA was subjected to qPCR to find out the limit of detection for the clinical sample.

4.3 Strategies of sequence specific magneto-capture of SARS-CoV-2 nucleic acid:

We used two types of in vitro sequence specific magneto capture assay on solid support- direct magneto capture (Scheme 2A) and indirect magneto capture (Scheme 2B) with the clinically significant 1000 and 100 copies of plasmid in aqueous solution. For direct magneto capture, 5' biotinylated oligonucleotides (b*) complementary to RdRp gene (b) was employed firstly to immobilize with streptavidin coated magnetic nanoparticles followed by annealing with target plasmid (b c*) to investigate the performance of on beads downstream readout capability by real time LAMP. For the indirect magneto capture, 5' biotinylated oligonucleotides was annealed with target (b c*) first, to form the binary complex followed by attachment of streptavidin coated MNP. The next steps are same for both of the sequence specific magneto capture studies. Using magnetic decantation wash, any polymerase inhibitors, non-target nucleic acid can be physically separated from the magnetic bead bound binary complex. The complex immobilized in magnetic nanoparticles or solid support added itself into the amplification mix (in situ amplification). The total extraction assay time for direct and indirect sequence specific magneto capture is 60 minutes and 30 minutes respectively. Clinical sample consist target nucleic acid with various polymerase inhibitors which effect downstream readouts. Presence of host genomic DNA sometimes interfere in the specificity and of downstream amplification. So. we assessed for the on-beads (in situ) amplification for direct

and indirect magneto extraction studies with 10^1-10^3 copies of plasmid in presence of host genomic DNA and 10% FBS to investigate the effectiveness of the magnetocapture.

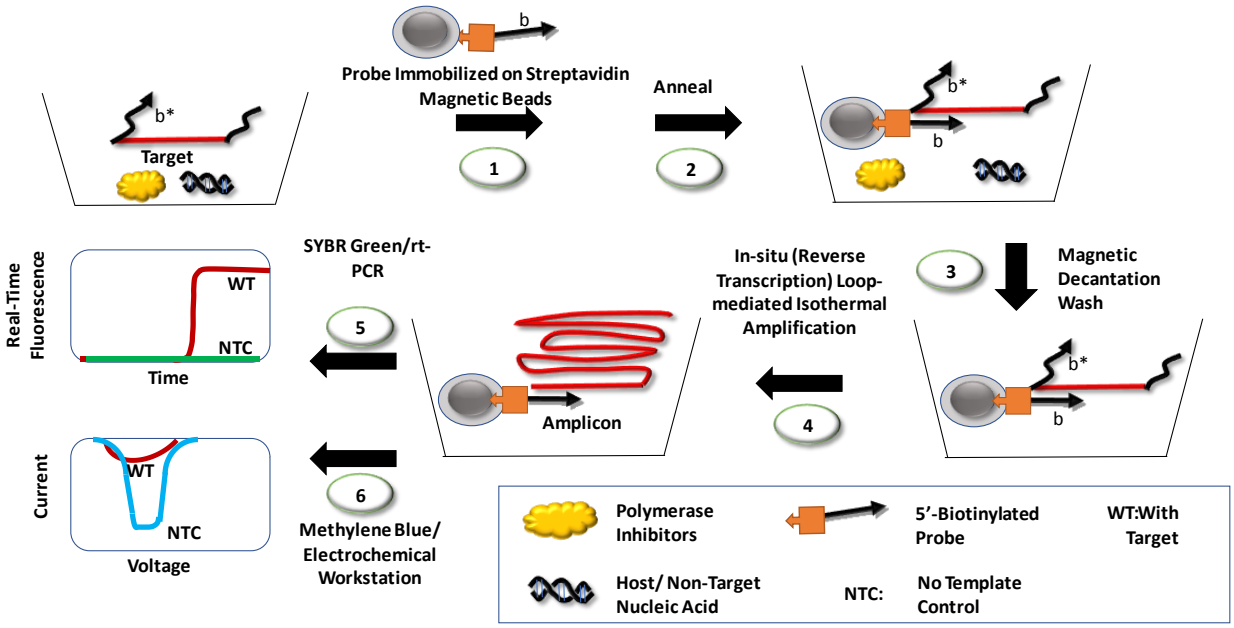

Scheme 2: A, Direct magneto-capture

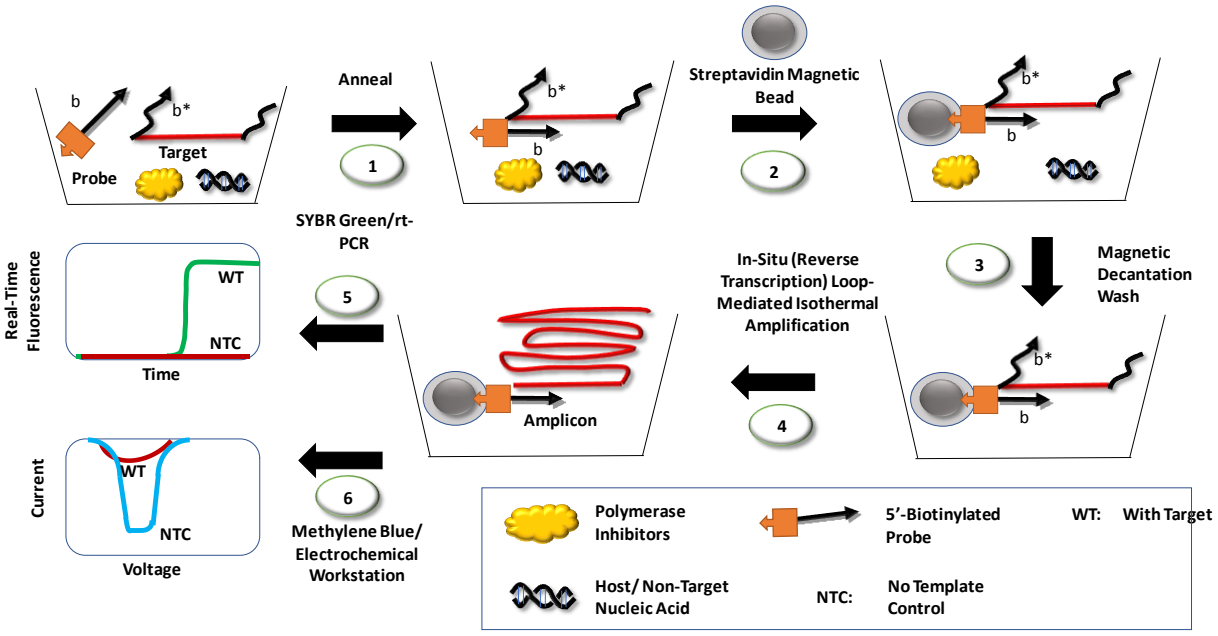

Scheme 2: B, Indirect magneto-capture.

Next, the whole assay was investigated with in vitro transcribed RNA obtained from RdRp gene containing plasmid.To find out the efficacy of indirect magneto-capture in-situ amplification assay for detecting target RdRp, plasmid spiked with human genomic DNA sample in aqueous solution or 5% FBS (fetal bovine serum) samples was employed. In each case, the magneto extraction was carried out on 10^2 and 10^3 copies present in 40 µL solution to find out the limit of detection of the assay.

4.4 Working strategy of sandwich aptamer based assay for viable pathogen detection followed by colorimetry:

The sandwich aptamer method was used for detecting live pathogens from biological samples. Firstly, biotinylated aptamers would bind with streptavidin coated magnetic nanoparticles which are described in scheme 3. While incubation with a biological fluid, this conjugated aptamer will then recognize the specific pathogen e.g., -*Staphylococcus aureus* (SA) from a biological sample. After washing off residual and non-bound aptamers, pre-synthesized hybridization chain reaction (HCR) nano-wires with secondary aptamer will come and initiate the binding and create a sandwich aptamer in which cells are entrapped. After three to four successive magnetic decantation with wash buffer we will investigate the colorimetry. In the case of HCR, the complementary DNAzyme sequence is part of the hairpin 1 (H1) probe. Hemin DNAzymes generate green color upon incubation with (2,2'-azino-bis (ethylbenzothiazoline-6-sulfonic acid)(ABTS) and H_2O_2. Thus, colorimetric readouts can be generated in a specific manner.

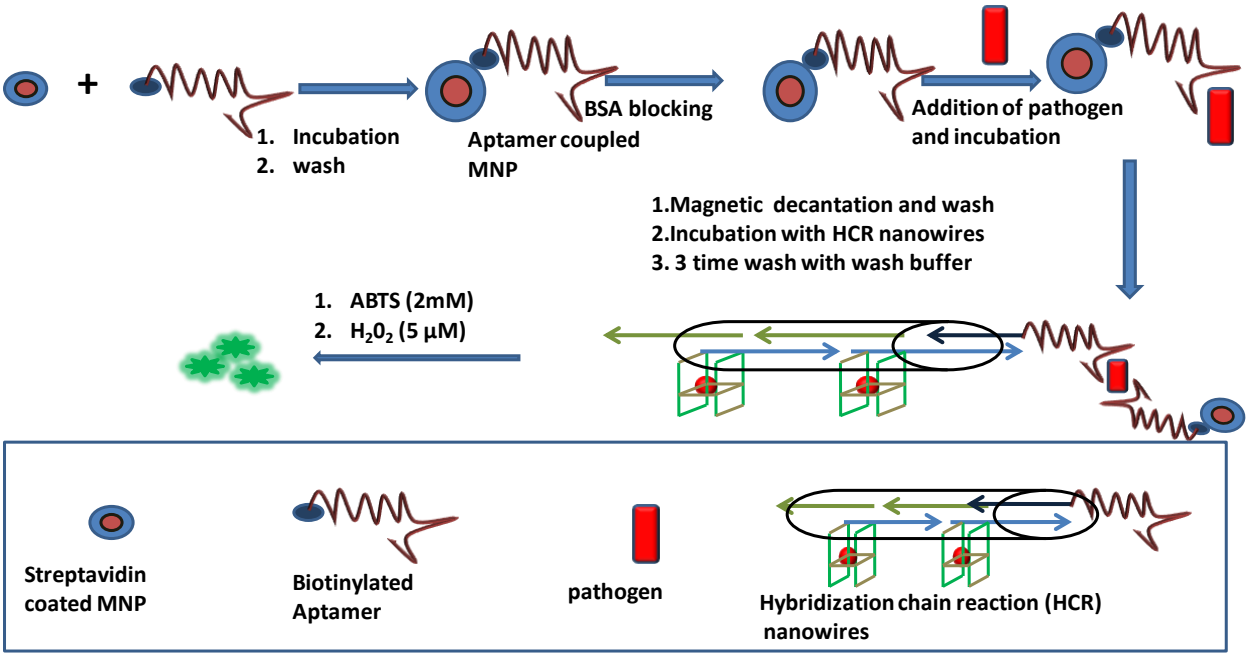

Scheme 3: Sandwich aptamer based assay for viable pathogen detection

4. Origination of proposed thesis:

The proposed thesis contains five chapters which includes the introduction, the three research objectives, and conclusions. A brief overview of chapter wise description of the proposed thesis is stated below:

Chapter 1 describes the essential introduction which includes the necessity of nucleic acid extraction for pathogen detection. The chapter will include conventional ways of pathogen detection and their drawbacks, the need of commonly used procedures for nucleic acid extraction and their cost/assay. The chapter will also include a detailed literature survey on commonly used magnetic beads based nucleic acid extraction such as chitosan coated, poly-amine coated, silica coated, cellulose coated magnetic nanoparticles. The survey will also include the current gold standard amplification methods and their drawbacks in resource constrained area. This chapter will also highlight the significance of isothermal amplification procedures over conventional nucleic acid amplification procedure in resource limited area.

Chapter 2 describes our attempts to develop novel chitosan and polyamine-coated magnetic nanoparticles which were coated by positively charged chitosan, methylated chitosan derivatives, or

spermine for isolating DNA from biological samples. Chitosan (CS) [(1→4)-2-amino-2-deoxy-β-D-glucan], a cationic polysaccharide consisting of N-acetyl glucosamine (GlcNAc) and glucosamine (GlcN), obtained from the deacetylation of chitin, has now widely used in the field of gene delivery because of its excellent nucleic acid binding capacity and biocompatability. Therefore, it can be used along with magnetic (Fe_3O_4) nanoparticle. We have synthesized various chitosan-iron oxide, magnetic nanoparticles (MNPs), characterized them using FT-IR spectroscopy and then subjected to DNA binding and isolation in a rapid (less than 30 min) assay. Since the ultimate goal was biomedical detection without using high cost instruments like PCR, the isolated DNA was then characterized by loop-mediated isothermal amplification (LAMP) and further gone for its limit of detection (LOD).

Chapter 3 describes a method development for the sequence specific capture of RNA containing RdRp gene of SARS-CoV-2 on a solid-phase magnetic bead support followed by an integrated in situ (on-bead) reverse transcriptase loop-mediated isothermal amplification (LAMP). The amplicons are subsequently detected by real-time fluorescence measurement and square wave voltametry (SWV). We also demonstrate that the assay, in either fluorescence or electrochemical read-out, do not require presence of a molecular beacon-like probe even when excess host nucleic acid is present. In addition, we show the assay utility in real life resembling scenario by extracting and detecting the RNA from a VTM-mimic clinical sample containing complex biofluid. assay could detect as low as 25 copies/µL of viral RdRp genes in less than 2.30 hours.

Chapter 4 describes the sandwich aptamer coupled with streptavidin coated magnetic nanoparticles covalently bound with Biotinylated aptamer for detecting the live pathogen from a biological sample e by an enzyme free detection method hybridization chain reaction (HCR). By this technique we tried to overrule the shortcomings of nucleic acid detection method in a very cost effective and in a time dependent manner. This method is coupled with colorimetry using G-quadruplex chemistry with hemin.

Chapter 5 concludes the findings of present work and suggests the scope of future improvisation of the work.

5. Conclusion:

In our work, we adopted a pH controlled and sequence-specific magneto-capture assay that was designed to be compatible with resource limited settings. These assays could be accomplished with a bench top magnetic stirrer or water bath with a magnet. Selecting LAMP for downstream read-out purpose also overrules the need of high cost thermal cyclers. The downstream LAMP was carried out in situ and elution from magnetic bead, and therefore the assay time was reduced. LAMP showed succeptibility with both real-time fluorescence as well as electrochemical readouts, and therefore was sacceptable for both centralized as well as resource-constrained field implementations. The all assays successfully exhibited the detection of 100 – 1000 copies/reaction for pure genomic DNA from *E.coli*, *E.coli* cell lysate, plasmid DNA and RNA carrying SARS-CoV-2 RdRp sequence from aqueous, human genomic DNA spiked, and serum spiked VTM-mimicking samples. Despite of the fact that, the assay was able to successfully detect 100 – 1000 copies/reaction in less time than the conventional methods and distinguish the same from NTC, it was inadequate to significantly differentiate the fluorescence signal between the 100 and 1000 copies. The reason could be due to our use of homemade LAMP mastermix and possibly be enhanced for commercial LAMP mastermix. Besides, a separate primer set with even higher specificity could also help in detecting and differentiating the 100 and 1000 copies bacterial and viral nucleic acid. The turnaround time (sample-to-answer) was 1.5 – 2 h, dictates the prospectives of -point-of-care detection. On the other hand, we have attempt to perform sandwich aptamer assay, where the aptamer was coupled with streptavidin coated magnetic nanoparticles bound with aptamer for detecting the live pathogen from a biological sample by an enzyme free detection method hybridization chain reaction (HCR) coupled with colorimetry. By this technique, we are hypothesizing to overrule the shortcomings of the nucleic acid detection method (inability to differentiate viable from nonviable cells) in a very cost-effective and time-dependent manner.

6. Publications:

1. Limited-resource preparable chitosan magnetic particles for extracting amplification-ready nucleic acid from complex biofluids. Sayantan Tripathy, Ashish Kumar Chalana, Arunansu

Talukdar, P. V. Rajesh, Abhijit Saha, Goutam Pramanik* and Souradyuti Ghosh *, Analyst, RSC, 2022,147, 165-177 . [IF-4.6,Q1]

2. Oxygen Vacancy Modulated MnO2 Bi-Electrode System for Attomole-Level Pathogen Nucleic Acid Sequence Detection. Tanvi Agarkar, Vandana Kuttappan Nair, Sayantan Tripathy, Vipin Chawla, Souradyuti Ghosh*, Ashvani Kumar* Electrochimica acta, Volume 407, 1 March 2022, 139876 Elsevier, (just accepted) [IF-6.9,Q1]
3. Magnetic beads based sequence specific nucleic acid extraction coupled with electrochemical loop mediated isothermal amplification for rapid detection of SARS-CoV-2. Sayantan Tripathy, Tanvi Agarkar, Ashvani Kumar, Mrittika Sengupta, Arunansu Talukdar, Souradyuti Ghosh* Sensors and Actuators B,Chemical Elsevier.[IF-7.3,Q1] (under revision)
4. Titanium Oxide-Vanadium Oxide nanocompositebased solid state dual-electrode sensor for nucleic acid detection Sayantan Tripathy, Tanvi Agarkar, Ashvani Kumar, Mrittika Sengupta, Arunansu Talukdar, Souradyuti Ghosh* ACS Analytical Chemistry [IF-6.9,Q1]
5. Aptamer-magnetic beads based Hybridization chain reaction for pathogen detection based on colorimetric readouts in resource limited area. Sayantan Tripathy, Arunansu Talukdar, and Souradyuti Ghosh * (manuscript prepared)

Patents:

1. Methods for identification of charged biopolymer. TEMP/E1/41874/2021-DEL
2. A method for nucleic acid extraction using coated magnetic particles and detection thereof. 202111004691. (Patent published).

Conference:

Presented a poster at conference in 2nd Virtual International symposium of RSC chemical biology and bioorganic group in University of Nottingham, United Kingdom

7. Reference:

(1) Bhattarai, S.; Sharma, B. K.; Subedi, N.; Ranabhat, S.; Baral, M. P. Burden of Serious Bacterial Infections and Multidrug-Resistant Organisms in an Adult Population of Nepal: A Comparative Analysis of Minimally Invasive Tissue Sampling Informed Mortality Surveillance of Community and Hospital Deaths. *Clin. Infect. Dis. Off. Publ. Infect. Dis. Soc. Am.* **2021**, *73* (Suppl_5), S415–S421. https://doi.org/10.1093/cid/ciab773.

(2) Bustin, S.; Mueller, R.; Shipley, G.; Nolan, T. COVID-19 and Diagnostic Testing for SARS-CoV-2 by RT-QPCR-Facts and Fallacies. *Int. J. Mol. Sci.* **2021**, *22* (5), 2459. https://doi.org/10.3390/ijms22052459.

(3) Methods for Rapid Detection of Foodborne Pathogens: An Overview https://scialert.net/abstract/?doi=ajft.2011.87.102 (accessed 2022 -03 -17). https://doi.org/10.3923/ajft.2011.87.102.

(4) Zhao, X.; Lin, C.-W.; Wang, J.; Oh, D. H. Advances in Rapid Detection Methods for Foodborne Pathogens. *J. Microbiol. Biotechnol.* **2014**, *24* (3), 297–312. https://doi.org/10.4014/jmb.1310.10013.

(5) Vidal, A. M. B.; Catapani, W. R. Enzyme-Linked Immunosorbent Assay (ELISA) Immunoassaying versus Microscopy: Advantages and Drawbacks for Diagnosing Giardiasis. *Sao Paulo Med. J. Rev. Paul. Med.* **2005**, *123* (6), 282–285. https://doi.org/10.1590/s1516-31802005000600006.

(6) White, D.; Gouffon, J.; Peacock, A.; Geyer, R.; Biernacki, A.; Davis, G.; Pryor, M.; Tabacco, M.; Sublette, K. Forensic Analysis by Comprehensive Rapid Detection of Pathogens and Contamination Concentrated in Biofilms in Drinking Water Systems for Water Resource Protection and Management. *Environ. Forensics - Env. FORENSICS* **2003**, *4*, 63–74. https://doi.org/10.1080/15275920303481.

(7) Schrader, C.; Schielke, A.; Ellerbroek, L.; Johne, R. PCR Inhibitors - Occurrence, Properties and Removal. *J. Appl. Microbiol.* **2012**, *113* (5), 1014–1026. https://doi.org/10.1111/j.1365-2672.2012.05384.x.

(8) El Bali, L.; Diman, A.; Bernard, A.; Roosens, N. H. C.; De Keersmaecker, S. C. J. Comparative Study of Seven Commercial Kits for Human DNA Extraction from Urine Samples Suitable for DNA Biomarker-Based Public Health Studies. *J. Biomol. Tech. JBT* **2014**, *25* (4), 96–110. https://doi.org/10.7171/jbt.14-2504-002.

(9) Anticona Huaynate, C. F.; Pajuelo Travezaño, M. J.; Correa, M.; Mayta Malpartida, H.; Oberhelman, R.; Murphy, L. L.; Paz-Soldan, V. A. Diagnostics Barriers and Innovations in Rural Areas: Insights from Junior Medical Doctors on the Frontlines of Rural Care in Peru. *BMC Health Serv. Res.* **2015**, *15*, 454. https://doi.org/10.1186/s12913-015-1114-7.

(10) Tang, C.; He, Z.; Liu, H.; Xu, Y.; Huang, H.; Yang, G.; Xiao, Z.; Li, S.; Liu, H.; Deng, Y.; Chen, Z.; Chen, H.; He, N. Application of Magnetic Nanoparticles in Nucleic Acid Detection. *J. Nanobiotechnology* **2020**, *18* (1), 62. https://doi.org/10.1186/s12951-020-00613-6.

(11) Yi, L.; Huang, Y.; Wu, T.; Wu, J. A Magnetic Nanoparticles-Based Method for DNA Extraction from the Saliva of Stroke Patients. *Neural Regen. Res.* **2013**, *8* (32), 3036–3046. https://doi.org/10.3969/j.issn.1673-5374.2013.32.007.

(12) Kami, D.; Takeda, S.; Itakura, Y.; Gojo, S.; Watanabe, M.; Toyoda, M. Application of Magnetic Nanoparticles to Gene Delivery. *Int. J. Mol. Sci.* **2011**, *12* (6), 3705–3722. https://doi.org/10.3390/ijms12063705.

(13) Maldonado-Camargo, L.; Unni, M.; Rinaldi, C. Magnetic Characterization of Iron Oxide Nanoparticles for Biomedical Applications. *Methods Mol. Biol. Clifton NJ* **2017**, *1570*, 47–71. https://doi.org/10.1007/978-1-4939-6840-4_4.

(14) Ling, D.; Hyeon, T. Chemical Design of Biocompatible Iron Oxide Nanoparticles for Medical Applications. *Small Weinh. Bergstr. Ger.* **2013**, *9* (9–10), 1450–1466. https://doi.org/10.1002/smll.201202111.

(15) Wei, H.; Hu, Y.; Wang, J.; Gao, X.; Qian, X.; Tang, M. Superparamagnetic Iron Oxide Nanoparticles: Cytotoxicity, Metabolism, and Cellular Behavior in Biomedicine Applications. *Int. J. Nanomedicine* **2021**, *16*, 6097–6113. https://doi.org/10.2147/IJN.S321984.

(16) Feng, Q.; Liu, Y.; Huang, J.; Chen, K.; Huang, J.; Xiao, K. Uptake, Distribution, Clearance, and Toxicity of Iron Oxide Nanoparticles with Different Sizes and Coatings. *Sci. Rep.* **2018**, *8* (1), 2082. https://doi.org/10.1038/s41598-018-19628-z.

(17) Sohrabijam, Z.; Saeidifar, M.; Zamanian, A. Enhancement of Magnetofection Efficiency Using Chitosan Coated Superparamagnetic Iron Oxide Nanoparticles and Calf Thymus DNA. *Colloids Surf. B Biointerfaces* **2017**, *152*, 169–175. https://doi.org/10.1016/j.colsurfb.2017.01.028.

(18) Hsu, S.; Ho, T.-T.; Tseng, T.-C. Nanoparticle Uptake and Gene Transfer Efficiency for MSCs on Chitosan and Chitosan-Hyaluronan Substrates. *Biomaterials* **2012**, *33* (14), 3639–3650. https://doi.org/10.1016/j.biomaterials.2012.02.005.

(19) Kievit, F. M.; Veiseh, O.; Bhattarai, N.; Fang, C.; Gunn, J. W.; Lee, D.; Ellenbogen, R. G.; Olson, J. M.; Zhang, M. PEI-PEG-Chitosan Copolymer Coated Iron Oxide Nanoparticles for Safe Gene Delivery: Synthesis, Complexation, and Transfection. *Adv. Funct. Mater.* **2009**, *19* (14), 2244–2251. https://doi.org/10.1002/adfm.200801844.

(20) Torres-Chavolla, E.; Alocilja, E. C. Nanoparticle Based DNA Biosensor for Tuberculosis Detection Using Thermophilic Helicase-Dependent Isothermal Amplification. *Biosens. Bioelectron.* **2011**, *26* (11), 4614–4618. https://doi.org/10.1016/j.bios.2011.04.055.

(21) Bai, Y.; Cui, Y.; Paoli, G. C.; Shi, C.; Wang, D.; Zhou, M.; Zhang, L.; Shi, X. Synthesis of Amino-Rich Silica-Coated Magnetic Nanoparticles for the Efficient Capture of DNA for PCR. *Colloids Surf. B Biointerfaces* **2016**, *145*, 257–266. https://doi.org/10.1016/j.colsurfb.2016.05.003.

(22) DNA aptamers against bacterial cells can be efficiently selected by a SELEX process using state-of-the art qPCR and ultra-deep sequencing - PubMed https://pubmed.ncbi.nlm.nih.gov/33262379/ (accessed 2022 -03 -17).

(23) Song, M. Y.; Nguyen, D.; Hong, S. W.; Kim, B. C. Broadly Reactive Aptamers Targeting Bacteria Belonging to Different Genera Using a Sequential Toggle Cell-SELEX. *Sci. Rep.* **2017**, *7*, 43641. https://doi.org/10.1038/srep43641.

(24) Point-of-care diagnostics for infectious diseases: From methods to devices - PubMed https://pubmed.ncbi.nlm.nih.gov/33584847/ (accessed 2022 -03 -17).

(25) Cao, Y.; Wang, L.; Duan, L.; Li, J.; Ma, J.; Xie, S.; Shi, L.; Li, H. Development of a Real-Time Fluorescence Loop-Mediated Isothermal Amplification Assay for Rapid and Quantitative Detection of Ustilago Maydis. *Sci. Rep.* **2017**, *7* (1), 13394. https://doi.org/10.1038/s41598-017-13881-4.

SCHOLAR BIOGRAPHY

Sayantan Tripathy was born in city of joy Calcutta, India. He received a Bachelor's in Science (Microbiology Honours) from the University of Calcutta and a Masters in Biochemistry with specialization in chemical toxicology from the Department of Biochemistry, University of Calcutta. He is pursuing his Ph.D. from Bennett University, Greater Noida. His Ph.D. is constrained in the area of nanoparticles based biosensor development for point of care diagnostics. His Ph.D. work elucidates the novel biosensing procedures in combination with material chemistry to overcome the drawbacks of conventional molecular diagnostic techniques. Before pursuing Ph.D. he was a research fellow in IISER-Kolkata and Shiv Nadar University and explored the research field of cancer signalling pathways and plant secondary metabolites.